



The  
University  
Of  
Sheffield.

# **ECM internalisation as a novel modulator of cancer cell growth/survival**

**Mona Nazemi**

A thesis submitted in partial fulfilment of the requirements for the degree of  
Doctor of Philosophy

The University of Sheffield  
Faculty of Science  
Department of Biomedical Science

April 2021

## Abstract

Tumour development is defined as a process in which cells constantly accumulate genetic mutations and epigenetic alterations. However, there is growing evidence that the tumour microenvironment including the extracellular matrix (ECM) also affects cancer cells survival, proliferation, growth, invasion and metastasis through cell-ECM interaction, cytokines, and growth factors. In addition, it is suggested that cancer cells rely on extracellular proteins during starvation, which is often observed in the tumour microenvironment due to elevated tumour growth rate and limited blood supply. Nonetheless, the role of ECM internalisation in cancer metabolism and regulatory mechanisms of this process have not been addressed in detail yet. Here we explored the role of ECM trafficking in terms of controlling breast cancer growth and survival. Our data demonstrate that the mechanisms through which cell-ECM interaction affects cancer cell growth varies by different starvation conditions. Under amino acid (AA) depletion, the presence of ECM could partially rescue the growth of invasive breast cancer cells (MDA-MB-231). Breast cancer cells were able to internalize and degrade collagen I and Matrigel under AA deficiency. In addition, inhibition of ECM uptake prevented cell growth under starvation. Our data show that presence of collagen I and Matrigel promotes cellular anabolic activity under AA starvation conditions by inducing mTORC1 activity. Mass-spectrometry data from AA starved cells on ECMs demonstrated significant increase in AA content as well as the upregulation of different metabolic pathways including phenylalanine and tyrosine metabolism, potentially increasing energy content of cells via fumarate formation. The data under non-essential AA (NEAA) starvation was also consistent to the AA starvation as cells required ECM internalization to rescue their growth. Monitoring candidate genes participating in ECM trafficking revealed three genes, RIN3, MAKP8IP3 and AP3D1 potentially having important role in trafficking of the ECM to the lysosome since their lack of function had adverse impact on invasive breast cancer cell growth under the NEAA deficiency. Under Glucose (Glc) starvation, MDA-MB-231 showed higher growth rate on ECM compared to the plastic. They could internalize ECM followed by lysosomal degradation. However, lack of ECM uptake did not oppose their growth. Whereas inhibition of focal adhesion kinase (FAK) activity substantially reduced their growth rate. Presence of ECM also enhanced mTORC1 activity in Glc starved cells. In contrast, ECM did not change metabolic content of cells after six days of Glc depletion. Thus, it is possible that the presence of ECM can trigger signalling

pathways downstream of FAK inducing mTORC1 activity and cell growth. These findings lead to the conclusion that the presence of ECM could facilitate cancer cells growth/survival in nutrient deficient conditions via various mechanisms. There are different types of tumours that are surrounded by a dense and fibrotic stroma including breast, lung, pancreatic, and colon tumours. Therefore, the findings of this study could potentially be generalised to other types of cancers to find a potential therapeutic target in future.

## Acknowledgement

First and the most important, I would like to thank my PhD supervisor, Dr Elena Rainero, for her constant support, guidance, and motivations throughout my PhD. She was so patient with me through this scientific journey. I also want to thank University of Sheffield, Faculty of Science for providing the funds for my research.

I would like to thank Dr Heather Walker and Dr Mark Collins at University of Sheffield Mass Spectrometry Centre, for their guidance. I also want to thank Professor Elizabeth Smyth for her advice for my thesis writing. I also want to thank Dr Stephen Brown for his help with microscopy.

I want to thank everyone in KA/SW/ER lab, past and present, for their scientific and emotional supports in the lab and during our coffee breaks. I would like to give a special thanks to Stella, Montse, Ben, Adam, Sarah, and Nan, for all the good times spending together and for all the jokes, laughs and support. Without you my time in the lab would be very boring.

Finally, I want to thank my family for their continued support throughout my PhD, and a special thanks to my Fiancé, Robert, who was always by my side and managed to tolerate all my moaning and nagging throughout this journey. This achievement would not have been possible without them. At the end, I would like to dedicate this thesis to the memory of my grandparents, I hope they are all proud of me.

## Declaration

I declare that this thesis has been solely the result of my own work and has not been submitted for any other degree at the University of Sheffield or any other institution. I can confirm that where I have quoted from the work of others, the source is always given.

Mona Nazemi

## Table of contents

<b>ABSTRACT .....</b>	<b>1</b>
<b>ACKNOWLEDGEMENT.....</b>	<b>3</b>
<b>DECLARATION .....</b>	<b>4</b>
<b>TABLE OF CONTENTS .....</b>	<b>5</b>
<b>LIST OF FIGURES .....</b>	<b>11</b>
<b>LIST OF TABLES.....</b>	<b>14</b>
<b>ABBREVIATIONS.....</b>	<b>15</b>
<b>CHAPTER 1: INTRODUCTION .....</b>	<b>19</b>
1.1 HALLMARKS OF CANCER .....	19
1.1.1 Sustaining proliferative signalling.....	20
1.1.2 Evading growth suppressors.....	21
1.1.3 Resisting cell death .....	21
1.1.4 Enabling replicative immortality. ....	22
1.1.5 Inducing angiogenesis .....	23
1.1.6 Invasion and metastasis .....	23
1.1.7 Evading immune destruction.....	24
1.2 BREAST CANCER.....	25
1.2.1 Incidence.....	25
1.2.2 Breast cancer classification .....	26
1.2.2.1 Molecular classification .....	26
1.2.2.2 Clinical classification .....	27
1.2.2.2.1 ER positive and HER-2 negative breast cancer .....	27
1.2.2.2.2 HER-2 positive breast cancer .....	28
1.2.2.2.3 Triple negative breast cancer.....	28
1.2.3 Models for study breast cancer .....	29
1.3 THE TUMOUR MICROENVIRONMENT .....	31
1.3.1 Cancer associated fibroblasts.....	32
1.3.2 The Extracellular matrix.....	33

1.3.2.1 Collagen.....	34
1.3.2.2 Fibronectin.....	37
1.3.2.3 Laminin.....	38
1.3.3 ECM remodelling in breast cancer .....	39
1.3.4 ECM receptors: integrins .....	43
1.3.5 The crosstalk between nutrient signalling and the ECM-integrin trafficking. ....	45
1.4 METABOLISM.....	47
1.4.1 Reprogramming energy metabolism.....	47
1.4.2 TCA cycle.....	49
1.4.3 Glycolysis .....	50
1.4.4 Glutaminolysis .....	52
1.4.5 Amino acid metabolism.....	54
1.4.6 CAFs and metabolism .....	57
1.4.7 Nutrient scavenging from microenvironment.....	58
1.5 AIM OF THE THESIS.....	61
<b>CHAPTER 2: MATERIALS AND METHODS .....</b>	<b>62</b>
2.1 MATERIALS.....	62
2.1.1 Reagents .....	62
2.1.2 Cell culture media.....	63
2.1.3 Solutions .....	64
2.1.4 siRNA.....	64
2.1.5 Primary antibodies.....	65
2.1.6 Secondary antibodies .....	65
2.2 METHODS .....	66
2.2.1 Cell culture.....	66
2.2.2 ECM preparation .....	66
2.2.2.1 Collagen I, Matrigel and Laminin coating.....	66
2.2.2.2 Preparation of cell-derived matrices. ....	67
2.2.3 Cell proliferation assay .....	67
2.2.3.1 Starvation media compositions .....	68
2.2.3.2 Media formulation (DMEM). ....	69
2.2.3.3 MEM Non-Essential Amino Acids Solution (100x) .....	70

2.2.3.4 MEM Essential amino acid solution (50x) .....	70
2.2.3.5 Media formulation (DMEM/F12). .....	71
2.2.3.6 Cell proliferation assay on CAF-CDM .....	73
2.2.3.7 Cell proliferation assay in the presence of pharmacological inhibitors.....	76
2.2.4 Measurement of ECM consumption .....	76
2.2.5 ECM cross-linking.....	76
2.2.6 ECM uptake assay.....	77
2.2.7 Cell division assay (EdU labelling).....	78
2.2.8 Measurement of mTORC1 activity (p-S6 labelling) .....	78
2.2.9 Measurement of cell apoptosis .....	82
2.2.10 Glucose Uptake Assay.....	82
2.2.11 Live imaging of ATP content .....	83
2.2.12 Western blot.....	83
2.2.13 Quantification of cellular focal adhesion content.....	84
2.2.14 Mass spectrometry .....	85
2.2.14.1 Non-targeted metabolite profiling.....	85
2.2.14.2 Data analysis .....	85
2.2.14.3 Targeted metabolite profiling.....	86
2.2.15 RNAi screen.....	86
2.2.15.1 Optimisation of RNAi-mediated gene knockdown .....	86
2.2.15.2 High throughput RNAi screening .....	87
2.2.15.2.1 Traffic-ome screen. ....	87
2.2.15.3 HPD and HPDL RNAi-mediated gene knockdown .....	89
2.2.16 Statistical analysis.....	90

### **CHAPTER 3: THE EXTRACELLULAR MATRIX SUPPORTS BREAST CANCER GROWTH UNDER AMINO ACID STARVATION BY REGULATING TYROSINE METABOLISM..... 91**

ABSTRACT .....	91
INTRODUCTION .....	91
RESULTS .....	92
The presence of ECM partially rescued breast cancer cell growth under starvation conditions. ....	92



Matrigel partially rescued the growth of non-invasive breast cancer cells under glutamine starvation.....	95
Collagen I and Matrigel increased cell division under starvation conditions.....	97
Collagen I and Matrigel rescued mTORC1 activity in starved cells. ....	98
ECM internalization inhibition opposed cell growth under amino acid starvation. ....	99
Inhibition of focal adhesion kinase did not affect cell growth on ECM under starvation. ....	101
ECM promoted cell growth under amino acid starvation by modulating tyrosine and phenylalanine metabolism. ....	103
DISCUSSION.....	107
MATERIALS AND METHODS .....	110
REFERENCES .....	113
<b>CHAPTER 4: THE ECM SUPPORTS BREAST CANCER CELL METABOLISM UNDER AMINO ACID STARVATION. ....</b>	<b>122</b>
4.1 INTRODUCTION .....	122
4.2 RESULTS.....	124
4.2.1 Cell proliferation assay optimisation.....	124
4.2.2 TIF-CDM, but not CAF-CDM, supported the growth of non-invasive breast cancer cells under glutamine starvation. ....	125
4.2.3 Laminin increased invasive breast cancer cell division under glutamine and amino acid starvation conditions. ....	127
4.2.4 Invasive breast cancer cells internalized and degraded laminin.....	128
4.2.5 Laminin did not support mTORC1 activity under starvation.....	129
4.2.6 V-ATPase inhibitor decreased cell growth. ....	130
4.2.7 Glucose uptake was not responsible for cell growth under amino acid starvation. ....	132
4.2.8 Cells on Matrigel had higher ATP content under amino acid starvation. ....	133
4.2.9 The presence of ECM increased glycolysis and TCA cycle intermediates under starvation.....	135
4.3 DISCUSSION.....	136

**CHAPTER 5: AN RNAI SCREEN IDENTIFIED AP3, RIN3 AND MAPK8IP3 AS NOVEL REGULATORS OF ECM-DEPENDENT CELL GROWTH UNDER STARVATION. .... 142**

5.1 INTRODUCTION .....	142
5.2 RESULTS.....	144
5.2.1 The presence of collagen rescued breast cancer cell growth under non-essential amino acid starvation. ....	144
5.2.2 ECM cross-linking opposed cell growth under NEAAs starvation. ....	146
5.2.3 RNAi screen setup and evaluation on Matrigel.....	147
5.2.4 The RNAi Traffic-ome screen.....	150
5.3 DISCUSSION.....	154

**CHAPTER 6: SIGNALLING PATHWAYS DOWNSTREAM OF CELL-ECM INTERACTION ENHANCE THE GROWTH/SURVIVAL OF GLUCOSE STARVED BREAST CANCER CELLS. .... 159**

6.1 INTRODUCTION .....	159
6.2 RESULTS.....	162
6.2.1 Optimising cell proliferation assays under glucose and serum starvation .....	162
6.2.2 Fibrillar ECMs partially rescued breast cancer cell growth under serum starvation. ....	163
6.2.3 The presence of ECM did not affect normal mammary epithelial cell and non-invasive breast cancer cell growth under serum starvation. ....	165
6.2.4 The presence of ECMs did not promote cell division under serum starvation in invasive breast cancer cells. ....	167
6.2.5 Collagen I, but not Matrigel or laminin, rescued the activity of mTORC1 under serum starvation.....	168
6.2.6 The presence of ECM partially rescued breast cancer cell growth under glucose starvation.....	169
6.2.7 The ECM did not affect cell growth of normal mammary epithelial cells and non-invasive breast cancer cells under glucose starvation. ....	173
6.2.8 The presence of ECMs did not promote cell division under glucose starvation in invasive breast cancer cells. ....	176
6.2.9 ECM affected the activity of mTORC1 under glucose starvation. ....	178

6.2.10 Blocking ECM internalization did not affect cell growth under glucose starvation. .....	180
6.2.11 FAK activity was required for cell growth on Matrigel and CDM under glucose starvation.....	183
6.2.12 Cells on plastic internalized more glucose compared to the cells on ECM.....	184
6.2.13 Cells on Matrigel had higher ATP content under glucose starvation.....	185
6.2.14 The presence of Matrigel did not change the metabolite content of cells under glucose starvation.....	187
6.3 DISCUSSION.....	188
6.3.1 Serum starvation .....	188
6.3.2 Glucose starvation .....	190
<b>CHAPTER 7. GENERAL DISCUSSION .....</b>	<b>195</b>
7.1 SUMMARY.....	195
7.2 ECMs PARTIALLY RESCUED CELL GROWTH UNDER DIFFERENT STARVATION CONDITIONS. ....	196
7.3 NORMAL MAMMARY EPITHELIAL CELLS AND NON-INVASIVE BREAST CANCER CELLS BEHAVED DIFFERENTLY ON ECM UNDER DIFFERENT STARVATION CONDITIONS. ....	198
7.4 THE ECM PROMOTED CELL GROWTH VIA DIFFERENT MECHANISMS UNDER VARIOUS STARVATION CONDITIONS. ....	199
7.4.1 Assessing rate of cell division and apoptosis on different ECMs and starvation conditions. ....	200
7.4.2 Potential mechanisms controlling mTORC1 activity on ECMs under different nutrient conditions. ....	202
7.4.3 Does the presence of ECM have signalling or metabolic impact? .....	203
7.5 METABOLIC PATHWAYS WERE ENHANCED ON ECMs IN AA STARVED CELLS. ....	204
7.6 CONCLUSION AND FUTURE DIRECTIONS .....	206
<b>CHAPTER 8: REFERENCES .....</b>	<b>208</b>

## List of Figures

### Chapter 1:

Figure 1.1. Hallmarks of Cancer. ....	19
Figure 1.2. Schematic image of breast cancer progression. ....	30
Figure 1.3. Collagen synthesis steps. ....	35
Figure 1.4. Fibronectin structure. ....	38
Figure 1.5. Laminin structure. ....	39
Figure 1.6. Changes in ECM during breast cancer progression. ....	40
Figure 1.7. Schematic representation of FA complex formation followed by integrin activation. ....	44
Figure 1.8. Crosstalk between integrin-ECM interaction and nutrient availability. ....	47
Figure 1.9. TCA cycle intermediates. ....	50
Figure 1.10. Glycolysis. ....	52
Figure 1.11. Metabolic pathways of non-essential amino acids. ....	56
Figure 1.12. Schematic representation of signalling pathways induces macropinocytosis and ECP internalization. ....	60

### Chapter 2:

Figure 2.1. Designing algorithm by CME to detect cells positive for actin staining. ....	75
Figure 2.2. Designing algorithm by CME to detect the intensity of pS6 staining per cell. ....	81

### Chapter 3:

Figure 1. The ECM rescued cell growth under starvation conditions. ....	95
Figure 2. The ECM did not affect normal epithelial cell and non-invasive breast cancer cell growth. ....	97
Figure 3. Collagen I and Matrigel induced cell proliferation under glutamine and amino acid starvations. ....	98
Figure 4. Collagen I and Matrigel rescued mTORC1 activity in starved cells. ....	98
Figure 5. MDA-MB-231 cells internalized and degraded collagen I and Matrigel. ....	101
Figure 6. FAK inhibition did not affect cell growth on collagen I, Matrigel and CAF-CDM under AA starvation. ....	102
Figure 7. Cells had different metabolite content on collagen I compared to plastic under amino acid starvation. ....	104

Figure 8. HPDL KD significantly opposed cell growth under AA starvation on collagen I. ....	106
Supplementary figure 1. MDA-MB-231 cell growth on ECMs under complete media.....	117
Supplementary figure 2. MCF10A and MCF10A-DCIS growth on ECMs under complete media. ....	118
Supplementary figure 3. The ECM did not affect apoptosis under starvation.....	119
Supplementary figure 4. MMP inhibition did not affect ECM uptake and cell growth under starvation. ....	120
Supplementary figure 5. Cells had different metabolite content on Matrigel compared to plastic under amino acid starvation. ....	121
<b>Chapter 4:</b>	
Figure 4.1. Optimising techniques for cell proliferation assay. ....	125
Figure 4.2. TIF-CDM rescued MCF10A-DCIS growth under glutamine starvation.....	126
Figure 4.3. Laminin induced cell proliferation under glutamine and amino acid starvations. ....	127
Figure 4.4. MDA-MB-231 cells internalized and degraded laminin under normal and starvation conditions. ....	128
Figure 4.5. Presence of laminin did not affect mTORC1 activity in starved cells. ....	129
Figure 4.6. Effect of V-ATPase inhibitor on cell growth and mTORC1 activity on Matrigel. .	131
Figure 4.7. The presence of ECM did not affect glucose uptake under amino acid starvation. ....	133
Figure 4.8. Cells on Matrigel had higher ATP content under starvation. ....	134
Figure 4.9. TCA cycle and glycolysis intermediates on collagen I and Matrigel compared to the plastic under starvation.....	136
<b>Chapter 5:</b>	
Figure 5.1. Schematic representation of ECM internalization pathways. ....	143
Figure 5.2. Collagen I and CDMs partially rescued cell growth under NEAAs starvation.....	145
Figure 5.3. ECM cross-linking opposed matrix-dependent cell growth under NEAA starvation. ....	146
Figure 5.4. Optimizing siRNA transfection on ECM. ....	149
Figure 5.5. High throughput RNAi screen set up. ....	151
Figure 5.6. Traffic-ome siRNA screening.....	153

Figure 5.7. Schematic representation of ECM trafficking pathways that AP3, JIN3 and RIN3 might be involved in under starvation conditions.....158

### **Chapter 6:**

Figure 6.1. Role of Growth factor signalling in nutrient consumption.....161

Figure 6.2. Collagen degradation occurred during cell proliferation.....162

Figure 6.3. Fibrillar matrices rescued cell growth under serum starvation.....164

Figure 6.4. MCF10A and MCF10A-DCIS growth under serum starvation.....166

Figure 6.5. ECMs did not affect cell division under serum starvation.....167

Figure 6.6. Collagen I rescued mTORC1 activity in serum starved cells. ....169

Figure 6.7. Cell growth under different glucose concentration. ....171

Figure 6.8. The ECM rescued cell growth under glucose starvation. ....172

Figure 6.9. The ECM did not affect MCF10A-DCIS growth under glucose starvation. ....174

Figure 6.10. MCF10A-DCIS growth on CAF-CDM.....175

Figure 6.11. ECMs did not rescue MCF10A growth under glucose starvation.....176

Figure 6.12. ECMs did not affect cell division or apoptosis under glucose starvation.....178

Figure 6.13. The ECM supported mTORC1 activation in glucose starved cells, and this was required for ECM-dependent cell growth. ....180

Figure 6.14. MDA-MB-231 cells internalized and degraded ECMs under glucose starvation condition, but this was not required for cell growth.....182

Figure 6.15. MMP inhibition did not affect cell growth under glucose starvation. ....183

Figure 6.16. FAK inhibition reduced cell growth on Matrigel and CAF-CDM under glucose starvation. ....184

Figure 6.17. The presence of ECM reduced 2-NBDG uptake under glucose starvation.....185

Figure 6.18. Cells on Matrigel had higher ATP content under starvation. ....186

Figure 6.19. The presence of Matrigel did not affect cellular metabolite content under glucose starvation.....187

### **Chapter 7:**

Figure 7.1. Mechanism of cell ECM interaction under different starvation conditions.....196

## List of Tables

Table 1.1: Molecular subtype of breast cancer .....	27
Table 1.2. Different types of collagen participate in IM and BM. ....	36
Table 1.3. ECMs and their integrin receptors .....	45
Table 1.4. List of essential and non-essential amino acids.....	54
Table 2.1. Reagents and suppliers.....	62
Table 2.2. Media, suppliers, and reference numbers.....	63
Table 2.3. Recipes of solutions. ....	64
Table 2.4. siRNA used for siRNA knockdown.....	64
Table 2.5. Primary antibodies. ....	65
Table 2.6. Secondary antibodies .....	65
Table 2.7. Composition of different media used for different cell lines. ....	68
Table 2.8. Concentration of different DMEM media. ....	69
Table 2.9. Concentration of amino acids in MEM NEAAs solution.....	70
Table 2.10. Concentration of amino acids in MEM solution .....	70
Table 2.11. Concentration of different DMEM/F12 media. ....	71
Table 2.12. Name, ID, and sequence of genes participating in Traffic-ome siRNA library.....	87
Table 7.1. Effect of different matrices on MDA-MB-231 growth under various starvation conditions.....	197

## Abbreviations

2-NBDG	2-(N-(7-Nitrobenz-2-oxa-1,3-diazol-4-yl) Amino)-2-Deoxyglucose
AA	Amino acid
ADH	Atypical ductal hyperplasia
AIs	Aromatase inhibitors
AML	Acute myeloid leukaemia
AMPK	AMP-activated protein kinase
AMPK	Adenosine monophosphate-activated kinase
AR	Androgen receptor
ASNS	Asparagine synthetase
ASS	Arginine succinate synthetase
ATF4	Activating transcription factor4
BA1	Bafilomycin A1
BCAAs	Branched chained amino acids
BCAT1	Branched-chain amino acid transaminase 1
bFGF	Basic FGF
BM	Basement membrane
BMF	Bone marrow fibroblasts
BSA	Bovine serum albumin
CAFs	Cancer associated fibroblast cells
CDM	Cell derived matrix
CHOP	C/EBP-homologous protein
CME	Costum Module Editor
CTL	Cytotoxic T cells
DCIS	Ductal carcinoma in situ
DCIS-MI	DCIS with microinvasion
DDR	Discoidin domain receptor
DEPTOR	DEP-domain-containing mTOR-interacting protein
DF1	DharmaFect-1
DFBS	Dialyzed FBS
DHAP	Dihydroxyacetone phosphate
DI-MS	Direct infusion mass spectrometry
DMEM	Dulbecco's Modified Eagle's Medium
DMSO	Dimethyl sulfoxide
EAAAs	Essential amino acids
ECAR	Extracellular acidification rate
ECM	Extracellular matrix
ECP	Extracellular protein
EdU	5-ethynyl-2'-deoxyuridine
EGF	Epidermal growth factor
Elf $\alpha$ 2	Eukaryotic Initiation Factor 2 $\alpha$
EMT	Epithelial mesenchymal transition
ER	Oestrogen receptor
ERE	Oestrogen responsive element



ERK1/2	Extracellular signal-regulated kinase-1/2
ESCRT	Endosomal sorting complex required for transport
FA	Focal adhesion
FACITs	Fibril associated collagens with interrupted triple helices
FADH	Flavin adenine dinucleotide
FAK	Focal adhesion Kinase
FAP	Fibroblast activation protein
FAT	Focal adhesion targeting
FBS	Fetal bovine serum
FERM	Four-point-one, Ezrin, Radixin, Moesin
FGF	Fibroblast growth factor
FH	Fumarate hydratase
FN	Fibronectin
GF	Growth factor
Glc	Glucose
Gln	Glutamine
GLS	Glutaminase
GS	Glutamine synthetase
GDH	Glutamate dehydrogenase
GOT	Glutamate–oxaloacetate transaminase
GPT	Glutamate–pyruvate transaminase
GRM3	Glutamate metabotropic receptor 3
HCC	Hepatocellular carcinoma
HER-2	Human epidermal growth factor receptor 2
HGF	Hepatocyte growth factor
HIF-1	Hypoxia-inducible factor-1
HK	Hexokinase
HNCSS	Head and neck squamous cell carcinoma
HPD	4-hydroxyphenylpyruvate dioxygenase
HPDL	4-hydroxyphenylpyruvate dioxygenase-like
HR	Hormone receptors
HS	Horse serum
ICW	In-Cell Western
IDH	Isocitrate dehydrogenase
IF	Interstitial fluid
IGF-1	Insulin-like growth factor -1
IGF-IR	Insulin like growth factor I receptor
IICs	Infiltrating immune cells
ILs	Interleukins
ILVs	Intraluminal vesicles
IM	Interstitial matrix
IR	Insulin receptor
KD	Knockdown
LAMP I	Lysosomal transmembrane proteins I
LAT1	L-type amino acid transporter

LCC	Laminin coiled coil
LDH	Lactate dehydrogenase enzyme
LG	Laminin globular
LIMP II	Lysosomal integral membrane proteins II
LKB1	Liver kinase B1
LN	Laminin N-terminal
MACITs	Membrane-associated collagens with Interrupted triple-helices
MAPK	Mitogen-activated protein kinase
MEF	Mouse embryonic fibroblasts
MLST8	Mammalian lethal with SEC13 protein 8
MMP	Matrix metalloprotease
MR	Mannose receptor
MS	Mass spectrometry
MT1-MMP	Membrane type 1 MMP
mTOR	Mechanistic target of Rapamycin
NADH	Nicotinamide adenine dinucleotide
NAPDH	Nicotinamide adenine dinucleotide phosphate
NEAAs	Non-essential amino acids
NF	Normal fibroblasts
NHS	N-hydroxysuccinimidyl
NK	Natural killer
NMMIIA	Non-muscle myosin IIA
NOX	NAPDH oxidase
Nt	Non-targeted
OCR	Oxygen consumption rate
PARP1	Poly (ADP-ribose) polymerase
PDAC	Pancreatic ductal adenocarcinoma
PDGF	Platelet derived growth factors
PDGFR $\beta$	Platelet-derived growth factor receptor beta
PFA	Paraformaldehyde
PGM1	Phosphoglucomutase 1
PHGDH	3-phosphoglycerate dehydrogenase
PK	Pyruvate kinase
PLK1	Polo Like Kinase 1
PPP	Pentose phosphate pathway
PR	Progesterone receptor
PRODH	Proline dehydrogenase
PS	Penicillin streptomycin
PSAT	Phosphoserine transaminase
PSCs	Pancreatic stellate cells
RAPTOR	Regulatory-associated protein of mTOR
RB	Retinoblastoma-associated
RT	Room temperature
S6	Ribosomal subunit S6
S6K	Ribosomal S6 kinase

SDH	Succinate dehydrogenase
SRSF	Sheffield RNAi Screening Facility
STAT3	Signal transducer and activator of transcription 3
TCA	Tricarboxylic acid
TEMED	Tetramethylethylenediamine
TGF- $\beta$	Transforming growth factor- $\beta$
TGN	Trans-Golgi network
TIF	Telomerase immortalised fibroblast
TIMP	Tissue inhibitor of metalloproteases
TME	Tumour micro-environment
TNBC	Triple negative breast cancer
TNF- $\alpha$	Tumour necrosis factor- $\alpha$
UBB	Ubiquitin B
V-ATPase	Vacuolar-ATPase
VEGF	Vascular endothelial growth factor
VEGFR2	VEGF receptor 2
$\alpha$ SMA	$\alpha$ -Smooth muscle actin

## Chapter 1: Introduction

### 1.1 Hallmarks of cancer

Cancer cells are characterised by ten common traits causing their transformation to tumorigenic and finally malignant cells. These traits are called “Hallmarks of cancer” permitting these cells to survive, proliferate and migrate at different levels of cancer progression (Figure 1.1) (Hanahan and Weinberg, 2011).

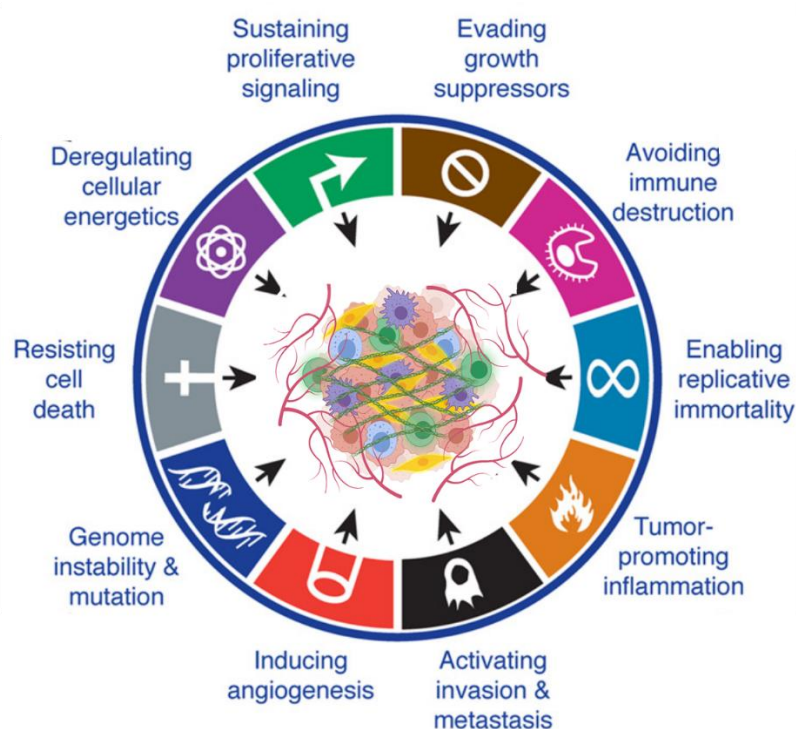


**Figure 1.1. Hallmarks of Cancer.** Hallmarks of Cancer are ten biological capabilities cells acquire during tumour development. Genome instability and tumour promoting inflammation are two hallmarks that enable cancer cells to obtain rest of the characteristics including evading growth suppressors, avoiding immune destruction, enabling replicative mortality, activating invasion and metastasis, inducing angiogenesis, resisting cell death, deregulating cellular energetics, and sustaining proliferative signalling (Figure is adapted from (Hanahan and Weinberg, 2011)).

Two of these hallmarks enabling cancer cells to acquire rest of the characteristics are:

1. Genome instability/mutation. Susceptibility of cells to mutagenic compounds, defects in DNA maintenance machinery, as well as deficiency in the system that monitor

genome integrity result in genome instability and mutation (Jackson and Bartek, 2009, Negrini et al., 2010).

2. Tumour promoting inflammation. Even though inflammation in the tumour microenvironment was interpreted as a sign of immune system attack to the neoplastic cells, it has a very paradoxical activity in favour of tumours. Inflammation is managed by immune cells around the tumour releasing mitogenic molecules, pro-angiogenic factors and enzymes that modify extracellular matrix (ECM) to promote cancer cells' metastasis and invasion. Therefore, inflammation could facilitate the emergence of other features of cancer cells (DeNardo et al., 2010, Grivennikov et al., 2010, Hanahan and Weinberg, 2011).

In addition to genomic changes, the property of microenvironment around the tumours enables cancer cells to obtain the tumorigenic characteristics being briefly explained in the following sections.

### **1.1.1 Sustaining proliferative signalling.**

One of the main features that discriminate cancer cells from normal cells is their ability of continuous proliferation and ultimately destruction of the tissue architecture. Cancer cells go through continuous proliferation by different mechanisms. Some of them constantly release growth factors (GFs) and benefit from autocrine growth stimulation. Some cancer cells release signalling molecules that induce normal stroma cells to release GFs in their micro-environment. They could also benefit from over-expression of their GF receptors making them over-sensitive to signalling molecules. In addition, there might be some structural alteration in the receptors that keep them constantly triggered (Hanahan and Weinberg, 2011, Bhowmick et al., 2004, Cheng et al., 2008). The tumour micro-environment (TME) also plays a critical role in terms of cancer cell proliferation. Angiogenesis in the TME provides a route for cancer cells to receive blood-born mitogenic GFs. It also facilitates the transfer and infiltration of specific types of leukocytes releasing different types of growth mediators including histamine, interleukins (ILs), heparins, transforming growth factor- $\beta$  (TGF- $\beta$ ), epidermal growth factor (EGF) and fibroblast growth factor (FGF). These growth mediators induce the proliferation and division of neoplastic and normal cells in the vicinity of the TME. Infiltrated leukocytes also release proteolytic enzymes modifying ECM to make the mitogenic

factors more available (Balkwill et al., 2005, Lu et al., 2011). Cancer associated fibroblast cells (CAFs) are also in charge of releasing various types of growth mediators such as EGF, insulin-like growth factor -1(IGF-1) and FGFs. Therefore, alongside gene mutation in cancer cells, the TME also provides a pro-proliferative environment for them (Hanahan and Coussens, 2012).

### **1.1.2 Evading growth suppressors**

Cancer cells stop the function of genes called tumour suppressor genes negatively regulating cell proliferation. Two most important tumour suppressor genes are retinoblastoma-associated (RB) and TP53. RB works as a cell cycle gatekeeper and inhibits G1 to S transition based on mostly external growth-inhibitory signals. While TP53 perceives different abnormalities and stresses inside the cell and stops cell proliferation or induces cell apoptosis based on the intensity of the damages (Hanahan and Weinberg, 2011). Another mechanism that in normal cells regulates proliferation is 'contact inhibition'. Contact inhibition stops cell proliferation when cells make a confluent monolayer. Even though contact inhibition was firstly found as an *in vitro* mechanism, it could be generalized to *in vivo* (Stramer and Mayor, 2017). Different mechanisms have been suggested for contact inhibition. For example, a tumour suppressor gene (*NF2*) triggers contact inhibition through coupling transmembrane tyrosine kinase receptors with cell surface adhesion molecules to increase cell-cell attachment and limit the access of GFs to their receptors (Curto et al., 2007, Okada et al., 2005).

### **1.1.3 Resisting cell death**

Mammalian cells are exposed to different disturbances inside the cell or in their microenvironment inducing signalling pathways that result in cell death. There are different types of cell death. Apoptosis is a programmed cell death which is highly regulated. There are biochemical events happening during apoptosis that result in cell death including cytoplasm shrinkage, nuclear fragmentation, and chromatin condensation that all accumulate in the apoptosis body being absorbed by other cells in their neighbourhood. Apoptosis could occur in response to DNA damage or depletion of survival factor signalling (Galluzzi et al., 2018). To avoid apoptosis, cancer cells upregulate anti-apoptotic, and survival signalling factors or downregulate pro-apoptotic proteins. In addition, loss of function for tumour suppressor

genes like TP53 cause disruption in sensing DNA damage and skipping apoptosis (Adams and Cory, 2007, Hanahan and Weinberg, 2011, Juntila and Evan, 2009, Lowe et al., 2004). Autophagic cell death is another type of death that happens when cells remove dysfunctional organelle through autophagosome fuse with lysosome. Autophagy can be a pro or anti tumorigenic process. In some types of cancer cells, autophagy is used as a cell death mechanism. Prolonged autophagy results in excessive degradation and damage of organelles and eventually cell death (Mathew et al., 2007). However, in other cancer cells like pancreatic cancer cells, the high demand of nutrients in proliferating cells can be met by autophagy, through nutrient recycling and protein degradation (Yang et al., 2011). Necrosis is a type of cell death that happens due to irreversible cell injury. During necrosis, no phagocytosis or lysosomal integration happens. In contrast to autophagy and apoptosis, necrosis works in favour of neoplastic cells (Galluzzi and Kroemer, 2008). Debris from necrotic cells could be consumed as a source of energy by proliferative cells in their neighbourhood. Necrotic cells also release some proinflammatory signals attracting immune cells, which have a tumour promoting effect (White et al., 2010). In addition, necrotic cells themselves might release some mitogenic factors that induce proliferation (Galluzzi and Kroemer, 2008, Grivennikov et al., 2010, White et al., 2010). CAFs could also assist cancer cells to avoid apoptosis. CAFs release some pro-survival factors such as IGF-1 and IGF-2. Moreover, they deposit and remodel ECMs in a way that they could make survival signals available for the cells in their vicinity (Lu et al., 2011).

#### **1.1.4 Enabling replicative immortality.**

To make a tumour, cancer cells need to cross the barriers against their unlimited proliferation. There is different evidence showing that telomeres, a region of hexanucleotide repeats at the end of the chromosomes, are involved in cancer cell consistent division. In normal cells, every proliferation result in shortening of telomeres. Hence, cells after a limited number of divisions enter a senescence phase in which they are still alive but non-proliferative. If telomere erosion happens causing genome instability, cells face a crisis phase and die. However, *in vitro* cell culture gives rise to the cells surviving the crisis phase and having non-stopped division. These cells are called immortalized. Cancer cells work like immortalized cells. They evade the crisis phase and instead keep proliferating. This ability of neoplastic cells is linked to the

expression of telomerase enzymes. Telomerase enzyme in immortalized or cancer cells protects telomeres from degradation and chromosomal fusion during DNA replication resulting in unlimited division and skipping the crisis phase (Blasco, 2005, Hanahan and Weinberg, 2011, Shay and Wright, 2000, Prasad et al., 2020).

### **1.1.5 Inducing angiogenesis**

In normal tissue, angiogenesis does not happen unless due to wound healing or women's menstrual cycle. However, tumour growth and metastasis are highly dependent on angiogenesis. Highly proliferative neoplastic cells need vasculature to receive nutrients and oxygen and remove their metabolic wastes. Vasculature formation happens either *de novo*, called vasculogenesis, or through sprouting of pre-existing vessels, called angiogenesis. Angiogenesis is stimulated as a response to cancer cells' need for oxygen and nutrients. Various types of signalling molecules have been identified as an angiogenesis activator including vascular endothelial growth factor (VEGF), TGF- $\beta$ , FGF and tumour necrosis factors (TNF). Both up regulation of angiogenesis factors and down regulation of angiogenesis inhibitors are needed for this process (Carmeliet, 2005, Hanahan and Weinberg, 2011, Nishida et al., 2006). Even though cellular and molecular procedures are the same in both normal and oncogenic angiogenesis, tumour blood vessels are highly branched, leaky, enlarged with inconsistent blood flow in the TME (Nagy et al., 2010, Baluk et al., 2005). There is also evidence that CAFs are involved in regulating tumours' angiogenesis. ECMs derived from CAFs can sequester signalling molecules and angiogenesis activators. In addition, introducing ECM remodelling enzymes such as MMPs facilitate the accessibility of angiogenic mediators for the cancer cells. CAFs themselves are also responsible of producing angiogenesis signalling factors such as FGF, VEGF and platelet derived growth factors (PDGF) (Crawford et al., 2009, Kalluri and Zeisberg, 2006, Rasanen and Vaheri, 2010).

### **1.1.6 Invasion and metastasis**

In the process of metastasis, carcinoma cells go through epithelial mesenchymal transition (EMT). During EMT cancer cells lose their adherens junctions (E-cadherin); release protease for ECM degradation and achieve fibroblastic morphology. These biological changes allow cancer cells to progress through the metastatic cascade composed of local invasion,



intravasation, extravasation, formation of micro- and finally macro-tumour in distant organs (Berx and van Roy, 2009, Hanahan and Weinberg, 2011, Peinado et al., 2011, Sabeh et al., 2009, Talmadge and Fidler, 2010). Stroma cells in the TME also facilitate cancer cells invasion. Releasing VEGF not only induces angiogenesis, but also its interaction with VEGF receptor 2 (VEGFR2) on endothelial cells relaxes the tight junction between them. Loose junction induces blood leakage and as a result facilitate intravasation of cancer cells (Peinado et al., 2011). The same process could happen during cancer cells extravasation. Infiltrating immune cells (IICs) also provides different types of proteases for remodelling and degrading ECMs, thus creating a path for cell metastasis (Lu et al., 2011). Macrophages also provide chemo-attraction to facilitate intravasation through releasing EGF (Qian and Pollard, 2010). CAFs play an important role in cell invasion. Providing metastasis path is mainly responsible for CAFs through depositing ECMs. In addition, CAFs induce invasion and EMT through releasing signalling molecules such as hepatocyte growth factor (HGF) and TGF- $\beta$  (Chaffer and Weinberg, 2011, Hanahan and Coussens, 2012, Kessenbrock et al., 2010).

### **1.1.7 Evading immune destruction**

It is believed that the immune system could monitor and destroy cells commencing tumorigenic transformation. Cancer cells can develop mechanisms to protect themselves from the immune system. There are some studies showing that mice with deficiency in some of their immune system components more frequently develop tumours compared to the normal mice (Hanahan and Weinberg, 2011, Kim et al., 2007, Teng et al., 2008). It is suggested that immunogenic tumours would be eradicated in immunocompetent hosts; while their weak immunogenic counterparts are able to hide from the immune system and grow in both immunocompetent and immunodeficient hosts (Smyth et al., 2006). There are also studies showing that in some types of cancers like ovarian and colon cancers, infiltration of cytotoxic T cells (CTL) and Natural killer (NK) cells into the TME improves the prognosis (Pages et al., 2010, Nelson, 2008). However, some immunogenic tumours acquire the ability to neutralize the immune destructive effect of CTLs or NK cells by releasing immunosuppressive factors like TGF- $\beta$  (Shields et al., 2010, Yang and Weinberg, 2008). CAFs in the TME produce immunosuppressive factors such as TGF- $\beta$ ; and induce recruitment of IICs by releasing chemokines. IICs use different immunosuppressive mechanisms to neutralize the anti-

tumorigenic effect of NKs and CTLs. In addition, aberrant angiogenesis cannot provide an efficient route toward the tumour for cytotoxic cells such as CTLs and NKs. (Onrust et al., 1996, Ruffell et al., 2012, Stover et al., 2007).

Tumours benefit from all cancer hallmarks, plus 'reprogramming energy metabolism' described in detail in section 1.4. However, each type of cancer shows specific properties which should be considered for the development of therapies. In the following section, characteristics of breast cancer will be explained in more detail.

## **1.2 Breast cancer**

### **1.2.1 Incidence**

Breast cancer is the most common type of cancer among women. In 2012 around 1.7 million women were diagnosed with breast cancer with 521,900 deaths worldwide. Between 1980 to 1990 in western countries the incidence of breast cancer was around 30%. However, due to changes in reproduction pattern and availability of diagnostic techniques such as mammography, the mortality rate is decreasing or being stabilized (Coughlin, 2019). In 2016, in the United Kingdom (UK), 54,960 cases of breast cancer were diagnosed which was 15.2% of all the cancers (Excluding non-melanoma skin cancer) diagnosed in the same year (National Disease Registration Service, 2020). Studies over a decade in the UK, between 1993-1995 and 2015-2017 shows that the incidence of breast cancer increased around 23% among women; and women aged between 65 to 69 showed the highest increase, 69%. Even though the incidence of breast cancer is increasing, the mortality rate has decreased around 19% in women over the past decade. The mortality rate between 2015 to 2017 was around 11,400 per year (Cancer Research UK, 2020). Breast cancer is a very heterogeneous disease, it could vary by alteration in oncogene and tumour suppressor genes, hormone and GF receptor expression, histological phenotype, molecular biomarkers and the TME. Identifying the molecular and cellular characteristics of breast cancer heterogeneity could help to find more specific treatment (Turashvili and Brogi, 2017).

## **1.2.2 Breast cancer classification**

Historically, classification of breast cancer was based on the cancer grade and histological types. In the grading system three factors are considered including tubule formation, nuclear pleomorphism, and mitotic count, which was first established by Bloom and Richardson (Bloom and Richardson, 1957). Cells are scored 1-3 for each category based on poor tubular formation, high pleomorphism and high mitotic count normalized by microscope field. Based on the scoring, cells fall into three categories called grade 1,2 or 3. Grade 1 cells show highest differentiation while grade 3 has the lowest differentiation rate. Grading can help to choose suitable therapy and predict the outcome (Vuong et al., 2014). Recently, other factors are considered in terms of tumour characteristics and therapy outcome. Expression of hormone receptors including oestrogen (ER) and progesterone receptor (PR) and human epidermal growth factor receptor 2 (HER2) are used to evaluate prognosis and cancer response to some endocrine treatments (Vuong et al., 2014).

### **1.2.2.1 Molecular classification**

Gene expression analysis of breast cancer cells through cDNA microarray sub-divide them into different groups showing various characteristics in terms of expression of different receptors, proliferation rate, and their response to various therapies. Gene expression analysis classifies breast cancer cells to four different molecular subtypes including luminal A, luminal B, basal like and HER-2 enriched. Luminal A and B both are ER positive. However, Luminal B over-expresses genes associated with proliferation, such as Ki-67. Hence, it is higher grade with poorer prognosis compared to luminal A. HER-2 receptors could be expressed alongside ER and PR and these tumours are subcategorized as Luminal B. While HER-2 overexpression with ER-/PR- is categorized as HER-2 enriched subtype. Overexpression of HER-2 and genes associated with proliferation in HER-2 enriched tumours result in high grade and poor outcome. Basal-like groups are named after basal epithelial cells as they have high similarity in their gene expression. In addition, they are triple negative and express none of the receptors which help them to escape from treatments targeting hormone receptors and HER-2 (Table 1.1) (Sorlie et al., 2001, Sorlie et al., 2003). Further efforts in terms of classification result in addition of two more ER negative breast cancer subtypes including claudin-low

tumours which are triple negative and apocrine tumours which are positive for androgen receptor (AR) (Prat et al., 2010, Farmer et al., 2005).

**Table 1.1: Molecular subtype of breast cancer**

Molecular subtype	Histological grade	Receptor status	Biological properties	Clinical response
<b>Luminal A</b>	1-2	ER+ PR+ HER2- Low Ki-67	50% of invasive breast cancer	Response to endocrine treatment. Good prognosis.
<b>Luminal B</b>	2-3	ER+ PR+ HER2+ or HER2- with high Ki-67	20% of invasive breast cancer, higher proliferation than luminal A.	Response to endocrine treatment not as good as luminal A. Worse prognosis compared to luminal A.
<b>HER-2 enriched</b>	2-3	ER- PR- HER2+	15% of invasive breast cancer. High proliferation. TP53 mutation.	Response to trastuzumab. Unfavourable prognosis.
<b>Basal-like</b>	3-3	Triple negative	~15% of invasive breast cancer. TP53 mutation. BRCA1 dysfunction. High proliferation.	No response to endocrine treatment and trastuzumab. Usually poor prognosis.

Table1.1 Characteristics of major molecular subtype of breast cancer (Vuong et al., 2014, Eliyatkin et al., 2015, Tang et al., 2016b).

### 1.2.2.2 Clinical classification

Decisions about the best effective way of treatment in breast cancer mainly rely on expression of hormone receptors (HR). Endocrine therapy improved the survival rate of patients to at least five years. However, the battle against resistance to the therapy, recurrence of the disease and triple negative cells is still on.

#### 1.2.2.2.1 ER positive and HER-2 negative breast cancer

Around 85% of breast cancer tumours are HR+ expressing ER and or PR. There are two types of ER,  $\alpha$  and  $\beta$ . ER $\alpha$  is one of the main markers of cancer prognosis. ER is located in either plasma membrane or cytoplasm. Binding of oestrogen to ER triggers its translocation to the

nucleus where it binds to the oestrogen responsive element (ERE) of promoters to induce downstream gene expression. This process makes the HR+ cells vulnerable to the ER inhibitors such as tamoxifen, that binds to ER and inhibits its proliferative effect; or aromatase inhibitors (AIs), that stop aromatase enzyme from catalysing the conversion of androgen into oestrogen (Tang et al., 2016b, Burns and Korach, 2012). However, 20% to 30% of the ER+ breast cancer will show resistance to the therapy. This resistance could be de novo, primary resistance with no previous treatment, or appear over a long time that tumours are being exposed to the therapy (Ring and Dowsett, 2004, Nass and Kalinski, 2015, Tang et al., 2016b).

#### **1.2.2.2.2 HER-2 positive breast cancer**

Around 20% of breast cancer tumours are HER-2+. HER-2 is a tyrosine kinase transmembrane receptor. Overexpression of HER-2 receptors make the cancer cells more responsive to the GFs including EGF. Therefore, HER-2+ cells are more aggressive and proliferative compared to the ER+/HER-2- cells (Pegram et al., 2004, O'Shaughnessy, 2005). On the other hand, HER-2+ cells are more susceptible to the HER-2 inhibitors such as monoclonal antibodies including trastuzumab and pertuzumab, or tyrosine kinase inhibitors including lapatinib (Tang et al., 2016b). Trastuzumab mechanism of action is to bind to the extracellular domain of HER-2 and inhibit tyrosine kinase activity of the intracellular domain, resulting in changes in the transcription of genes linked to cell proliferation and survival. In addition, trastuzumab could induce the destruction of cancer cells through immune cell recruitment (Hudis, 2007). Around 65% of patients being treated by trastuzumab show de novo resistance, and 70% of patients with early response to the therapy will develop resistance later (Vu and Claret, 2012). There is also an aberrant type of HER-2+ that does not contain the extracellular domain and is constitutively active. Presence of this type of HER-2+ is associated usually with aggressiveness, poor outcome, and resistance to trastuzumab therapy (Scaltriti et al., 2007, Arribas et al., 2011).

#### **1.2.2.2.3 Triple negative breast cancer**

Around 15% of the population of breast cancer is triple negative (TNBC). TNBC is a type of cancer that is HR and HER-2 negative. Therefore, targeting receptors through endocrine therapy or HER-2 inhibitors cannot be used as an effective mode of treatment. Patients with TNBC suffer from poor prognosis due to high tumour grade, higher rate of recurrence and

lack of targeted therapy (Dent et al., 2007, Anders and Carey, 2008). It has been a challenge to find markers for TNBC. Androgen receptors are expressed in 40% of TNBC. AR inhibition in TNBC decreases tumour growth (Giovannelli et al., 2018). EGF receptor (EGFR) is another target as 60% of TNBC express EGFR (Brand et al., 2014). Poly (ADP-ribose) polymerase (PARP1) enzyme can also be targeted to induce cell death. PARP1 is associated with molecular pathways that result in DNA damage repair. When PARP1 is inhibited, an alternative mechanism called homologous recombination is used to repair DNA. Both BRCA1 and BRCA2 are engaged in this process. BRCA1 mutation is associated with TNBC type of cancer making them responsive to PARP1 inhibition and DNA damage accumulation result in cell death (Anders and Carey, 2008). Common therapy for TNBC is combination of surgery, radiotherapy, and chemotherapy. However, TNBC could become resistant in response to some chemotherapy (Perez, 2009). Therefore, more studies are needed to find specific targets for efficient treatment of TNBC.

### **1.2.3 Models for study breast cancer**

Evolution of breast cancer as an heterogenous disease is due to different genetic changes such as mutation, copy number amplification, rearrangement, and epigenetic alteration. Breast cancer progression starts from benign hyperplasia of epithelial cells of mammary ducts, developing to atypical ductal hyperplasia (ADH), ductal carcinoma in situ (DCIS), DCIS with microinvasion and invasive ductal cancer (Figure 1.2). To have a proper model to study the stages from normal epithelial to malignant cells, a series of human cell lines, MCF10, are used. MCF10-M are mortal epithelial cells taken from a patient with fibrocystic breast. To have a stable cell line, two immortalized cell lines, MCF10A (attached cells) and MCF10F (floating cells) have been originated from spontaneous immortalization of MCF10-M (Dawson et al., 1996, Rhee et al., 2008, So et al., 2012). MCF10A belongs to a Basal-like molecular subtype due to the lack of ER, PR and HER2 expression (Soule et al., 1990, Subik et al., 2010). MCF10A cells are still categorized as normal due to their inability in making tumours in immunodeficient mice, lack of anchorage-independent growth, relying on GFs and hormones to grow in the cell culture (Soule et al., 1990). Nonetheless, transfection of MCF10A cells with constitutively active *HRAS* gives rise to cells with benign proliferation (MCF-10AT1 and MCF-10AT1 kcl2) which generate lesions similar to ADH. MCF-10AT1 cells have a non-invasive

derivative, MCF-10DCIS.com cell line, which form lesions like DCIS; and, invasive ones, MCF-10CA1a (MCF-10CA1h cl2, MCF-10CA1d cl1 and MCF-10CA1a cl1), which are able to make invasive ductal carcinomas (Rhee et al., 2008, So et al., 2012).

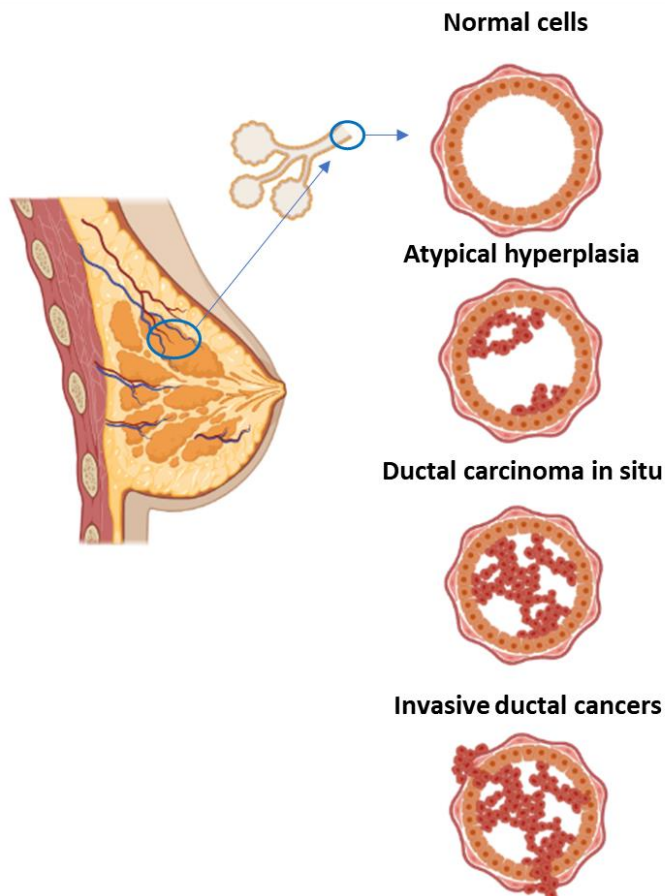


**Figure 1.2. Schematic image of breast cancer progression.** Cancer cell growth starts from benign hyperplasia of epithelial cells of mammary ducts, then it evolves to atypical ductal hyperplasia, with a little abnormality in cell shape, ductal carcinoma in situ with cells showing features of cancer cells. And at the end they acquire invasive ductal cancer phenotype. Image is “Created with BioRender.com.”

Different genetic changes in proto-oncogenes and tumour suppressor genes induce the mentioned transformations. Constitutive activation of *HRAS* in non-malignant mammary epithelial cells gives rise to benign MCF-10AT1, as mentioned above. However, to acquire the invasive characteristics of MCF10CA1a cells, further induction of C-Myc, cyclin D and insulin like growth factor I receptor (IGF-IR) are needed. These proteins are respectively in charge of regulation of cell proliferation, cell cycle, and breast cancer cell growth and survival. Erk1/2, Akt, signal transducer and activator of transcription 3 (Stat3), and Pak4 are other signalling

molecules highly expressed in the invasive cell line, MCF10CA1a. These are believed to be responsible for cell cycle progression and motility through mediating cellular response to external signalling factors such as cytokines and GFs (Rhee et al., 2008, So et al., 2012). Therefore, MCF10 cell lines can be used as a model to evaluate the activity of different signalling pathways and the effect of therapeutics at different stages of cancer progression and during their transition from localised to invasive cancer. In addition, working on cell lines being categorized as TNBC gives this opportunity to discover specific targets to develop novel treatments against this subtype.

There are other cell lines, including MDA-MB-231, MDA-MB-231-UR, MCF-12A, HBL101, HS598T, BT-20, MCF-10F, 468 and BT-48, that fall into Basal-like subtype because of them being negative for ER, PR, HER-2 expression while expressing EGFR. All these cell lines can facilitate targeting TNBC (Subik et al., 2010). For instance, among these cell lines, MDA-MB-231 is a very aggressive and metastatic cell line that 100% expresses Ki-67, a proliferation marker. MDA-MB-231 cell line was first isolated from pleural effusions from a breast cancer patient (Cailleau et al., 1974). Their high proliferation and invasion rate make MDA-MB-231 cells a desirable model to identify genes participating in metastasis and identify their interaction with the TME inside the breast as a primary tumour or distant tissues as a secondary tumour (Minn et al., 2005).

Acquiring cancer properties is not confined to genetic changes. Interaction with stroma cells and extracellular proteins facilitate tumour progression as well. Thus, both genetic alteration in epithelial cells and the TME can be considered as stimuli for growth, invasion, and metastasis (Bergamaschi et al., 2008).

### **1.3 The tumour microenvironment**

Tumour development comprises acquiring the fundamental changes in cancer cells, described by Hanahan and Weinberg and summarised in section 1.1. Even though these developments are direct result of genome instability in cancer cells, host response to these changes results in development of tumour tissue consisting of host cells and ECM scaffolds called TME (Hanahan and Weinberg, 2011, Hanahan and Coussens, 2012). The TME is composed of non-malignant cells arranged in a dynamic network of ECM working in mutual close contact with cancer cells to promote their malignancy. The cellular components of the TME comprise cells



from the immune system, endothelial cells, pericytes, blood cells, adipocytes, mesenchymal stroma cells and fibroblasts. At an early stage of tumour development, the TME negatively regulates tumour growth. However, tumours reciprocal interaction with the TME has manipulative effect in favour of cancer cells (Maman and Witz, 2018, Zhuang et al., 2019, Valkenburg et al., 2018). ECM deposition and remodelling by fibroblasts help cell invasion and make the signalling molecules trapped in the ECM available. Endothelial cells and pericytes facilitate angiogenesis and metastasis. Adipocytes release GFs and cytokines. Immune cells induce EMT and help cancer cells to hide from killer cells and acquired immune surveillance (Brown, 2014, Hida et al., 2013, Ruffell and Coussens, 2015, van Beijnum et al., 2015, Choi et al., 2018, Kozin et al., 2010). In the past decade, the TME has been considered as an important target for the cancer therapy (Turley et al., 2015).

### **1.3.1 Cancer associated fibroblasts**

Fibroblasts are spindle-like cells with mesenchymal origin. Fibroblasts are the main source of ECM production. However, they are normally quiescent and located in connective tissues among ECM fibres. In response to chronic and acute inflammation, wound healing and fibrosis, fibroblasts become activated. Activated fibroblasts, known as myofibroblast, are morphologically and molecularly different from the quiescent ones (Liu et al., 2019, Kalluri, 2016). Activated fibroblasts express myofibroblast markers,  $\alpha$ -Smooth muscle actin ( $\alpha$ SMA), platelet-derived growth factor receptor beta (PDGFR $\beta$ ) and fibroblast activation protein (FAP). They have a stellate shape. They are metabolically active, proliferative, and migratory. Once fibroblasts are activated, they release chemokines and cytokines, recruit immune cells, produce, and remodel ECM, and provide physical forces to obtain tissue architecture and homeostasis (Kalluri, 2016, Poltavets et al., 2018).

CAFs are the active form of fibroblasts and the most abundant cellular component of the TME. Release of GFs such as TGF $\beta$ , FGF2 and PDGF from tumour cells induce recruitment of fibroblasts and their transformation to CAFs (Nissen et al., 2019). High concentration of CAFs in the TME is usually correlated to poor prognosis in different cancers including breast cancer (Surowiak et al., 2007, Kellermann et al., 2007). CAFs could also originate from non-fibroblast cell types. Epithelial and endothelial cells can go through mesenchymal transition, adopt fibroblast phenotype, and express fibroblast specific protein 1 (Iwano et al., 2002, Zeisberg et

al., 2007). It was also shown that exposure of adipose-derived stem cells to conditioned media from breast cancer cells containing TGF $\beta$ 1 differentiate them to CAF (Jotzu et al., 2010). Fibrocytes, mesenchymal cells originated from monocytes and mesenchymal stem cells originated from the bone marrow could be also recruited in the TME and transformed into CAFs (Barth et al., 2002, Jung et al., 2013, Zhu et al., 2014). Compared to activated fibroblasts, CAFs express higher amount of myofibroblast markers, and increase synthesis and remodelling of collagen and other ECM components (Kalluri and Zeisberg, 2006). CAFs can release different types of GFs and pro-inflammatory cytokines to induce angiogenesis and recruit more immunosuppressive cells into the tumour niche to affect cancer cell proliferation, migration, angiogenesis, and immune surveillance (Ahmadzadeh and Rosenberg, 2005, Feig et al., 2013, Nissen et al., 2019). The major job of CAFs in the TME is contributing to the synthesis of fibrous tissue (desmoplasia) around the tumour and remodelling of the ECM. CAFs increase the release of matrix metalloproteinase (MMPs) and lysyl oxidase (LOX) proteins to induce collagen cross-linking, re-alignment, and fibre elongation (Pankova et al., 2016, Hanley et al., 2016). Desmoplastic stroma around the tissue usually correlate to poor prognosis and severe cancer (Saadi et al., 2010, Surowiak et al., 2007).

### **1.3.2 The Extracellular matrix**

ECM is a substantial part of the microenvironment in all tissues. Genome sequencing of organisms revealed all the proteins that contribute to the ECM, called 'matrisome'. Matrisome proteins are divided into two different categories. First, the components that constitute the ECM called 'core matrisome'. Second, the proteins that are associated with the ECM are called 'associated matrisome'. Core matrisome components include around 300 genes. 35 genes for proteoglycans, 43 genes for collagens and the rest are for glycoproteins including fibronectin, laminin, tenascins, thrombospondin etc. Matrisome associated proteins include around 778 genes subcategorized into ECM regulators such as MMPs and LOX, ECM affiliated proteins such as galectins and semaphorins, and secreted factors including cytokines and GFs (Naba et al., 2012).

ECM consists of both basement membrane (BM) and interstitial matrix (IM) mainly composed of proteins, proteoglycans, glycoproteins, and glycosaminoglycan (Nissen et al., 2019). BM is mainly composed of collagen IV, fibronectin, entactin and laminins, which separate epithelial

and epithelial cells from IM. Collagen IV keeps the epithelial cell structure intact while laminin provides an adhesion site for them (Theocharis et al., 2016). The IM comprises fibrous proteins such as fibrillar collagen, glycoproteins (fibronectin and tenascin C) and proteoglycans. In most of the tissues, collagen type I and type III are the major components of the ECM. ECM components provide tensile strength and chemical cues to keep tissue homeostasis through regulating different mechanisms inside and outside the cells such cell migration, anchorage, biomechanical forces, and GF signalling induction (Insua-Rodriguez and Oskarsson, 2016, Lu et al., 2012). The ECM provides a dynamic environment for cells which interact and regulate cells' behaviour. During tumour formation, recruitment of CAFs with their reciprocal interactions with cancer cells totally alter ECM's dynamics. Breast malignant tissues usually show desmoplastic properties with higher amount of fibrillar collagen deposition, more ECM remodelling enzymes and alteration in GFs availability providing a pro-tumorigenic environment (Pankova et al., 2016, Insua-Rodriguez and Oskarsson, 2016).

### **1.3.2.1 Collagen**

The main component of the ECM is collagen and 30% of the whole-body protein is composed of collagen. Up to this point 28 different types of collagen have been recognized. Even though collagens have different structures, they all are made of right-handed triple helix composed of three  $\alpha$ -chains. These  $\alpha$ -chains contain repeating Gly-X-Y triplet. Gly is glycine and X and Y could be substituted by any other AAs. However, X and Y are mainly replaced by proline and hydroxyproline, respectively. Each triple-helix could be built of three similar or different  $\alpha$ -chains wrapping around the central axis with the glycine face inward of the helix. The small hydrogen atom side chain of glycine causes the inter-chain hydrogen bond and secures the triple helix (Okuyama et al., 1981, Bella et al., 1994). Prior to final triple helix formation, collagens go through different modification processes such as hydroxylation, glycosylation, phosphorylation and cross-linking in the endoplasmic reticulum (ER). The end product of the ER, the procollagen, is transported to the Golgi to face the last modifications and self-assembly to make fibrillar collagen (Figure 1.3) (Gelse et al., 2003, Nissen et al., 2019, Theocharis et al., 2016, Myllyharju and Kivirikko, 2004).

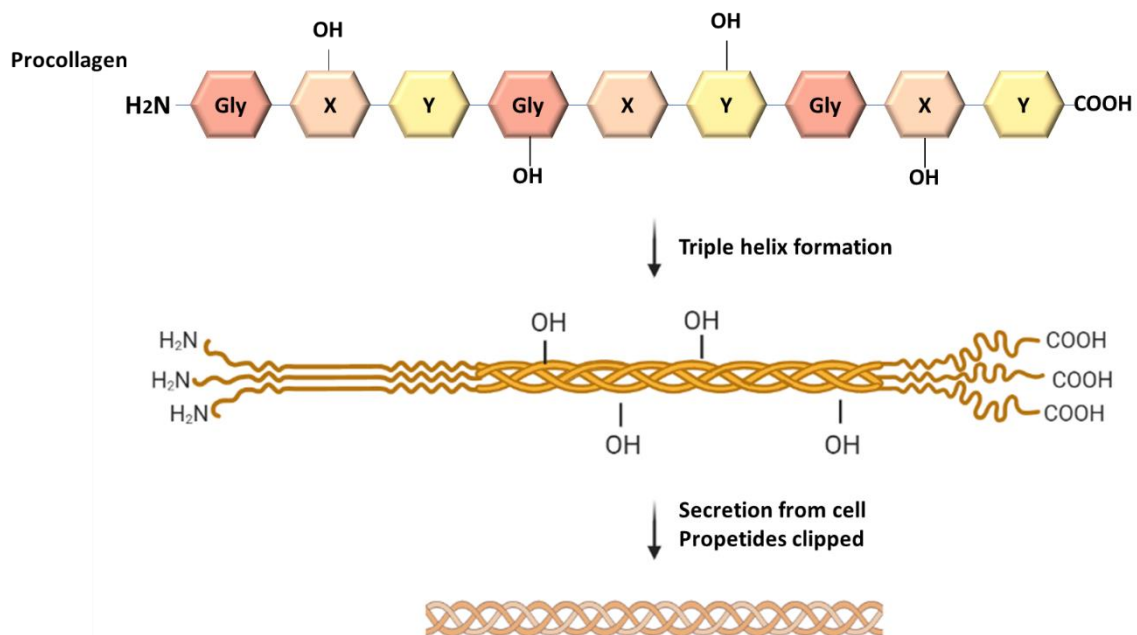


**Figure 1.3. Collagen synthesis steps.** In collagen's  $\alpha$ -chains, glycine is in every three residues. Following X and Y could be substituted by any other amino acids. Assembly of  $\alpha$ -chains followed by pro-collagen triple-helix assembly are processed in the ER. Procollagen traffic from the ER to the Golgi to go through final modifications. Finally, after pro-collagen secretion to the extracellular area, N and C terminal will be cleaved and they will be cross-linked via enzymes located outside the cell. Image is "Created with BioRender.com."

There are different subcategories of collagens based on their structure. Fibrillar collagen, anchoring fibrils, membrane-associated collagens with Interrupted triple-helices (MACITs), fibril associated collagens with interrupted triple helices (FACITs) and network forming collagen (Table 1.2). The main components of the IM are fibrillar collagen type I, II, III, V, XI, XXIV, XXVII and network making collagen VI; while the BM is mainly composed of network making collagen type IV and VIII (Table 1.2) (Nissen et al., 2019). As described in Table 1.2, collagen composition of both BM and IM could participate in tumour development and progression. Pancreatic cancer cells show elevated survival and growth rate in environments with elevated deposition of collagen (Armstrong et al., 2004). In line with that, breast cancer cells have higher metastasis and invasion rate in environments with high collagen fibrils; and cancer progression is significantly induced when mammary glands produce greater amount of collagen, laminin, and fibronectin fragments during weaning-induced involution (McDaniel et al., 2006, Provenzano et al., 2008). Collagen remodelling enzymes, LOX and MMPs, have a pivotal role in modifying collagens in favour of tumour progression (Insua-Rodriguez and Oskarsson, 2016).

**Table 1.2. Different types of collagen participate in IM and BM.**

Structure	Type	Tissue distribution	Cancer tissue distribution	Tumorigenicity effect
<b>Fibrillar</b>	I	Dermis, tandem, bone, ligament	Bone, colorectal, ovarian, lung and breast cancer	Invasion, apoptosis, and proliferation
	II	Cartilage, vitreous	Chondrosarcoma	Death and survival
	III	Intestine, lung, liver, skin, vascular system	Colorectal, breast, pancreas and Head and neck squamous cell carcinoma (HNSCC)	Invasion, proliferation, and metastasis
	V	Co-distribute with collagen type I and III	Breast cancer	Growth
	XI	skeletal muscle, trabecular bone, tendons, testis, trachea, articular cartilage, lung, placenta, and brain	Colorectal, HNSCC cancer breast, lung, gastric, pancreas and ovarian cancer	Invasion, proliferation, and metastasis
	XXIV	Bone, kidney, ovaries, muscle, testis, and spleen.	HNSCC	Proliferation
	XXVII	Cartilage, bone, eye, lung, heart, and arteries	NA	NA
<b>Network</b>	IV	Basement membrane	Pancreas cancer	Growth and migration (Ohlund et al., 2009)
	VI	cornea, lung, skin, adipose, tendon, cartilage, skeletal muscle, and dermis	Colorectal, breast, glioma, ovarian, pancreatic and melanoma cancer	Proliferation, invasion, inflammation, and metastasis
	VIII	Basement membrane, heart, kidney, dermis, and brain	Colorectal cancer	NA (Willumsen et al., 2019)

Table 1.2. Description of the distribution of collagens participating in BM and IM in normal and cancerous tissues. The table is adapted from (Fang et al., 2014, Nissen et al., 2019).

### 1.3.2.2 Fibronectin

Even though fibronectin (FN) has one single gene, extended alternative splicing gives rise to two major different types, plasma fibronectin and cellular fibronectin (Schwarzbauer et al., 1983). Plasma FN is released from hepatocytes and located in blood; while cellular fibronectin is a component of the ECM found in most of the tissues. FN is composed of two subunits linked together by disulphide bonds in their C terminal (Wagner and Hynes, 1979). Each subunit is composed of three modules, types I, II and III (Figure 1.4) (Petersen et al., 1983, Schwarzbauer and DeSimone, 2011). FN has collagen, fibrin, heparin, and cell binding sites. Cell-fibronectin interaction happens through integrin and syndecans (Cell surface receptors) and it can regulate cell adhesion, migration, and differentiation (Schwarzbauer and DeSimone, 2011, Bowditch et al., 1994). FN can be produced by both cancer cells and CAFs in the TME. Upregulation of FN in TME has been linked to invasiveness of cancer cells including lung carcinoma and breast cancer. Migratory cells also induce FN production in the environment they reside after metastasis by releasing different cytokines (Kaplan et al., 2005, Fernandez-Garcia et al., 2014). STAT3 pathway and Mitogen-activated protein kinase (MAPK) pathway could be induced through cell-FN interaction, resulting in more invasion and metastasis associated with poor prognosis and clinical outcome in breast cancer (Qian et al., 2011, Balanis et al., 2013, Bae et al., 2013).

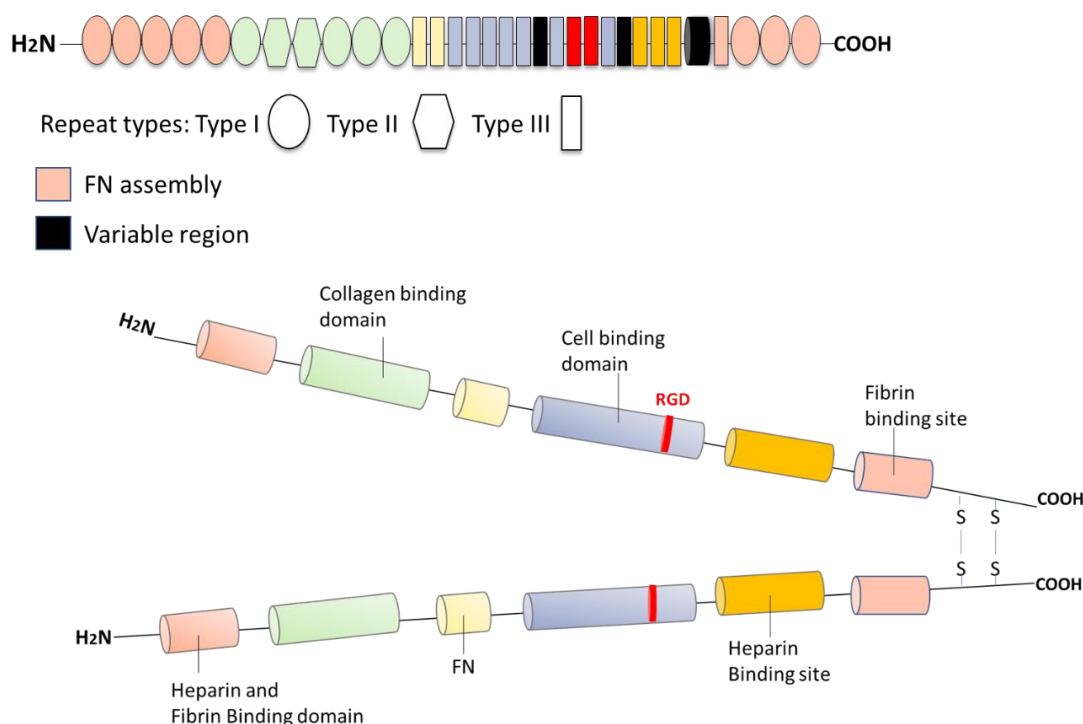


**Figure 1.4. Fibronectin structure.** The fibronectin molecule is composed of different binding motifs and has specific affinity toward heparin, fibrin, integrin, cells, and intramolecular units that enable self-assembly of the molecule. These binding motifs are built by three fibronectin repeats, I, II and III. Two fibronectins build a dimer by c-terminal disulphide bonds (Figure is adapted from (Mouw et al., 2014)).

### 1.3.2.3 Laminin

Laminin is a large heterotrimeric protein that is composed of three chains,  $\alpha$ ,  $\beta$  and  $\gamma$ , that join each other in a triple-helical coiled-coil domain to form a cross-shaped configuration. Each chain is encoded by an individual gene. Different laminin chains share a common structure. They have a globular N-terminal domain (LN domain) followed by a straight LE domain.  $\beta$  and  $\gamma$  chain make trimerization happen through their laminin coiled-coil (LCC) domain following LE, while  $\alpha$  chain C-terminal consists of five laminin globular (LG) domains (Figure 1.5) (Theocharis et al., 2016, Timpl and Brown, 1994). Various combinations of laminin chains, LAM $\alpha$ 1–5, LAM $\beta$ 1–3, and LAM $\gamma$ 1–3, give rise to 16 different isoforms of laminin (Durbeej, 2010). Laminin has different binding regions including, cell, collagen, integrin, entactin and dystroglycan binding regions (Aumailley, 2013). Laminin self-binding through LN domain or their binding to entactin significantly participate into the BM structure (Willem et al., 2002). Laminin also provides proper substrate for migration of epithelial and endothelial cells in wound healing and angiogenesis (Willem et al., 2002, Malinda et al., 2008). Laminin could have both anti and pro tumorigenic effects. Laminin-111 (LM-111), the main component of the BM, has anti-tumorigenic effect by preventing methylation of E-cadherin promoter and therefore increasing E-cadherin expression and cell-cell adhesion (Benton et al., 2009). In contrast, expression of LM-332 in breast tissue correlates to invasion and anchorage-independent survival (Kwon et al., 2012, Carpenter et al., 2009).

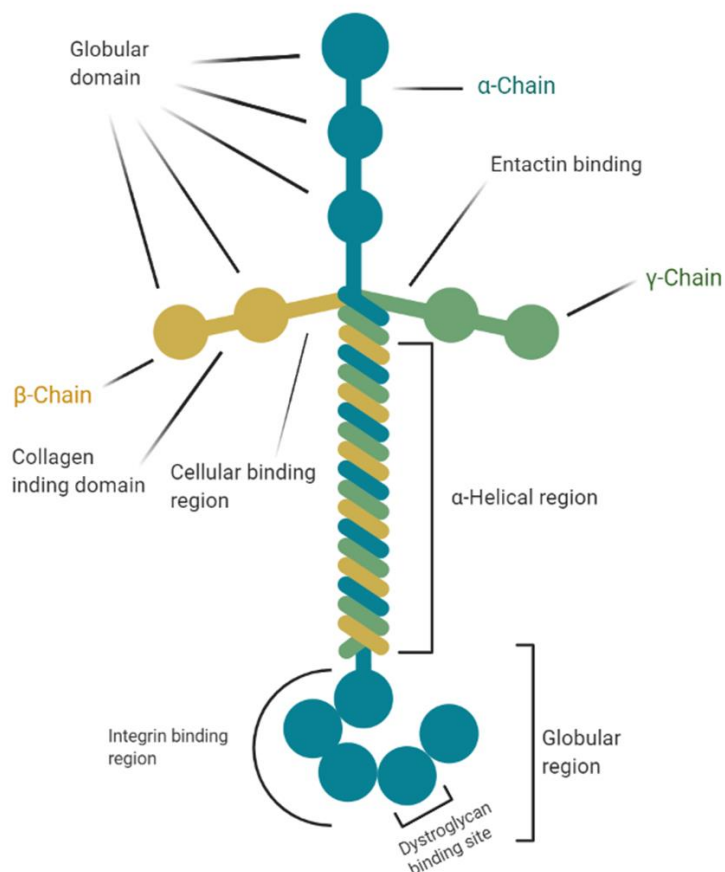


**Figure 1.5. Laminin structure.** Laminin is composed of three chains,  $\alpha$ -chain,  $\beta$ -chain, and  $\gamma$ -chain making a Y shaped structure. Each of these chains contains different binding domains shown in the figure. Image is “Created with BioRender.com.”

### 1.3.3 ECM remodelling in breast cancer

ECMs are a major component of the TME, and they are in direct contact with tumour cells. Tumorigenic phenotypes of cancer cells such as proliferation, migration and dissemination depend on both cell genotype and ECM content. It is believed that there are significant changes in gene expression related to cell anchorage (cadherin and integrin) and ECM remodelling (MMP and Lox) between normal and breast cancer epithelial cells. In breast cancer, high breast tissue density, disruption of BM, increase in remodelling enzymes, matricellular proteins, and proteoglycans are associated with a shift to more malignant and invasive tumours (Figure 1.6) (Insua-Rodriguez and Oskarsson, 2016).



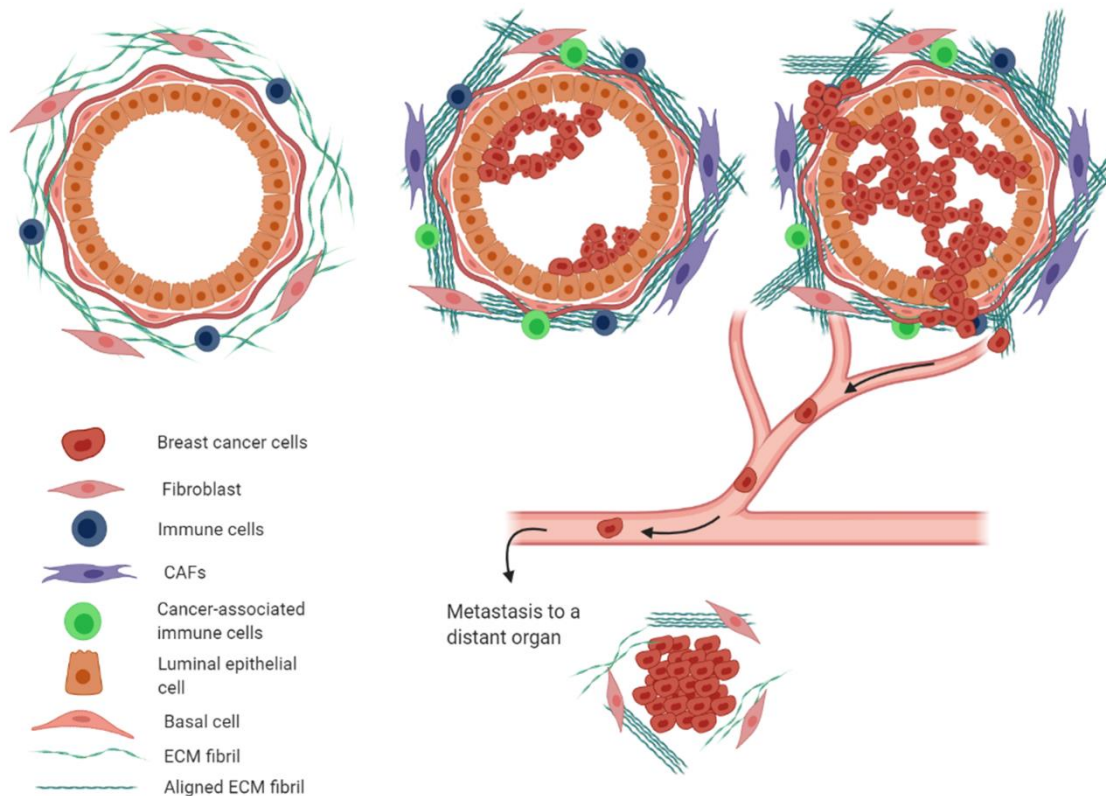


**Figure 1.6. Changes in ECM during breast cancer progression.** Changes in the composition and mechanical properties of ECMs affects transformation from normal mammary epithelial cells to malignant cells. The normal mammary epithelial cells locate around the lumen of the ducts, and they are surrounded by basal cells covered by intact BM. Stroma around the normal mammary gland is composed of random fibrillar collagen, fibroblasts and immune cells keeping tissue haemostasis. During malignancy, the stroma composition changes due to the presence of CAFs and cancer-associated immune cells. Increase in the amount of fibrillar collagen (I, III and V), hyaluronan, fibronectin and lox enzymes increase ECM stiffness promoting tumour invasiveness. Invasion of breast cancer cells is concomitant to BM disruption resulting in a decrease in collagen IV and LM-111 and an increase in the activity of ECM remodelling enzymes including MMPs, cathepsins and heparinase. Besides, during invasion, ECM fibrils undergo higher cross-linking. They are also organised in perpendicular orientation toward the lumen to provide the route for cancer cells to migrate (Insua-Rodriguez and Oskarsson, 2016, Kaushik et al., 2016). Image is “Created with BioRender.com.”

In terms of collagen, in malignant tumours, mRNA expression of procollagen I and III is confined to stroma cells and it is higher compared to benign tumours (Kauppila et al., 1998). Increase in secretion of collagen I is linked to the higher adhesion, sprouting and invasiveness of MDA-MB-231 and MCF7 breast cancer cells (Kim et al., 2014). As MDA-MB-231 are more aggressive than MCF7 cells, their injection to mouse mammary gland results in more collagen deposition and cross-linking, showing that there is a correlation between rate of aggressiveness and ability of modifying the TME (Liverani et al., 2017). Transplantation of

breast cancer tumours in transgenic mice with higher collagen density in the mammary gland also showed more proliferation, invasion, and lung metastasis (Provenzano et al., 2008). Both *in vitro* and *in vivo* (mouse xenograft model) study also revealed that the stroma from mammary glands undergoing weaning-induced involution significantly increases breast cancer cell, MDA-MB-231, invasion with higher rate of angiogenesis compared to Matrigel or stroma from nulliparous mouse. Stroma in weaning-induced regression has higher MMP activity, high level of fibrillar collagen and proteolytic fragment of fibronectin and laminin (McDaniel et al., 2006).

FN is a major component of ECM promoting cell differentiation, migration, and dissemination. Comparing CAFs derived FN to FN derived from normal fibroblasts (NF) revealed some differences. FN derived from CAFs is organized in parallel lines aligned with each other; whereas NF-FN is like a mesh. Aligned FN induces cancer cells directional migration through  $\alpha V$  integrin (Erdogan et al., 2017). Inhibition of FN expression along with MMPs inhibition reduce *in vivo* metastasis and *in vitro* migration in breast cancer cells (MDA-MB-231) (Hong et al., 2014). However, downregulation of a micro-RNA family, which inhibits malignant transformation in CAFs, induced ECM stiffness through increase in FN and LOX expression and resulted in poor outcome in breast cancer patients (Tang et al., 2016a). In addition, co-expression of fibronectin with  $\beta 1$  integrin in breast tumours is linked to low survival rate (Yao et al., 2007).

Laminin interaction with cancer cells could also regulate their behaviour. LM511 deposited by breast cancer stem cells works as an integrin  $\alpha 6\beta 1$  ligand to activate TAZ and induce self-renewal and tumour initiation (Chang et al., 2015). Cleavage of LM-332 by MMP-2 also reveals its EGF-like domain which binds to the EGFR of breast epithelial cells (MCF10A) and induces their migration (Schenk et al., 2003).

Major changes in the ECM are mediated by LOXs enzymes or MMPs. Expression of these enzymes in CAFs leads to ECM cross-linking, fibre alignment and degradation (Nissen et al., 2019). CAFs with higher expression of activated fibroblast markers such as  $\alpha$ SMA show higher LOX expression, resulting in collagen I increased stiffness and eventually higher proliferation of breast cancer cells (Cox et al., 2013). In various cancers including breast cancer, LOX is overexpressed resulting in changes in ECM directionality, stiffness, and topology (Mohan et al., 2020). Expression of LOX is enhanced in mammary tumours with higher metastasis rate

compared to the ones with little invasion. Inhibition of LOX activity decreases stiffness of ECM resulting in lower cancer cell intravasation and metastasis in breast cancer (Pickup et al., 2013). Injection of organoid into the LOX pre-conditioned mammary gland promotes growth and invasion of cancer cells through collagen stiffening, which result in focal adhesion assembly and PI3K signalling (Levental et al., 2009).

Invasive phenotype of cancer cells heavily relies on the ability of degrading the ECM. MMPs are a proteolytic enzyme family that have a major role in ECM degradation associated with metastasis and invasion. Expression of some types of MMPs such as MMP-2, MMP-14, MMP-9, and tissue inhibitor of metalloproteases (TIMP)-2 in breast cancer is associated with poor prognosis and could be used as an indicator for survival rate (Talvensaaari-Mattila et al., 1998, Tetu et al., 2006, Yousef et al., 2014). Overexpression of MMP-9 is mostly seen in invasive breast cancer cells such as triple negative ones and it is tightly correlated with metastasis, shorter latency in relapse and lower survival rate after relapse in patients (Yousef et al., 2014). The stroma from mammary glands undergoing involution show a high rate of MMP activity in addition to high levels of collagen, fibronectin, and laminin deposition. *In vivo* study on weaning-induced involuting mammary glands show that activity elevation for MMP-2 and MMP-9 could correlate to their higher rate of liver, kidney, and lung metastasis (McDaniel et al., 2006). Early studies show that some MMPs, such as stromelysin-3, are exclusively expressed by fibroblasts around breast cancer tumours (Basset et al., 1990). Interaction of neoplastic cells with fibroblasts through different signalling molecules including tumour necrosis factor- $\alpha$  (TNF- $\alpha$ ), PDGF, EGF, basic FGF (bFGF) induce their activation and MMPs expression which eventually induce the invasive growth (Basset et al., 1990, Stuelten et al., 2005). Liberating the fibroblast associated-MMPs is also a mechanism that cancer cells take advantage of. Invasive breast cancer cells (MDA-MB-231) induce the release of MMPs such as MMP-2 bound to the membrane of normal bone marrow fibroblasts (BMF) and increase ECM degradation to facilitate their migration into other tissues (Saad et al., 2002).

The physical composition of the ECM could regulate different aspects of cellular behaviour ranging from proliferation, invasion, growth, metastasis, to another major factor controlling cancer progression, which is metabolism.

### 1.3.4 ECM receptors: integrins

There are different types of cell receptors that mediate the cell-ECM interactions including discoidin domain receptor (DDR) family, syndecans, CD44 and integrins (Sainio and Jarvelainen, 2020). Integrins are cell adhesion receptors which mainly recognize ECMs and cell adhesion proteins as ligands. They are a family of heterodimeric molecules composed of two transmembrane subunits,  $\alpha$  and  $\beta$ , non-covalently bound together. At least 18 different  $\alpha$  subunits and 8  $\beta$  subunits genes have been discovered in mammals, resulting in 24 different combinations of  $\alpha\beta$  heterodimer that can engage various ECM components (Table 1.3). Each integrin subunit is composed of a large extracellular domain, a single transmembrane domain, and a short intracellular domain (Takada et al., 2007). Transition of integrins from low affinity and inactive receptors to active receptors with high affinity majorly depends on their conformation alteration. Inactivated integrins have a hairpin like structure where their ligand binding domain faces toward the membrane. Whereas their active version is more extended with the ligand domain facing away from the membrane and exposed to ECM (Xiong et al., 2001, Tiwari et al., 2011). Activation of integrins take place through a bidirectional signal transportation: 'inside-out' and 'outside-in' signalling. In inside-out signalling, proteins containing a FERM (Four-point-one, Ezrin, Radixin, Moesin) domain such as talin and kindilin bind to the integrin intracellular domain and induce receptor extension and ECM binding. In outside-in signalling, binding of integrin to ECMs induce recruitment to talin of more adaptor proteins in focal adhesion (FA) to strengthen ECM-cytoskeleton signalling. In this case, integrins can work as force sensors, transferring forces applied by ECMs to cells through FA proteins resulting in triggering different signalling pathways or changes in gene expression. On the other hand, forces from cytoskeletons could also be transferred to ECM through FAs that allows integrins to pull ECM and sense mechanical cues (Klotzsch et al., 2009, Maziveyi and Alahari, 2017). Proteins engaging in FA complexes participate in different signalling pathways inside the cell. However, tyrosine phosphorylation is the main signalling pathway involved in recruiting more proteins to FAs. There are two dominant tyrosine kinases participating in FA signalling, FA kinase (FAK) and SRC. Integrin-talin interaction support recruitments of FAK. FAK is a non-receptor kinase consisting of two protein binding domain, N-terminal FERM domain and C-terminal FAT (Focal adhesion targeting) domain that makes it a proper platform for recruitment of other proteins. Integrin-ligand binding results in FAK

autophosphorylation providing a SH2 binding domain in FAK to engage with proteins carrying SH2 domain including SRC (Maziveyi and Alahari, 2017). Engagement of SRC and FAK leads to phosphorylation and recruitment of other proteins such as paxillin and vinculin. Paxillin has a leucine and aspartate rich domain that could bind directly to vinculin (Figure 1.7) (Maziveyi and Alahari, 2017, Burridge et al., 1992). Vinculin is a tension sensor conveying mechanical forces from ECM to the actin filaments (Grashoff et al., 2010). Therefore, FA provides a bi-directional pathway for the cytoskeleton-ECM interaction.

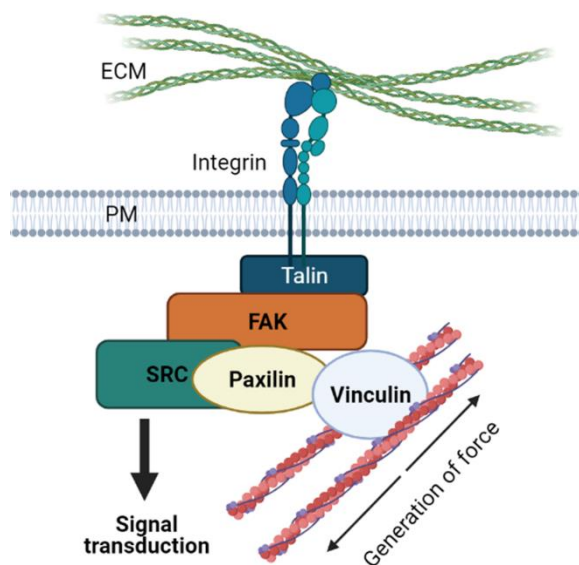


**Figure 1.7. Schematic representation of FA complex formation followed by integrin activation.** Engagement of integrin with ECM results in integrin clustering and focal adhesion complex recruitment cause signal transmission inside the cell and integrin-actin cytoskeleton interaction (Maziveyi and Alahari, 2017). Image is “Created with BioRender.com.”

Integrin trafficking has been shown to happen for both active and inactive receptors. Integrins can be internalized through different endocytosis pathways including clathrin-dependent endocytosis, caveolin-dependent endocytosis, and macropinocytosis (De Franceschi et al., 2015, Gu et al., 2011). Internalized integrins follow two different pathways: being recycled to provide further cell-ECM adhesion or being degraded inside the lysosomes (De Franceschi et al., 2015). Discovery of ECM molecules in endocytosis vesicles reveals that there is ECM-integrin co-endocytosis. In addition, ECM turnover can rely on both remodelling enzymes outside the cells and ECM internalization and degradation inside the cell. As an example, fibronectin engaged with  $\beta 1$  integrin can go through caveolin-1 dependent endocytosis

pathway followed by lysosomal degradation (Sottile and Chandler, 2005). Also, the size of fibronectin can affect its endocytosis. Prior to fibronectin endocytosis along with  $\alpha 5\beta 1$  integrin, fibronectin degradation by MMP-14 is critical (Shi and Sottile, 2011).

**Table 1.3. ECMs and their integrin receptors.**

Ligands	Integrins
Collagen	$\alpha 10\beta 1$ , $\alpha 2\beta 1$ , $\alpha 1\beta 1$ , $\alpha 11\beta 1$ , $\alpha X\beta 2$
Fibronectin	$\alpha 11\beta 3$ , $\alpha V\beta 3$ , $\alpha V\beta 6$ , $\alpha V\beta 1$ , $\alpha 5\beta 1$ , $\alpha 8\beta 1$ , $\alpha 4\beta 1$ , $\alpha 4\beta 7$ , $\alpha D\beta 2$
Laminin	$\alpha 3\beta 1$ , $\alpha 6\beta 1$ , $\alpha 6\beta 4$ , $\alpha 7\beta 1$ , $\alpha 1\beta 1$ , $\alpha 2\beta 1$ , $\alpha 10\beta 1$ , $\alpha 3\beta 1$

Table 1.3. Integrin-ECM interaction (Humphries et al., 2006, Takada et al., 2007).

### 1.3.5 The crosstalk between nutrient signalling and the ECM-integrin trafficking.

Triggering signalling pathways through trafficking of extracellular protein (ECP) bound integrin could directly or indirectly affect cell metabolism. Mechanistic target of Rapamycin (mTOR) is one of the signalling pathways that could be regulated by integrin trafficking. mTOR is a serine-threonine protein kinase forming two independent complexes, mTORC1 and mTORC2. mTORC1 signalling pathway activity relies on nutrient and GF availability (Kim et al., 2013a, Kim et al., 2013b, Zoncu et al., 2011b). Presence of AAs, GFs and other sources of energy induce mTORC1 activity. Activation of mTORC1 triggers downstream signalling pathways responsible for anabolic processes including nucleotide, lipid, and protein synthesis. However, nutrient deficiency restrains the activity of mTORC1 permitting cells to use other sources of nutrient acquisition like autophagy (Korolchuk et al., 2011). It has been demonstrated that mimicking nutrient deficiency via deactivation of mTORC1 activity could effectively increase integrin internalization. Glucose (Glc) depletion induces FN bound  $\alpha 5\beta 1$  integrin translocation from focal adhesions to fibrillar adhesions beneath the nucleus, followed by an Arf4-dependent internalization pathway. Transport of FN-bound  $\alpha 5\beta 1$  integrin to lysosomes eventually leads to mTOR1 recruitment and activation. Activation of mTORC1 negatively regulates integrin internalization implying that simulating nutrient deficient

environments by inhibiting mTORC1 activity results in a higher ligand-bound  $\alpha 5\beta 1$  integrin endocytosis (Rainero et al., 2015a). Addition of laminin to the environment where normal mammary epithelial cells suffer from serum and GF deficiency increased laminin bound  $\beta 4$  integrin internalization. After internalization, laminin is conducted to the lysosome where it is degraded resulting in higher AA content of the cells. Eventually, the increase in cellular AA concentration induces mTORC1 activity to avoid excess uptake of extracellular proteins. Studies on mice under dietary restriction also confirmed that mammary epithelial cells have a tendency to induce laminin internalization from BM or other types of ECMs during nutrient deficiency (Muranen et al., 2017). Therefore, ECM uptake following integrins trafficking under nutrient depleted conditions could hypothetically supply a source of nutrients for cells as ECMs are rich in AAs and sugars.

AMP-activated protein kinase (AMPK) is a serine-threonine kinase responding to the nutrient availability. AMPK activation blocks any anabolic process of the cells and gives the opportunity to the catabolic pathways to provide energy and nutrients for the cells during nutrient starvation (Hardie et al., 2012). In fibroblasts, activation of AMPK has inhibitory effect on  $\alpha 5\beta 1$  integrins activity. AMPK activation due to lack of nutrient/energy blocks tensin3 expression. Translocation of  $\alpha 5\beta 1$  integrins from focal adhesions to fibrillar adhesions is accompanied by replacement of talin with tensin. Therefore, AMPK has an inhibitory role for the activation of  $\alpha 5\beta 1$  integrins in fibroblasts. In AMPK KO mouse embryonic fibroblasts (MEFs), activity of  $\alpha 5\beta 1$  is increased which directly lead to more fibronectin biogenesis and fibrillar adhesion leading to a stiffer environment (Georgiadou et al., 2017).

Sensing mechanical properties of the microenvironment by integrins could also affect cell metabolism. CD98hc is an integrin co-receptor and AA transporter. CD98hc can assess mechanical forces from the environment resulting in integrin and RhoA activation to increase cell stiffness. It has been shown that interruption in mechanosensing due to C330S mutation in CD98hc can disrupt sphingolipid synthesis in fibroblasts. Sphingolipids are types of lipids located in the plasma membranes. Sphingolipids have structural functions. In addition, they modulate transmembrane protein dynamics. Absence of CD98hc reduces sphingolipid availability disrupting translocation and activation of SRC kinase and GEF-H1 which is responsible for RhoA activation (Boulter et al., 2018). Therefore, presence of ECP as a source of nutrient or biomechanical force can affect cell metabolic status suggesting that

experiencing different microenvironments during metastasis can affect cancer cell behaviour (Nazemi and Rainero, 2020).

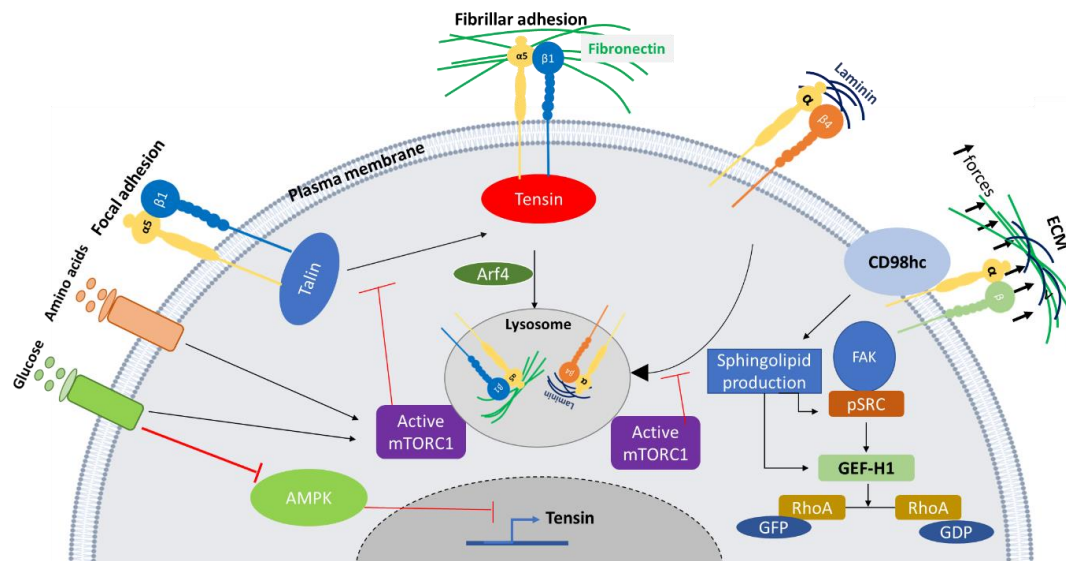


**Figure 1.8. Crosstalk between integrin-ECM interaction and nutrient availability.** Glucose and serum starvation respectively induce fibronectin and laminin bound integrin to be internalized inside the cell followed by lysosomal degradation. Besides, extraction of nutrients from ECMs inside the lysosome reactivate mTORC1 signalling, blocking further integrin internalization to avoid excess uptake of ECPs. Activation of AMPK during starvation, however, blocks tensin expression resulting in integrin inactivation. CD98hc activation is due to biomechanical forces from ECMs causing sphingolipid production and RhoA activation (Nazemi and Rainero, 2020).

## 1.4 Metabolism

### 1.4.1 Reprogramming energy metabolism

In normal somatic cells, the presence of intact blood vessels provides adequate oxygen and nutrients for the cells. However, nutrient uptake is not triggered simply by the presence of nutrients in the surrounding environment. Interaction of cells with soluble GFs and the ECM through membrane receptors are required to regulate nutrient consumption (Thompson, 2011, Grassian et al., 2011). Due to high proliferation rate and inadequate oxygen/blood delivery, cancer cells need to optimize their metabolism to acquire the maximum amount of nutrients from the environment and to overcome nutrient-poor conditions. Metabolic alterations in cancer cells comprise all phases of metabolism in the cells, including nutrient uptake, intracellular metabolic pathways, and metabolite dependent gene regulation. The main biosynthetic needs of cells are accomplished by Glc and Gln uptake working as carbon



building blocks for macromolecules production. They also work as electron transfer intermediates in the electron transfer chain in the form of nicotinamide adenine dinucleotide (NADH) and reduced flavin adenine dinucleotide (FADH) to help ATP production (Pavlova and Thompson, 2016).

Significantly, enhanced Glc consumption because of metabolic demands of cancer cells was first described by Otto Warburg (Warburg et al., 1927). In normal cells, in the presence of oxygen, most of the pyruvates enter the tricarboxylic acid (TCA) cycle in mitochondria to produce 36 molecules of ATP. In contrast, during hypoxia, differentiated cells use anaerobic glycolysis and produce lactate allowing glycolysis to continue with less ATP production. However, cancer cells and proliferating cells, regardless of presence of oxygen, use the glycolytic pathway, called aerobic glycolysis or Warburg effect (Vander Heiden et al., 2009).

At that time, Warburg was convinced that cancer cells had a respiration deficiency making them rely on glycolysis (Hanahan and Weinberg, 2011, Warburg, 1956). Warburg's hypothesis that the tendency of cancer cells toward aerobic glycolysis was because of inhibition of the TCA cycle was proven wrong. Later studies demonstrated that tumour cells have an intact mitochondria, and they can use oxidative phosphorylation to meet their ATP needs. In addition, some non-cancerous proliferative cells benefit from aerobic glycolysis showing that it has some advantage in terms of biosynthesis (Cavalli et al., 1997, Brand et al., 1986).

Now the question is why neoplastic cells prefer converting pyruvate from glycolysis to lactate over feeding to the TCA cycle? Demand of ATP in proliferative cells is just slightly higher than quiescent cells. However, their need for precursor molecules and NADPH is significantly higher than non-proliferative cells. Glycolysis is a main source for production of precursor molecules (Figure 1.10), whereas the TCA cycle focuses on production of ATP and NADH, which are negative regulators of glycolysis. Conversion of pyruvate to lactate gives the opportunity to cells to decrease ATP accumulation, therefore releasing the ATP-mediated inhibition of glycolysis (Pavlova and Thompson, 2016). In addition, even though the number of ATP molecules per Glc generated by glycolysis is lower than by the TCA cycle, ATP production is faster, which makes glycolysis more profitable for proliferative cells with high demands of energy (Pfeiffer et al., 2001).

In general, cancer cells might have some preferences over different metabolic pathways in different conditions. Each metabolic pathway could be reinforced through different genetic or non-genetic changes. In the following sections the basics of each metabolic pathway with their alteration due to cancer cells metabolic rewiring will be briefly explained.

### 1.4.2 TCA cycle

The TCA cycle is a cell respiration machinery composed of a series of chemical reactions happening in the mitochondrial matrix in the presence of oxygen, providing energy, redox balance, and macromolecules (Anderson et al., 2018). The TCA cycle is fed through different sources including, Glc, glutamine (Gln), and fatty acid. Since pyruvate made from glycolysis is mainly consumed to produce lactate in cancer cells, Gln and fatty acid play a major role to replenish TCA cycle intermediates (Figure 1.9) (Described in below sections) (DeBerardinis et al., 2007, Eagle, 1955). The main input of the TCA cycle is acetyl-CoA. Acetyl-CoA is obtained from pyruvate, fatty acids and different AAs including phenylalanine, tyrosine, leucine, isoleucine, and tryptophan. Conversion of Acetyl-CoA to other TCA cycle intermediates trigger redox reactions generating reduced NADH and FADH. Later, NADH and FADH along with oxygen were consumed in oxidative phosphorylation reactions to form ATP (Akram, 2014).

In addition to the mutations in cancer cells inducing uptake of Gln, Glc, and other fuel sources of the TCA cycle (Described in the sections below), cancer progression has also been shown to rely on the derailed function of TCA cycle enzymes. Succinate dehydrogenase (SDH) catalyses the oxidation of succinate to fumarate and participates in TCA cycle and electron transport chain in mitochondria. SDH is known as a tumour suppressor gene whose mutation results in neoplastic transformation through succinate and ROS accumulation, both resulting in hypoxia-inducible factor-1 (HIF-1) induction (Gottlieb and Tomlinson, 2005). Fumarate hydratase (FH) catalyses the conversion of fumarate to l-malate and has a role in AA synthesis and urea cycle. FH mutation is one of the first germline mutations discovered in adult testicular tumours as well as in patients with ovarian mucinous cystadenoma (Ylisaukko-oja et al., 2006, Carvajal-Carmona et al., 2006). Isocitrate dehydrogenase (IDH) catalyses isocitrate to alpha-ketoglutarate transformation. IDH mutation in acute myeloid leukaemia (AML) suppresses hematopoietic cell differentiation (Yen et al., 2017). It is also one of the markers of secondary glioblastomas (Ohgaki and Kleihues, 2013). Overall, TCA cycle

dysregulation and accumulation of the intermediate metabolites inside the cells, due to the mutation in TCA cycle enzymes, could convey some oncogenic signalling pathways that facilitate tumour growth or survival.

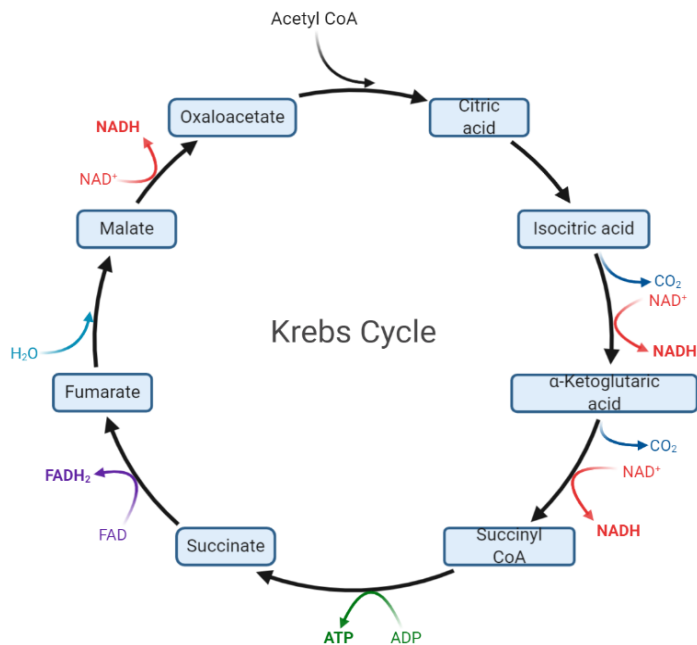


**Figure 1.9. TCA cycle intermediates.** The aim of the TCA cycle is to release energy via oxidation of Acetyl-CoA. During this metabolic pathway, consumption of acetate from acetyl-CoA and H<sub>2</sub>O reduces NAD<sup>+</sup> to NADH and releases CO<sub>2</sub>. NADH are fed to the electron transport pathway in the mitochondria membrane to produce ATP. Image is “Created with BioRender.com.”

### 1.4.3 Glycolysis

Glycolysis is a series of metabolic processes that use one molecule of Glc to generate two molecules of pyruvate and two molecules of ATP. In the first phase of glycolytic metabolic reactions, consumption of two molecules of ATP fuel the reaction in which Glc is catabolized into fructose-1,6-bisphosphate through sequential reactions triggered by different enzymes, including hexokinase, phosphor-glucose isomerase, and phosphofruktokinase. In the second phase of glycolysis, fructose-1,6-bisphosphate is catalysed into two molecules of pyruvate, four molecules of ATP and two molecules of NADH. In aerobic conditions, pyruvate is oxidized and fed into the TCA cycle through acetyl-CoA to make 36 molecules of ATP, CO<sub>2</sub>, and H<sub>2</sub>O. In contrast, in anaerobic conditions, pyruvate is catalysed into lactate by the lactate dehydrogenase enzyme (LDH) (Figure 1.10) (Pelicano et al., 2006). Even though the main product of glycolysis is known as pyruvate, some of glycolysis intermediates could branch off

and participate in production of precursors in different pathways, demonstrating why relying on glycolysis could be more advantageous for proliferative cells. In the pentose phosphate pathway (PPP), partial oxidation of glucose-6-phosphate gives rise to NADPH and ribose-5-phosphate which is a component of nucleotides (Jiang et al., 2011). Fructose-6-phosphate could also branch off and participate in the production of hexosamines (Itkonen et al., 2013, Spiro, 2002, Wellen et al., 2010). Dihydroxyacetone phosphate (DHAP) could be converted into glycerol-3-phosphate to produce phospholipids. The most well-known of these pathways is using 3-phosphoglycerate as a precursor to produce serine and glycine. Pyruvate could also be involved in AA metabolism by participating in the production of some non-essential AAs (NEAA) including asparagine and aspartate through metabolic pathways mediated by different enzymes such as pyruvate-carboxylase and glutamate and oxaloacetate transaminases (Figure 1.10 and 1.11) (Pavlova and Thompson, 2016, Locasale et al., 2011, Pelicano et al., 2006).

Considerable increase of both Glc and Gln uptake in cancer cells and their correlation to poor prognosis have been studied since the mid-1900s (Som et al., 1980, Warburg et al., 1927, Eagle, 1955). Activation of PI3K/Akt and Ras signalling pathway induce Glc internalization by promoting the expression of a Glc transporter, Glut1; and their aberrant activation which facilitates constant Glc uptake in cancer cells (Wieman et al., 2007, Murakami et al., 1992). Transformation of glucose to glucose-6-phosphate is upregulated in cancer cells due to excessive expression of different isoforms of hexokinase (HK). HK could be considered as a target for cancer therapy (Ko et al., 2001). Inhibition of HK in breast cancer cells induce apoptosis; while in melanoma and leukaemia HK suppression results in lower production of ATP (Kwiatkowska et al., 2016, Nakano et al., 2011). Transformation of phosphoenolpyruvate to pyruvate in glycolysis is catalysed by pyruvate kinase (PK). There are four isoforms of PK in mammals; isoform M2 (PKM2) was shown to be upregulated in different tumours resulting in higher metabolism and tumour growth. Targeting PKM2 as a cancer therapy could increase the effect of chemotherapy (Shi et al., 2010, Akins et al., 2018). Therefore, higher Glc uptake and excessive expression of key glycolytic enzymes can induce tumorigenicity in cancer cells. Moreover, degradation of an ECM component, hyaluronan, has been shown to promote glycolysis via increasing Glut1 trafficking to the plasma membrane, resulting in higher

migration rate in breast cancer cells. Thus, ECMs can also indirectly regulate cancer cells metabolic status and invasion (Sullivan et al., 2018).

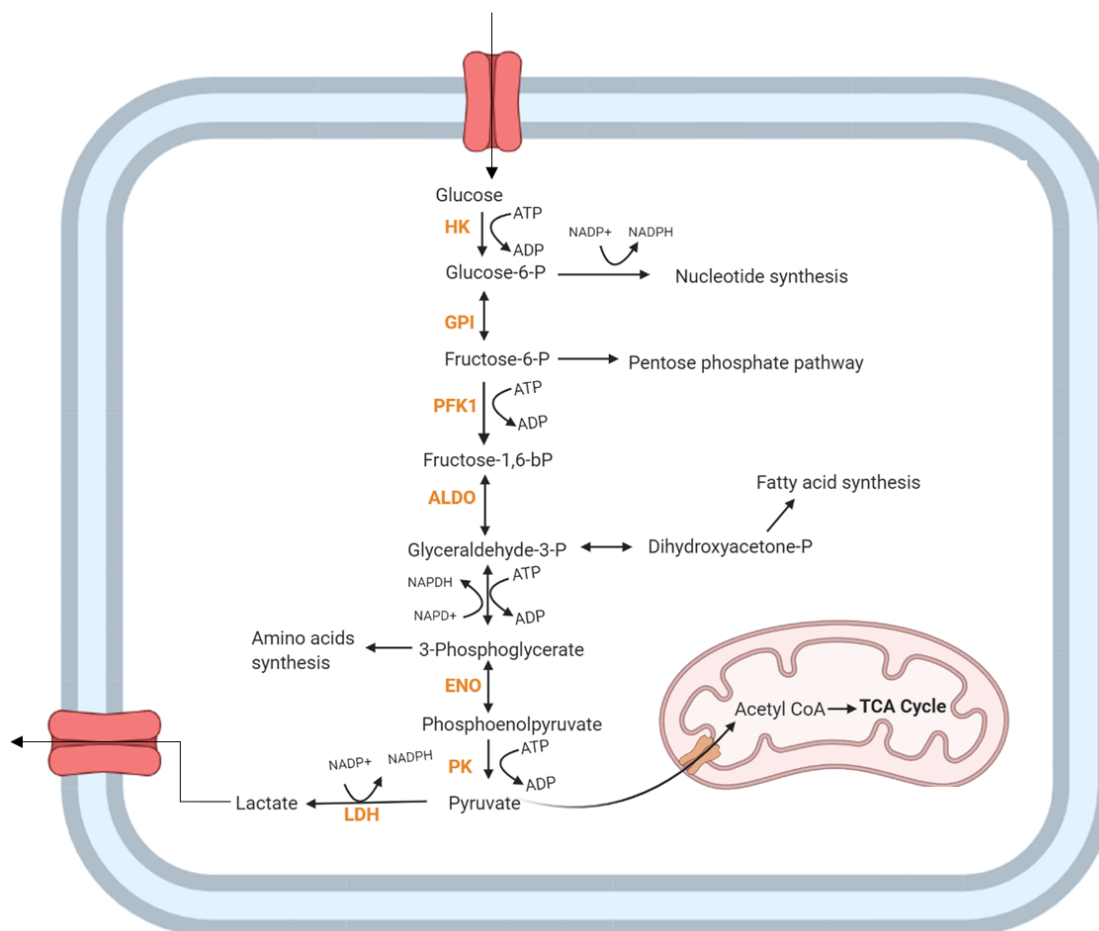


**Figure 1.10. Glycolysis.** During glycolysis, glucose is converted to pyruvate and lactate. Cells secrete lactate to the extracellular environment. However, pyruvate is fed into the TCA cycle via Acetyl-CoA. Some of the glycolysis intermediates are used as a precursor for nucleotide, amino acid, and fatty acid synthesis (Figure is adapted from (Baenke, 2012)). Image is “Created with BioRender.com.”.

#### 1.4.4 Glutaminolysis

Glutamine is the most abundant AA in plasma (Bergstrom et al., 1974). Even though Gln is known as a NEAA, proliferative cells such as cancer cells need external sources to meet their high demand (Lacey and Wilmore, 1990). Some cells mainly rely on Gln uptake to replenish their TCA cycle, which is called Gln anaplerosis, to provide energy. Gln also provides reduced nitrogen as a building block of nitrogen-containing compounds including NEAAs, pyrimidine and purine nucleotides and glucosamine-6-phosphatase (Nicklin et al., 2009). Glutaminolysis, the process of feeding the TCA cycle by Gln, happens through conversion of Gln to glutamate

by glutaminase enzymes (GLS1/GLS2). Glutamate can be converted to  $\alpha$ -ketoglutarate, one of the TCA intermediates, through different pathways. In the process of  $\alpha$ -ketoglutarate formation, glutamate can be catalysed by glutamate dehydrogenase (GDH) or some transaminase enzymes including glutamate–oxaloacetate transaminase (GOT), glutamate–pyruvate transaminase (GPT), and phosphoserine transaminase (PSAT). Glutamate transformation via transaminase results in production of different NEAAs. GOT, PSAT and GPT can promote generation of aspartate, serine, and alanine respectively in the process of  $\alpha$ -ketoglutarate formation. Aspartate can be converted to asparagine or be used as a building block for nucleotide formation.  $\alpha$ -ketoglutarate can be transformed to citrate and being released from mitochondria to the cytoplasm. Citrate could be catalysed to Acetyl-CoA working as a precursor of fatty acids and lipids inside the cells. In general, Gln anaplerosis can also provide NEAAs and nucleotide precursors to the cells (Yang et al., 2017). Efflux of cytoplasmic Gln is also coupled with import of AAs such as leucine, iso-Leucine, tyrosine, valine, methionine, tryptophan, and phenylalanine through L-type amino acid transporter (LAT1) (Figure 1.11) (Yanagida et al., 2001).

According to studies on Gln, the oncogenic protein, C-Myc, prompts the transcription of Gln transporters, ASCT2 and ASN2, to increase Gln uptake. C-Myc also induces GLS over-expression in mitochondria increasing Gln metabolism. Inhibition of GLS1 in prostate and breast cancer cells decreases their growth rate. However, tumour suppressor proteins of the Rb family, participating in G1 cell cycle checkpoint, negatively regulate Gln consumption inside the cell (Wang et al., 2011, Reynolds et al., 2014, Gao et al., 2009, Qie et al., 2014). Cancer cell Gln dependency is also linked to their invasiveness. Highly invasive ovarian cancer cells need Gln uptake for their growth while low invasive ones are Gln independent. Invasive ovarian cancer cells have higher glutaminolysis rate due to elevated expression of GLS and GOT enzymes, which has been linked to their poor prognosis (Yang et al., 2014). It has previously been shown that the rate of GLS protein is dependent on tumour stage. Higher stage and grade of breast cancer cells rely more on Gln. In addition, the amount of GLS is significantly higher in cells negative for both ER and PR implying that they rely more on external sources of Gln (Demas et al., 2019). Gln to glutamate conversion is also linked to metastasis of breast cancer cells. Presence of glutamate in the TME facilitates invasion. Invasive breast cancer cells release glutamate into the environment. Glutamate activates

metabotropic glutamate receptors (GRM3) responding to extracellular glutamate. Activation of GRM3 stimulates MMP-14 recycling happening via Rab27 GTPase. Recycling of MMP-14 from late endosome to plasma membrane increases fibrillar collagen degradation, resulting in higher invasion (Dornier et al., 2017). Gln addicted cancer cells could easily face Gln deprivation due to their high Gln uptake and inadequacy in Gln transport via blood vessels. Tumour cells might rely on alternative sources, like ECPs or CAFs, in their microenvironment to meet their Gln needs (for more details please refer to section 1.4.6 and 1.4.7)

### 1.4.5 Amino acid metabolism

Amino acids are the main building blocks of protein. The human body can endogenously synthesize a group of AAs called NEAAs. However, the rest of the AAs that must be received from an exogenous source are called essential AAs (EAAs) (Table 1.4) (Vettore et al., 2020).

**Table 1.4. List of essential and non-essential amino acids.**

Non-essential amino acids	Essential amino acids
Alanine	Histidine
Asparagine	Isoleucine
Aspartic acid	Lysine
Arginine	Leucine
Cysteine	Phenylalanine
Glutamine	Methionine
Glycine	Tryptophan
Glutamic acid	Threonine
Serine	Valine

Proline	
Tyrosine	

Changes in the rate of different AA synthesis or consumption in favour of cell survival or growth is common in cancer cells. In breast cancer cells, the catabolism of proline via proline dehydrogenase (PRODH) is elevated, resulting in higher ATP production and maintenance of spheroid growth and metastasis of cancer cells (Elia et al., 2017). ECM stiffness increases proline synthesis in lung adenocarcinoma through increase in PYCR1, a key enzyme for proline synthesis, resulting in higher proliferation of cells (Guo et al., 2019). Serine synthesis is also upregulated in different types of cancer. The enzyme that is responsible for the early stage of serine synthesis is 3-phosphoglycerate dehydrogenase (PHGDH). PHGDH upregulation is more common in triple-negative breast cancer cells and its high expression is correlated to lower survival rate and shorter relapse time (Locasale et al., 2011, Pollari et al., 2011). PHGDH expression in glioma cells and cervical cancer is also linked to high tumour grade and lower survival rate (Liu et al., 2013, Jing et al., 2013). Serine can also be converted to glycine and cysteine. An *in vivo* study showed that tumour transplants in the mouse mammary gland decrease the level of plasma cysteine (Al-Awadi et al., 2008). In addition, hypermethylation of cysteine dioxygenase in breast cancer cells induces ROS detoxification and survival (Jeschke et al., 2013). Glycine also facilitates cancer cells detoxification via participating in glutathione production, which is an essential antioxidant (di Salvo et al., 2013). Cancer cell glycine consumption and biosynthesis correlates with their proliferation and metastasis; and breast cancer patients with high reliance on glycine show higher mortality rate (Jain et al., 2012).

In cancer cells, high proliferation rates result in higher metabolic demand. Therefore, they rely on external sources to provide NEAAs, a process called NEAAs auxotrophy. NEAAs auxotrophy is linked to different mutations in genes expressing NEAA synthesis enzymes. Argininosuccinate synthetase (ASS) transfers amino groups from aspartate to synthesize arginine from citrulline. In some cancer cells, mutation in ASS genes limits the synthesis of arginine (Szlosarek et al., 2006). Asparagine synthesis could also be eliminated in cancer cells via mutation in asparagine synthetase (ASNS) transferring amide groups from Gln to make asparagine from aspartate (Richards and Kilberg, 2006). Mutation in Gln synthetase (GS) also



makes the cells rely on exogenous Gln (Tardito et al., 2015). Leukaemia stem cells rely on access to external sources of AAs to survive and supply energy from the oxidative phosphorylation process (Jones et al., 2018). Depletion of Gln in human glioblastoma results in lower ATP production and cell apoptosis. However, providing asparagine to the cells under Gln starvation could rescue the cells from apoptosis (Zhang et al., 2014). Therefore, access of cancer cells to external sources of AAs to meet their metabolic demands is necessary in different conditions. Mechanotransduction upon ECM stiffness causes an aspartate/glutamate crosstalk between CAFs and cancer cells, where cancer cells receive aspartate from CAFs for purine and pyrimidine biosynthesis and supporting cancer cell growth and metastasis (Bertero et al., 2019). Lack of Glc and serum derived-nutrients in the TME of pancreatic ductal adenocarcinoma (PDAC) induce stroma-associated pancreatic stellate cells (PSCs) autophagy. Knockdown of proteins contributing to autophagy decreases the levels of both intracellular and secreted alanine in PDAC. Thus, it is believed that autophagy is the source of alanine in the TME for cancer cells. Deficiency in Glc and other nutrients make alanine a major carbon source for TCA cycle, NEAAs and lipid synthesis in PDACs (Sousa et al., 2016). Therefore, Glc and Gln starvation could be compensated by other alternative sources of nutrients which will be discussed in the next section.

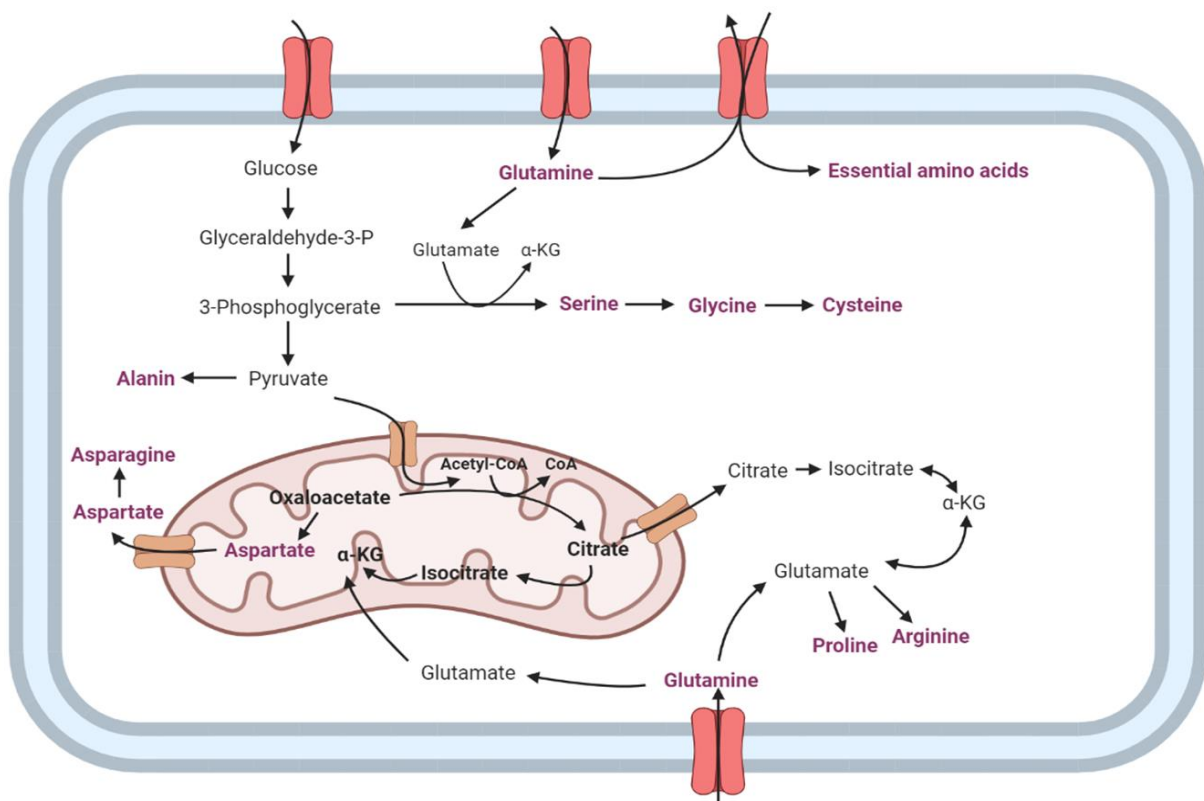


**Figure 1.11. Metabolic pathways of non-essential amino acids.** Major metabolic pathways contributing to amino acid metabolism are glycolysis, glutaminolysis and TCA cycle. Cells receive their essential amino acids from external sources. There are some glutamine transporters that efflux glutamine in exchange of essential amino acids (Bhutia and Ganapathy, 2016). Glutamine is utilized as a precursor for proline, arginine, aspartate, and serine production. Aspartate and serine can be converted to asparagine and glycine, respectively (Figure is adapted from (Baenke, 2012)). Image is "Created with BioRender.com."

#### 1.4.6 CAFs and metabolism

'Deregulating cellular energetics' is one of the cancer cells hallmarks (Hanahan and Weinberg, 2011). Even though many studies focused on the autonomous role of cells in charge of metabolic reprogramming, recently the role of the TME has been considered. Among cells in the TME, CAFs show a major reciprocal metabolic interaction with cancer cells to support their growth.

A study on ovarian cancer cells revealed that co-culture of CAFs with cancer cells induce metastasis via increasing energy content and glycolysis in cancer cells. Secretion of TGF- $\beta$  in the TME induces the P38-MAPK signalling pathway in CAFs resulting in secretion of cytokines such as IL-6, CCL5 and CXCL10. Cytokines increase glycogen mobilisation and higher phosphoglucomutase 1 (PGM1) expression. Higher activity of PGM1 in ovarian cancer cells in the presence of CAFs induces conversion of glycogen to glycolysis intermediates. Therefore, higher glycolysis activity in cells results in higher proliferation and invasion (Curtis et al., 2019). CAFs also release exosomes carrying AAs, TCA intermediates and lipids. Nutrient deprived conditions increase the uptake of these exosomes in pancreatic and prostate cancer cells. Heavy carbon labelling of exosomes content revealed that by taking the exosomes inside the cancer cells, their content contributed to production of AAs and TCA cycle intermediates (Zhao et al., 2016). CAFs associated with ovarian cancer cells show increased Gln anabolic pathways as a response to cancer cells residing in Gln starvation environments. Ovarian cancer cells increase Gln synthesis in CAFs under Gln starvation. Secretion of Gln from CAFs helps cancer cells to maintain their growth under Gln deficiency condition (Yang et al., 2016).

CAFs can also induce the 'reverse Warburg effect'. Higher levels of glycolysis in CAFs increases the secretion of lactate. The presence of lactate in the TME increases the TCA cycle and NAD<sup>+</sup>/NADH level in prostate cancer cells in the vicinity of CAFs. Higher mitochondria mass

and activity increase oxidative phosphorylation (OXPHOS) pathway in cancer cells, resulting in higher metastasis rate and chemotherapy resistance (Ippolito et al., 2019). Similarly, secretion of pyruvate from CAFs in the lymphoma microenvironment increases TCA cycle intermediates, decreases reactive oxygen production, and eventually increases cell survival (Sakamoto et al., 2019).

There is some evidence showing that ECM stiffness could also manipulate breast cancer cells and CAF metabolism. Stiff ECM induces a metabolic crosstalk between carcinoma and CAFs through NEAA flux. Carcinoma cells increase Gln uptake and glutamate release in the TME on stiffer substrates; whereas, in CAFs, glutamate is internalized, and aspartate is secreted. Following, CAFs-derived aspartate is consumed by cancer cells and participates in nucleotide formation and finally cell proliferation (Bertero et al., 2018).

Therefore, Interaction of cancer cells with CAFs provides different sources of nutrients for cancer cells such as AAs and lipids facilitating growth, invasion, and survival of cancer cells under different nutrient conditions.

#### **1.4.7 Nutrient scavenging from microenvironment**

High rate of tumour growth and inadequate vasculature forming or blood supply inside the tumours substantially increase the chance of nutrient deficiency in TME (Weis and Cheresh, 2011). Therefore, cancer cells adapt to use alternative sources of nutrients, such as albumin or collagen from the TME to meet their metabolic needs.

Leaky blood vessels and shortage of lymphatic vessels around the tumours permit cancer cells to have access to blood serum and its protein content such as albumin. (Stehle et al., 1997, Son et al., 2013). Higher tendency toward proteins in blood serum is the result of different types of nutrient deficiency in cancer cells. In addition, constitutive activation of Ras induces macropinocytosis facilitating ECPs internalization. Under AA starvation, albumin macropinocytosis followed by lysosomal degradation in Ras-driven PDACs and Ras-transformed mouse embryonic fibroblasts (MEFs), increases AA content of the cells. Presence of AAs inside the cells induces mTORC1 activity and eventually protein synthesis and growth. It has been also shown that simulating nutrient deficiency via inhibiting mTORC1 signalling pathway encourages cells to rely on ECPs. In contrast, activation of mTORC1 inhibits lysosomal

degradation of ECPs to avoid excessive uptake of proteins from extracellular sources (Commisso et al., 2013, Kamphorst et al., 2015, Palm et al., 2015). Cells have also access to the cell debris from cells that died due to lack of nutrient or oxygen. AA and Glc starvation in K-Ras-driven pancreatic cancer cells and PTEN-deficient prostate cancer cell lines induces scavenging cell debris. Nutrient deficiency in these cells promotes AMPK activation (by increasing Rac1 activation) leading to macropinosome formation, mTORC1 inactivation and cell debris scavenging. Extracting nutrients from cell debris finally assists cells to have higher proliferation and cell biomass production rate (Kim et al., 2018). Cancer cells are also surrounded by a network of ECM components inside the tumours. Low Glc and Gln conditions induce PDAC cells to uptake collagen I and IV through macropinocytosis or receptor-dependent endocytosis, respectively. PDAC cells extract proline via digestion of collagen I and IV inside the lysosomes. Proline could be fed into the TCA cycle and result in higher ATP production and cell survival through ERK1/2 activation (Olivares et al., 2017). It has been revealed that in MEFs, ECPs uptake happens as the result of GF dependent macropinocytosis through PI3 kinase activation. Based on the nutrient condition, PI3K triggers different downstream signalling pathways. Under AA deficiency conditions, activation of Rac1 and PLC $\gamma$  as a PI3K downstream target induces macropinocytosis and provides nutrients via ECP uptake. However, in the presence of AAs and Glc, another PI3k effector, Akt, is activated resulting in activation of mTORC1 signalling. Activation of mTORC1 signalling pathway forces cells to rely on free AA instead of macropinocytosis of macromolecules from the environment (Palm et al., 2017). PDAC cells are heterogeneous in terms of macropinocytosis. Some have constitutive macropinocytosis not influenced by the amount of nutrients, while others display inducible macropinocytosis. In the cells with inducible macropinocytosis, Gln starvation induces transcriptional upregulation of EGFR ligands. EGFR ligand binding causes Ras and EGFR-Pak signalling activation, which leads to ECPs macropinocytosis and lysosomal degradation (Lee et al., 2019). In addition, *in vivo* studies also demonstrate that hypoalbuminemia is observed in some cancer patients, suggesting that the tumours could rely on albumin as an alternative source of nutrients (Fearon et al., 1998). Another *in vivo* study revealed that PDAC cells inside the tumour do albumin macropinocytosis followed by AA extraction. In contrast, normal cells in the vicinity of tumours do not have the ability to benefit from the albumin uptake (Figure 1.12) (Davidson et al., 2017). Therefore, cancer cells can rely on alternative nutrient sources such as albumin, laminin, collagen, or cell debris via

different mechanisms to adapt to the nutrient deficient environment and maximize their nutrient uptake (Figure 1.12) (Nazemi and Rainero, 2020).

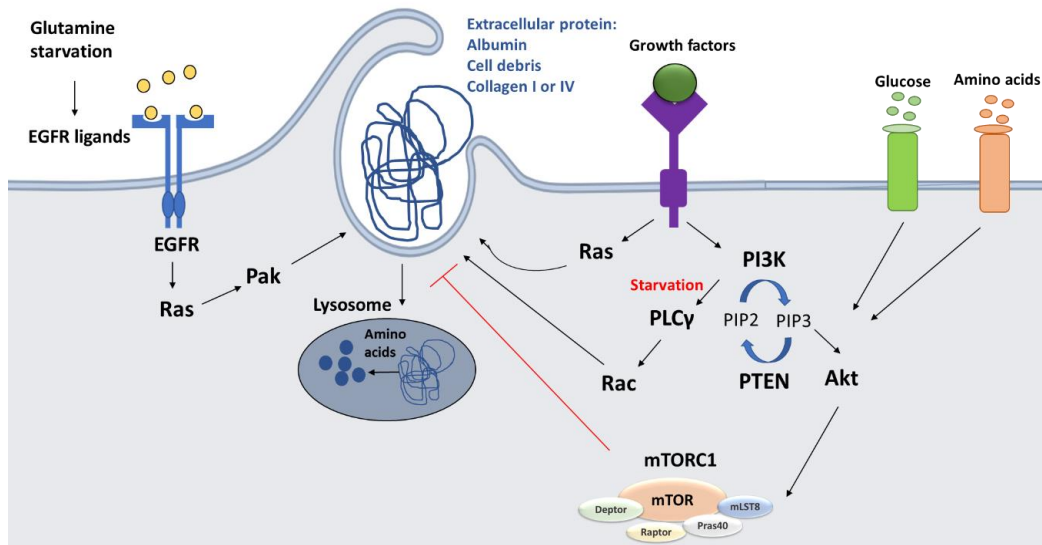


**Figure 1.12. Schematic representation of signalling pathways induces macropinocytosis and ECP internalization.** Amino acid and glucose starvation induce macropinocytosis of ECPs via Ras or GF dependent macropinocytosis. ECP internalization is usually followed by lysosome degradation and amino acid extraction. Amino acids can later be fed into the TCA cycle intermediates and facilitate ATP production (Nazemi and Rainero, 2020).

## 1.5 Aim of the thesis

As the ECM is produced by stromal cells constantly around the tumours, we hypothesise that invasive breast cancer cells might have adopted the characteristic to use ECM components as either a substitute source of nutrients during starvation, through internalization and lysosomal degradation, or as signalling molecules to trigger signalling pathways to induce survival/growth. Therefore, the aim of this study is to monitor mammary cancer cell behaviour in terms of ECM uptake during starvation and dissecting the signalling pathways following that.

To do so, we will examine whether the presence of different types of ECM (collagen, laminin, Matrigel and cell-derived matrices) could support cell growth under specific nutrient starvation conditions (AA, Gln, Glc and serum starvation) by:

- Specifying which types of ECM induce cell growth/survival under starvation conditions.
- Determining whether ECM internalization and lysosomal degradation is required to support growth during the different starvation conditions.
- Dissecting whether ECM-dependent cell growth is linked to mTOR activation.
- Determining whether signalling downstream of cell-ECM interaction is involved in cell growth under starvation.
- Analysing metabolic changes inside the cells due to the presence of ECM.
- Investigating the role of different genes participating in ECM trafficking on ECM-dependent cell growth under starvation via an RNAi gene silencing screen.

## Chapter 2: Materials and Methods

### 2.1 Materials

#### 2.1.1 Reagents

**Table 2.1. Reagents and suppliers.**

Reagent	Supplier
0.45µm filter	Gilson
10cm <sup>2</sup> petri dishes	Greiner bio-one
11130-MEM amino acid solution (50x) liquid	Gibco
11140- MEM non-essential amino acid solution (100x) liquid	Gibco
2-Deoxy-D-Glucose	Sigma
2-NBDG Glucose Uptake Assay Kit	Abcam
3.5cm <sup>2</sup> glass-bottom dishes	SPL Life Science
384-well glass-bottom plates	Perkin Elmer
6-well tissue culture plates	Greiner bio-one
96-well glass bottom plates	Greiner bio-one
96-well plastic bottom plates	FALCON
Alexa fluor <sup>TM</sup> 555/488/647 Phalloidin	Invitrogen
Bafilomycin A1	Alfa Aesar
BioTracker ATP-Red Live Cell Dye	Merck
Bovine Serum albumin	Sigma-Aldrich
CellEvent <sup>TM</sup> Caspase-3/7 Green Detection	Invitrogen
Collagen type I (Rat tail high concentration)	Corning
D-glucose anhydrase	Fisher chemical
D-Glucose- <sup>13</sup> C <sup>6</sup>	Sigma-Aldrich
DharmaFect 1 (DF1) Reagent	Dharmacone
Dialyzed FBS	Gibco
Dimethyl sulfoxide (DMSO)	Fisher Scientific
DNase I	Sigma
DRAQ5 <sup>TM</sup>	Rocher
E64d (Aloxistatin)	AdooQ Bioscience
Epidermal growth factor	Sigma
Fetal Bovine Serum	Gibco
Filipin	Sigma
Gelatin	Sigma
Glutamine stable 100x	biowest
Glutaraldehyde solution	Sigma Aldrich
Glycine	Sigma
GM6001	APEXBIO
Hoechst 33342	Invitrogen

Hydrocortisone	Sigma
PVDF membrane	IMMOBILON-FL
Insulin solution human	Sigma
IRDye 800CW N-Hydroxysuccinimide (NHS Ester	LI-COR
L-Ascorbic acid	Sigma
Laminin/entactin complex	Corning
Laemmli Sample Buffer	Bio-Rad
Matrigel	Corning
NH <sub>4</sub> OH	Fluka Analytical
NHS-Fluorescein	Thermo Scientists
Oligomycin A	AdooQ Bioscience
PBS containing calcium and magnesium	Sigma
Penicillin/Streptomycin (PS)	Life Technologies
PF573228	AdooQ Bioscience
Paraformaldehyde	Fluka Chemika
Protein ladder	Colour protein standard broad range. Bio-Labs
QiaShredder	QIAGEN
siGLO Red/Green Transfection Indicator (20 nmol)	Thermo Fisher
Triton-X100	Sigma
Trypan blue stain 0.4%	Gibco by life technologies
Trypsin EDTA solution 1x	Sigma
Tween-20	Sigma
Vectashield mounting reagent +DAPI	VECTOR

## 2.1.2 Cell culture media

**Table 2.2. Media, suppliers, and reference numbers.**

Media	Supplier	Ref No
DMEM, high glucose, no glutamine	Gibco	11960-044
DMEM, no glucose	Gibco	11966-025
DMEM, no amino acids	US Biological life science	
DMEM, high glucose, pyruvate	Gibco	41966-029
DMEM, no glucose, no glutamine	Gibco	A14430-01
EBSS, calcium, magnesium, phenol red	Gibco	24010-043
DMEM/F-12, HEPES	Gibco	31330-038
DMEM/F-12, no glutamine	Gibco	21331-020



SILAC Advanced DMEM/F-12 Flex	Gibco	A24943-01
-------------------------------	-------	-----------

### 2.1.3 Solutions

**Table 2.3. Recipes of solutions.**

Solutions	Recipe
TBS	10mM Tris-HCl pH7.4, 150mM NaCl
TBS-T	TBS, 0.1% Tween-20 (v/v)
Towbin buffer 10x	1.92M Glycin, 0.25M Tris
Transfer buffer	10% 10x Towbin buffer, 20% methanol
Sample Buffer	31.5 mM Tris-HCl, pH 6.8 buffer 10% glycerol 1% SDS 0.005% Bromophenol Blue
1% SDS lysis buffer	1% SDS (v/v), 50mM Tris-HCl pH7.0
Cell extraction buffer	20mM NH <sub>4</sub> OH, 0.5% Triton X-100 (v/v) in PBS with calcium and magnesium
Metabolite extraction solution	5 MeOH: 3 AcN: 2 H <sub>2</sub> O

### 2.1.4 siRNA

**Table 2.4. siRNA used for siRNA knockdown.**

Target	siRNA	Supplier
Non-targeting (NT)	SiGenome control Non-Targeting siRNA pool #1	Thermo Fisher
Non-targeting (NT)	ON TARGET plus non-targeting siRNA pool #4	Dharmacon
siRNA library for Traffic-om	ON-TARGETplus siGENOME <sup>®</sup> Human siRNA Library for Traffic-om	Dharmacon
Polyubiquitin-B (UBB)	SiGenome Smart Pool Human UBB	Dharmacon
Serine/threonine-protein kinase PLK1	SiGenome Smart Pool Human PLK1	Dharmacon
HPD	ON TARGET plus human HPD (3242) siRNA SMART Pool	Dharmacon

HPDL	ON TARGET plus human HPDL (84842) siRNA SMART Pool	Dharmacon
------	--	-----------

### 2.1.5 Primary antibodies

Table 2.5. Primary antibodies.

Protein	Host	Technique (dilution)	Supplier
Phospho-S6 Ribosomal Protein (ser235/236)	Rabbit	Immunostaining (1:100)	Cell signalling
Phospho-FAK (Tyr397)	Rabbit	Western blot (1:1000)	Thermo Fisher
GAPDH	Mouse	Western blot (1:500)	Cell signalling
Paxillin	Mouse	Immunostaining (1:200)	BD bioscience

### 2.1.6 Secondary antibodies

Table 2.6. Secondary antibodies

Antibody	Host	Technique	Supplier
Alexa-fluor 594 $\alpha$ -Rabbit IgG	Goat	Immunostaining (1:1000)	Cell signalling
Alexa-fluor 488 $\alpha$ -Mouse IgG	Goat	Immunostaining (1:1000)	Cell signalling
IRDye® 800CW Anti Mouse IgG	Goat	Western blot (1:30K)	LI-COR
IRDye® 680CW Anti Rabbit IgG	Donkey	Western blot (1:20K)	LI-COR

## **2.2 Methods**

### **2.2.1 Cell culture**

MDA-MB-231 cells, telomerase immortalised fibroblast (TIF) cells and CAFs were cultured in high glucose Dulbecco's Modified Eagle's Medium (DMEM) supplemented with 10% fetal bovine serum (FBS) and 1% penicillin streptomycin (PS). Cells were grown at 5% CO<sub>2</sub> and 37°C and passaged every 3 to 4 days. CAFs were from breast cancer and were generated in Professor Akira Orimo's lab, Paterson Institute, Manchester. MCF10A-DCIS cells were cultured in DMEM/F12 supplemented with 5% Horse serum (HS), 20 ng/ml EGF and 1% PS. MCF10A cells were cultured in DMEM/F12 supplemented with 5% HS, 20 ng/ml EGF, 0.5mg/ml hydrocortisone, 10µg/ml insulin and 1% PS.

To passage the cells, media was removed, cells were washed once in PBS, and incubated in 0.25% trypsin for 2 minutes at 5% CO<sub>2</sub>, 37°C. After cells were detached, they were resuspended in complete growth media and plated at the needed density in tissue culture dishes.

Cryofreezing was performed for long term storage. Cells from a 10cm<sup>2</sup> dish at around 90% confluency were trypsinized and resuspended in complete media, and then centrifuged at 1000rpm for 3 minutes at room temperature (RT). Pelleted cells were resuspended in 1ml freezing solution containing 10% DMSO, 25% complete media and 65% FBS. Vials were transferred to -80°C for a few days. Then, they were transferred to liquid nitrogen for long-term storage.

### **2.2.2 ECM preparation**

#### **2.2.2.1 Collagen I, Matrigel and Laminin coating.**

To coat plates/dishes, collagen I, Matrigel and laminin were diluted with cold PBS on ice to have 2mg/ml, 3mg/ml, and 3.5 mg/ml concentration, respectively. Diluted ECM were added to each well/dish and properly spread on the bottom with pipette tips. Plates/dishes coated with ECM were transferred to the incubator at 5% CO<sub>2</sub>, and 37°C for 3hrs for polymerization. To avoid dryness, after three hours, PBS were added to each well/dish and the matrices were kept into the incubator overnight.

### 2.2.2.2 Preparation of cell-derived matrices.

Cell-derived matrix (CDM) was generated from TIFs and CAFs. CDMs were generated either in a 6-well plate or 96-well glass-bottom plate. Plates were first coated with 0.2% gelatine in PBS and incubated at 37°C for 1hr. Gelatine was washed twice with PBS followed by being cross-linked with 1% glutaraldehyde in PBS at RT for 30 minutes. Glutaraldehyde was removed and the wells were washed twice with PBS. Cross-linker was quenched in 1M glycine at RT for 20 minutes, followed by two PBS washes, and an incubation in complete media at 5% CO<sub>2</sub> and 37°C for 30 minutes. In 96-well plates, 6x10<sup>3</sup> cells and in 6-well plates 2x10<sup>5</sup> cells were seeded per well. Cells were incubated at 5% CO<sub>2</sub>, 37°C until being fully confluent (1 or 2 days). Once the cells were 100% confluent, the media was changed to complete growth media containing 50µg/mL ascorbic acid, and it was refreshed every two days. To prepare CDMs, TIFs were kept under media supplemented with ascorbic acid for 6 days while CAFs were kept under the same condition for 7 days. The media was aspirated, and the cells were washed once with PBS containing calcium and magnesium (PBS<sup>++</sup>). The cells were incubated with the extraction buffer containing 20mM NH<sub>4</sub>OH and 0.5% triton in PBS<sup>++</sup> for 2 minutes at RT until no intact cells were visible by phase contrast microscopy. The extraction buffer was removed and the CDM was washed twice with PBS<sup>++</sup>. Residual DNA was digested with 10µg/mL DNase I in PBS<sup>++</sup> at 5% CO<sub>2</sub>, 37°C for 1hr. Following two PBS<sup>++</sup> washes, the CDMs were stored at 4°C in PBS<sup>++</sup> containing 1% PS.

### 2.2.3 Cell proliferation assay

To monitor cell proliferation on ECM compared to plastic under different starvation conditions, 96-well plates containing TIF-CDM or collagen I, Matrigel and laminin as described in section 2.2.2.1 and 2.2.2.2 were prepared and left in PBS. Three wells were allocated to each condition as technical replicates. The following day, the PBS was removed from each well and 10<sup>3</sup> cells/well were seeded under full growth media. After 5hrs incubation in 5% CO<sub>2</sub> and 37°C, the full growth media was replaced with 200µL of the starvation media shown in table 2.7 or Plasmax. Plasmax was kindly provided by Dr Tardito, The Beatson Institute, Glasgow. The details of Plasmax composition were previously described by Vande Voorde et al 2019 (Vande Voorde et al., 2019). In all the media where FBS was needed, we used dialyzed FBS (DFBS). The manufacturing process of DFBS is designed to significantly reduce the number

of low weight molecules in the serum including AAs, cytokines, salts, and hormones. After incubating cells under starvation conditions, cells were fixed every two days up to day six or eight by adding 4% paraformaldehyde (PFA) for 15mins RT followed by two PBS washes.

### 2.2.3.1 Starvation media compositions

**Table 2.7. Composition of different media used for different cell lines.**

Cell line	Starvation conditions	Media composition
1. MDA-MB-231	Glucose and glutamine starvation	1. DMEM [-] D-glucose, [-] L-glutamine [+] 10% DFBS
1. MDA-MB-231 2. MCF10A 3. MCF10A-DCIS	Serum starvation	1. DMEM [+] 4.5 g/L D-glucose [+] L-glutamine 2, 3. DMEF/F12 4.5 g/L D-glucose [+] L-glutamine
1. MDA-MB-231 2. MCF10A 3. MCF10A-DCIS	Amino acid starvation	1. DMEM [+]4.5 g/L D-glucose [+] 10% DFBS 2, 3. DMEM [+]4.5 g/L D-glucose [+] 10% HS
1. MDA-MB-231	Non-essential amino acid starvation	1. DMEM [+]4.5 g/L D-glucose [+] 10%DFBS [+]1/50 MEM amino acid solution (50x) liquid
2. MDA-MB-231	Essential-amino acid starvation	1. DMEM [+]4.5 g/L D-glucose [+] 10%DFBS [+]1/100 MEM non-essential amino acid solution (100x) liquid
1. MDA-MB-231 2. MCF10A 3. MCF10A-DCIS	Glutamine starvation	1. DMEM [+] 4.5 g/L D-glucose [+] 10%DFBS 2. DMEM [+] 4.5 g/L D-glucose [+] 10% HS 3. DMEM/F12 [+] 4.5 g/L D-glucose [+] 5% HS
1. MDA-MB-231 2. MCF10 3. MCF10A-DCIS	Glucose starvation	1. DMEM [+] L-glutamine [+] 10%DFBS. 2. DMEM [+] L-glutamine [+] 10% HS. 3. DMEM/F12 [+] L-glutamine [+] 5% HS.

### 2.2.3.2 Media formulation (DMEM).

Table 2.8. Concentration of different DMEM media.

Components	DMEM, high glucose, pyruvate (mg/L)	DMEM Low Glucose, w/o Amino	DMEM, high glucose, no glutamine	DMEM, no glucose
<b>Amino Acids</b>				
Glycine	30	Absent	30	30
L-Arginine hydrochloride	84	Absent	84	84
L-Cystine 2HCl	63	Absent	63	63
L-Glutamine	580	Absent	Absent	580
L-Histidine hydrochloride-H <sub>2</sub> O	42	Absent	42	42
L-Isoleucine	105	Absent	105	105
L-Leucine	105	Absent	105	105
L-Lysine hydrochloride	146	Absent	146	146
L-Methionine	30	Absent	30	30
L-Phenylalanine	66	Absent	66	66
L-Serine	42	Absent	42	42
L-Threonine	95	Absent	95	95
L-Tryptophan	16	Absent	16	16
L-Tyrosine disodium salt dihydrate	72	Absent	104	104
L-Valine	94	Absent	94	94
<b>Vitamins</b>				
Choline chloride	4	4	4	4
D-Calcium pantothenate	4	4	4	4
Folic Acid	4	4	4	4
Niacinamide	4	4	4	4
Pyridoxine hydrochloride	4	4	4	4
Riboflavin	0.4	0.4	0.4	0.4
Thiamine hydrochloride	4	4	4	4
i-Inositol	7.2	7.2	7.2	7.2
<b>Inorganic Salts</b>				
Calcium Chloride (CaCl <sub>2</sub> ·2H <sub>2</sub> O)	264	265	200	200
Ferric Nitrate (Fe(NO <sub>3</sub> ) <sub>3</sub> ·9H <sub>2</sub> O)	0.1	0.1	0.1	0.1
Magnesium Sulfate (MgSO <sub>4</sub> ·7H <sub>2</sub> O)	200	97.67	97	97
Potassium Chloride (KCl)	400	400	400	400
Sodium Bicarbonate (NaHCO <sub>3</sub> )	3700	Absent	3700	3700
Sodium Chloride (NaCl)	6400	6400	6400	6400
Sodium Phosphate monobasic (NaH <sub>2</sub> PO <sub>4</sub> ·2H <sub>2</sub> O)	141	109	125	125

Other Components				
D-Glucose (Dextrose)	4500	1000	4500	Absent
Phenol Red	15	15.9	15	15
Sodium Pyruvate	110	Absent	Absent	Absent

### 2.2.3.3 MEM Non-Essential Amino Acids Solution (100x)

Table 2.9. Concentration of amino acids in MEM NEAAs solution.

Amino Acids	Concentration (mg/L)
Glycine	750
L-Alanine	890
L-Asparagine	1320
L-Aspartic acid	1330
L-Glutamic Acid	1470
L-Proline	1150
L-Serine	1050

### 2.2.3.4 MEM Essential amino acid solution (50x)

Table 2.10. Concentration of amino acids in MEM solution

Amino Acids	Concentration (mg/L)
L-Arginine hydrochloride	6320
L-Cystine	1200
L-Histidine hydrochloride-H <sub>2</sub> O	2100
L-Isoleucine	2620
L-Leucine	2620
L-Lysine hydrochloride	3625
L-Methionine	755
L-Phenylalanine	1650
L-Threonine	2380
L-Tryptophan	510
L-Tyrosine	1800
L-Valine	2340

### 2.2.3.5 Media formulation (DMEM/F12).

Table 2.11. Concentration of different DMEM/F12 media.

Components	DMEM/F-12, HEPES (mg/L)	DMEM/F-12, no glutamine, no HEPES (mg/L)	SILAC Advanced DMEM/F-12 Flex Media, no glucose (mg/L)
<b>Amino Acids</b>			
Glycine	18.75	18.75	18.75
L-Alanine	4.45	4.45	4.45
L-Arginine hydrochloride	147.5	147.5	Absent
L-Asparagine-H <sub>2</sub> O	7.5	7.5	7.5
L-Aspartic acid	6.65	6.65	6.65
L-Cysteine hydrochloride-H <sub>2</sub> O	17.56	17.56	17.56
L-Cystine 2HCl	31.29	31.29	31.29
L-Glutamic Acid	7.35	7.35	7.35
L-Glutamine	365	Absent	Absent
L-Histidine hydrochloride-H <sub>2</sub> O	31.48	31.48	31.48
L-Isoleucine	54.47	54.47	54.47
L-Leucine	59.05	59.05	59.05
L-Lysine hydrochloride	91.25	91.25	Absent
L-Methionine	17.24	17.24	17.24
L-Phenylalanine	35.48	35.48	35.48
L-Proline	17.25	17.25	17.25
L-Serine	26.25	26.25	26.25
L-Threonine	53.45	53.45	53.45
L-Tryptophan	9.02	9.02	9.02
L-Tyrosine disodium salt dihydrate	55.79	55.79	55.79
L-Valine	52.85	25.85	25.85
<b>Vitamins</b>			
Biotin	0.0035	0.0035	0.0035
Choline chloride	8.98	8.98	8.98
D-Calcium pantothenate	2.24	2.24	2.24
Folic Acid	2.65	2.65	2.65
Niacinamide	2.02	2.02	2.02
Pyridoxine hydrochloride	2	2	2
Riboflavin	0.219	0.219	0.219
Thiamine hydrochloride	2.17	2.17	2.17
Vitamin B12	0.68	0.68	0.68
i-Inositol	12.6	12.6	12.6
<b>Inorganic Salts</b>			
Calcium Chloride (CaCl <sub>2</sub> ) (anhyd.)	116.6	116.6	116.6



<b>Cupric sulfate (CuSO<sub>4</sub>·5H<sub>2</sub>O)</b>	0.0013	0.0013	0.0013
<b>Ferric Nitrate (Fe(NO<sub>3</sub>)<sub>3</sub>·9H<sub>2</sub>O)</b>	0.05	0.05	0.05
<b>Ferrous Sulfate (FeSO<sub>4</sub>·7H<sub>2</sub>O)</b>	0.417	0.417	0.417
<b>Magnesium Chloride (MgCl<sub>2</sub>·6H<sub>2</sub>O)</b>	61	28.64	28.64
<b>Magnesium Sulfate (MgSO<sub>4</sub>·7H<sub>2</sub>O)</b>	100	48.84	48.84
<b>Potassium Chloride (KCl)</b>	311.8	311.8	311.8
<b>Sodium Bicarbonate (NaHCO<sub>3</sub>)</b>	1200	2438	2438
<b>Sodium Chloride (NaCl)</b>	6995.5	6995.5	6995.5
<b>Sodium Phosphate dibasic (Na<sub>2</sub>HPO<sub>4</sub>·7H<sub>2</sub>O)</b>	134	71	71
<b>Sodium Phosphate monobasic (NaH<sub>2</sub>PO<sub>4</sub>·H<sub>2</sub>O)</b>	62.5	62.5	62.5
<b>Zinc sulfate (ZnSO<sub>4</sub>·7H<sub>2</sub>O)</b>	0.432	0.432	0.432
<b>Other Components</b>			
<b>D-Glucose (Dextrose)</b>	3151	3151	Absent
<b>HEPES</b>	3574.5	Absent	Absent
<b>Hypoxanthine Na</b>	2.39	2.39	2.39
<b>Linoleic Acid</b>	0.042	0.042	0.042
<b>Lipoic Acid</b>	0.105	0.105	0.105
<b>Phenol Red</b>	8.1	8.1	Absent
<b>Putrescine 2HCl</b>	0.081	0.081	0.081
<b>Sodium Pyruvate</b>	55	55	55
<b>Thymidine</b>	0.365	0.365	0.365

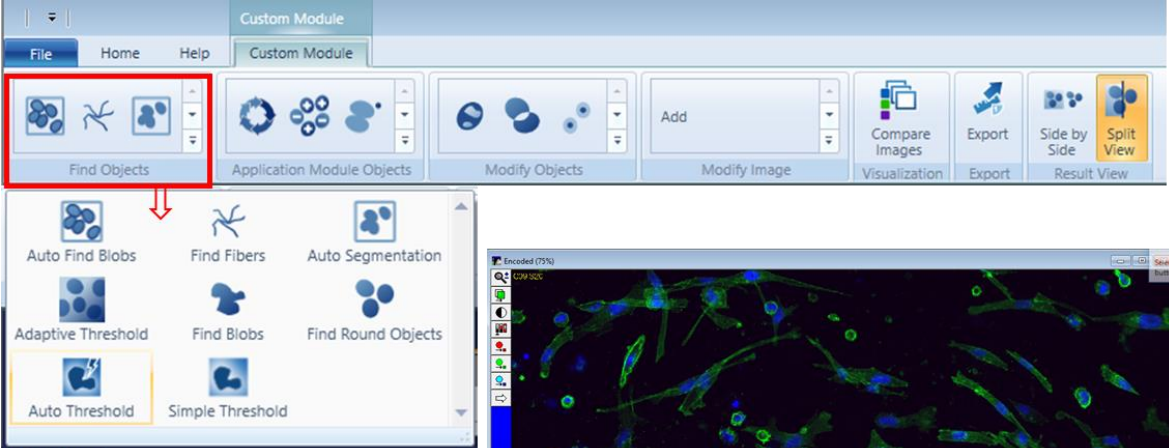
Cell proliferation was quantified using two different techniques 1) Nuclei staining with DRAQ5 and staining intensity per well detection with the Licor Odyssey imaging system. DRAQ5 is a far-red fluorescing DNA probe used for normalization of cell number in In-Cell Western (ICW) Assays (<https://www.licor.com/documents/zfig072j08h7bf4wgc4m>). 5µM DRAQ5 in PBS was added to the cells for 1hr at RT with a gentle rocking. Cells were washed two times with PBS, 20 to 30 minutes to avoid the background fluorescence, and kept in PBS for imaging with the Licor Odyssey imaging system. DRAQ5 was detected with a 700nm channel with 200µm resolution by an Odyssey Sa instrument. The signal intensity, which was the total intensity minus total background, of each well was quantified with Image Studio Lit software. 2) Using Hoechst nuclei staining and imaging by ImageXpress micro. In this technique, cells were fixed with 4% PFA containing 10µg/ml Hoechst 33342 for 15 mins, followed by two PBS washes. Image analyses of cells stained with Hoechst 33342 was done by MetaXpress and Costum Module Editor software (CME) in the Sheffield RNAi Screening Facility (SRSF). To obtain cell

number, plates were imaged by ImageXpress micro with 2x objective and DAPI filter. Images were acquired at multiple sites to cover the entire well. With 2x magnification, 4 sites/well in 96-well plate and one site/well for 384-plates covers the whole well. The CME application was used to design an algorithm to detect every nucleus in each image based on the range of nuclei intensity and size (Figure 2.1).

#### **2.2.3.6 Cell proliferation assay on CAF-CDM**

Even though fibroblast extraction was performed when preparing CAF-CDMs, it was realized that some CAF nuclei remained in the CDM, which could affect the accuracy of cell counting for proliferation assays. To overcome this, cell seeding, fixation and Hoechst 3342 nuclei staining was performed following the same protocol described in section 2.2.3. In addition, cells were permeabilized for 5 min with 0.25% Triton X-100 and stained with Phalloidin Alexa Fluor 488 diluted 1:400 in PBS for 30mins to stain the actin cytoskeleton. Cells were washed twice with PBS and were left in PBS for imaging. Images were collected by ImageXpress micro and analysed by MetaXpress and CME software. To obtain cell number, plates were imaged by ImageXpress micro with 10x objective and with both DAPI and GFP filter. To measure cell number, an algorithm was designed to detect and mask GFP (Phalloidin) wavelength (Figure 2.1).

**A**



**B**

**1 Setup**

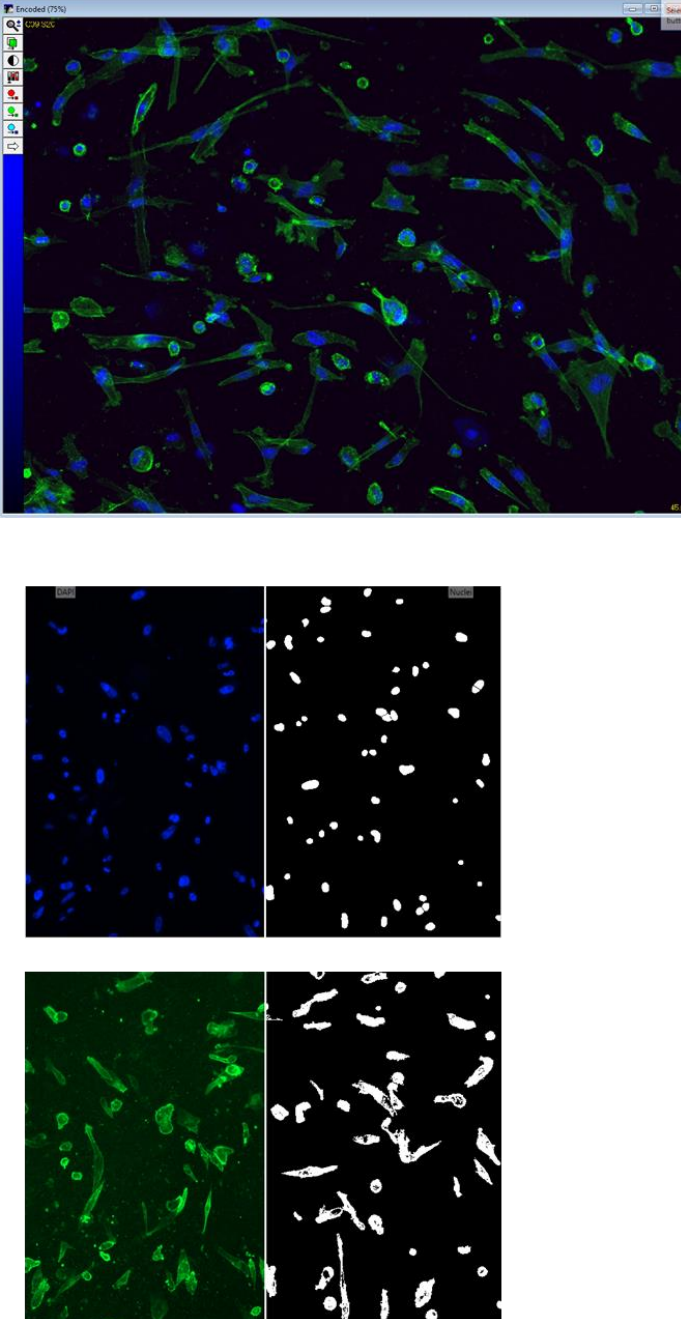
Image Names: DAPI, GFP  
 Channels: DAPI, GFP

**2 Find Round Objects**

Source: DAPI  
 Approximate Minimum Width ( $\mu\text{m}$ ): 5  
 Approximate Maximum Width ( $\mu\text{m}$ ): 40  
 Intensity Above Local Background: 25  
 Result: Nuclei

**3 Adaptive Threshold**

Source: GFP  
 Approximate Minimum Width ( $\mu\text{m}$ ): 10  
 Approximate Maximum Width ( $\mu\text{m}$ ): 30  
 Intensity Above Local Background: 15  
 Result: Actin



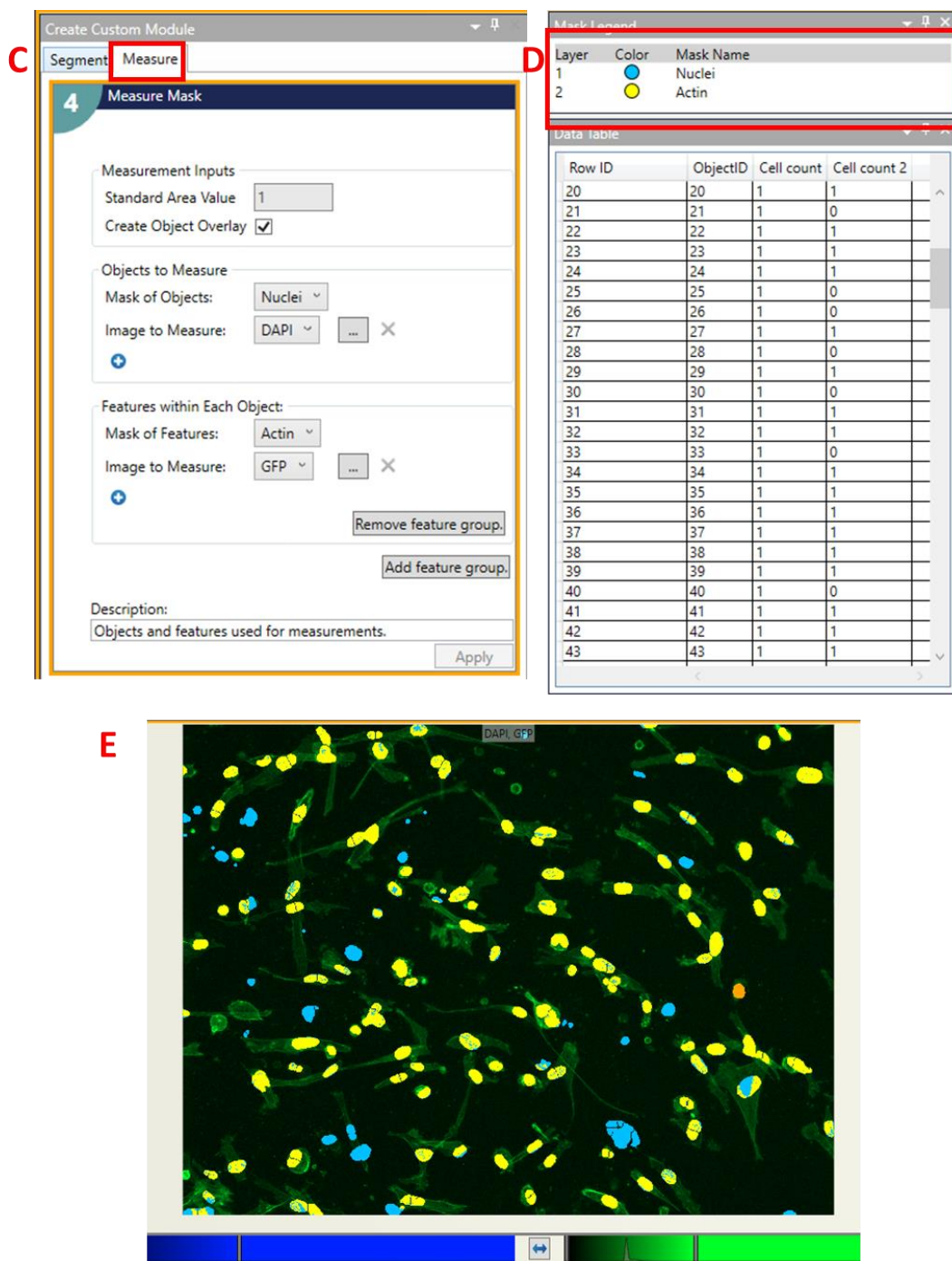


**Figure 2.1. Designing algorithm by CME to detect cells positive for actin staining.** To extract data from images, an algorithm was designed by CME software. For this purpose, (A) Find object tools was selected to mask objects in grayscale images based on the fluorescent intensity and area. (B) To do segmentation 'Find Blobs' were selected to detect nuclei staining, and 'Adaptive Threshold' was selected to detect actin staining. To mask nuclei and actin staining, 'Approximate Minimum and Maximum Width' of selected objects and the 'Level of Intensity above the Local Background' were defined. (C) Once all the objects of interests were marked, we decided what was going to be the 'Main objective' to measure the 'Features' within each object. Here our main object was nuclei mask and the features object we were looking for within them was GFP wavelength or actin. (D) Applying this measurement to each mask identified (E) cells positive for actin (yellow nuclei) or negative for actin (blue nuclei).

### **2.2.3.7 Cell proliferation assay in the presence of pharmacological inhibitors**

96-well plates were coated with ECM as described in section 2.2.2.1 and 2.2.2.2.  $10^3$  MDA-MB-231 cells/well were seeded in full growth media. After 5hrs incubation in 5% CO<sub>2</sub> and 37°C, full growth media was replaced with 200µL of the starvation media as shown in table 2.7. Either 10µM of GM6001 (MMP inhibitor), 0.5 µM PF573228 (FAK inhibitor), 200nM Bafilomycin A (V-ATPase inhibitor), 5µg/ml Filipin (lipid raft-mediated endocytosis inhibitor), or DMSO as control were added to each well every two days up to day six or day three for Bafilomycin A and Filipin. Sample fixation and staining was performed as described above in section 2.2.3.

### **2.2.4 Measurement of ECM consumption**

96-well plates were coated with 15µl/well of 2mg/ml collagen I and 3mg/ml Matrigel as described in section 2.2.2.1. Polymerized ECM were incubated with 50µl of 0.2µg/ml IRDye 800CW N-hydroxysuccinimidyl (NHS) ester reactive dye for 1hr at RT with gentle rocking. NHS reactive dyes bind to free amine groups on lysine residues and form a stable conjugate. Labelled matrices were left overnight in PBS at 5% CO<sub>2</sub> and 37°C. Cells were seeded the following day, and media was replaced with starvation conditions after 5hr. Cells were fixed on day 2 and day 8. Intensity of NHS-Ester bound to collagen I or Matrigel was quantified by imaging with the Licor Odyssey imaging system. The NHS was detected with 800nm channel with 200µm resolution. Image analysis was done by Image Studio Lite.

### **2.2.5 ECM cross-linking**

After ECM polymerisation/preparation as described in section 2.2.2, ECMs were treated with 10% glutaraldehyde for 30mins at RT, followed by two PBS washes. The cross-linker was quenched in 1M glycine at RT for 20 minutes, followed by two PBS washes. Cross-linked ECMs were kept in PBS at 5% CO<sub>2</sub> and 37°C over-night.

### 2.2.6 ECM uptake assay

To monitor the internalization of ECM, 3.5cm<sup>2</sup> glass-bottomed dishes were coated with either 100µl of 1mg/ml collagen I, 70µl of 3mg/ml Matrigel or 80µl of 3.5mg/ml laminin. Dishes coated with ECM were incubated at 5% CO<sub>2</sub>, and 37°C for 3hrs for polymerization. Following that, ECMs were labelled with 10µg/ml N-Hydroxysuccinimide-Fluorescein (diluted in PBS) for 1hr at RT on a gentle rocker, followed by two PBS washes. 10<sup>5</sup> MDA-MB-231 cells per dish were seeded in full growth media. After a 5hr incubation in 5% CO<sub>2</sub> and 37°C, full growth media were replaced with 1ml of the indicated starvation media in the presence of 20µM lysosome inhibitor (E64d) or DMSO (control). E64d and DMSO were added after two days, and cells were fixed at day three by adding 4% PFA for 15mins at RT followed by a PBS wash. To permeabilize, cells were treated with 0.25% triton X-100 for 5mins followed by two PBS washes. For actin cytoskeleton staining, cells were incubated with Phalloidin Alexa Fluor 555 diluted 1:400 in PBS for 10mins followed by two PBS washes and one wash with distilled water (dH<sub>2</sub>O). To avoid dryness and preserve the samples, 2-3 drops of Vectashield mounting medium containing DAPI were added to the dishes, which were then sealed with parafilm and kept at 4°C. Cells were visualised by confocal microscopy using a Nikon A1 microscope and 60x 1.4NA oil immersion objective. To cover the full area of cells, Z stacks with 1 µm intervals were collected. To quantify ECM uptake, a similar protocol to the one described in Comisso et al., 2014 was followed. ECM uptake was measured in ImageJ by specifying both cell area and then the area of ECM inside each cell and using the following formula for normalization.

$$\frac{ECM\ area}{Cell\ area} \times 100$$

To monitor internalization of cross-linked ECMs, ECM cross-linking (as described in section 2.2.5) was done after the ECMs were labelled with N-Hydroxysuccinimide-Fluorescein.

To track ECM uptake in the presence of MMP inhibition, 10µM of MMP inhibitor (GM6001) and 20µM E64d were added to the cells immediately after replacing the full growth media with the starvation conditions and 48hrs later.

### 2.2.7 Cell division assay (EdU labelling)

To monitor the cell's ability to proliferate, Click-iT EdU Imaging Kits (Invitrogen) were used. EdU (5-ethynyl-2'-deoxyuridine) is a nucleoside analogue of thymidine and is incorporated into the DNA during DNA synthesis. This labelling is based on a click reaction, a copper-catalysed covalent reaction between the EdU containing the alkyne and the Alexa Fluor 555 dye containing the azide.

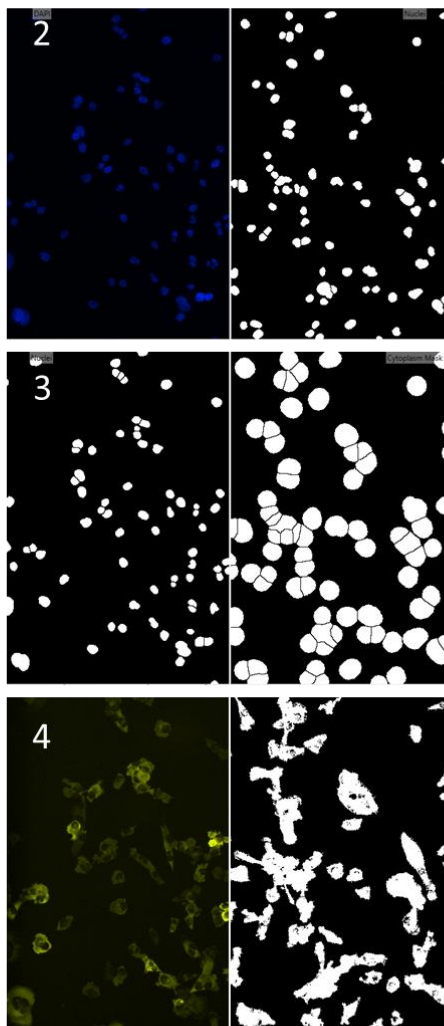
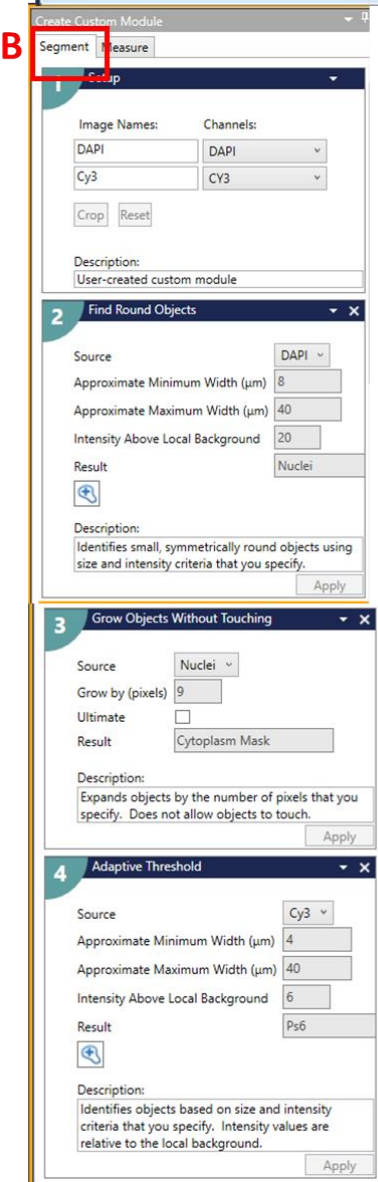
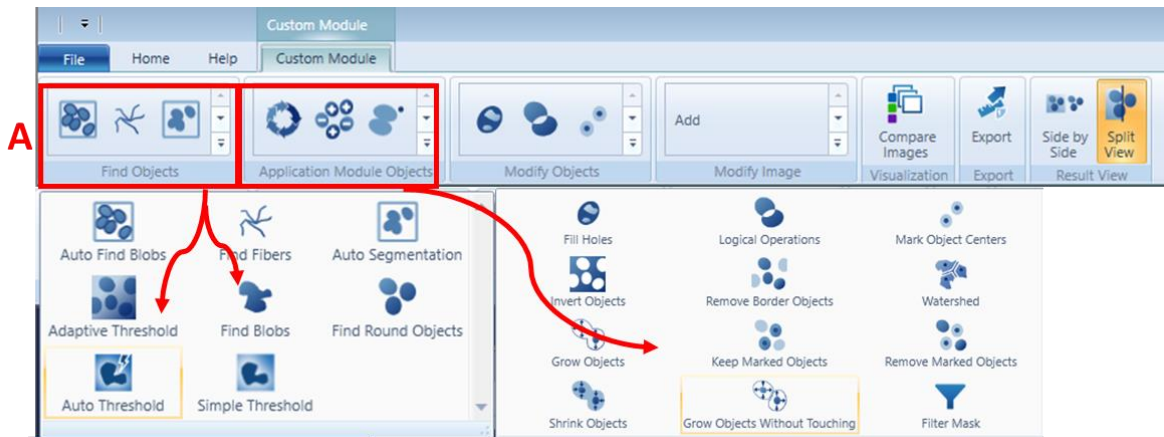
As described in section 2.2.2.1 plates were coated with desired ECM and  $10^3$  MDA-MB-231 cells/well were seeded under full growth media. After a 5hr incubation at 5% CO<sub>2</sub> and 37°C, the full growth media was replaced with 200µL of the starvation media (Table 2.7). At day six of starvation, cells were treated with 5µM EdU. To do this, 100µl of media from each well was removed and replaced by 100µl of fresh starvation media containing 10µM EdU. Cells were incubated with EdU for two days at 5% CO<sub>2</sub> and 37°C. At day eight, cells were fixed with 4% PFA containing 10µg/ml Hoechst 33342 for 15mins at RT followed by a PBS wash. To permeabilize, cells were treated with 0.25% triton X-100 for 5mins followed by two PBS washes and two washes with 3% bovine serum albumin (BSA). Cells were incubated with EdU detection cocktail (Invitrogen, Click-iT EdU Alexa Fluor 555) for 30 min at RT with gentle rocking. To prepare 1.5ml of total volume of the cocktail, following amounts of the kit components were mixed in order, 1290 µl 1x Click-iT reaction buffer (component D), 60 µl Copper (II) sulfate solution (Component E, 100 mM CuSO<sub>4</sub>) and 3.75 µl Alexa Fluor 555 azide (Component B, in 70 µl DMSO) and 150µl reaction buffer additive (Component F). Cells were washed twice with PBS and were kept in PBS for imaging. Images were collected by ImageXpress micro detecting DAPI and Cy3 wavelength through 2x objective and four fields per well were taken. Data analysis was done by MetaXpress and CME software. To measure the percentage of cells positive for EdU labelling, an algorithm was designed in CME which could detect all the nuclei (Figure 2.1) and the nuclei are positive for EdU.

### 2.2.8 Measurement of mTORC1 activity (p-S6 labelling)

We examined the rate of phosphorylation of an mTORC1 downstream target, ribosomal subunit S6 (p-S6), as an indicator for mTORC1 activity. Plates were coated with desired ECM as described in section 2.2.2.1, and  $10^3$  MDA-MB-231 cells/well were seeded in full growth

media. After a 5hr incubation at 5% CO<sub>2</sub> and 37°C, the full growth media was replaced with 200µL of the Gln, Glc, or AA starvation media. Where indicated, cells were incubated with either 200nM Bafilomycin A or DMSO as a control. Bafilomycin A or DMSO were added to the cells every day up to day three. Bafilomycin A is a V-ATPase inhibitor which causes deacidification of lysosome and consequently inhibits lysosomal degradation (Yoshimori et al., 1991). After three days of starvation, cells were fixed with 4% PFA containing 10µg/ml Hoechst 33342 for 15mins at RT followed by a PBS wash. To permeabilize, cells were treated with 0.25% triton X-100 for 5mins followed by two PBS washes. Unspecific binding sites were blocked by incubating with 3%BSA at RT with gentle rocking. Cells were incubated with the primary antibody, anti-Phospho-S6 Ribosomal protein, diluted 1:100 in PBS overnight at 4°C. The primary antibody was removed, and cells were washed twice with PBS for 5mins to 10mins each time. Cells were incubated with secondary antibody (anti-Rabbit IgG Alexa Fluor 594) diluted 1:1000 in PBS for 1hr at RT with gentle rocking. Cells were washed twice with PBS for 10 to 30mins and were kept in PBS for imaging. Images were collected by ImageXpress micro detecting DAPI and Cy3 wavelengths through 10x objective and around 48 fields per well were taken. Image analysis was done by MetaXpress and CME software. To measure the intensity of p-S6 labelling, an algorithm was designed to detect and mask the DAPI wavelength (Nuclei) as the main objects. Because S6 is a cytoplasmic protein, the masks detecting the nuclei were grown to cover the cytoplasmic area as well. Then the grown nuclei masks were used as the main objects and Cy3 (p-S6 labelling) wavelength integrated intensity was detected as a feature within each object (Figure 2.2).





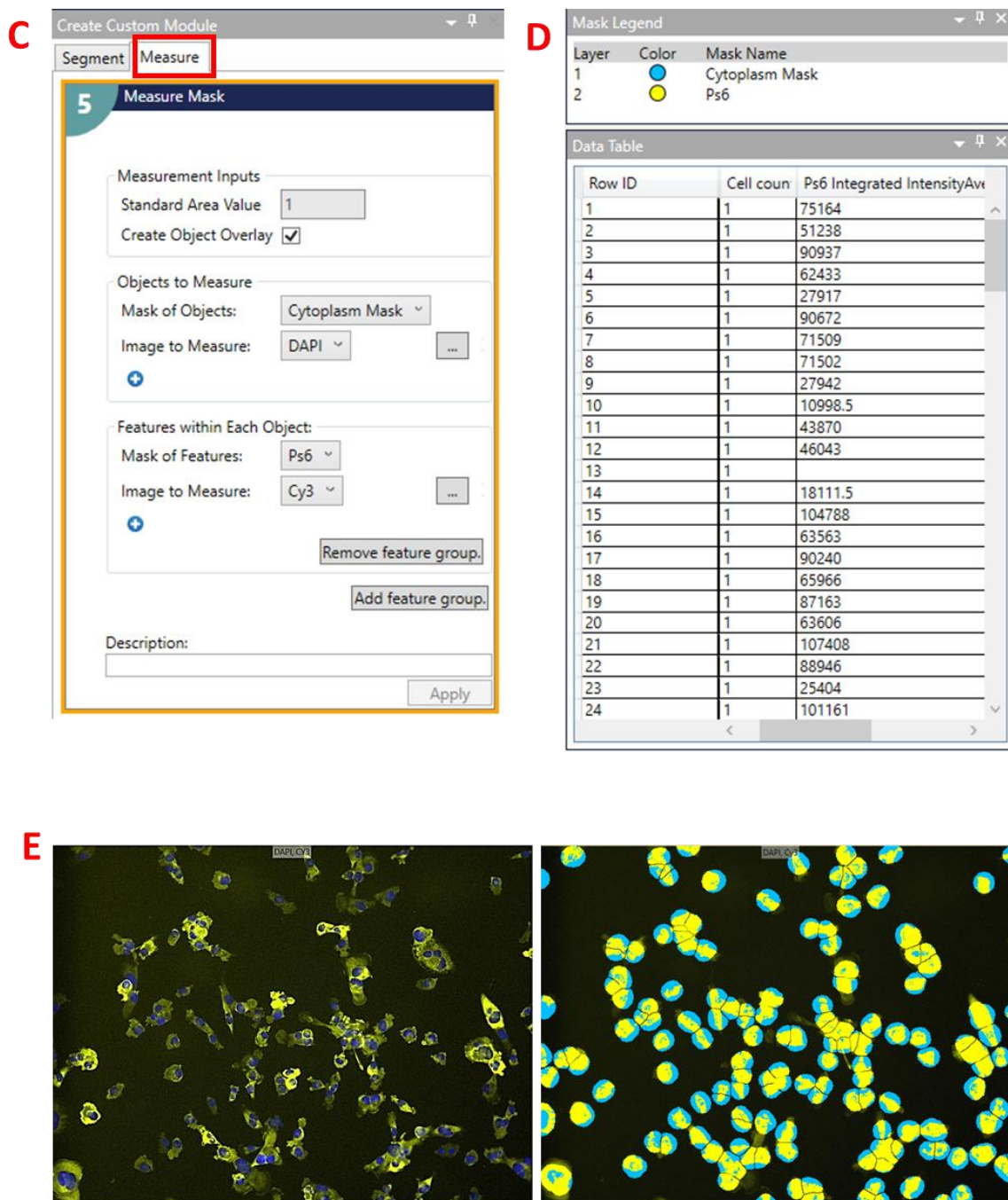


**Figure 2.2. Designing algorithm by CME to detect the intensity of p-S6 staining per cell.** (A and B) Find object tools was selected to mask objects in grayscale images based on the fluorescent intensity and area. To do the segmentation 'Find Blobs' were selected to detect nuclei staining, 'Grow Objects Without Touching' was used to grow the nuclei mask to cover the cytoplasm (cytoplasm mask), and 'Adaptive Threshold' was used to mask p-S6 staining. To mask objects, 'Approximate Minimum and Maximum Width' of selected objects and the 'Level of Intensity above the Local Background' were defined. (C) 'Cytoplasm mask' was considered as 'Main object' to measure integrated intensity of p-S6 (Features within each object) within. (D and E) Applying this measurement to each mask identifies the intensity of p-S6 per cell (yellow area within each mask).

### 2.2.9 Measurement of cell apoptosis

Plates were coated with desired ECM as described in section 2.2.2.1,  $10^3$  MDA-MB-231 cells/well were seeded in full growth media. After 5hrs incubation at 5% CO<sub>2</sub> and 37°C, the full growth media was replaced with 200µL of the starvation media (Table 2.7). Cells were kept under starvation conditions either for 3 or 8 days. At day 3 or 8, the starvation media were replaced by 5µM CellEvent™ Caspase-3/7 Green Detection Reagent diluted into PBS, containing calcium and magnesium, and 5% DFBS for 1.5hrs at 5% CO<sub>2</sub> and 37°C. Cells were fixed with 4% PFA containing 10µg/ml Hoechst 33342 for 15mins at RT followed by a PBS wash. Images were collected by ImageXpress micro detecting DAPI and GFP wavelengths through 10x objective and around 20 fields per well were imaged. Image analysis was done by MetaXpress and CME software. To measure the percentage of cells positive for Caspase-3/7, an algorithm was designed to detect and mask the DAPI wavelength (Nuclei) as the main objects. Because Caspase-3/7 is a cytoplasmic protein, the masks detecting the nuclei were grown to cover some cytoplasm. Then the grown nuclei masks were used as the main objects to detect GFP (Cas-3/7 labelling) wavelength as a feature within each object.

### 2.2.10 Glucose uptake assay

96-well plates were coated with collagen I and Matrigel, cells were seeded and starved as described in section 2.2.9. Cells were kept under starvation conditions either on ECM or plastic for six days. At day six, 100µM of 2-(N-(7-Nitrobenz-2-oxa-1,3-diazol-4-yl) Amino)-2-Deoxyglucose (2-NBDG) was added to the cells for 1hr at 5% CO<sub>2</sub> and 37°C. The media was removed, and cells were washed twice with ice-cold PBS. Cells were fixed with 4% PFA containing 10µg/ml Hoechst 33342 for 15mins at RT followed by a PBS wash. Cells were then incubated for 1hr with Phalloidin Alexa Fluor 647 diluted 1:400 in PBS, followed by two PBS washes. Images were collected by ImageXpress micro and analysed by MetaXpress and CME software. To measure the intensity of 2-NBDG staining, an algorithm was designed to detect and mask DAPI wavelength (Nuclei staining) as the main objects. Because 2-NBDG is found in the cytoplasm, the masks detecting the nuclei were grown to cover the cytoplasm. Then grown nuclei masks were used as the main objects to detect Cy3 (2-NBDG) wavelength integrated intensity as a feature within each object.

### 2.2.11 Live imaging of ATP content

96-well plates were coated with collagen I or Matrigel as described in section 2.2.2.1.  $10^3$  MDA-MB-231 cells/well were seeded in full growth media. After 5hrs incubation in 5% CO<sub>2</sub> and 37°C, the full growth media was replaced with 200µL of the starvation media (Table 2.7). Cells were kept under the indicated starvation conditions either for 3 or 8 days. At day 3 or 8, 126.4µM Oligomycin A were added to the cells for 1hr at 5% CO<sub>2</sub> and 37°C. The control group received DMSO as a vehicle. 10µM BioTracker ATP-Red Live Cell Dye was added to the cells for 15min at 5% CO<sub>2</sub> and 37°C. The media was removed, and cells were washed with PBS. Cells were incubated with complete media without phenol red containing 10µg/ml Hoechst 33342 for 15min at 5% CO<sub>2</sub> and 37°C, then washed and replaced by complete media with no phenol red and no Hoechst for imaging. Live-cell imaging was performed with ImageXpress micro detecting DAPI and Cy3 wavelengths through a 10x objective and around 48 fields per well were imaged. Image analysis was done by MetaXpress and CME. To measure the intensity of cells positive for BioTracker ATP-Red Live Cell Dye, a similar algorithm to the one described in section 2.2.8 was used in which the integrated intensity of the Cy3 wavelength was detected as a feature within each object.

### 2.2.12 Western blot

MDA-MB-231 cells were trypsinized and  $10^6$  cells were collected in each Falcon tube. Cells received 0.2, 0.5, 0.7 and 1µM P573228 (FAK inhibitor) for 30mins at 5% CO<sub>2</sub> and 37°C, while they were kept in suspension. Cells were transferred to a 6-well plate which had been coated with 900µL of 0.5mg/ml collagen I. Cells were allowed to adhere to collagen I for 30 mins at 5% CO<sub>2</sub> and 37°C. The media was aspirated, and cells were put on ice. After two washes with ice-cold PBS (~2ml), 100µl per well of lysis buffer (50mM Tris pH7 and 1% SDS) were added and lysates were collected and transferred to QiaShredder columns, which were spun for 5mins at 6000rpm. The filter was discarded, and the extracted proteins were kept at -20°C.

To run the samples, 12% gels were prepared. 10ml of resolving gel containing 3.3ml H<sub>2</sub>O, 5ml of 30% acrylamide mix, 2.5ml of 1.5 M Tris (pH 8), 0.1ml of 10% ammonium persulfate and 0.004ml of tetramethylethylenediamine (TEMED) were prepared. 5ml of resolving gel were added to each cast for 30mins at RT. After polymerization, 2ml of stacking gel was added on

top. 4ml of stocking gel contained 2.7ml H<sub>2</sub>O, 0.67ml of 30% acrylamide mix, 0.5ml of 1 M Tris (pH 6.8), 0.04ml of 10% ammonium persulfate and 0.004ml of TEMED.

Samples were fully thawed at RT. 15µl of 2x sample buffers were added to 15µl of each sample and were heated at ~70°C for 5 min. 30µl of sample and 8µl of protein ladder were loaded into the 12% gel and ran at 100V for ~2hr 30min. Proteins were transferred from the gel to FL-PVDF membranes in a transfer buffer for 75mins at 100V. Membranes were washed three times with TBS-T (Tris-Buffered Saline, 0.1% Tween) and blocked in 5% w/v skimmed milk powder in TBS-T for 1hr at RT. Membranes were then incubated with primary antibodies, 1:500 GAPDH and 1:1000 pFAK in TBS-T + 5%w/v skimmed milk overnight at 4°C. Membranes were washed three times in TBS-T for 10min on the rocker at RT. Membranes were incubated with secondary antibodies, IRDye® 800CW anti-mouse IgG for GAPDH (1/30,000) and IRDye® 680CW anti-rabbit IgG for pFAK (1/20,000) in TBS-T + 0.01% SDS, for 1hr at RT on the rocker. Membranes were washed three times in TBS-T for 10min on the rocker at RT followed by being rinsed with water. Images were taken at the Licor Odyssey system. Each band intensity was quantified with the Image Studio Lite software.

### **2.2.13 Quantification of cellular focal adhesion content**

35mm<sup>2</sup> glass-bottomed dishes were coated with ECM. 4x10<sup>4</sup> MDA-MB-231 cells were seeded and incubated at 5% CO<sub>2</sub> and 37°C for 5hrs. The full growth media was then replaced with AA starvation condition. After three days of starvation, cells were fixed with 4%PFA for 15 mins and permeabilized with 0.25% triton X-100 for 5mins, followed by 1hr incubation in 3% BSA as a blocking buffer. Cells were incubated with anti-mouse Paxillin primary antibody (1:200 dilution in PBS) at RT for 1hr. Cells were washed three times with PBS for 20mins and incubated with Alexa-Fluor 488 α-Mouse IgG secondary antibody (1:1000 dilution in PBS) for 1hr at RT with gentle shaking and protected from light. Cells were washed twice with PBS and once with H<sub>2</sub>O. Vectashield mounting reagent containing DAPI was added on top. Cells were visualised by confocal microscopy using a Nikon A1 microscope and 60x 1.4NA oil immersion objective. To quantify the number of focal adhesions, both cell and paxillin area for each cell were measured. Then, areas of paxillin were normalized by cell area as described in section 2.2.6.

## 2.2.14 Mass spectrometry

### 2.2.14.1 Non-targeted metabolite profiling

MDA-MB-231 cells were seeded on 96-well plates coated with ECM under the full growth media. After a 5hr incubation at 5% CO<sub>2</sub> and 37°C, the full growth media was replaced with the starvation media. Cells were kept under starvation for six days; the media was removed, and cells were washed with ice-cold PBS three times. The PBS were aspirated very carefully after the last wash to remove every remaining drop of PBS. The extraction solution (cold; 5 MeOH: 3 AcN: 2 H<sub>2</sub>O) was added for 5min at 4°C with low agitation. Metabolites were transferred to eppendorf tubes and centrifuged at 4°C and 14000 rpm for 10 mins. Each sample was transferred into HPLC vials. The samples were directly injected into a Waters G2 Synapt mass spectrometer in electrospray mode within the Sheffield Faculty of Science Mass Spectrometry Centre. Three technical replicates of each sample were run, technical replicates were a combination of nine individual wells, and the replicates were combined to obtain an average intensity. The dataset only includes peaks present in all three replicates. The intensity is a measure of abundance of any particular mass. The data is binned into 0.2amu m/z bins and the m/z in each bin is used to identify putative IDs using the HumanCyc database.

### 2.2.14.2 Data analysis

The mass spectrometry data were analysed using Perseus software version 1.5.6.0. There were three samples for each group. First, each group was defined for the late t-test. Here, we had two groups that each contained three technical repeats. Then, the minimal number of valid values that each row needs to have in the expression columns to survive the filtering process was defined, which was 3 in this study. The intensity of each metabolite was normalized by the median intensity of all the metabolites in each sample/column. T-test was done between two groups of samples to show the differences between their metabolic contents. To do the t-test, S0, which defines the artificial within groups variance, was set to 0.1 and false discovery rate (FDR) to 0.05. Hence, test results below p<0.05 were reported as significant. To find the metabolic pathways being upregulated in cells on ECM compared to the plastic, the metabolites significantly upregulated in MDA-MB-231 cells on ECM were compared to homo sapiens KEGG pathway library via <https://www.metaboanalyst.ca/> to find pathways with significantly higher enrichment, p<0.05.

### **2.2.14.3 Targeted metabolite profiling**

MDA-MB-231 cells were seeded on 6-well plates coated with ECM under full growth media. After a 5hr incubation at 5% CO<sub>2</sub> and 37°C, the full growth media were replaced with the AA starvation media. Cells were kept under starvation for six days; the media was removed, and metabolites were extracted as described above (section 2.2.14.1). Then, mass spectrometer Waters Synapt G2-Si coupled to Waters Acquity UPLC was used to separate phenylalanine, tyrosine and fumaric acid with Column Waters BEH Amide 150x2.1mm. The injection was 10µl. The flow rate was 0.4ml/min. To identify the targeted metabolites, the retention time of the compound coming off the column and the mass of the compound were matched with the standards.

### **2.2.15 RNAi screen**

#### **2.2.15.1 Optimisation of RNAi-mediated gene knockdown**

Glass-bottomed 384-well plates were coated with 5µl 2mg/ml collagen I and 5µl 3mg/ml Matrigel. 5µl of 150nM siGlo, SiGenome control Non-Targeting siRNA, SiGenome Smart Pool Human UBB or SiGenome Smart Pool Human PLK1 were added on top of the ECMs. 0.06µl of DharmaFect 1 (DF1) (Transfection reagent) was diluted in 4.94µl of DMEM. 5µl of diluted DF1 were transferred to each well. Plates were left 30mins inside the hood at RT to let the siRNA and DF1 make complexes.  $6 \times 10^2$  cells in 15µl DMEM media containing 10%FBS, but no antibiotics, were transferred to each well. The final concentration of siRNA reached 30nM. Cells were transferred to the incubator with 5% CO<sub>2</sub> and 37°C over-night. The full growth media was replaced by 50µl of fresh complete or NEAA starvation media. After 3 or 6 days, cells were fixed and incubated with 10µg/ml Hoechst 33342 and Phalloidin Alexa Fluor 555 1:400 in PBS for 30mins followed by two PBS washes. Images were collected by ImageXpress micro and analysed by MetaXpress and CME software. To measure the number of cells showing siGlo uptake, an algorithm was designed to detect Cy3 wavelength (actin) as the main object. Then, GFP wavelength (siGlo) was detected as a feature within each main object.

### 2.2.15.2 High throughput RNAi screening

The non-target (Nt) siRNA showing highest compatibility to MDA-MB-231 cells were chosen from ON-TARGET plus Non-targeting Control siRNAs (Dharmacon) from pools #1 to #5. For the screening, two 384-well plates containing 150nM siRNA library for Traffic-ome (Dharmacon ON-TARGETplus siGENOME® Human siRNA Library) (Table 2.12) were used. This library was already prepared and frozen at -80°C by Sheffield RNAi Screening Facility (SRSF). The library was designed by Professor Elizabeth Smyth and Dr Andrew Peden (University of Sheffield, Department of Biomedical Science). The screening was done on MDA-MB-231 cells, which were split the day before to have 70%-80% confluence at the screening start day. siRNA libraries were thawed and centrifuged for 1minute to avoid loss of any siRNA. 5µl of diluted DF1 were added to each well as described in section 2.2.15.1. 15µl of complete media with no antibiotic were added to each well. The final siRNA concentration reached to 30nM in each well with the addition of DF1 and media. 15µl of media containing  $7 \times 10^2$  MDA-MB-231 cells were added per well in two separate glass-bottomed 384-well plates pre-coated with 5µl 3mg/ml Matrigel. Cells were incubated for 5hrs at 5% CO<sub>2</sub> and 37°C. After the cells were attached to the Matrigel, the media was fully removed. 30nM siRNA library was transferred to the cells on ECM by the Hamilton robot. Cells were incubated at 5% CO<sub>2</sub> and 37°C overnight. Full growth media was replaced by 50µl of NEAA free media or fresh complete media the day after. Cells were incubated for 6 days at 37°C and 5% CO<sub>2</sub>. On day 6, cells were fixed with 4% PFA, stained with Hoechst 33342 and imaged by ImageXpressmicro with a 2× objective and DAPI filters.

#### 2.2.15.2.1 Traffic-ome screen.

**Table 2.12. Name, ID, and sequence of genes participating in Traffic-ome siRNA library.**

Gene symbol	Gene ID	Gene accession	GI number	Sequence
STX1A	6804	NM_004603	4759181	GGAACACGCGGUAGACUUAU
STX2	2054	NM_001980	37577286	UAGACAAGCUCUCAUGAA
STX3	6809	NM_004177	34147491	GAUCAUUGACUCACAGAUU
STX4	6810	NM_004604	34147603	GGACAAUUCGGCAGACUUAU
STX5	6811	NM_003164	94400931	CAGAACAUUGAGUCGACAA
STX6	10228	NM_005819	58294156	GCAGUUAUGUUGGAAGAUU
STX7	8417	NM_003569	4507294	GAGUUUGUUGCUCGAGUAA
STX8	9482	NM_004853	4759187	AAUGAAACCAGGCGGGUAA



STX10	8677	NM_003765	4507284	GGAAGAGACCAUCGGUAUA
STX11	8676	NM_003764	33667037	AGCACUGAAUAUCGAACAA
STX12	23673	NM_177424	28933464	CCACAAAUCAGCUCGCCAA
STX16	8675	NM_001001434	47778944	GUAUGAUGUUGGCCGGAUU
STX17	55014	NM_017919	8923603	CGAUCCAAUAUCCGAGAAA
STX18	53407	NM_016930	39725935	CUGUCUGAGUCAACGAAUA
STX19	415117	NM_001001850	49258195	GAGAAGGUUUAGUCUACUU
SNAP23	8773	NM_130798	18765730	UAACAGAACUCAACAAAUG
SNAP25	6616	NM_130811	18765734	CUGGAAAGCACCCGUCGUA
SNAP29	9342	NM_004782	18765736	GAAGCUAUAAGUACAAGUA
SNAP47	116841	NM_053052	26024192	CCACUCACCUUACGAAAUU
VAMP1	6843	NM_016830	40549443	UACAUGACCAGUAACAGA
VAMP2	6844	NM_014232	7657674	GCGCAAUACUGGUGGAAA
VAMP3	9341	NM_004781	42544205	GGAUUACUGUUCUGGUUUAU
VAMP4	8674	NM_003762	42544206	CAACUUCGAAGGCAAUUGU
VAMP5	10791	NM_006634	31543930	UGACGGAAUUAUGCGUAA
VAMP7	6845	NM_005638	27545446	GUACUCACAUGGCAUUUAU
VAMP8	8673	NM_003761	14043025	CCACUGGUGCCUUCUCUUA
YKT6	10652	NM_006555	34304384	GCUCAAAGCCGCAUACGAU
SEC22A	26984	NM_012430	14591918	GGGCAAGGCUCGCCGAUUUAU
SEC22B	9554	NM_004892	34335289	AAUAGUGUAUGUCGGAUUC
SEC22C	9117	NM_032970	21536309	CCUCCAGGCCAUACGCUUU
BET1	10282	NM_005868	83779007	GGAACUAUGGCUAUGCUAA
BET1L	51272	NM_016526	34365798	UCCCUUAGGACUCGGAUUU
GOSR2	9570	NM_054022	60499002	ACGAAUCACUGCAGUUUAA
GOSR1	9527	NM_001007025	55770857	CAGAAGAACUGAGCUAUUU
VT11A	143187	NM_145206	21624647	CGUGAAAGACUUCGGGAAA
VT11B	10490	NM_006370	5454165	CCAAAGUAUUGAACGUUCU
USE1	55850	NM_018467	49574516	UGAAGGUCCACGCGAGCAA
BNIP1	662	NM_013978	153946402	GGUCCUCUAUAUUGUGAAA
STXBP1	6812	NM_001032221	73760414	GGACCUUGUUUGUCGAAGA
STXBP2	6813	NM_006949	5902127	GAGCGGAGUUAUUCGGAGU
STXBP3	6814	NM_007269	6005885	AGAGUGACAUGAUUCGUAA
VPS33A	65082	NM_022916	91206458	GGGCGUAACCUUCGCUGAA
VPS33B	26276	NM_018668	18105057	CCAGUAUGAUCGCCGGAGA
VPS45	11311	NM_007259	91822913	GCAUAAACAACAAUCGGAU
SCFD1	23256	NM_182835	33469977	AAGCAUUGGUGCACAUGU
EXOC6	54536	NM_001013848	62243651	GAUAAUUGCUGUCCUAGA
EXOC7	23265	NM_015219	62241043	CUAAGCACCUAUAUCUGUA
STXBP6	29091	NM_014178	46048194	GGUUAUUGGUAUCGAUCCU
STXBP5L	9515	XM_938898	88970941	AGACACGGCCAGUGCGAAU

GOPC	57120	NM_001017408	62868212	GGCCUUGGCAUUUCAUUA
RABEP1	9135	NM_004703	49574500	UGAGAGACAUGCAGCGAAU
GAPVD1	26130	NM_015635	51093831	AAGAAGUGGCCAAUCGAUA
RABGEF1	27342	NM_014504	7657495	AAAUUAAGCCUCCGAUUA
RIN1	9610	NM_004292	68989255	AGAAGCUGCUGUCGCCUAA
RIN2	54453	NM_018993	35493905	GGUCUGGACAAGCGAGGAA
RIN3	79890	NM_024832	40353728	UCAGAUUGAUUGCGUUCUA
ALS2	57679	NM_020919	40316934	GAAUGUGUCCUUCGACUAA
SH3GL2	6456	NM_003026	4506930	CAACCUAAACCACGAAUGA
RAB22A	57403	NM_020673	34577103	GGACUACGCCGACUCUAUU
RAB21	23011	NM_014999	7661921	GAUAACUGUUCACGCCUAA
RAB31	11031	NM_006868	33589860	UGAAGGAUGCUAAGGAAUA
ARHGAP26	23092	NM_015071	32189359	GCACUACUGUACAUUAUCAA
SNX9	51429	NM_016224	23111056	GUAACCGGAUCUAUGAUUA
EHD1	10938	NM_006795	30240931	CCGCAAGCUCAACGCGUUU
MICAL1	64780	NM_022765	20127615	UGGAGAACAUUGUGUACUA
APPL2	55198	NM_018171	82617617	CUAGUAGAGAUGC GCGAUA
RBSN	64145	NM_022340	70980546	CGUGAAGCUCUACGAGAAA
OCRL	4952	NM_001587	21396492	GAACGAAGGUACCGGAAAG
PICALM	8301	NM_001008660	56788367	CAACAGGCAUGAUAGGAUA
RAPH1	65059	NM_025252	47132517	GGAAACAGUAAGCGUCAAA
ARHGDI1	396	NM_004309	34147601	GGUGUGGAGUACCGGAUAA
FLOT1	10211	NM_005803	6552331	GCAAGAGAAGUCCCAACUAA
ANKFY1	51479	NM_020740	31317251	GGUGUUAUGUCUCUAGUGA
APPL1	26060	NM_012096	6912241	GAAACUAUGCGCCAAAUUCU

### 2.2.15.3 HPD and HPDL RNAi-mediated gene knockdown

Glass-bottomed 96-well plates were coated with 15µl 2mg/ml collagen I. 20µl of 150nM ON TARGET plus Human HPDL and HPD smart pool were added on top of the ECM. 0.24µl of DF1 was diluted in 19.86µl of DMEM. 20µl of diluted DF1 were transferred to each well. Plates were left 30mins inside the hood at RT to let DF1 and siRNAs make complex.  $3 \times 10^3$  cells in 60µl DMEM media containing 10%FBS, but no antibiotics, were transferred to each well. The final concentration of siRNA reached 30nM. Cells were transferred to the incubator with 5% CO<sub>2</sub> and 37°C over-night. The full growth media was replaced by 200µl of fresh complete or depleted media for up to 6 days. At day 2 and 6, cells were fixed and incubated with 10µg/ml

Hoechst 33342. Images were collected by ImageXpress micro and analysed by MetaXpress and CME software.

### **2.2.16 Statistical analysis**

Graphs were created by GraphPad Prism software and t-test and ANOVA tests were performed. To compare two datasets, an unpaired t-test was performed. To compare more than two data set, one-way ANOVA was used when there was one independent variable. Two-way ANOVA was performed when there were two independent variables. Statistical analysis for non-targeted metabolic profiling was performed by Perseus software and used Student t-test (described in section 2.2.14.2).

## Chapter 3: The extracellular matrix supports breast cancer growth under amino acid starvation by regulating tyrosine metabolism.

This result chapter is prepared in a format of paper which is soon going to be published in bioRxiv.

Mona Nazemi conceived, planned, and carried out most of the experiments. Montserrat Llanses Martinez performed an experiment for Matrigel uptake in the presence of Filipin (Figure 5H). Heather Walker ran Mass-spectrometry for the samples (Figure 7 and Supplementary Figure 5).

### Abstract

Breast cancer tumours are embedded in a collagen I rich the extracellular matrix (ECM) network where nutrients are scarce due to angiogenesis deficiency and elevated tumour growth. Metabolic adaptation is required for the breast cancer cells to endure this condition. Here, we demonstrated the presence of ECM rescued cell growth under amino acid (AA) starvation, through a mechanism that required ECM uptake. ECM internalisation, followed by lysosomal degradation, contributed to upregulation of amino acid content in the cells, including tyrosine and phenylalanine. Finally, we revealed that cells on ECM increased the phenylalanine and tyrosine metabolism pathway, potentially feeding into the TCA cycle via fumarate production. Interestingly, this pathway was required for ECM-dependent cell growth under amino acid starvation. Collectively, our results highlight that the ECM surrounding breast cancer tumours represents an alternative source of nutrients to support cancer cell growth by regulating phenylalanine and tyrosine metabolism.

### Introduction

Breast cancer is the most common type of cancer among women. In 2012 around 1.7 million women were diagnosed with breast cancer with 521,900 deaths worldwide (Coughlin, 2019). There are different factors that increase the risk of breast cancer, including the density of stroma around the tumour (Provenzano et al., 2008, Kim et al., 2014). There is growing evidence that the tumour microenvironment (TME) facilitates tumour growth and survival (Hanahan and Coussens, 2012). The TME consists of stromal cells and extracellular matrix (ECM). The ECM is a highly dynamic three-dimensional network of macromolecules providing structural and mechanical support to the tissues while interacting with cells through different receptors (Bergamaschi et al., 2008, Insua-Rodriguez and Oskarsson, 2016). In breast cancer, high breast tissue density is associated with a shift to malignancy and invasion. In malignant tumours, mRNA expression of procollagen I and III is higher compared to benign tumours (Kauppila et al., 1998). Increase in secretion of collagen is linked to higher adhesion, sprouting and invasiveness of breast cancer cells (Kim et al., 2014, Liverani et al., 2017, Provenzano et al., 2008). The stroma of mammary glands during post-lactational involution, with high level of fibrillar collagen and proteolytic fragment of fibronectin and laminin, also supports breast cancer metastasis (McDaniel et al., 2006).

Due to angiogenesis deficiency, the TME is usually nutrient deprived (Baluk et al., 2005, Nagy et al., 2010). Different studies showed that cancer cells benefit from extracellular proteins

during food scarcity (Muranen et al., 2017, Palm et al., 2015, Rainero et al., 2015b). The main biosynthetic needs of cells are accomplished by glucose (Glc) and glutamine (Gln) uptake working as carbon building blocks for macromolecules production (Pavlova and Thompson, 2016). Gln is the most abundant amino acid (AA) in the plasma providing reduced nitrogen as a building block of nitrogen-containing compounds including non-essential AAs (NEAAs), pyrimidine and purine nucleotides (Nicklin et al., 2009, Bergstrom et al., 1974). Even though Gln is known as a NEAA, proliferative cells such as cancer cells need the external sources to meet their high demand (Lacey and Wilmore, 1990). Although cancer cells are mainly dependent on their microenvironment to provide the nutrients, tumour blood vessels are highly branched, leaky, enlarged with inconsistent blood flow, resulting in inefficient nutrient transportation and starvation (Nagy et al., 2010, Baluk et al., 2005). One of the cancer hallmarks is the reprogramming of energy metabolism, which provides metabolic flexibility allowing the cells to adapt to different nutrient conditions (Hanahan and Weinberg, 2011). There are alternative sources that cancer cells can benefit from during starvation. In Ras-driven pancreatic ductal adenocarcinoma cells (PDACs) AA and Gln starvation induced albumin and collagen internalization respectively, followed by lysosomal degradation and AA extraction (Commisso et al., 2013, Kamphorst et al., 2015, Palm et al., 2015, Olivares et al., 2017). Serum and growth factor (GF) starvation also induced normal mammary epithelial cells to uptake laminin to raise their AA content (Muranen et al., 2017). Despite this growing data, the role of internalization of different components of the ECM in breast cancer cells' metabolism and regulatory mechanisms of this process have not been addressed in detail yet.

To determine whether the ECM surrounding breast cancer cells could provide a metabolically favourable microenvironment, here we investigated the effect of the presence of ECM on breast cancer growth and metabolism under Gln and full AA starvation. We found that the growth of starved invasive breast cancer cells, but not non-transformed mammary epithelial cells or non-invasive breast cancer cells, could partially be rescued by the presence of different types of ECM. Indeed, Matrigel and collagen I induced MDA-MB-231 cell division and enhanced mTORC1 activity under AA starvation. Interestingly, ECM endocytosis was required for cancer cell growth under starvation, as matrix cross-linking or reduction of ECM internalisation by the endocytosis inhibitor, Filipin, significantly reduced ECM-dependent cell growth. Moreover, examining metabolic content of cells on collagen I and Matrigel, compared to plastic, showed higher AA content and upregulation of phenylalanine and tyrosine metabolism during AA scarcity. Phenylalanine and tyrosine metabolism can lead to the production of the TCA cycle intermediate fumarate, resulting in higher cell growth. Indeed, inhibition of tyrosine and phenylalanine metabolism opposed ECM-dependent breast cancer cell growth under AA starvation.

## Results

### **The presence of ECM partially rescued breast cancer cell growth under starvation conditions.**

To assess whether the presence of ECMs could help survival or growth of invasive breast cancer cells under nutrient deprivation, MDA-MB-231 cells were seeded either on plastic or different components of the ECM under Gln or AA deficiency condition. Observing cell growth on collagen I, Matrigel and laminin in comparison to the plastic displayed consistent results.

MDA-MB-231 cells showed significantly higher cell number and growth rate in plates coated with collagen I, Matrigel and laminin compared to the cells on plastic after eight days of Gln or AA starvation (Figure 1A-F). Our data also indicated that receiving all the essential nutrients make cell growth independent of ECM, as there were no remarkable differences in cell number on ECM compared to the plastic under the complete media (Supplementary figure 1A-C). To test the effect of Gln and AA deficiency on the cell growth in a more physiologic condition, MDA-MB-231 were seeded on matrices derived from normal telomerase-immortalized fibroblasts (TIFs) or cancer associated fibroblasts (CAFs) extracted from the breast tumours. There are different studies showing that the ECM surrounding tumours released by CAFs has different structure and composition compared to the ECM derived from normal fibroblasts (Pankova et al., 2016, Hanley et al., 2016). Desmoplastic stroma around the tissue usually correlates to poor prognosis and severe cancer (Saadi et al., 2010, Surowiak et al., 2007). Here, cell derived matrices (CDM) from TIFs rescued the growth of cells under Gln deficiency but not AA starvation, whereas, on CAF-CDM cell number was significantly higher after eight days of Gln or AA starvation (Figure 1G-H). This data implies that CAF-CDM might provide a more favourable environment for cancer cells' growth compared to the TIF-CDM under AA deprivation. In parallel, to reproduce the *in vivo* metabolic environment, Plasmax, a physiological medium, was used. Plasmax is designed to contain metabolites and nutrients at the same concentration of human blood to avoid adverse effects of commercial media on cancer cells (Vande Voorde et al., 2019). To simulate starvation conditions, Plasmax was diluted with PBS. Our data from cell growth on diluted Plasmax showed that cells on collagen I, Matrigel and CAF-CDM had significantly better growth compared to the cells on plastic (Figure 1I-J). Taken together, these data demonstrate that the presence of ECM positively affected invasive breast cancer cell growth under nutrient depletion condition.

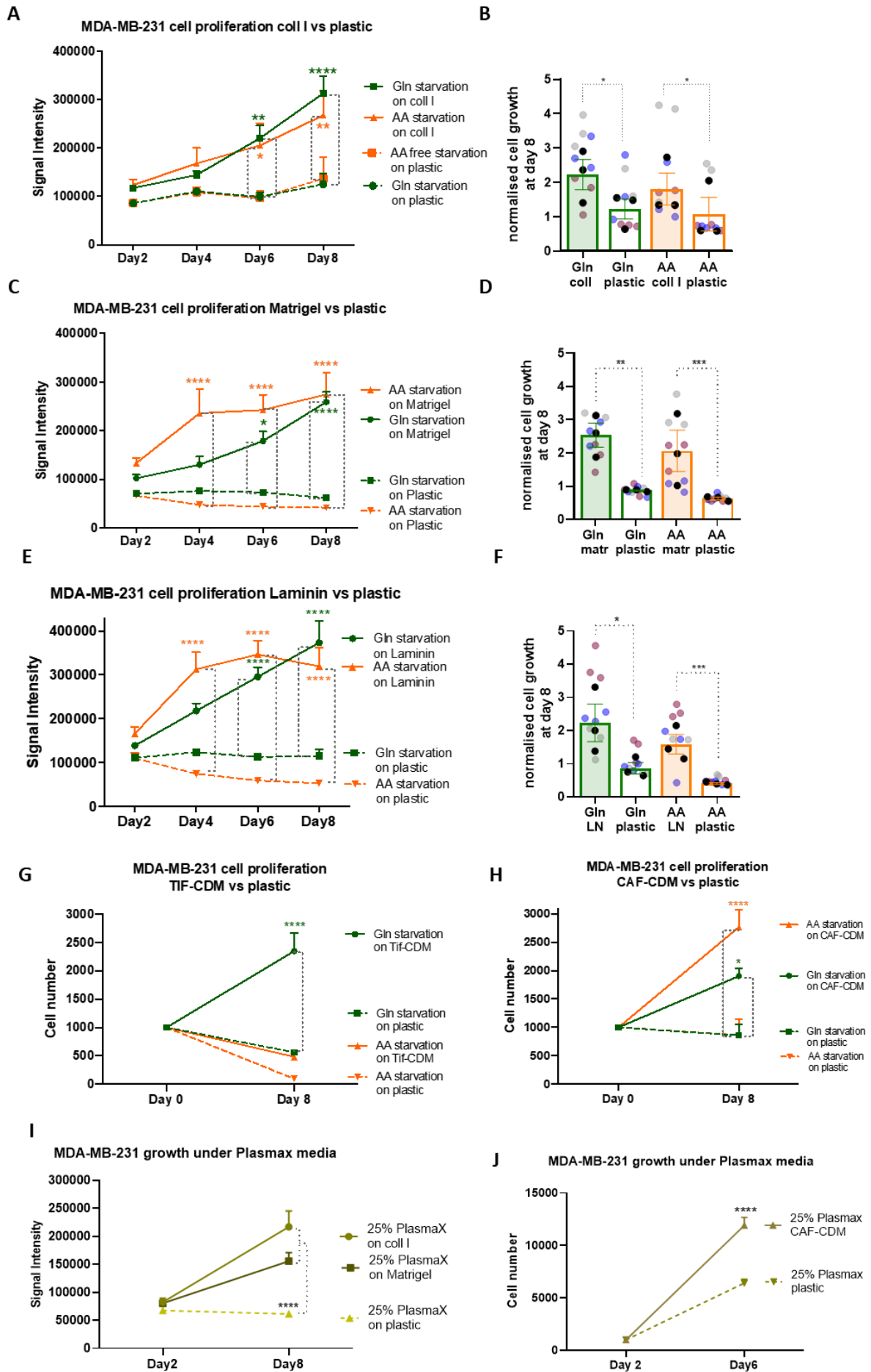


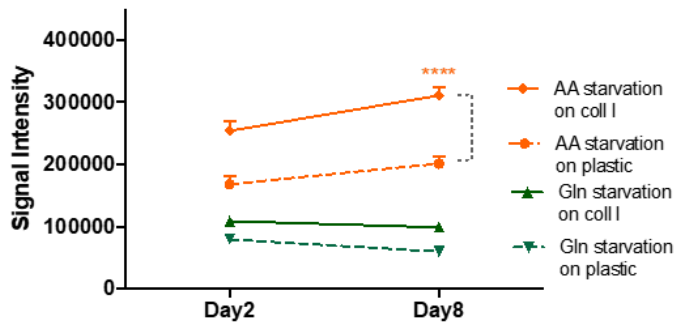
**Figure 1. The ECM rescued cell growth under starvation conditions.** MDA-MB-231 cells were seeded either on plastic or on plates coated with (A-B) collagen I (2mg/ml), (C-D) Matrigel (3mg/ml) and (E-F) laminin/entactin (3.5mg/ml) for eight days under glutamine (Gln) and amino acid (AA) starvation. Cell proliferation was measured by DRAQ5 nuclear staining quantification with the Licor Odyssey system every two days up to day eight. Signal intensity from cells under each condition were collected by Image Studio Lit software. (G) MDA-MB-231 cells were seeded either on plastic or plates containing TIFs-CDM or (H) CAF-CDM under Gln or AA starvation condition for eight days. Cell proliferation was measured via Hoechst nuclear staining. Images were collected by ImageXpress micro and analysed by MetaXpress software. (I) cells were seeded either on plastic or on plates coated with collagen I (2mg/ml) or Matrigel (3mg/ml) in the presence of Plasmax media diluted 1:4 in PBS for eight days. Cell proliferation was measured by DRAQ5 nuclear staining. (J) cells were seeded either on plastic or on plates containing CAF-CDM in the presence of Plasmax media diluted 1:4 in PBS for six days. Cell proliferation was measured via Hoechst nuclear staining. Images were collected by ImageXpress micro and analysed by MetaXpress software. Values are mean  $\pm$  SEM and are representative of at least three independent experiments (the black dots in the bar graphs represent the mean of individual experiments). \* $p < 0.05$ , \*\* $p < 0.01$ , \*\*\* $p < 0.001$ , \*\*\*\* $p < 0.0001$  ANOVA test.

### **Matrigel partially rescued the growth of non-invasive breast cancer cells under glutamine starvation.**

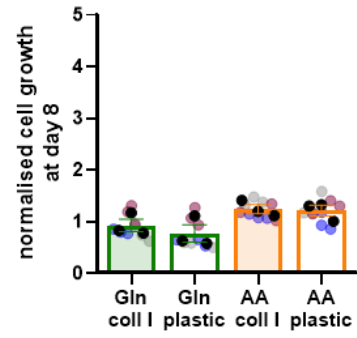
To assess whether the ECM only affects the growth of highly invasive breast cancer cells, the growth rate of normal mammary epithelial cells (MCF10A) and non-invasive breast cancer cells (MCF10A-DCIS) was tested. Breast cancer progression starts from benign hyperplasia of epithelial cells of the mammary duct, then it evolves to atypical ductal hyperplasia, with a little abnormality in cell shape, and ductal carcinoma in situ (DCIS), with cells showing features of cancer cells. At the end, the cells acquire the invasive ductal cancer phenotype (Dawson et al., 1996, Rhee et al., 2008, So et al., 2012). To assess cell lines with different tumorigenicity, MCF10A and MCF10A-DCIS were seeded either on plastic, collagen I and Matrigel under Gln or AA depleted media for eight days. In contrast to MDA-MB-231 cells (Figure 1), MCF10A cell growth pattern under starvation on collagen I and Matrigel was similar to plastic. Although cell number was higher on collagen I and Matrigel under AA starvation compared to the plastic (Figure 2A and C), cells did not show higher growth rate (Figure 2B and D). Experiments on MCF10A-DCIS cells, representative of non-invasive breast cancer cells, showed no significant changes in cell number on collagen I or Matrigel under AA depleted media compared to the plastic (Figure 2E-H). In terms of Gln deficiency, cells on plastic and collagen I followed a similar pattern of growth with no remarkable differences in their cell number during the starvation time (Figure 2E-H). However, MCF10A-DCIS cells on Matrigel had significantly higher cell number and growth rate at day eight of post Gln starvation compared to the plastic (Figure 2G-H). These data suggest that the ability of using ECM to compensate for nutrient starvation could have been gradually developed in cancer progression while the cells are becoming more invasive.



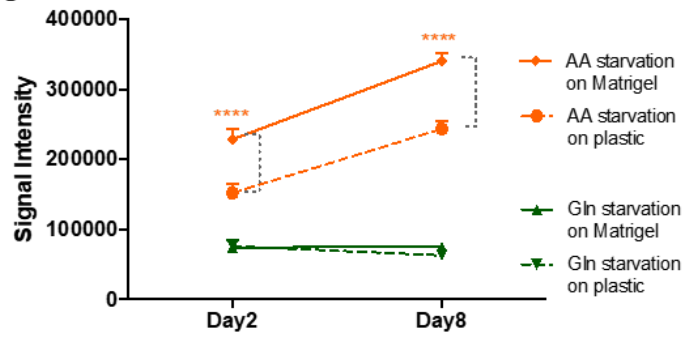
**A** MCF10A cell proliferation coll I vs plastic



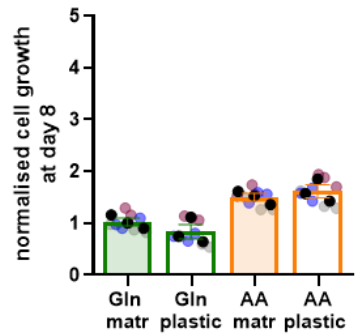
**B**



**C** MCF10A cell proliferation Matrigel vs plastic

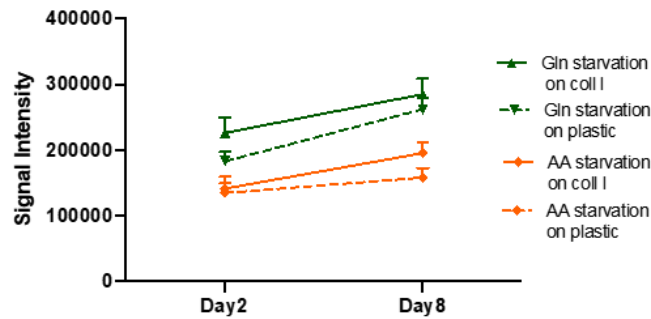


**D**

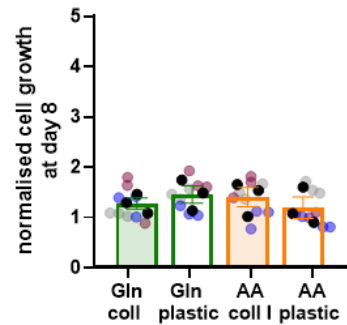


**E**

MCF10A-DCIS proliferation coll I vs plastic

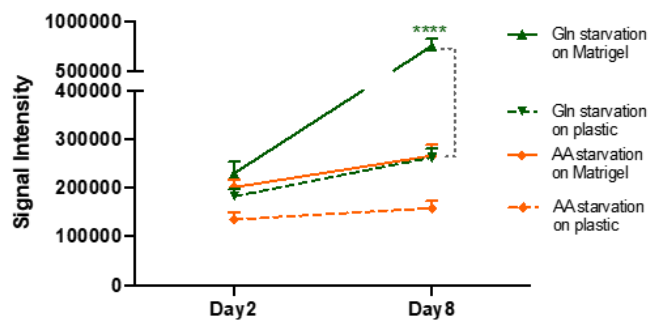


**F**



**G**

MCF10A-DCIS proliferation Matrigel vs plastic



**H**

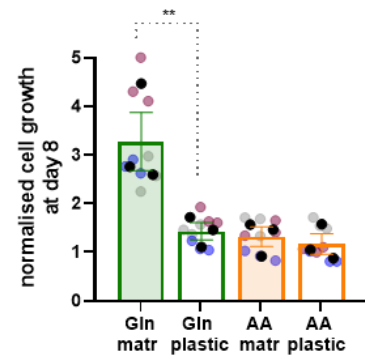


**Figure 2. The ECM did not affect normal epithelial cells and non-invasive breast cancer cell growth.** MCF10A and MCF10A-DCIS cells were seeded either on plastic or on plates coated with (A-B and E-F) 2mg/ml collagen I, (C-D and G-H) 3mg/ml Matrigel for eight days under Gln and AA starvation. Cell proliferation was measured by DRAQ5 nuclear staining quantification with the Licor Odyssey system on day two and day eight post starvation. Signal intensity from cells under each condition were collected by Image Studio Lit software. Values are mean  $\pm$  SEM and are representative of at least three independent experiments (the black dots in the bar graphs represent the mean of individual experiments). \*\* $p < 0.01$ , \*\*\*\* $p < 0.0001$  ANOVA test.

### Collagen I and Matrigel increased cell division under starvation conditions.

Above data demonstrate that MDA-MB-231 cell number was higher on ECM compared to plastic during eight days of AA and Gln starvation (Figure 1). However, the ECM mechanism of action was still unknown. We therefore asked whether being surrounded by collagen I and Matrigel either induced cell survival, proliferation, or both. To answer this question, we used 5-Ethynyl-2'-deoxyuridine (EdU) as a thymidine analogue to identify cells which passed through DNA synthesis and mitosis. Cells were starved for six days when they received EdU. EdU incorporation was measured after two days, on day eight of post starvation. According to the data comparing cell division on ECM with plastic, MDA-MB-231 cells had significantly higher EdU incorporation on collagen I and Matrigel under Gln and AA starvation conditions compared to the cells seeded on plastic (Figure 3A-B). Whereas cells growing in complete media were around 100% EdU positive on both ECM and plastic (Figure 3A-B). To clarify whether the ECM also played an anti-apoptosis role, cell death was assessed by measuring the number of cells positive for an apoptosis marker, activated caspase-3/7, at day three and eight post AA starvation. The data revealed that, although the apoptosis rate increased between day three and day eight under all nutrient condition, there were no significant differences between the apoptosis rate on collagen I and Matrigel compared to the plastic either at day 3 or day 8 under AA depleted media (Supplementary figure 3A-B). Thus, our data indicate that collagen I and Matrigel induce invasive breast cancer cell proliferation under AA starvation, without having an anti-apoptotic effect.

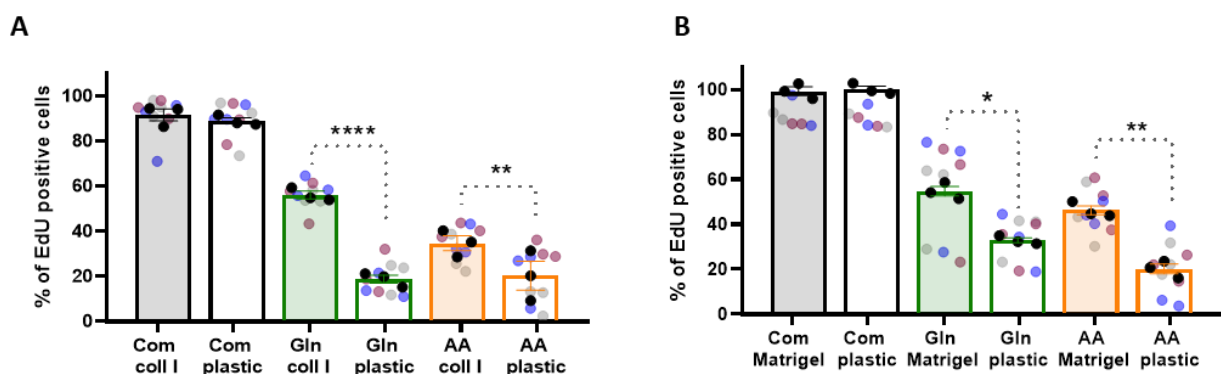


**Figure 3. Collagen I and Matrigel induced cell proliferation under glutamine and amino acid starvations.** MDA-MB-231 cells were seeded either on plastic or plastic coated with (A) 2mg/ml collagen I or (B) 3mg/ml Matrigel under Gln and AA starvation conditions. Cells were incubated with EdU on day six post starvation, fixed and stained with Hoechst and Click iT EdU imaging kit on day 8. Images were collected by ImageXpress micro and analysed by MetaXpress software. Values are mean  $\pm$  SEM and are representative of three independent experiments (the black dots represent the mean of individual experiments). \* $p < 0.05$ , \*\* $p < 0.01$ , \*\*\*\*  $p < 0.0001$  ANOVA test.

### Collagen I and Matrigel rescued mTORC1 activity in starved cells.

We next tested whether higher proliferation rate of cells on ECM linked to mTORC1 activity. The mTOR signalling pathway is the pivotal regulator of anabolic and catabolic processes in the cells. Receiving AA, GFs and energy activates mTORC1 triggering downstream anabolic signalling pathways. However, the lack of AA and GFs deactivates mTORC1 and induces catabolism resulting in lysosome biogenesis and autophagy (Mossmann et al., 2018). Therefore, we investigated whether higher proliferation rate of cells on collagen I and Matrigel was linked to higher mTORC1 activity in starved MDA-MB-231 cells. To do this, we examined the phosphorylation of an mTORC1 downstream target, ribosomal subunit S6 (S6), as an indicator for mTORC1 activity. MDA-MB-231 cells, which were starved for three days either on collagen I, Matrigel or plastic, were fixed and stained for phospho-S6 (p-S6). Quantifying the intensity of p-S6, as expected, demonstrated that AA starvation resulted in a significant reduction in mTORC1 activity on plastic. Interestingly, the presence of the ECM could fully rescue mTORC1 activation under starvation (Figure 4A-B). Together, these results suggest that collagen I and Matrigel might work as alternative sources of AA for starved MDA-MB-231 cells to remarkably increase mTORC1 activity.

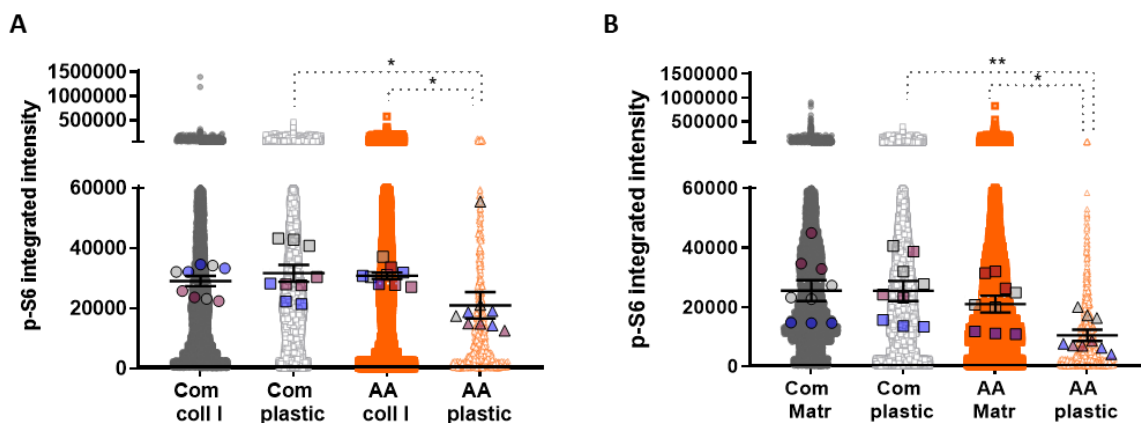


**Figure 4. Collagen I and Matrigel rescued mTORC1 activity in starved cells.** MDA-MB-231 cells were plated either on plastic or plastic coated with (A) 2mg/ml collagen I or (B) 3mg/ml Matrigel under complete media or AA starvation. Cells were fixed and stained for p-S6 and nuclei at day three. Images were collected by ImageXpress micro and analysed by MetaXpress and Costum Module Editor (CME) software. Values are mean  $\pm$  SEM and are representative of three independent experiments. (The bigger dots represent the mean of individual experiments). \* $p < 0.05$ , \*\* $p < 0.01$  ANOVA test.

### **ECM internalisation inhibition opposed cell growth under amino acid starvation.**

It was previously shown that cancer cells rely on scavenging extracellular proteins and extracting AAs from them under starvation to maintain their survival and growth (Olivares et al., 2017, Kamphorst et al., 2015). To examine whether invasive breast cancer cells have the ability to internalize the ECM under different starvation conditions, we tracked the journey of the ECM inside the cells in the presence of a lysosomal protease inhibitor (E64d), to prevent lysosomal degradation. Uptake of fluorescently labelled collagen I (Figure 5A) and Matrigel (Figure 5B) was monitored under AA depleted media three days post starvation. The quantification of collagen I and Matrigel uptake demonstrated that under all nutrient condition, MDA-MB-231 cells significantly accumulated higher amount of collagen I and Matrigel inside the cell if lysosomal degradation is inhibited (Figure 5A-B), showing that ECM components go through lysosomal degradation following internalization. We then wanted to investigate whether the growth of cancer cells relies on ECM internalization under nutrient deficiency conditions. To assess this hypothesis, collagen I and Matrigel coated plates were treated with 10% glutaraldehyde to chemically cross-link amine groups of proteins. Our data confirmed that cross-linking completely opposed collagen I and Matrigel internalisation (Figure 5C-D). Moreover, the data collected from cell growth on cross-linked collagen I and Matrigel demonstrated that MDA-MB-231 growth under complete media did not depend on ECM uptake (Figure 5E). In contrast, lack of collagen I and Matrigel uptake due to cross-linking completely opposed cell growth under AA starvation (Figure 5F). ECM cross-linking has been shown to increase matrix stiffness, thereby affecting cell adhesion and integrin signalling (Levental et al., 2009). To examine the signalling effect of ECM crosslinking, the number of focal adhesions (FAs) per cell were measured on normal and cross-linked ECM in complete media, by staining the cell for the FA protein, paxillin. Our results showed that the number of FAs on collagen I was slightly reduced by the cross-linking. However, Matrigel cross-linking did not change the number of FAs (Figure 5G), suggesting that the effect of ECM cross-linking on cell growth was not due to adhesion defects. To further assess whether lack of ECM internalization reduced cell growth under starvation, cells were treated with Filipin. Filipin is a cholesterol binding agent that prevents lipid raft-mediated endocytosis (Dutta and Donaldson, 2012). Our data revealed that Filipin treatment significantly reduces Matrigel uptake and cell growth on Matrigel under AA starvation (Figure 5H and J); whereas it does not affect cell growth under complete media (Figure 5I).

ECM cross-linking has been reported to also prevent MMP-mediated degradation (Pourfarhangi et al., 2018). To investigate whether matrix metalloproteinase (MMP)-dependent ECM degradation is required for internalization, we treated the cells with a broad spectrum MMP inhibitor (GM6001) under complete and AA depleted media. MMPs are a proteolytic enzyme family that have a major role in ECM degradation associated with metastasis and invasion. Expression of different types of MMPs such as MMP-2, MMP-14 and MMP-9 in breast cancer is associated with poor prognosis and could be used as an indicator for survival rate (Talvensaari-Mattila et al., 1998, Tetu et al., 2006, Yousef et al., 2014). Our data showed that MMP inhibition did not affect collagen I and Matrigel uptake and cell growth under AA starvation (Supplementary figure 4). Parallel to our results, it has previously been shown that inhibition of extracellular proteolytic enzymes including MMP did not change the amount of internalized ECM (Everts et al., 1989, Han et al., 2015). Altogether, these results indicate that ECM internalization is necessary for breast cancer cell growth under AA

starvation while ECM extracellular degradation is not required for ECM internalization and cell growth.

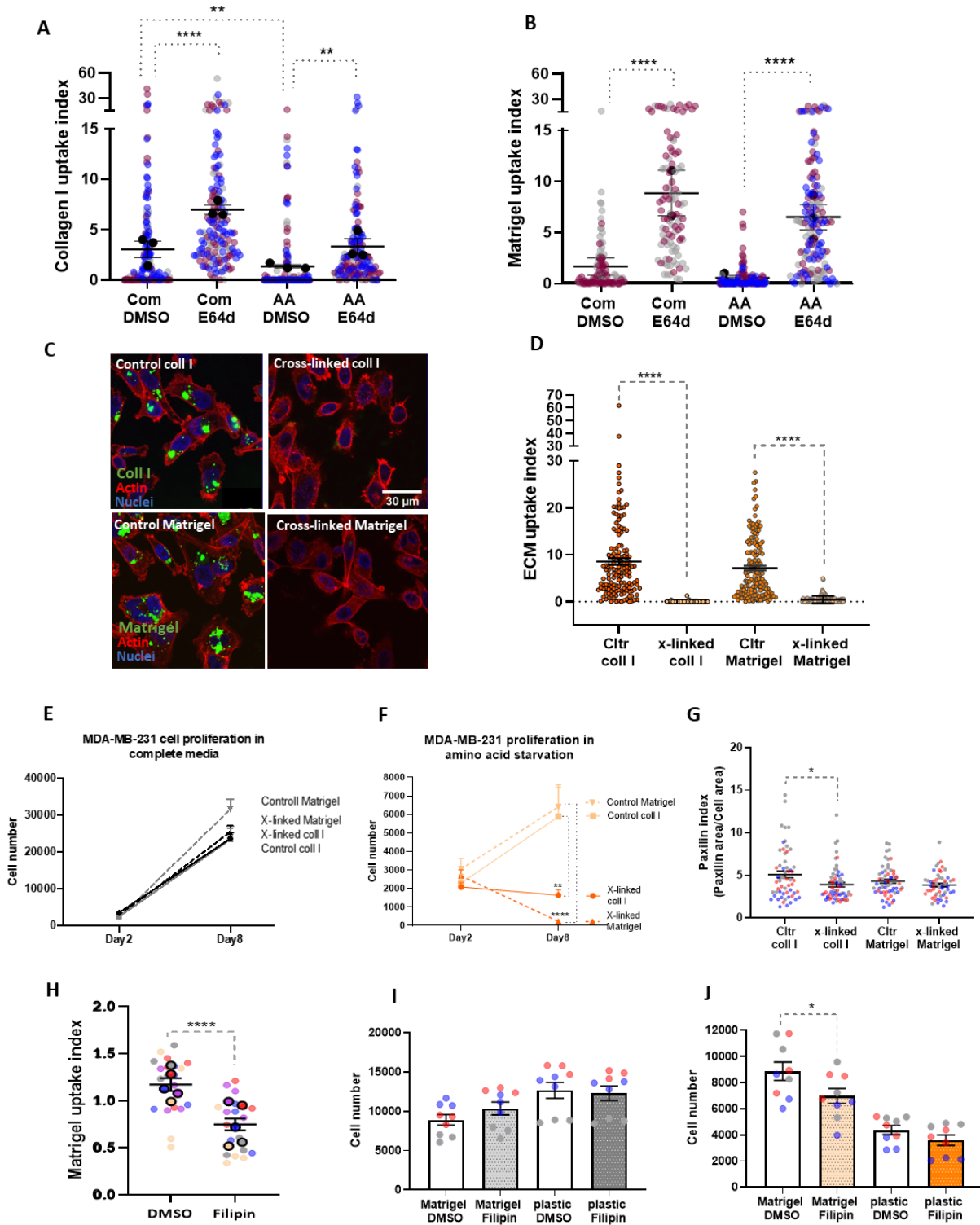


**Figure 5. MDA-MB-231 cells internalized and degraded collagen I and Matrigel.** MDA-MB-231 cells were plated under complete (Com) or AA depleted media on dishes coated with N-Hydroxysuccinimide-fluorescein labelled (A) 1mg/ml collagen I (green) or (B) 3mg/ml Matrigel for three days, in the presence of the lysosomal inhibitor E64d (20 $\mu$ M) or DMSO (control). (C-D) Dishes were coated with 2mg/ml collagen I or 3mg/ml Matrigel, treated with 10% glutaraldehyde for 30 mins or left untreated and labelled with N-Hydroxysuccinimide-fluorescein. Cells were plated on the cross-linked matrices for three days under AA starvation in the presence of the lysosomal inhibitor E64d (20 $\mu$ M). Cells were fixed and stained for actin (red) and nuclei (blue). Images were collected by a Nikon A1 confocal microscope. (E-F) MDA-MB-231 cells were seeded on untreated (control) or cross-linked (X-linked) collagen I (2mg/ml) or Matrigel (3mg/ml) under complete media or AA starvation and stained with Hoechst. Images were collected by ImageXpress micro and analysed by MetaXpress software. Values are mean  $\pm$  SEM and are representative of three independent experiments. (G) MDA-MB-231 cells were plated under complete media on dishes coated with normal (control) or cross-linked collagen I (2mg/ml) or Matrigel (3mg/ml) for three days. Cells were fixed and stained for Paxillin, actin and nuclei. Images were collected by a Nikon A1 confocal microscope. (H) MDA-MB-231 cells were plated under complete media on dishes coated with N-Hydroxysuccinimide-fluorescein labelled Matrigel (3mg/ml) in the presence of 5 $\mu$ g/ml Filipin or DMSO control. MDA-MB-231 cells were plated under (I) complete media or (J) AA starvation condition on plastic or plates coated with 3mg/ml Matrigel. Cells received 5 $\mu$ g/ml Filipin or DMSO as control everyday up to day three. Cell proliferation was measured through Hoechst nuclei staining. Images were collected by ImageXpress micro and analysed by MetaXpress software. Graphs are shown in A, B and D are representative of around 150 cells and in G around 60 cells per condition (the bigger dots represent the mean of individual experiments). \* $p$ <0.05, \*\* $p$ <0.01 and \*\*\*\* $p$ <0.0001 ANOVA test.

### **Inhibition of focal adhesion kinase did not affect cell growth on ECM under starvation.**

ECM cross-linking has been shown to affect cell-ECM adhesion (Pourfarhangi et al., 2018). Binding of ECM components to the integrin family of ECM receptors induces recruitment of focal adhesion proteins on the intracellular domain of integrin triggering different signalling pathways inside the cells (Burrige et al., 1992, Maziveyi and Alahari, 2017). Focal adhesion kinase (FAK) is a non-receptor kinase located in the FAs. FAK mediates signalling pathways initiated by integrins to regulate different cell behaviours, including proliferation, migration, and survival. FAK is also over-expressed in some cancers, and it is linked to their aggressiveness (Aboubakar Nana et al., 2019). To test whether the inhibition of focal adhesion signalling could affect cell growth under different nutrient conditions, MDA-MB-231 cells were treated with focal adhesion kinase (FAK) inhibitor, PF573228. Firstly, the auto-phosphorylation of FAK<sup>Tyr397</sup> was measured under different concentrations of PF573228. Our results revealed around 80% inhibition of FAK activity with 0.5 $\mu$ M PF573228 concentration (Figure 6A-B). Therefore, to assess the effect of FAK inhibition on cell growth, MDA-MB-231 were seeded either on collagen I, Matrigel or CAF-CDM under complete media or AA starvation condition, in the presence of 0.5 $\mu$ M PF573228 or DMSO as control (Figure 6C-F). Monitoring cell growth up to day six post starvation revealed no significant difference between the control group and the cells receiving the FAK inhibitor on collagen I and Matrigel (Figure 6C-D), either in complete or AA-depleted media. Cells growing on CAF-CDM also showed no significant differences in cell number at day six under AA starvation. However, in the complete media the cell number was significantly lower in the presence of the FAK inhibitors compared to the control group (Figure 6E-F). In addition, no changes in quantity of FAs were observed in cells under AA starvation compared to the complete media. (Figure

6G). Taken together, these data indicate that signalling events following cell-ECM interaction did not affect cell growth under starvation conditions and ECM-dependent cell growth is mainly mediated by ECM component internalisation followed by lysosomal degradation.

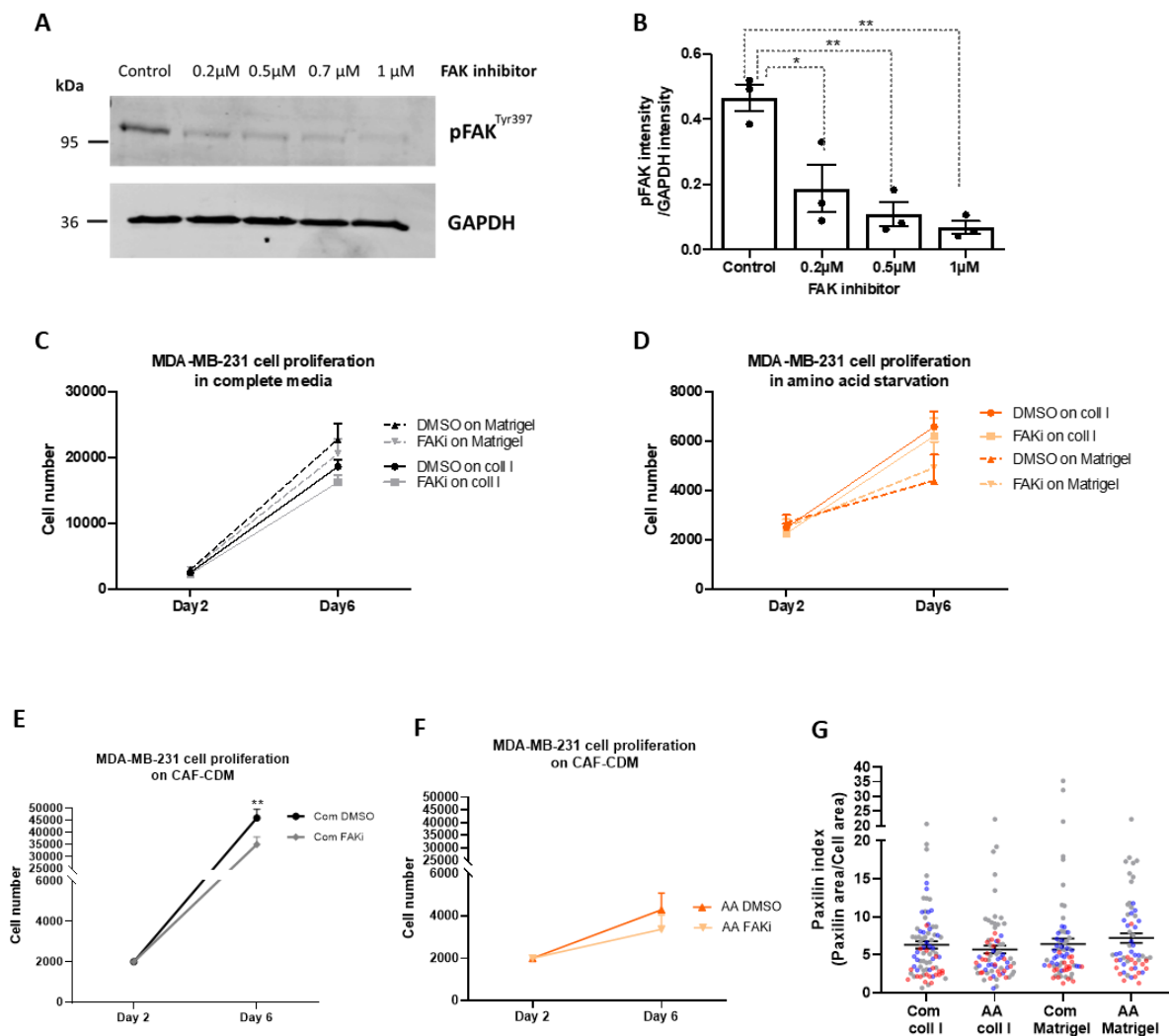


**Figure 6. FAK inhibition did not affect cell growth on collagen I, Matrigel and CAF-CDM under AA starvation.** (A-B) MDA-MB-231 cells were suspended in complete media containing either 0.2 μM, 0.5 μM, 0.7 μM or 1 μM of PF573228 or vehicle for 30 mins. Cells were seeded on collagen I for 30 mins under the same media. Cells were lysed and proteins were analysed via western blotting with antibodies recognising pFAK<sup>Tyr397</sup> and GAPDH. The intensity of the bands was quantified with Licor Odyssey technology. Values are mean ± SEM and are representative of three independent experiments. \*p < 0.05, and \*\*p < 0.01 ANOVA test. (C-F) MDA-MB-231 cells were seeded on either 2mg/ml collagen I, 3mg/ml Matrigel or CAF-CDM under complete media or AA starvation for six days. Cells received 0.5 μM PF573228 (FAKi) or DMSO (control) every two days. Cells were fixed at day two and day six and stained with Hoechst. Images were collected by ImageXpress micro and analysed by MetaXpress software. \*\*p < 0.01 ANOVA test. (G) Cells were plated under complete media or AA starvation on dishes coated with collagen I (2mg/ml) or Matrigel (3mg/ml) for three days. Cells were fixed and stained for Paxillin, actin and nuclei. Images were collected by a Nikon A1 confocal microscope. Values are mean ± SEM and are representative of three independent experiments.

### **ECM promoted cell growth under amino acid starvation by modulating tyrosine and phenylalanine metabolism.**

Because cancer cells were able to internalize ECM components and degrade them in the lysosomes (Figure 5A-B), and mTORC1 activity was enhanced under AA starvation on ECM (Figure 4), we reasoned that the presence of collagen I and Matrigel might lead to increase the intracellular AA level. To investigate the differences in the cell metabolite content, we performed direct infusion mass spectrometry (DI-MS) of MDA-MB-231 cells either on plastic, collagen I or Matrigel under AA starvation. The data showed that the intracellular level of many AAs was upregulated on collagen I compared to the plastic. There were significantly increase in level of mostly essential AAs (EAAs) including phenylalanine, threonine, tryptophan, leucine, isoleucine, and methionine in addition to cysteine, tyrosine, and hydroxy proline as NEAAs, on collagen I and Matrigel (Figure 7A and supplementary figure 5A). Metabolomic pathway analysis also revealed that phenylalanine and tyrosine metabolism was significantly enriched in cells on both collagen I and Matrigel compared to the plastic under AA starvation (Figure 7C-D and supplementary figure 5C-D). Comparing metabolites being significantly upregulated on collagen I and Matrigel revealed that around 36% of them are common in both groups (Data not shown). To confirm the upregulation of phenylalanine and tyrosine metabolic pathway on ECM, we performed ultra-performance liquid chromatography-tandem mass spectrometry (UPLC-MS/MS) to measure the concentration of phenylalanine, tyrosine, and fumarate in cells growing on collagen I compared to the plastic under AA starvation. Phenylalanine and tyrosine metabolic pathway give rise to formation of fumarate, which can be fed into the TCA cycle (Figure 8A). The data collected from UPLC-MS/MS revealed the upregulation of phenylalanine, tyrosine and fumarate in cells seeded on collagen I under AA deficiency compared to cells seeded on plastic (Figure 7E).



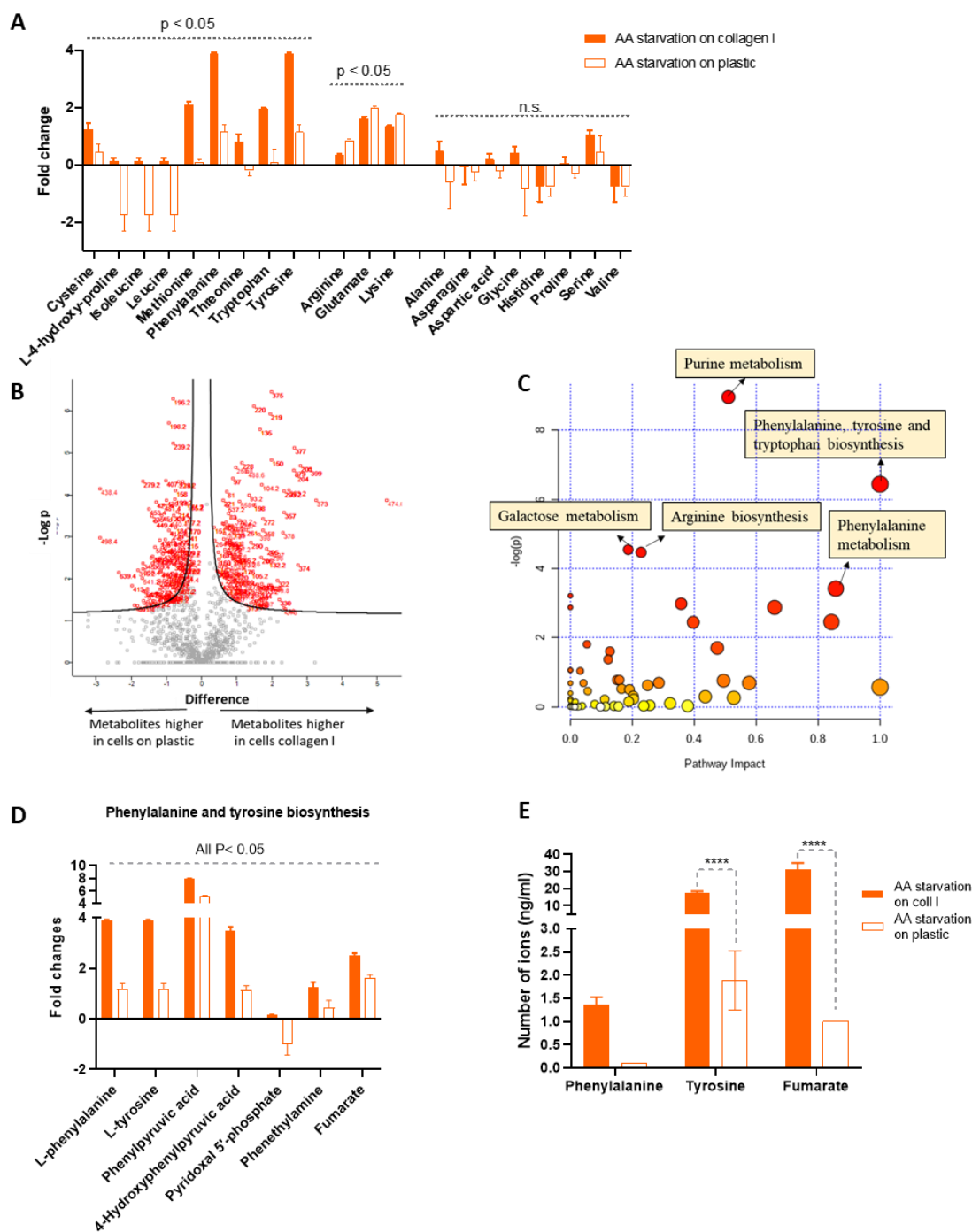


**Figure 7. Cells had different metabolite content on collagen I compared to plastic under amino acid starvation.** Cells were starved for 6 days either on collagen I or plastic. (A) Fold changes of amino acid levels and (D) fold changes of phenylalanine and tyrosine metabolism pathway intermediates in MDA-MB-231, which are normalized to the median of total metabolites in each condition. P values were measured by Student's t-test. (B) Volcano plot of cells on collagen I and plastic comparing the fold changes and P value of individual metabolites,  $p$ -value  $< 0.05$ . Each number is representative of the bins allocated to different metabolites which are statistically significant. (C) Highlights the most enriched pathways,  $p$ -value  $< 0.05$ . (E) MDA-MB-231 cells were grown on collagen I or plastic under amino acid starvation for 6 days, phenylalanine, tyrosine and fumarate concentrations were measured via UPLC-MS/MS. Values are mean  $\pm$  SEM and are representative of three biological replicates. \*\*\*\* $P < 0.0001$  ANOVA test.

Phenylalanine metabolism is composed of a series of metabolic reactions, resulting to the production of fumarate, which can enter the tricarboxylic acid cycle (TCA), leading to energy production. We reasoned that, if the ECM supported cell growth by promoting phenylalanine metabolism, the knockdown (KD) of enzymes involved in this pathway would inhibit ECM-dependent cell growth under AA deprivation. To test this, MDA-MB-231 cells were transfected with siRNA against 4-hydroxyphenylpyruvate dioxygenase (HPD), and 4-hydroxyphenylpyruvate dioxygenase-like (HPDL) (Figure 8A). Indeed, the inhibition of HPDL, but not HPD completely opposed cell growth on collagen I under AA starvation (Figure 8C). In complete media on collagen I, both HPDL and HPD resulted in a small but statistically significant reduction in cell growth, while on plastic HPDL KD did not have any impact on cell numbers. (Figure 8B and D). Taken together, these data demonstrated that ECM-dependent cell growth under AA starvation is mediated by the activation of phenylalanine and tyrosine metabolism, leading to fumarate production.

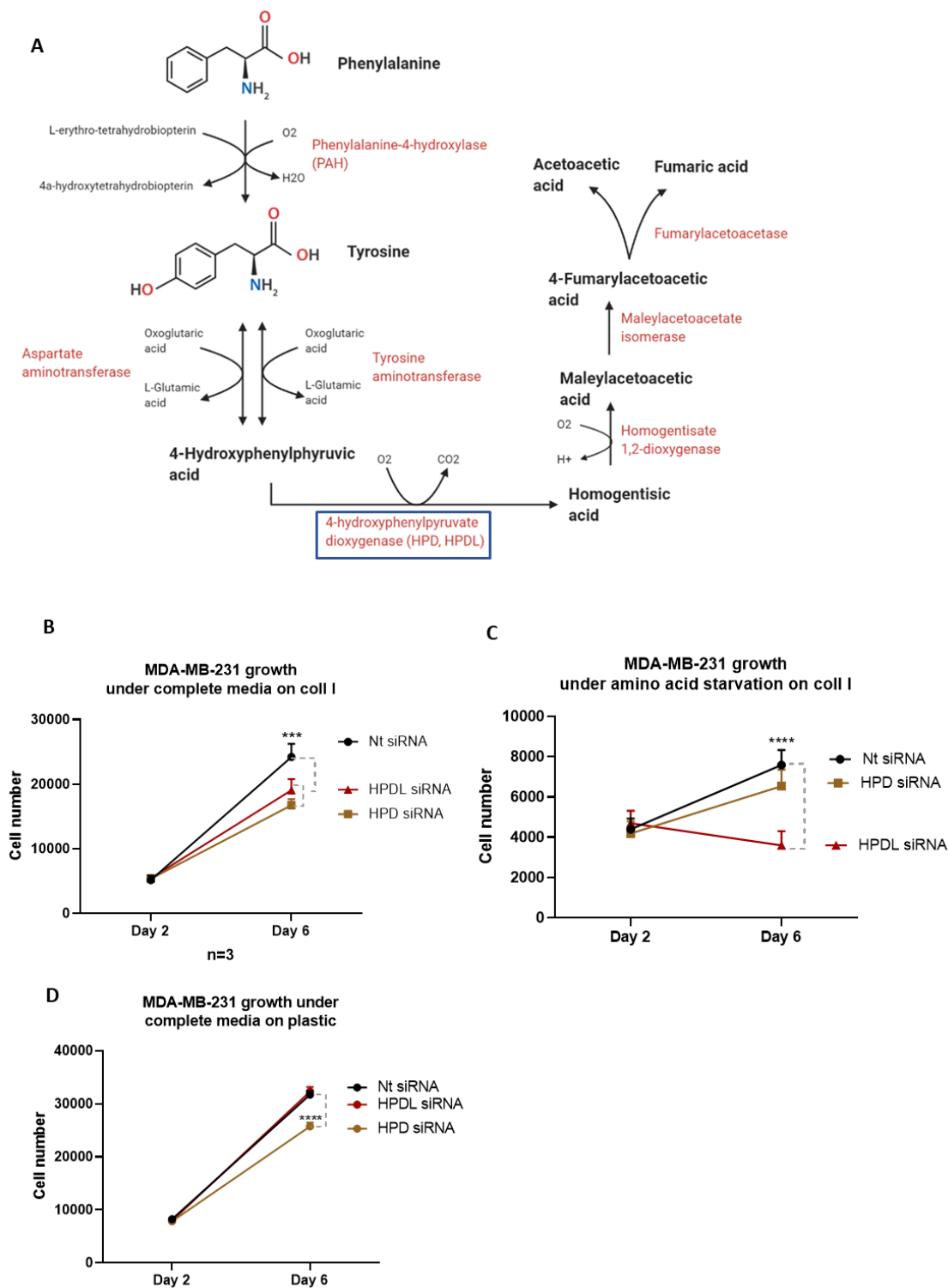


**Figure 8. HPDL KD significantly opposed cell growth under AA starvation on collagen I.** (A) Schematic representation of phenylalanine and tyrosine metabolism pathways. siRNA gene silencing was done for HPD and HPDL for MDA-MB-231 cells transfected with siRNA targeting HPD, HPDL or non-targeting control (Nt siRNA) on collagen I (A) under complete media, and (B) under AA starvation or (C) on plastic under complete media. Cells were fixed at day two and day six post KD. Cell proliferation was measured through Hoechst nuclei staining. Images were collected by ImageXpress micro and analysed by MetaXpress software. \*\*\* $p < 0.001$ , and \*\*\*\* $p < 0.0001$  ANOVA test.

## Discussion

Cancer cells to maintain their high proliferation rate need to optimize their metabolism to acquire the maximum amount of nutrients from the environment (Pavlova and Thompson, 2016). However, nutrient delivery to tumours is inefficient due to lowering vascularization and deformed vessels (Forster et al., 2017). Breast cancer cells are embedded into a highly fibrotic microenvironment with unlimited access to various ECM components (Kim et al., 2014). Different studies suggested that cancer cells rely on extracellular protein internalization during starvation (Commisso et al., 2013, Kamphorst et al., 2015, Muranen et al., 2017, Palm et al., 2015, Rainero et al., 2015a). Here, we highlight that the ECM surrounding breast cancer tumours represents an alternative source of nutrients to support cancer cell growth through ECM internalization and lysosomal degradation followed by regulating phenylalanine and tyrosine metabolism.

In this study, we showed that the presence of collagen I, Matrigel, laminin and CAF-CDM induced the growth of MDA-MB-231 cells under Gln and AA starvation, while CDM derived from normal fibroblasts (TIF) was unable to support cell growth in AA depleted media. It was previously shown that the unique composition of CAF-CDM induces invasiveness of breast cancer cells while CDM from TIF does not have this property (Hernandez-Fernaud et al., 2017). Our data indicate that CDM derived from CAFs could also provide a more favourable environment for cells to grow under AA starvation compared to CDM from noncancerous fibroblasts. However, cells had similar growth rate when they were growing under complete media regardless of them being seeded on plastic, CAF-CDM or TIF-CDM. Contrary to our data, it was previously shown that lower stiffness of CDM from TIF compared to CAF-CDM restricts cancer cell growth via downregulation of the YAP/TAZ mechanotransduction pathway in MDA-MB-231 cells (Kaukonen et al., 2016). In that study TIF cells were producing CDM for 10 days and cell proliferation was examined at day six. In our study the time allocated for TIF-CDM production was six days and cell growth was assessed at day eight. Therefore, shorter time for CDM production might result in different composition and structural characteristics of CDMs. In addition, longer time for cell growth assessment might have given the cells more opportunity to adapt and compensate for their lower growth rate.

In addition, our data comparing the growth rate of invasive breast cancer cells to normal mammary epithelial cells and non-invasive breast cancer cells highlighted that the ability of using ECM to compensate cell growth under starvation could have been gradually developed in cancer cells while they were becoming more invasive. There are studies showing that highly invasive breast cancer cells are more prepared to switch between different metabolic pathways as a mechanism to adapt to different nutrient availability and environmental stress compared to their non-metastasis counterparts (Simoës et al., 2015). In addition, Gln deficiency has more deleterious effects on invasive ovarian cancer cells (SKOV3) compared to low invasive tumours (OVCAR3) as invasive cells mainly rely on Gln to produce energy (Yang et al., 2014). However, in these studies the effect of ECM on cell behaviour was not taken into the account. Here, we showed that the lack of Gln also affected the growth of non-invasive breast cancer cells, suggesting that this effect could be cell line dependent. Moreover, the presence of Matrigel, but not collagen I, could rescue MCF10A-DCIS cell growth under Gln depletion. Matrigel is a basement membrane (BM) extract. Non-invasive breast cancer cells reside inside the mammary duct and are in contact with the BM (Muschler and Streuli, 2010) suggesting the reason why Matrigel has more compensatory effect compared to the collagen I. Collagen I is the main component of interstitial matrix with no contact with mammary

epithelial cells (Muschler and Streuli, 2010). In addition, our data showed that the presence of collagen I and Matrigel did not rescue the growth of normal mammary epithelial cells under AA starvation. In contrast, normal mammary epithelial cells were shown to be able compensated serum deficiency in their environment by scavenging laminin (Muranen et al., 2017). However, soluble laminin was used by Muranen et al., while in our study all the ECMs were in the form of matrices. In addition, we observed partial rescue of cell growth of serum starved MCF10A cells on collagen I (data not shown) suggesting that normal mammary epithelial cells' response to presence of ECM might vary based on different starvation conditions.

Our study demonstrated that higher MDA-MB-231 cell number on collagen I and Matrigel under starvation was linked to their higher division rate while their apoptosis was similar to the cells growing on plastic. Although it has been previously shown that coating culture area with 2D collagen I protects MCF-7 cells from apoptosis under serum starvation (Badaoui et al., 2018), our study demonstrated that under AA starvation there is no differences in apoptosis between cells on collagen I, Matrigel or plastic. However, other types of cell death could be affected by the presence of ECM and further work is required to investigate this. Starvation is the condition that the activity of mTORC1 is prevented to allow cells use alternative sources of nutrient obtainment like autophagy (Korolchuk et al., 2011, Yang et al., 2011). There are studies showing that mTORC1 could be reactivated by providing extracellular protein to cells under AA deficiency (Muranen et al., 2017, Palm et al., 2015) through a positive feedback loop as inhibition of mTORC1 induce ECP scavenging (Muranen et al., 2017, Palm et al., 2015, Rainero et al., 2015a). Therefore, here we could suggest that higher proliferation rate in starved MDA-MB-231 in the presence of collagen I and Matrigel is associated with the higher mTORC1 activity inducing anabolic processes. Furthermore, we revealed that the presence of ECM fully restored mTORC1 activity in cells under starvation, whereas the ECM could only partially rescue the growth under starvation. Our data are consistent with the observation that mTORC1 activity restrains growth if cells rely on scavenging ECP as a source of AAs. Indeed, it was shown that AA scarcity induced protein scavenging independent of mTORC1 activity. High activity of mTORC1 resulted in a higher translation rate. Cells that rely on ECP cannot support the high rate of translation and growth at the same time, due to their lower access to free AAs. Therefore, persistence of mTORC1 activity while cells rely on ECP resulted in lower growth due to insufficient AA sources (Nofal et al., 2017), which brings up the question whether mTORC1 inhibition is an efficient target for cancer therapy.

We showed that cell growth relies on ECM uptake and lysosomal degradation in AA depleted media. In support of this, we demonstrated that breast cancer cells are able to internalize ECM followed by lysosomal degradation under starvation. In addition, lack of ECM internalization through either ECM cross-linking or inhibition of lipid raft-mediated endocytosis opposed cell growth under AA depleted media. There are some concerns about the cytotoxicity of chemical cross-linkers such as glutaraldehyde (Oryan et al., 2018). In our study, cells had the same growth rate on both normal and cross-linked ECM under complete media. It was also previously revealed that exposing collagen I to glutaraldehyde for crosslinking for less than one hour (we treated ECMs with glutaraldehyde for 30mins) did not significantly affect growth and metabolic activity of the cells (Lai and Ma, 2013). Moreover, we showed that inhibiting MMP activity did not affect cell growth and ECM internalization under starvation. This is consistent with previous observations indicating that, even though

MMPs can facilitate ECM internalization, cells were shown to internalize intact ECM *in vivo* and *in vitro* in the presence of MMP inhibitors (Madsen et al., 2013, Han et al., 2015). It is still possible that other proteases might be involved in promoting ECM internalisation and further work is required to elucidate this.

In addition, inhibiting signalling pathways downstream of ECM receptors, which induce cell proliferation and invasion by activating FAK (Begum et al., 2017), did not affect cell proliferation under nutrient starvation. FAK phosphorylation triggers downstream signalling pathways ultimately resulting in upregulation of cyclin D1 expression and G1 to S transition (Lee et al., 2015, Serrels et al., 2012). Highly metastatic cells have been shown to have higher FAK phosphorylation in comparison to their low metastasis counterparts. In addition, inhibition of either FAK or  $\beta$ 1 integrin reduced cell proliferation in 3D environments but not in 2D (Shibue and Weinberg, 2009). In our study, to assure that lack of cell growth is not solely due to the FAK inhibition, we optimised a dose of FAK inhibitor reducing FAK phosphorylation around 80% with non-significant effect on cell proliferation. Application of that specific dose of FAK inhibitor did not affect cell proliferation under starvation. These data imply that the role of the ECM here is through endocytosis and lysosomal degradation and not signalling. However, further work is needed to fully characterise the contribution of integrin signalling in this condition.

Several studies revealed that cancer cells could rely on scavenging extracellular proteins to provide AA and energy in nutrient deprived conditions (Commisso et al., 2013, Davidson et al., 2017, Kamphorst et al., 2015, Muranen et al., 2017, Olivares et al., 2017, Palm et al., 2015). Here, accumulation of AAs in cells under AA depleted media indicate that invasive breast cancer cells catabolize collagen I and Matrigel and derive AAs from their breakdown. It was previously shown that PDAC cells extracted proline from collagen I and IV under nutrient deprived conditions and this rescued cell growth (Olivares et al., 2017). Interestingly, we did not observe proline upregulation in cells on ECM compared to plastic under AA starvation. In our study, cells were AA starved, while in study by Olivares et al (2017) cells were under low Glc or low Gln conditions (Olivares et al., 2017). Therefore, differences in starvation conditions could be the reason why we did not see proline upregulation. However, all AA accumulated in the cells on ECM in our study, except cysteine, were also shown to be upregulated in serum starved mammary epithelial cells treated with laminin (Muranen et al., 2017). Further studies are needed to realize why cells upregulate different types of AA on ECM. Whether is it related to the starvation condition, type of ECM or type of cells?

By performing metabolomic pathway analyses, we identified the upregulation of different metabolic pathways, including phenylalanine and tyrosine metabolism, leading to the generation of TCA cycle intermediates. These data raise the possibility that insoluble ECM proteins-derived provide AA could promote invasive breast cancer cell proliferation and energy production by upregulating metabolic pathways that could feed the TCA cycle. Interestingly, a comparison between control, benign and invasive ductal carcinoma tissue samples has revealed a significant increase in tyrosine level and phenylalanine/tyrosine biosynthesis in invasive cells (More et al., 2018). Alongside, we showed that if we prevent the conversion of 4-Hydroxyphenylpyruvic acid (HPD substrate) to homogentisic acid (HPD product), we prevent cell growth, with stronger effect being apparent on collagen I under AA starvation. HPD is an iron-dependant dioxygenase that has important role in tyrosine catabolism and its deficiency has been shown to cause disease like tyrosinemia and hawkinsinuria. Tyrosine breakdown eventually can feed in TCA cycle via fumarate formation.

It was previously shown that breast cancer cells (MDA-MB-231 and MCF7) have a substantially higher HPD expression compared to the adjacent normal tissue. HPD expression was correlated to the histological grade and clinical stage of breast cancer (Wang et al., 2019). Taken together tyrosine metabolism and HPD activation are essential for breast cancer cell growth and could potentially be used as a target for cancer therapy. HPDL shares 44% sequence similarity with HPD, and it is the only mammalian paralogue of HPD. Similarity between AA sequences of HPD and HPDL suggest that they might have similar substrates. HPD is mainly located in cytoplasm while HPDL has been suggested to also localise in mitochondria (Ghosh et al., 2020). We showed that under AA starvation, HPDL KD, but not HPD KD, completely opposed ECM-dependent cell growth. HPDL KD also results in lower growth rate in invasive breast cancer cells only on collagen I, but not plastic, under the complete media. In colon adenocarcinoma cells, it has been shown that HPDL KD reduced oxygen consumption, implying that it could play a role in controlling mitochondria functions. In addition, cells with HPDL gene silencing did not show tyrosine accumulation or tyrosine catabolism dysfunction, suggesting that HPDL could have tyrosine metabolism independent functions (Ghosh et al., 2020). Therefore, further studies are required to characterise the mechanism through which HPDL controls ECM-dependent cell proliferation. Future work will measure changes in tyrosine and fumarate concentrations upon HPDL KD in cells plated on ECMs, to find whether HPDL is required for tyrosine metabolism and fumarate production.

Taken together, our results highlight a novel role for ECM providing nutrients to AA starved invasive breast cancer cells via ECM internalization followed by phenylalanine and tyrosine metabolism upregulation. This raises the possibility that targeting phenylalanine and tyrosine metabolism could be a viable strategy to slow down breast cancer tumour growth, eventually leading to the generation of improved therapies for breast cancer patients.

## Materials and Methods

**Reagents.** Primary antibodies for Phospho-S6 Ribosomal Protein ser235/236 and GAPDH were from Cell Signalling, Phospho-FAK (Tyr397) from Thermo Fisher and Paxilin from Bdbioscience. Secondary antibodies for Alexa-fluor 594  $\alpha$ -Rabbit IgG and Alexa-fluor 488  $\alpha$ - Mouse IgG were from Cell Signalling, IRDye<sup>®</sup> 800CW and IRDye<sup>®</sup> 680CW were from LI-COR. Alexa fluor TM 555 Phalloidin, Click-iT EdU Imaging Kits and Hoechst 33342 was from Invitrogen. Nuclear stain DRAQ5 was from LICOR. Collagen I, Matrigel and Laminin/entactin complex were from Corning. All media and dialyzed FBS were from Gibco except DMEM with no amino acid which was from US Biological life science and Plasmax which was kindly provided by Dr Tardito, The Beatson Institute, Glasgow. The details of Plasmax composition are previously described by Vande Voorde et al 2019 (Vande Voorde et al., 2019). E64d (Aloxistatin) and PF573228 was from AdooQ Bioscience.

**Cell culture.** MDA-MB-231 cells, telomerase immortalised fibroblast (TIF) cells and CAFs, which were from breast cancer and were generated in Professor Akira Orimo's lab, Paterson Institute, Manchester, were cultured in High glucose Dulbecco's Modified Eagle's Medium (DMEM) supplemented with 10% fetal bovine serum (FBS) and 1% penicillin streptomycin (PS). Cells were grown at 5% CO<sub>2</sub> and 37°C and passaged every 3 to 4 days. MCF10A-DCIS cells were cultured in DMEM/F12 supplemented with 5% Horse serum (HS), 20 ng/ml EGF and 1% PS. MCF10A cells were cultured in DMEM/F12 supplemented with 5% HS, 20 ng/ml EGF, 0.5mg/ml hydrocortisone, 10 $\mu$ g/ml insulin and 1% PS. Cells were grown at 5% CO<sub>2</sub> and 37°C and passaged every 3 to 4 days.

**ECM preparation.** To coat plates/dishes, collagen I, Matrigel and laminin/entactin were diluted with cold PBS on ice to have 2mg/ml, 3mg/ml, and 3.5 mg/ml concentration respectively in 15 $\mu$ l/well, followed by 3hrs incubation at 5% CO<sub>2</sub>, and 37°C for polymerization. Cell derived matrix (CDM) was generated from TIF and CAF cells as described in Kaukonen et al., 2017 (Kaukonen et al., 2017). Briefly, plates were coated with 0.2% gelatine in PBS and incubated at 37° for 1hr, followed by being cross-linked with 1% glutaraldehyde in PBS at room temperature (RT) for 30 minutes. Glutaraldehyde was removed and quenched in 1M glycine at RT for 20 minutes, followed

by two PBS washes, and an incubation in full media at 5% CO<sub>2</sub> and 37°C for 30 minutes. CAF or TIF cells were seeded and incubated at 5% CO<sub>2</sub>, 37°C until being fully confluent (1 or 2 days). Once the cells were 100% confluent, the media was replaced to complete growth media containing 50µg/mL ascorbic acid, and it was refreshed every two days. TIFs were kept under media supplemented with ascorbic acid for six days while CAFs for seven days. The media was aspirated, and the cells washed once with PBS containing calcium and magnesium (PBS++). The cells were incubated with the extraction solution containing 20mM NH<sub>4</sub>OH and 0.5% triton in PBS++ for 2 minutes at RT until no intact cells were visible by phase contrast microscopy. Residual DNA was digested with 10µg/mL DNase I at 5% CO<sub>2</sub>, 37°C for 1hr. The CDMs were stored in PBS++ at 4°C.

**Starvation conditions.** Media used for starvation were supplemented with either 10% dialyzed FBS for MDA-MB-231 cell line or 10% HS, 10µg/ml insulin and 20 ng/ml EGF for MCF10A and or 5% HS and 20 ng/ml EGF for MCF10A-DCIS. Cells were plated in complete media for 5hrs, then the media was replaced with starvation media as indicated in the table 1.

**Table 1. Starvation media**

Media	Supplier	Ref No
<b>DMEM, high glucose, no glutamine</b>	Gibco	11960-044
<b>DMEM, no amino acids</b>	US Biological life science	D9800-13
<b>DMEM/F-12, no glutamine</b>	Gibco	21331-020

**Proliferation assays.** 96-well plates containing CAF-CDM, TIF-CDM, collagen I, Matrigel or laminin/entactin, as described above, were prepared. Three wells were allocated to each condition as technical replicates. 10<sup>3</sup> cells/well were seeded under full growth media. After 5hr incubation in 5% CO<sub>2</sub> and 37°C, the full growth media was replaced with 200µL of the starvation media shown in table1 or Plasmax. Plasmax was kindly provided by Dr Tardito, The Beatson Institute, Glasgow. Cells were fixed every two days up to day six or eight by adding 4% paraformaldehyde (PFA) for 15mins at RT followed by two PBS washes. Cell number was quantified using nuclear stains: DRAQ5 or Hoechst. 5µM DRAQ5 in PBS was added to the cells for 1hr at RT with a gentle rocking. Cells were washed two times with PBS for 30 minutes to avoid the background fluorescence and kept in PBS for imaging with the Licor Odyssey imaging system. DRAQ5 was detected with a 700nm channel with 200µm resolution by an Odyssey Sa instrument. The signal intensity, which was the total intensity minus total background, of each well was quantified with Image Studio Lit software. For the Hoechst nuclei staining, cells were fixed with 4% PFA containing 10µg/ml Hoechst 33342 for 15mins, followed by two PBS washes. Image analyses of cells were done by MetaXpress micro and Costum Module Editor software (CME) in the Sheffield RNAi Screening Facility (SRSF).

**ECM uptake assays.** To monitor the internalization of ECM, dishes coated with collagen I and Matrigel were labelled with 10µg/ml N-Hydroxysuccinimide-fluorescein (diluted in PBS) for 1hr at RT on a gentle rocker, followed by two PBS washes. Cells were seeded in full growth media. After a 5hr incubation at 5% CO<sub>2</sub> and 37°C, full growth media were replaced with AA starvation with the presence of 20µM lysosome inhibitor (E64d) or DMSO (control). E64d and DMSO were added again after 48hrs, and cells were fixed at day three by adding 4% PFA for 15mins at RT. To permeabilize, cells were treated with 0.25% triton X-100 for 5mins. For actin cytoskeleton staining, cells were incubated with Phalloidin Alexa Fluor 555 diluted 1:400 in PBS for 10 mins. To preserve the samples, 2-3 drops of Vectashield mounting medium containing DAPI were added to the dishes. Cells were visualised by confocal microscopy using a Nikon A1 microscope. Collagen I and Matrigel uptake indexes were quantified as described previously by Commisso et al. (Commisso et al., 2014).

**Cell division assays.** To monitor the cell's ability to proliferate Click-iT EdU Imaging Kits were used. MDA-MB-231 cells were plated on either ECM or plastic. At day six of starvation, cells were treated with 5µM EdU. Cells were incubated with EdU for two days at 5% CO<sub>2</sub> and 37°C. At day eight, cells were fixed with 4% PFA containing 10µg/ml Hoechst 33342 for 15mins at RT. To permeabilize, cells were treated with 0.25% triton X-100 for 5mins followed by two PBS washes and two washes with 3% bovine serum albumin (BSA). Cells were incubated with EdU detection cocktail (Invitrogen, Click-iT EdU Alexa Fluor 555) for 30 min at RT with gentle rocking. Cells were



washed twice with PBS and were kept in PBS for imaging. Images were collected by ImageXpress micro and analysed by MetaXpress and costum module editor software.

**Immunofluorescence.** Cells were fixed with 4% PFA containing 10 $\mu$ g/ml Hoechst 33342 for 15 mins at RT followed by a PBS wash. To permeabilize, cells were treated with 0.25% triton X-100 for 5mins followed by two PBS washes. Unspecific binding sites were blocked by incubating with 3% BSA at RT with gentle rocking. Cells were incubated with the Phospho-S6 Ribosomal (p-S6) Protein primary antibody overnight at 4°C. The primary antibody was removed, and cells were washed twice with PBS for 5mins to 10mins each time. Cells were incubated with secondary antibody 1hr at RT with gentle rocking. Cells were washed twice with PBS for 10 to 30mins and were kept in PBS for imaging. Images were collected by ImageXpress micro and analysed by MetaXpress and CME software.

**Western Blotting.** The culture media was aspirated, and cells were placed on ice. After two washes with ice-cold PBS, lysis buffer (50mM Tris pH7 and 1% SDS) were added and lysates were collected and transferred to a QiaShredder column (QIAGEN), which were spun for 5min at 14000 rpm. The filter was discarded, and the extracted proteins were kept at -20°C. To run the samples, 12% gels were prepared. Samples were fully thawed at RT and loaded into the 12% gel and ran at 100V for ~2hr 30min. Proteins were transferred from the gel to FL-PVDF membranes for 75mins at 100V. Membranes were washed three times with TBS-T (Tris-Buffered Saline, 0.1% Tween) and blocked in 5% w/v skimmed milk powder in TBS-T for 1hr at RT. Membranes were then incubated with primary antibodies overnight at 4°C. After washing the primary antibody, membranes were incubated with the secondary antibodies in TBS-T + 0.01% SDS, for 1hr at RT on the rocker. Membranes were washed three times in TBS-T for 10min on the rocker at RT followed by being rinsed with water. Images were taken at the Licor Odyssey system. Each band intensity was quantified with Image Studio Lite software.

**Non-targeted metabolite profiling.** MDA-MB-231 cells were seeded on 96-well plates coated with ECM under full growth media. After a 5hr incubation at 5% CO<sub>2</sub> and 37°C, the full growth media were replaced with the AA starvation media. Cells were kept under starvation for six days; the media was removed, and cells were washed with ice-cold PBS three times. The PBS were aspirated and the extraction solution (cold; 5 MeOH: 3 AcN: 2 H<sub>2</sub>O) was added for 5min at 4°C with low agitation. Metabolites were transferred to eppendorf tubes and centrifuged at 4°C and 14000 rpm for 10 mins. Samples were transferred into HPLC vials. The samples were directly injected into a Waters G2 Synapt mass spectrometer in electrospray mode within the Sheffield Faculty of Science Mass Spectrometry Centre. Three technical replicates of each sample were run, and the replicates were combined to obtain an average intensity. The dataset only includes peaks present in all three replicates. The intensity is a measure of abundance of any particular mass. The data is binned into 0.2amu m/z bins and the m/z in each bin is used to identify putative IDs using HumanCyc database.

**Targeted metabolite profiling.** MDA-MB-231 cells were seeded on 6-well plates coated with ECM under full growth media. After a 5hr incubation at 5% CO<sub>2</sub> and 37°C, the full growth media were replaced with the AA starvation media. Cells were kept under starvation for six days; the media was removed, and metabolites were extracted as described above. Then, mass spectrometer Waters Synapt G2-Si coupled to Waters Acquity UPLC was used to separate phenylalanine, tyrosine and fumaric acid with Column Waters BEH Amide 150x2.1mm. The injection was 10 $\mu$ l. The flow rate was 0.4ml/min.

**RNAi-mediated gene knockdown.** Glass-bottomed 96-well plates were coated with 15 $\mu$ l 2mg/ml collagen I. 20 $\mu$ l of 150nM ON TARGET plus Human HPDL and HPD smart pool were added on top of the ECM. 0.24 $\mu$ l of DF1 was diluted in 19.86 $\mu$ l of DMEM. 20 $\mu$ l of diluted DF 1 (Transfection reagent) were transferred to each well. Plates were left 30mins inside the hood at RT to let DF1 and siRNAs make complexes. 3 $\times$ 10<sup>3</sup> cells in 60 $\mu$ l DMEM media containing 10%FBS, but no antibiotics, were transferred to each well. The final concentration of siRNA reached 30nM. Cells were transferred to the incubator with 5% CO<sub>2</sub> and 37°C over-night. The full growth media was replaced by 200 $\mu$ l of fresh complete or AA starvation media for up to 6 days. At day 2 and 6, cells were fixed and incubated with 10 $\mu$ g/ml Hoechst 33342. Images were collected by ImageXpress micro and analysed by MetaXpress and CME software.

**Statistical analysis.** Graphs were created by GraphPad Prism software and t-test and ANOVA tests were performed. To compare two datasets, an unpaired t-test was performed. To compare more than two data set, one-way ANOVA was used when there was one independent variable. Two-way ANOVA was performed when

there were two independent variables. Statistical analysis for non-targeted metabolic profiling was performed by Perseus software and used Student t-test.

### Acknowledgments

Many Thanks to Dr Heather Walker, Biological Mass Spectrometry Facility Manager of University of Sheffield, for running the MS for our samples, to Montserrat Llanses Martinez for providing the data for Matrigel uptake in the presence of Filipin (Figure 5H), to Professor Akira Orimo's lab, Paterson Institute, Manchester to generously provide CAF cell line, and to Dr Tardito, The Beatson Institute, Glasgow for providing Plasmax media.

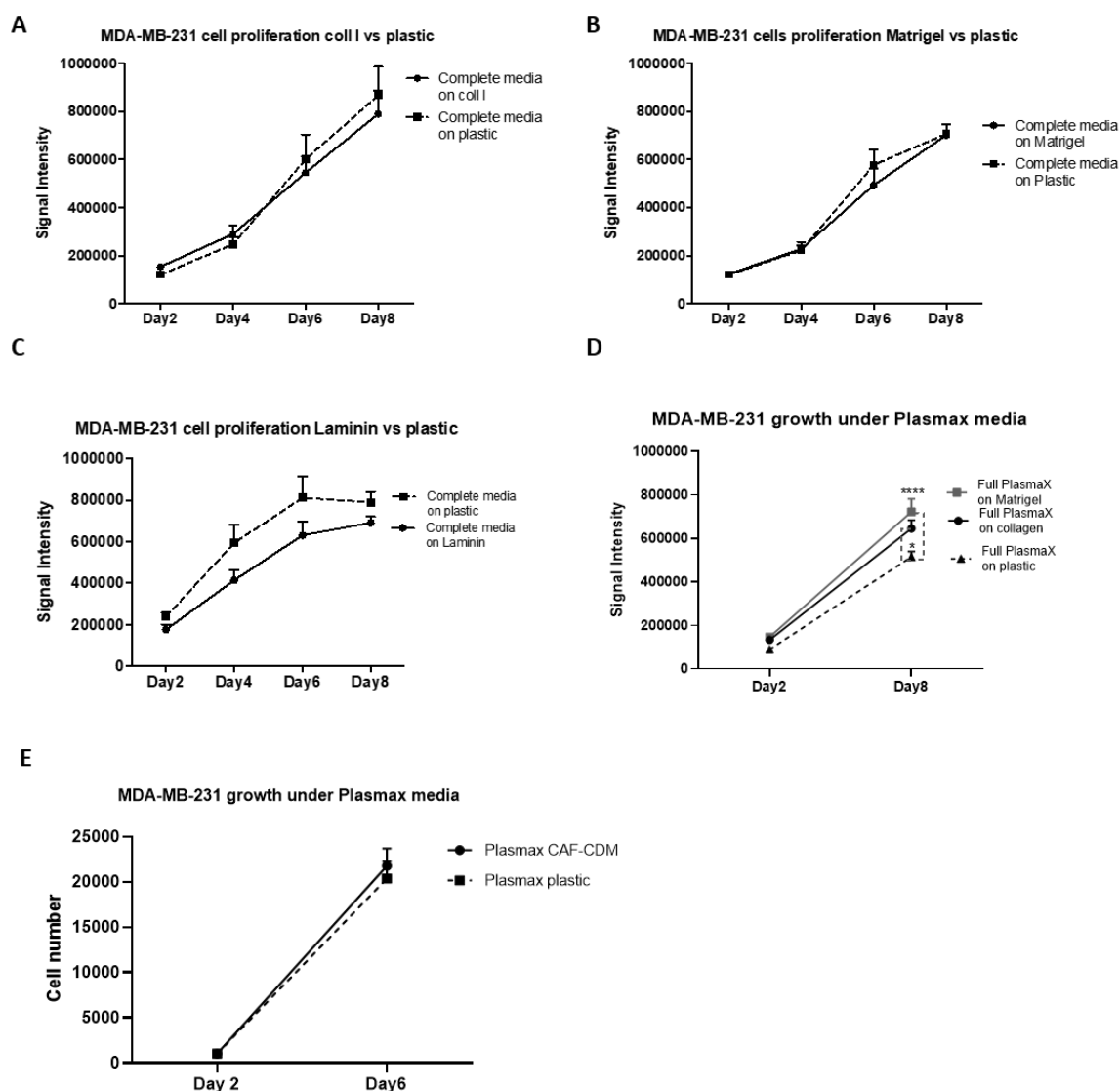
### References

1. Coughlin, S.S. Epidemiology of Breast Cancer in Women. *Adv Exp Med Biol* 1152, 9-29 (2019).
2. Provenzano, P.P. et al. Collagen density promotes mammary tumor initiation and progression. *BMC Med* 6, 11 (2008).
3. Kim, S.H. et al. Role of secreted type I collagen derived from stromal cells in two breast cancer cell lines. *Oncol Lett* 8, 507-512 (2014).
4. Hanahan, D. & Coussens, L.M. Accessories to the crime: functions of cells recruited to the tumor microenvironment. *Cancer Cell* 21, 309-322 (2012).
5. Bergamaschi, A. et al. Extracellular matrix signature identifies breast cancer subgroups with different clinical outcome. *J Pathol* 214, 357-367 (2008).
6. Insua-Rodriguez, J. & Oskarsson, T. The extracellular matrix in breast cancer. *Adv Drug Deliv Rev* 97, 41-55 (2016).
7. Kauppila, S., Stenback, F., Risteli, J., Jukkola, A. & Risteli, L. Aberrant type I and type III collagen gene expression in human breast cancer in vivo. *J Pathol* 186, 262-268 (1998).
8. Liverani, C. et al. Investigating the Mechanobiology of Cancer Cell-ECM Interaction Through Collagen-Based 3D Scaffolds. *Cell Mol Bioeng* 10, 223-234 (2017).
9. McDaniel, S.M. et al. Remodeling of the mammary microenvironment after lactation promotes breast tumor cell metastasis. *Am J Pathol* 168, 608-620 (2006).
10. Baluk, P., Hashizume, H. & McDonald, D.M. Cellular abnormalities of blood vessels as targets in cancer. *Curr Opin Genet Dev* 15, 102-111 (2005).
11. Nagy, J.A., Chang, S.H., Shih, S.C., Dvorak, A.M. & Dvorak, H.F. Heterogeneity of the tumor vasculature. *Semin Thromb Hemost* 36, 321-331 (2010).
12. Muranen, T. et al. Starved epithelial cells uptake extracellular matrix for survival. *Nat Commun* 8, 13989 (2017).
13. Palm, W. et al. The Utilization of Extracellular Proteins as Nutrients Is Suppressed by mTORC1. *Cell* 162, 259-270 (2015).
14. Rainero, E. et al. Ligand-Occupied Integrin Internalization Links Nutrient Signaling to Invasive Migration. *Cell Rep* (2015).
15. Pavlova, N.N. & Thompson, C.B. The Emerging Hallmarks of Cancer Metabolism. *Cell Metab* 23, 27-47 (2016).
16. Nicklin, P. et al. Bidirectional transport of amino acids regulates mTOR and autophagy. *Cell* 136, 521-534 (2009).
17. Bergstrom, J., Furst, P., Noree, L.O. & Vinnars, E. Intracellular free amino acid concentration in human muscle tissue. *J Appl Physiol* 36, 693-697 (1974).
18. Lacey, J.M. & Wilmore, D.W. Is glutamine a conditionally essential amino acid? *Nutr Rev* 48, 297-309 (1990).
19. Hanahan, D. & Weinberg, R.A. Hallmarks of cancer: the next generation. *Cell* 144, 646-674 (2011).
20. Comisso, C. et al. Macropinocytosis of protein is an amino acid supply route in Ras-transformed cells. *Nature* 497, 633-637 (2013).

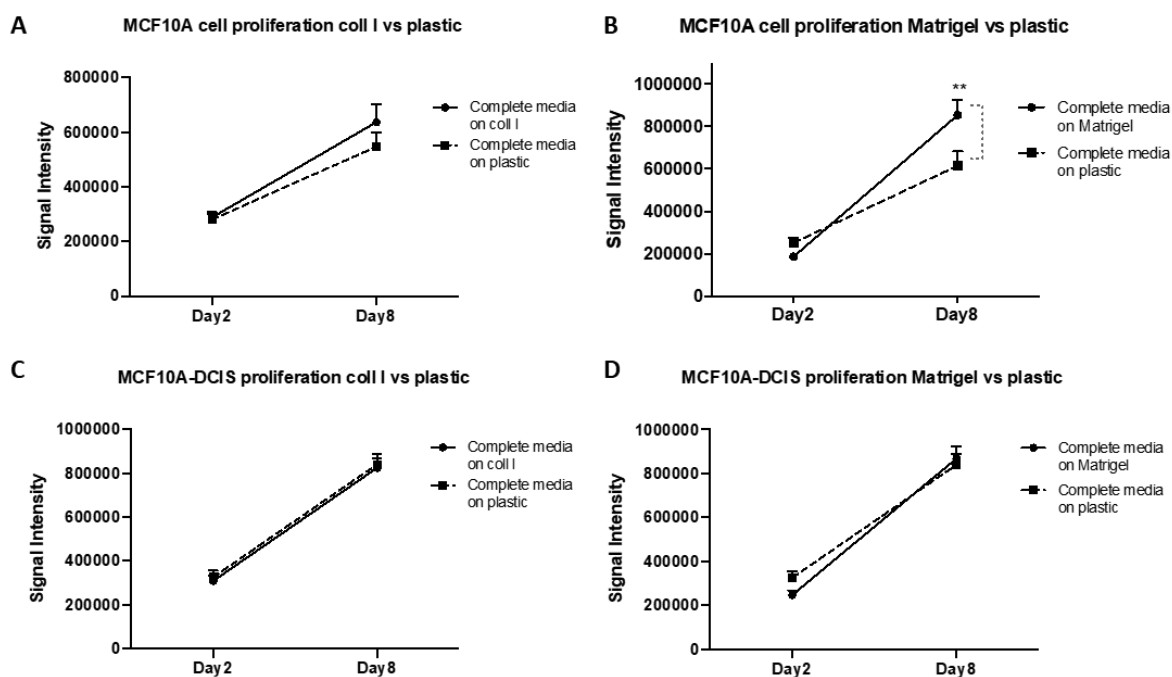
21. Kamphorst, J.J. et al. Human pancreatic cancer tumors are nutrient poor and tumor cells actively scavenge extracellular protein. *Cancer Res* 75, 544-553 (2015).
22. Olivares, O. et al. Collagen-derived proline promotes pancreatic ductal adenocarcinoma cell survival under nutrient limited conditions. *Nat Commun* 8, 16031 (2017).
23. Pankova, D. et al. Cancer-Associated Fibroblasts Induce a Collagen Cross-link Switch in Tumor Stroma. *Mol Cancer Res* 14, 287-295 (2016).
24. Hanley, C.J. et al. A subset of myofibroblastic cancer-associated fibroblasts regulate collagen fiber elongation, which is prognostic in multiple cancers. *Oncotarget* 7, 6159-6174 (2016).
25. Saadi, A. et al. Stromal genes discriminate preinvasive from invasive disease, predict outcome, and highlight inflammatory pathways in digestive cancers. *Proc Natl Acad Sci U S A* 107, 2177-2182 (2010).
26. Surowiak, P. et al. Occurrence of stromal myofibroblasts in the invasive ductal breast cancer tissue is an unfavourable prognostic factor. *Anticancer Res* 27, 2917-2924 (2007).
27. Vande Voorde, J. et al. Improving the metabolic fidelity of cancer models with a physiological cell culture medium. *Sci Adv* 5, eaau7314 (2019).
28. Dawson, P.J., Wolman, S.R., Tait, L., Heppner, G.H. & Miller, F.R. MCF10AT: a model for the evolution of cancer from proliferative breast disease. *Am J Pathol* 148, 313-319 (1996).
29. Rhee, D.K., Park, S.H. & Jang, Y.K. Molecular signatures associated with transformation and progression to breast cancer in the isogenic MCF10 model. *Genomics* 92, 419-428 (2008).
30. So, J.Y., Lee, H.J., Kramata, P., Minden, A. & Suh, N. Differential Expression of Key Signaling Proteins in MCF10 Cell Lines, a Human Breast Cancer Progression Model. *Mol Cell Pharmacol* 4, 31-40 (2012).
31. Mossmann, D., Park, S. & Hall, M.N. mTOR signalling and cellular metabolism are mutual determinants in cancer. *Nat Rev Cancer* 18, 744-757 (2018).
32. Dutta, D. & Donaldson, J.G. Search for inhibitors of endocytosis: Intended specificity and unintended consequences. *Cell Logist* 2, 203-208 (2012).
33. Talvensaaari-Mattila, A., Paakko, P., Hoyhtya, M., Blanco-Sequeiros, G. & Turpeenniemi-Hujanen, T. Matrix metalloproteinase-2 immunoreactive protein: a marker of aggressiveness in breast carcinoma. *Cancer* 83, 1153-1162 (1998).
34. Tetu, B. et al. The influence of MMP-14, TIMP-2 and MMP-2 expression on breast cancer prognosis. *Breast Cancer Res* 8, R28 (2006).
35. Yousef, E.M., Tahir, M.R., St-Pierre, Y. & Gaboury, L.A. MMP-9 expression varies according to molecular subtypes of breast cancer. *BMC Cancer* 14, 609 (2014).
36. Everts, V., Hembry, R.M., Reynolds, J.J. & Beertsen, W. Metalloproteinases are not involved in the phagocytosis of collagen fibrils by fibroblasts. *Matrix* 9, 266-276 (1989).
37. Han, S., Li, Y.Y. & Chan, B.P. Protease inhibitors enhance extracellular collagen fibril deposition in human mesenchymal stem cells. *Stem Cell Res Ther* 6, 197 (2015).
38. Burridge, K., Turner, C.E. & Romer, L.H. Tyrosine phosphorylation of paxillin and pp125FAK accompanies cell adhesion to extracellular matrix: a role in cytoskeletal assembly. *J Cell Biol* 119, 893-903 (1992).
39. Maziveyi, M. & Alahari, S.K. Cell matrix adhesions in cancer: The proteins that form the glue. *Oncotarget* 8, 48471-48487 (2017).
40. Aboubakar Nana, F. et al. Therapeutic Potential of Focal Adhesion Kinase Inhibition in Small Cell Lung Cancer. *Mol Cancer Ther* 18, 17-27 (2019).
41. Slack-Davis, J.K. et al. Cellular characterization of a novel focal adhesion kinase inhibitor. *J Biol Chem* 282, 14845-14852 (2007).
42. Ghosh, S.G. et al. Biallelic variants in HPDL, encoding 4-hydroxyphenylpyruvate dioxygenase-like protein, lead to an infantile neurodegenerative condition. *Genet Med* (2020).
43. Forster, J.C., Harriss-Phillips, W.M., Douglass, M.J. & Bezak, E. A review of the development of tumor vasculature and its effects on the tumor microenvironment. *Hypoxia (Auckl)* 5, 21-32 (2017).

44. Rainero, E. et al. Ligand-Occupied Integrin Internalization Links Nutrient Signaling to Invasive Migration. *Cell Rep* 10, 398-413 (2015).
45. Hernandez-Fernaund, J.R. et al. Secreted CLIC3 drives cancer progression through its glutathione-dependent oxidoreductase activity. *Nat Commun* 8, 14206 (2017).
46. Kaukonen, R. et al. Normal stroma suppresses cancer cell proliferation via mechanosensitive regulation of JMJD1a-mediated transcription. *Nat Commun* 7, 12237 (2016).
47. Simoes, R.V. et al. Metabolic plasticity of metastatic breast cancer cells: adaptation to changes in the microenvironment. *Neoplasia* 17, 671-684 (2015).
48. Yang, L. et al. Metabolic shifts toward glutamine regulate tumor growth, invasion and bioenergetics in ovarian cancer. *Mol Syst Biol* 10, 728 (2014).
49. Muschler, J. & Streuli, C.H. Cell-matrix interactions in mammary gland development and breast cancer. *Cold Spring Harb Perspect Biol* 2, a003202 (2010).
50. Buchheit, C.L., Weigel, K.J. & Schafer, Z.T. Cancer cell survival during detachment from the ECM: multiple barriers to tumour progression. *Nat Rev Cancer* 14, 632-641 (2014).
51. Badaoui, M. et al. Collagen type 1 promotes survival of human breast cancer cells by overexpressing Kv10.1 potassium and Orai1 calcium channels through DDR1-dependent pathway. *Oncotarget* 9, 24653-24671 (2018).
52. Korolchuk, V.I. et al. Lysosomal positioning coordinates cellular nutrient responses. *Nat Cell Biol* 13, 453-460 (2011).
53. Yang, S. et al. Pancreatic cancers require autophagy for tumor growth. *Genes Dev* 25, 717-729 (2011).
54. Nofal, M., Zhang, K., Han, S. & Rabinowitz, J.D. mTOR Inhibition Restores Amino Acid Balance in Cells Dependent on Catabolism of Extracellular Protein. *Mol Cell* 67, 936-946 e935 (2017).
55. Oryan, A., Kamali, A., Moshiri, A., Baharvand, H. & Daemi, H. Chemical crosslinking of biopolymeric scaffolds: Current knowledge and future directions of crosslinked engineered bone scaffolds. *Int J Biol Macromol* 107, 678-688 (2018).
56. Lai, J.Y. & Ma, D.H. Glutaraldehyde cross-linking of amniotic membranes affects their nanofibrous structures and limbal epithelial cell culture characteristics. *Int J Nanomedicine* 8, 4157-4168 (2013).
57. Madsen, D.H. et al. M2-like macrophages are responsible for collagen degradation through a mannose receptor-mediated pathway. *J Cell Biol* 202, 951-966 (2013).
58. Begum, A. et al. The extracellular matrix and focal adhesion kinase signaling regulate cancer stem cell function in pancreatic ductal adenocarcinoma. *PLoS One* 12, e0180181 (2017).
59. Lee, B.Y., Timpson, P., Horvath, L.G. & Daly, R.J. FAK signaling in human cancer as a target for therapeutics. *Pharmacol Ther* 146, 132-149 (2015).
60. Serrels, A. et al. The role of focal adhesion kinase catalytic activity on the proliferation and migration of squamous cell carcinoma cells. *Int J Cancer* 131, 287-297 (2012).
61. Shibue, T. & Weinberg, R.A. Integrin beta1-focal adhesion kinase signaling directs the proliferation of metastatic cancer cells disseminated in the lungs. *Proc Natl Acad Sci U S A* 106, 10290-10295 (2009).
62. Desgrosellier, J.S. et al. An integrin alpha(v)beta(3)-c-Src oncogenic unit promotes anchorage-independence and tumor progression. *Nat Med* 15, 1163-1169 (2009).
63. Pirone, D.M. et al. An inhibitory role for FAK in regulating proliferation: a link between limited adhesion and RhoA-ROCK signaling. *J Cell Biol* 174, 277-288 (2006).
64. Davidson, S.M. et al. Direct evidence for cancer-cell-autonomous extracellular protein catabolism in pancreatic tumors. *Nat Med* 23, 235-241 (2017).
65. More, T.H. et al. Metabolomic alterations in invasive ductal carcinoma of breast: A comprehensive metabolomic study using tissue and serum samples. *Oncotarget* 9, 2678-2696 (2018).
66. Wang, X. et al. HPD overexpression predicts poor prognosis in breast cancer. *Pathol Res Pract* 215, 152524 (2019).

67. Kaukonen, R., Jacquemet, G., Hamidi, H. & Ivaska, J. Cell-derived matrices for studying cell proliferation and directional migration in a complex 3D microenvironment. *Nat Protoc* 12, 2376-2390 (2017).
68. Comisso, C., Flinn, R.J. & Bar-Sagi, D. Determining the macropinocytic index of cells through a quantitative image-based assay. *Nat Protoc* 9, 182-192 (2014).

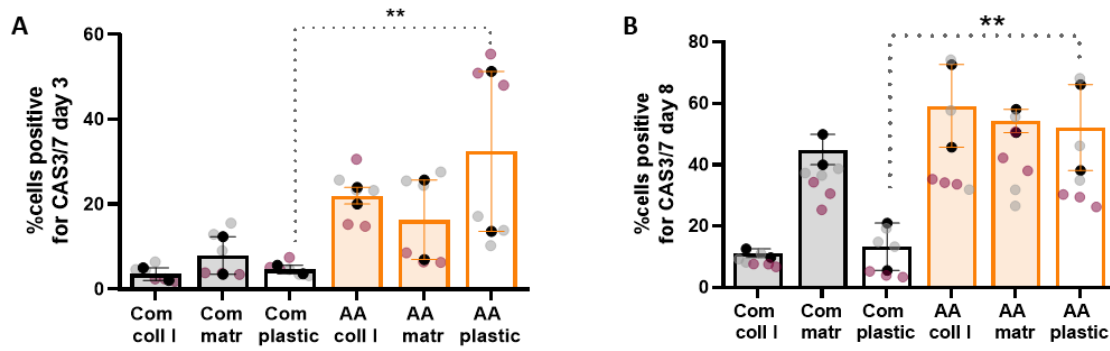


**Supplementary figure 1. MDA-MB-231 cell growth on ECMs under complete media.** MDA-MB-231 cells were seeded either on plastic or on plates coated with (A) collagen I (2mg/ml), (B) Matrigel (3mg/ml) and (C) laminin/entactin (3.5mg/ml) for eight days in complete media containing glutamine, glucose and 10% DFBS. (D) MDA-MB-231 cells were seeded either on plastic or on plates coated with collagen I (2mg/ml) and Matrigel (3mg/ml) in Plasmax with 2.5% DFBS. Cell proliferation was measured by DRAQ5 nuclear staining quantification with the Licor Odyssey system. Signal intensity from cells under each condition were collected by Image Studio Lit software. (E) MDA-MB-231 cells were seeded either on plastic or on plates coated with CAF-CDM in Plasmax with 10% DFBS. Cell proliferation was measured via Hoechst nuclear staining. Images were collected by ImageXpress micro and analysed by MetaXpress software. Values are mean  $\pm$  SEM and are representative of at least three independent experiments. \*\*\*\*  $p < 0.0001$  ANOVA test.



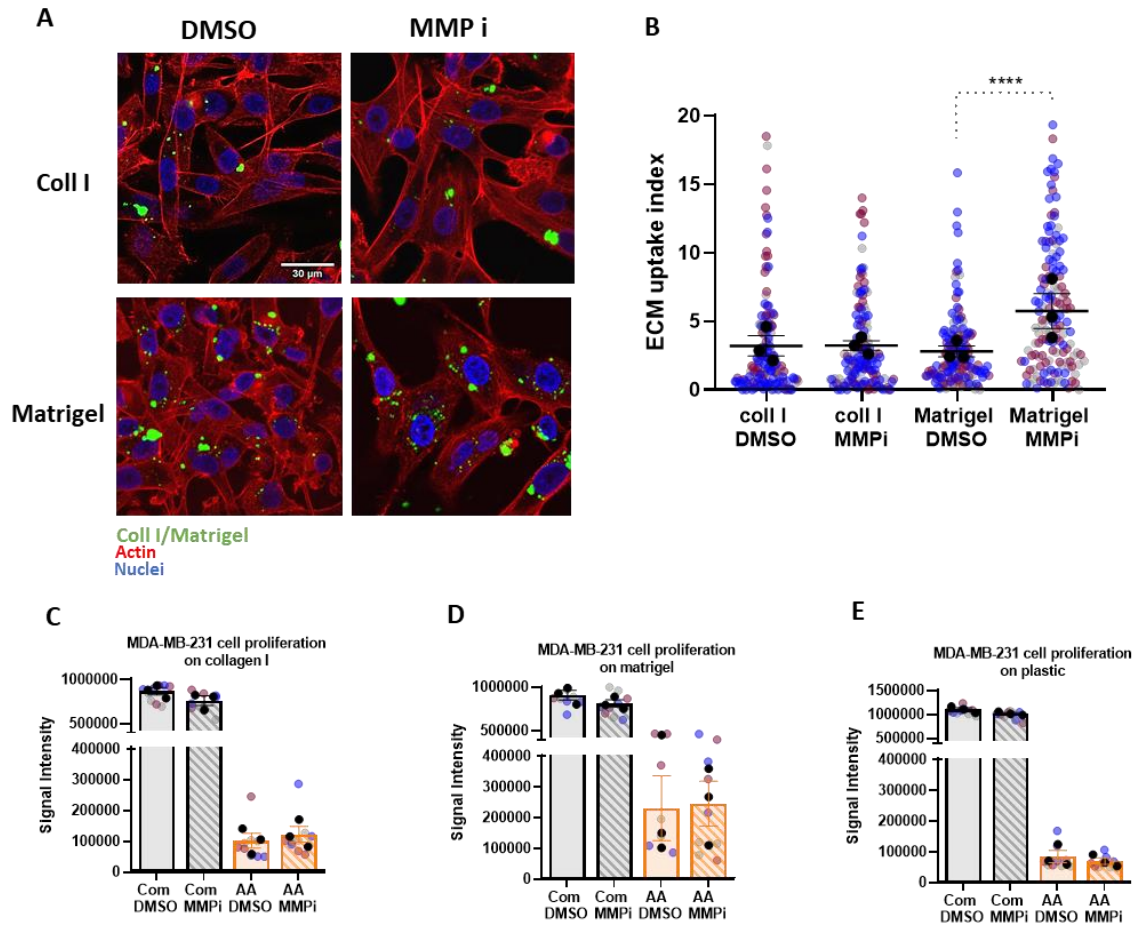
**Supplementary figure 2. MCF10A and MCF10A-DCIS growth on ECMs under complete media.**

MCF10A cells were seeded either on plastic or on plates coated with (A) collagen I (2mg/ml), (B) Matrigel (3mg/ml) for eight days in complete media containing glutamine, glucose and 10% HS. MCF10A-DCIS cells were seeded either on plastic or on plates coated with (C) collagen I (2mg/ml) and (D) Matrigel (3mg/ml) for eight days under complete media containing glutamine, glucose and 5% HS. Cell proliferation was measured by DRAQ5 nuclear staining quantification with the Licor Odyssey system. Signal intensity from cells under each condition were collected by Image Studio Lit software. Values are mean  $\pm$  SEM and are representative of at least three independent experiments. \*\* $p < 0.01$  ANOVA test.

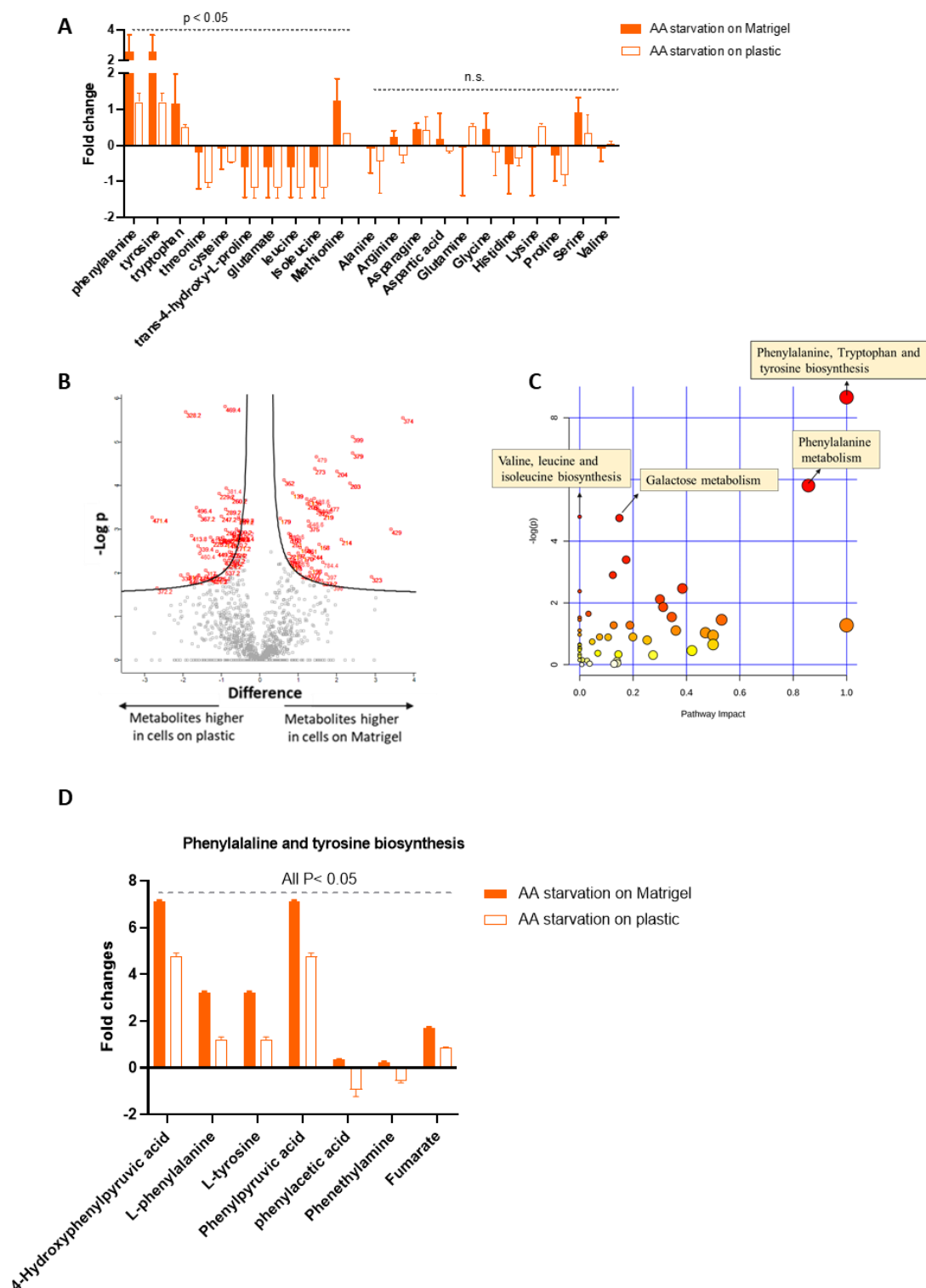


**Supplementary figure 3. The ECM did not affect apoptosis under starvation.** MDA-MB-231 cells were seeded on either plastic or plates coated with collagen I (2mg/ml) and Matrigel (3mg/ml) under AA starvation or complete media. Cells were stained for activated cas-3/7 at day (A) three or (B) eight post starvation. Images were collected by ImageXpress micro and analysed by CME software. Values are mean  $\pm$  SEM and are representative of two independent experiments. (the black dots represent the mean of individual experiments). \*\* $p < 0.01$  ANOVA test.





**Supplementary figure 4. MMP inhibition did not affect ECM uptake and cell growth under starvation.** (A and B) MDA-MB-231 were seeded either on N-Hydroxysuccinimide-fluorescein labelled collagen I (2mg/ml) or Matrigel (3mg/ml) under complete media and in the presence of lysosomal protease inhibitor, E64d (20 $\mu$ M). MMP inhibitors GM6001 (10 $\mu$ M) or DMSO (control) were added to cells every two days up to day three. Cells were fixed and stained for actin (red) and nuclei (blue). Images were collected by a Nikon A1 confocal microscope. \*\*\*\*  $p < 0.0001$  ANOVA test. To assess cell proliferation, MDA-MB-231 were seeded on (C) collagen I (2mg/ml), (D) Matrigel (3mg/ml), or (E) plastic under complete or AA depleted media. GM6001 (10 $\mu$ M) or DMSO (control) were added to cells every two days. Cell proliferation was measured by DRAQ5 nuclear staining quantification with the Licor Odyssey system on day six post starvation. Values are mean  $\pm$  SEM and are representative of three independent experiments. (The black dots represent the mean of individual experiments).



**Supplementary figure 5. Cells had different metabolite content on Matrigel compared to plastic under amino acid starvation.** Cells starved for 6 days either on Matrigel or plastic. (A and D) Fold changes of amino acids (A) and tyrosine and phenylalanine metabolism pathway intermediates (D) levels in MDA-MB-231 normalized to the median of total metabolites in each condition. P values were measured by Student's t-test. (B) Volcano plot of cells on Matrigel and plastic comparing the fold changes and P value of individual metabolites.  $p$ -value  $< 0.05$ . Each number is representative of the bins allocated to different metabolites which are statistically significant. (C) Highlights the most enriched pathways,  $p$ -value  $< 0.05$ .

## Chapter 4: The ECM supports breast cancer cell metabolism under amino acid starvation.

### 4.1 Introduction

This chapter contains data which provide some background to the work presented in the format of a paper in chapter 3. In addition, in this chapter we searched deeper into the metabolic changes due to the presence of ECM under AA starvation.

Previously we found that the presence of ECM rescued the growth of invasive breast cancer cells under AA deficiency. In particular, cells were shown to internalize and degrade ECM components inside the lysosomes and inhibition of internalization opposed cell growth under AA starvation. Metabolomic analysis revealed that the presence of collagen I and Matrigel remarkably changed the metabolite content of cells under AA depleted media. On ECM, cells mostly presented higher EAAs content, leading to mTORC1 signalling activation under AA starvation.

Cells can sense nutrient fluctuations in the environment and respond to them by balancing between anabolic and catabolic processes inside the cells. Mechanistic target of Rapamycin (mTOR) signalling pathway is the pivotal regulator of anabolic and catabolic processes. When nutrients are available, mTOR enhances anabolic processes such as nucleotide, proteins and lipid biosynthesis and prevents lysosomal biogenesis and cellular autophagy. On the other hand, during nutrient deficiency, mTOR signalling pathway is inhibited to allow cells to promote catabolic activity to provide adequate amounts of nutrients to the cells. Any mutation in this pathway could cause metabolic disorder and cancer stimulation (Kim et al., 2013a, Kim et al., 2013b, Zoncu et al., 2011b). mTOR is a serine-threonine protein kinase forming two independent complexes, mTORC1 and mTORC2. mTORC1 regulates cell growth in response to the presence of AAs and GFs, while mTORC2 is involved in actin organization. mTORC1 is composed of three main components; 1) regulatory-associated protein of mTOR (RAPTOR) recruiting substrates for phosphorylation in mTORC1 complex and is responsible for the subcellular localisation of mTORC1; 2) DEP-domain-containing mTOR-interacting protein (DEPTOR), working both as mTORC1 endogenous inhibitor and substrate; 3) mammalian lethal with SEC13 protein 8 (mLST8), stabilizing the kinase domain of mTORC1

(Kim et al., 2013a, Liu and Sabatini, 2020). Working platform for mTORC1 is the lysosome. Activation of mTORC1 is dependent on GFs and nutrients. Availability of nutrients induce recruitment of mTORC1 on lysosomes where they become activated through GFs' downstream signalling (Mossmann et al., 2018). Binding of GFs to tyrosine kinase receptors trigger PI3K/Akt and Ras/MAPK signalling pathways eventually activates mTORC1 (Mendoza et al., 2011). Presence of AAs induce association of Rag GTPase to RAPTOR in mTORC1 resulting in its activation and lysosomal recruitment. Gln triggers RAG GTPase activation via glutaminolysis. During glutaminolysis, Gln converts to  $\alpha$ -ketoglutarate which activates mTORC1 via enhancing the GTP loading of RAG-GTPase. However, leucine and arginine have independent mechanisms to activate RAG-GTPase. Leucine and arginine negatively regulate the activity of Rag-GTPase inhibitors, sestrin2 and CASTOR1 (Jewell et al., 2015, Wolfson and Sabatini, 2017). Glc also activates mTORC1 via inducing ATP production through glycolysis and the TCA cycle. Lack of Glc or inhibition of energy production result in the accumulation of AMP, which activates the mTORC1 inhibitor, AMPK (Inoki et al., 2012, Hardie et al., 2012). Removal of GFs, sources of energy, and AAs from the intercellular environment leads to mTORC1 inactivation and displacement from lysosome to the cytoplasm (Sato et al., 2008, Martinez-Carreres et al., 2017). Starvation is the condition when the activity of mTORC1 is prevented to allow cells to rely on other sources of nutrient consumption like autophagy (Korolchuk et al., 2011). Several studies showed that mTORC1 inhibition induced by starvation increase the scavenging of ECPs, such as albumin (Palm et al., 2015), laminin (Muranen et al., 2017) and fibronectin (Rainero et al., 2015a) as a compensatory mechanism. Inhibition of mTORC1 activity has been suggested as a strategy to limit cancer progression (Tian et al., 2019). However, mTORC1 might not be a favourable target for cancer therapy since its inactivation could help cancer cells to survive by adapting their metabolic pathways to rely on alternative sources of nutrients such as ECPs.

In this chapter we showed that cells can internalize and degrade laminin under starvation. Presence of Laminin can partially rescue cell growth and cell division under starvation while it does not enhance mTORC1 activity. In addition, we demonstrated that cells under AA starvation uptake more Glc compared to the cells under complete media on both ECM and plastic. However, presence of ECM increased glycolysis and TCA cycle intermediates and cells on Matrigel showed higher ATP content.

## 4.2 Results

### 4.2.1 Cell proliferation assay optimisation.

In the previous chapter, we quantified cell growth via detecting the signal intensity of the nuclei stained by DRAQ5. To assess whether this quantification technique was accurate, between  $10^3$  to  $2 \times 10^4$  MDA-MB-231 cells were plated on clear, flat-bottomed 96-well plates for 5hrs. Cells were fixed and stained with DRAQ5. Signal intensity per well was detected with the Licor Odyssey imaging system. Our data showed that intensity detected from DRAQ5 staining is directly proportional to the cell number (Figure 4.1A).

We have shown in chapter 3 that breast cancer cells were able to internalize and degrade the ECM under different starvation conditions. To assure that the ECM was not completely degraded by the cells during the proliferation assay, plates were coated with either collagen I or Matrigel. Polymerized ECM were incubated with a fluorescently labelled N-Hydroxysuccinimide Ester reactive dye binding to free amine groups on lysine residues to form a stable conjugate. MDA-MB-231 cells were seeded on the labelled matrices the following day, and media was replaced with starvation conditions after 5hrs. Cells were fixed at day two and day eight post starvation. Intensity of N-Hydroxysuccinimide Ester bound to collagen I or Matrigel under each condition was quantified by imaging with the Licor Odyssey imaging system. Collected data from plates covered by collagen I and Matrigel revealed that there was still matrix remaining at the end of the experiments, suggesting that the cells did not completely digest the matrix. However, there was a clear reduction in the amount of collagen I between day 2 and day 8 for all the media conditions, while this is a lot less pronounced for Matrigel. In addition, the starvations did not affect the total amount of ECM present compared to the complete media. (Figure 4.1B-C). Altogether, these data indicate that the quantification of DRAQ5 staining intensity by the Licor odyssey system can be used to measure cell proliferation. Moreover, the amount of ECM used to assess cell proliferation up to day eight was sufficient, as there was still detectable ECM inside the plates by the end of the experiment.

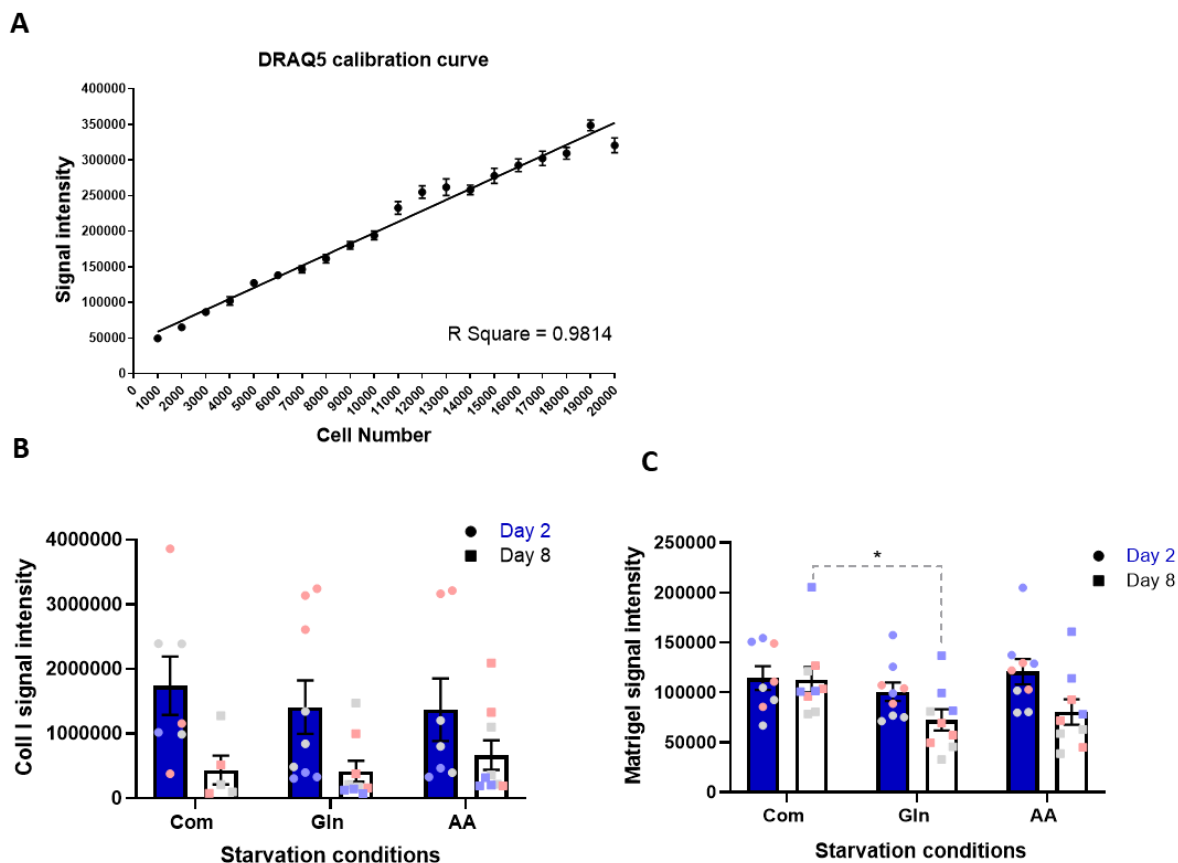


**Figure 4.1. Optimising techniques for cell proliferation assay.** (A) MDA-MB-231 cells were seeded on flat bottom 96-well plate. After 5hrs incubation in 5% CO<sub>2</sub> and 37°C, cells were fixed and stained with DRAQ5 nuclear staining. Signal intensity from well under each condition was collected and quantified with the Licor Odyssey system. R Square = 0.9814 linear regression test. Plates were coated with 15µl (B) 2mg/ml collagen I or (C) 3mg/ml Matrigel. Matrices were stained with 0.2µg/ml N-Hydroxysuccinimide ester. 10<sup>3</sup> MDA-MB-231 cells were seeded on ECMs under complete media (Com), glutamine (Gln) and amino acid (AA) starvation, fixed, imaged, and quantified with the Licor Odyssey system. Values are mean ± SEM and are representative of three independent experiments. \* p<0.05 ANOVA test.

#### 4.2.2 TIF-CDM, but not CAF-CDM, supported the growth of non-invasive breast cancer cells under glutamine starvation.

We have previously shown in chapter 3 that the presence of Matrigel, but not collagen I, can partially rescue the growth of MCF10A-DCIS cells under the Gln starvation (Chp3 figure 2E-H). To test the effect of Gln deficiency on the cell growth in a more physiologic condition, MCF10a-DCIS were seeded on matrices derived from TIFs or CAFs extracted from the breast tumours. As shown in figure 4.2, cells on TIF-CDM had significantly higher cell number and growth rate after eight days of Gln starvation compared to the plastic (Figure 4.2A-B).

However, cells plated on CAF-CDM did not show any difference in growth rate compared to the cells on plastic in Gln depleted media (Figure 4.2C-D). Altogether, these data indicate that TIF-CDM, but not CAF-CDM, was able to support MCF10A-DCIS cell growth under Gln starvation.

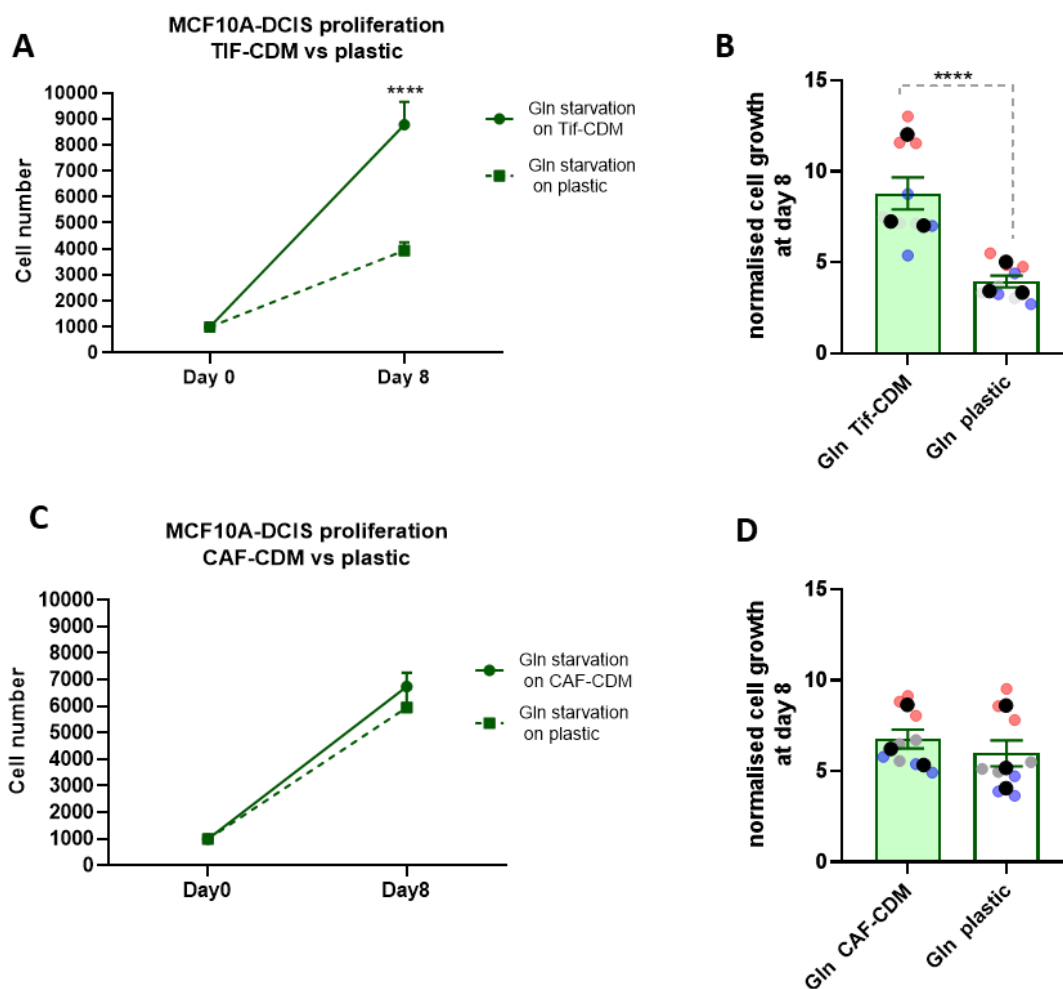


**Figure 4.2. TIF-CDM rescued MCF10A-DCIS growth under glutamine starvation.** MCF10A-DCIS cells were seeded either on plastic or on (A-B) TIF-CDM or (C-D) CAF-CDM under Gln starvation condition for eight days. On day zero  $10^3$  cells were seeded under each condition in each well of 96-well plate. In each experiment, three wells were allocated to each condition. On day eight, cell proliferation was measured via Hoechst nuclear staining. Images were collected by ImageXpress micro and analysed by MetaXpress software. Values are mean  $\pm$  SEM and are representative of at least three independent experiments (the black dots represent the mean of individual experiments). \*\*\*\*  $p < 0.0001$  ANOVA test.

### 4.2.3 Laminin increased invasive breast cancer cell division under glutamine and amino acid starvation conditions.

We showed in chapter 3 that laminin could partially rescue the growth of the cells under Gln and AA starvation (Chp3 figure 1E-F). To confirm whether laminin could induce cell division, MDA-MB-231 cells were seeded either on plastic or plates coated with laminin under Gln and AA depleted media. Cells received EdU on day six post starvation, were fixed and stained at day eight (Described in detail in section 2.2.7). Our result demonstrated that cells on laminin have a significantly higher EdU incorporation compared to the cells growing on plastic under Gln and AA deficiency (Figure 4.3), while no difference was observed in complete media. Altogether, higher percentage of replicative cells on laminin, collagen I and Matrigel indicates that presence of ECM facilitates cell proliferation under starvation.

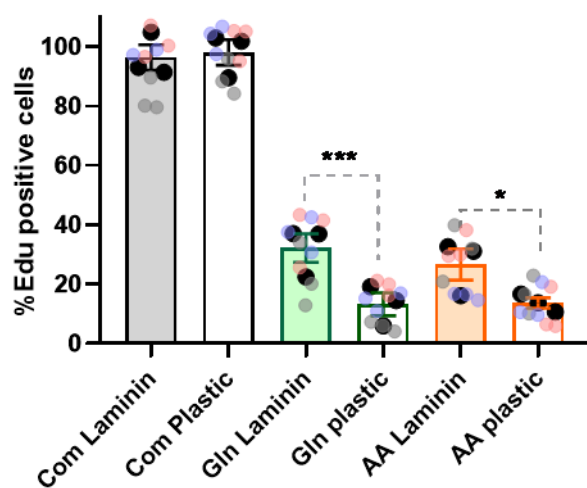


**Figure 4.3. Laminin induced cell proliferation under glutamine and amino acid starvations.** MDA-MB-231 cells were seeded either on plastic or plastic coated with laminin/entactin (3.5mg/ml) under Gln and AA starvation conditions. Cells were incubated with EdU on day six post starvation, fixed and stained with Hoechst and Click iT EdU imaging kit on day 8. Images were collected by ImageXpress micro and analysed by MetaXpress software. Values are mean  $\pm$  SEM and are representative of three independent experiments (the black dots represent the mean of individual experiments). \* $p < 0.05$  and \*\*\* $p < 0.001$ , ANOVA test.



#### 4.2.4 Invasive breast cancer cells internalized and degraded laminin.

Our results showed that MDA-MB-231 cells had higher growth rate on laminin compared to the plastic under starvation (Chp3 figure 1E-F). In addition, the data from EdU labelling experiments confirmed that under Gln and AA starvation laminin induced cell replication (Figure 4.3). Monitoring collagen I, and Matrigel uptake previously demonstrated that invasive breast cancer cells could internalize the ECM and degrade it inside the lysosomes under different nutrient conditions (Chp3 figure 5A-B). Therefore, to examine whether cells also internalized the laminin, we tracked the journey of laminin inside the cells in the presence of a lysosomal protease inhibitor (E64d). Uptake of fluorescent-labelled laminin was monitored under complete, Gln and AA depleted media. Our results showed that MDA-MB-231 cells internalized laminin followed by lysosomal degradation under both Gln and AA deficiency (Figure 4.4), since the presence of the lysosomal protease inhibitor resulted in a profound increase in the amount of laminin which could be detected inside the cells.

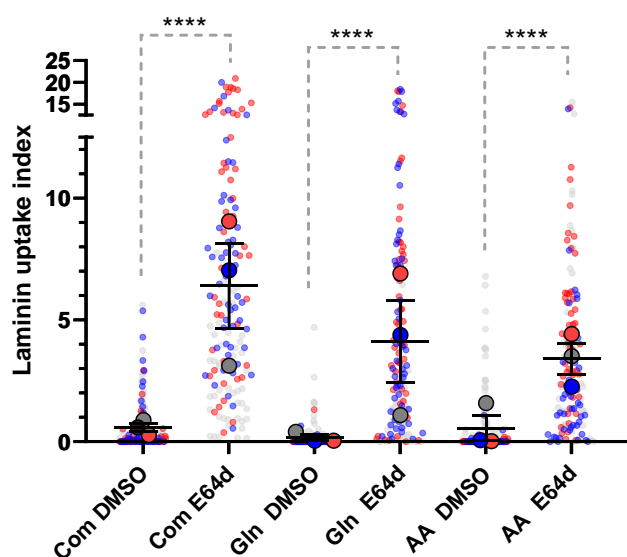


**Figure 4.4. MDA-MB-231 cells internalized and degraded laminin under normal and starvation conditions.** MDA-MB-231 cells were plated under complete (Com) or Gln and AA depleted media on dishes coated with N-Hydroxysuccinimide-fluorescein labelled laminin/entactin (3.5mg/ml) for three days, in the presence of the lysosomal inhibitor E64d (20 $\mu$ M) or DMSO (control). Cells were visualised by confocal microscopy using a Nikon A1 microscope (described in more details in section 2.2.6). Laminin uptake index was quantified with Image J. Values are mean  $\pm$  SEM and are representative of three independent experiments including around 150 cells per condition (the bigger dots represent the mean of individual experiments). \*\*\*\* p<0.0001 ANOVA test.

#### 4.2.5 Laminin did not support mTORC1 activity under starvation.

In chapter 3 we showed that Matrigel and collagen I fully rescued mTORC1 activity in starved cells (Chp3 figure 4). We also showed that cells can internalize laminin followed by lysosomal degradation under starvation condition (Figure 4.4). In another study, it was shown that laminin increased cell growth and promoted mTORC1 activation in normal mammary epithelial cells (Muranen et al., 2017). Therefore, we tested whether the presence of laminin was able to increase mTORC1 activity in starved MDA-MB-231 cells, by examining the phosphorylation of an mTORC1 downstream target, S6, as an indicator for mTORC1 activity. Cells were seeded on laminin or plastic in AA depleted condition for three days. mTORC1 activity was measured by quantifying p-S6 intensity. Our data demonstrated that laminin did not affect p-S6 intensity under AA starvation (Figure 4.5). Taken together, these data indicate that the ability of laminin to rescue invasive breast cancer cell growth is independent of mTORC1 signalling.

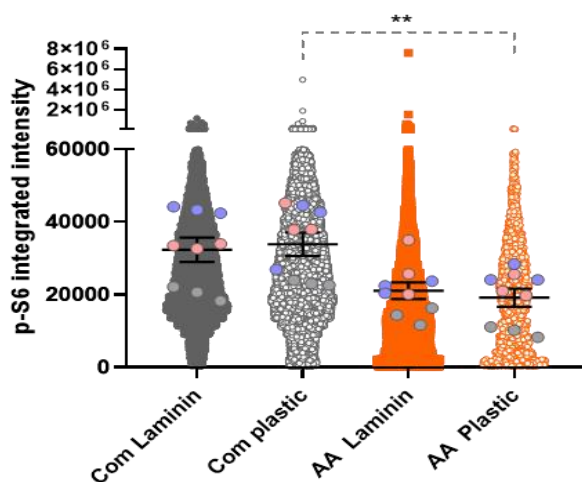


**Figure 4.5. Presence of laminin did not affect mTORC1 activity in starved cells.** MDA-MB-231 cells were plated either on plastic or plastic coated with laminin/entactin (3.5mg/ml) under complete media or AA starvation condition. Cells were fixed and stained for p-S6 and nuclei at day three. Images were collected by ImageXpress micro and analysed by CME software. Values are mean  $\pm$  SEM and are representative of three independent experiments. (The dots represent the mean of individual experiments). \*\* $p < 0.01$  ANOVA test.

#### 4.2.6 V-ATPase inhibitor decreased cell growth.

Vacuolar (V)-ATPase is a multi-subunit proton pump complex. It maintains the activity of lysosomes via lowering the pH. V-ATPase has two main domains: a peripheral domain, or V1, located in cytoplasm to supervise ATP hydrolysis and an integral domain, or V0, embedded in membrane, responsible for transferring protons from the cytoplasm to the lumen of the lysosome (Forgac, 2007). Inhibiting V-ATPase activity causes deacidification of lysosome and consequently constrain lysosomal protease degradation (Abu-Remaileh et al., 2017). V-ATPase activity has also been shown to be required for AA sensing and mTORC1 activation. Accumulation of AAs inside the lysosomes induces a signal transferred to Rag GTPases via the V-ATPase–Ragulator interaction leading to mTORC1 lysosomal recruitment and activation (Zoncu et al., 2011a). The data presented in chapter 3 demonstrated that the presence of ECM rescued mTORC1 activity which could be a result of the ECM being degraded in the lysosomes to extract AAs. To test this, MDA-MB-231 cells were treated with Bafilomycin A1 (BA1), a V-ATPase inhibitor. Our data showed that, in full media, V-ATPase inhibition decreased cell number and mTORC1 activity on both Matrigel and plastic (Figure 4.6A-B). Under AA starvation, the treatment of cells with BA1 completely blocked the ability of Matrigel to promote cell growth without further impeding the growth of starved cells on plastic (Figure 4.6C). We also expected to observe reduction in mTORC1 activity in cells on Matrigel in the presence of BA1, however, mTORC1 activity did not show any change upon BA1 treatment compared to the control group under AA starvation (Figure 4.6D). Taken together, these data suggest that inhibiting the V-ATPase activity in the presence of soluble nutrients decreased mTORC1 activity and cell growth regardless of cells being on ECM or not. In contrast, the inhibitory effect of BA1 on cell growth under AA starvation on Matrigel suggests that cells might need ECM degradation in the lysosomes to rescue their growth. However, the Matrigel-induced rescue of mTORC1 function was independent of V-ATPase activity.

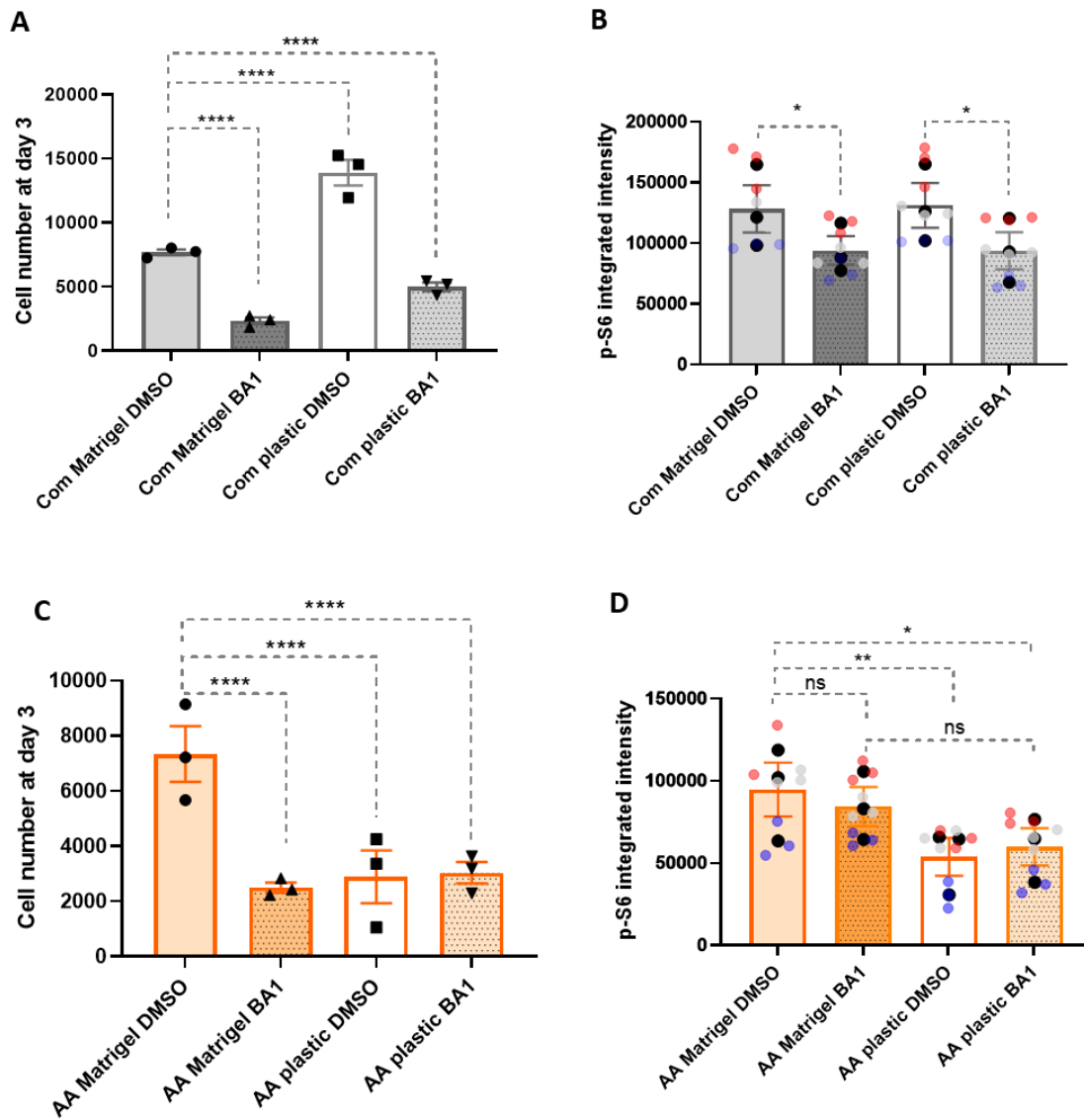


**Figure 4.6. Effect of V-ATPase inhibitor on cell growth and mTORC1 activity on Matrigel.** MDA-MB-231 cells were plated either on plastic or plastic coated Matrigel (3mg/ml) under (A-B) complete media, or (C-E) AA starvation. 200nM Bafilomycin A1 or DMSO (control) were added to each condition every day. Cells were fixed and stained for p-S6 and nuclei at day three. Images were collected by ImageXpress micro and analysed by CME software. Values are mean  $\pm$  SEM and are representative of three independent experiments. (The black dots represent the mean of individual experiments). \* $p < 0.05$ , \*\* $p < 0.01$ , \*\*\*\*  $p < 0.0001$  ANOVA test.

#### **4.2.7 Glucose uptake was not responsible for cell growth under amino acid starvation.**

Previously we showed that deacidifying lysosomes to inhibit their protease activity and ECM degradation did not affect mTORC1 signalling under AA starvation. Despite it was preventing cell growth. Therefore, cells might rely on another source of nutrients or GFs to reactivate mTORC1 in the presence of ECM. Studies have shown that availability of Glc induces mTORC1 activity (Liu and Sabatini, 2020). It has been revealed that NEAA biogenesis could occur through Glc uptake. Breast cancer cells could use Glc to produce serine and glycine, which can be fed into the folate and methionine cycle to produce cysteine (Geck and Toker, 2016). In addition, ECM degradation promotes GLUT1 expression and Glc uptake (Sullivan et al., 2018). Since cells under AA starvation have access to Glc, we hypothesised that the ECM could promote cell growth and mTORC1 activity by upregulating Glc uptake. To address this, MDA-MB-231 cells were seeded either on collagen I, Matrigel or plastic under AA starvation conditions. Cells received 2-NBDG, a fluorescent tracer for Glc, for 1hr at day six post starvation. Quantifying the percentage of cells positive for the Glc tracer showed that there was no significant difference between cells on plastic or collagen I under AA starvation. However, the percentage of 2-NBDG positive cells was significantly higher under AA starvation compared to the cells growing under complete media regardless of cells being on collagen I or not (Figure 4.7A). Measuring the intensity of 2-NBDG per cell showed that there was more Glc uptake under AA starvation on plastic compared to the collagen I. In addition, on plastic, cells under AA depleted media showed higher 2-NBDG uptake compared to the cells under the complete media (Figure 4.7B). Similarly, data from cells seeded on Matrigel revealed that there was no difference in the percentage of cells positive for 2-NBDG on Matrigel compared to the plastic under AA starvation. However, a significantly higher percentage of AA starved cells were positive for 2-NBDG compared to the cells under complete media (Figure 4.7C). Cells on Matrigel did not show significant changes in the intensity of 2-NBDG per cell compared to the plastic (Figure 4.7D). Overall, our data showed that cells on Matrigel or collagen I under AA starvation did not enhance Glc uptake compared to cells on plastic.

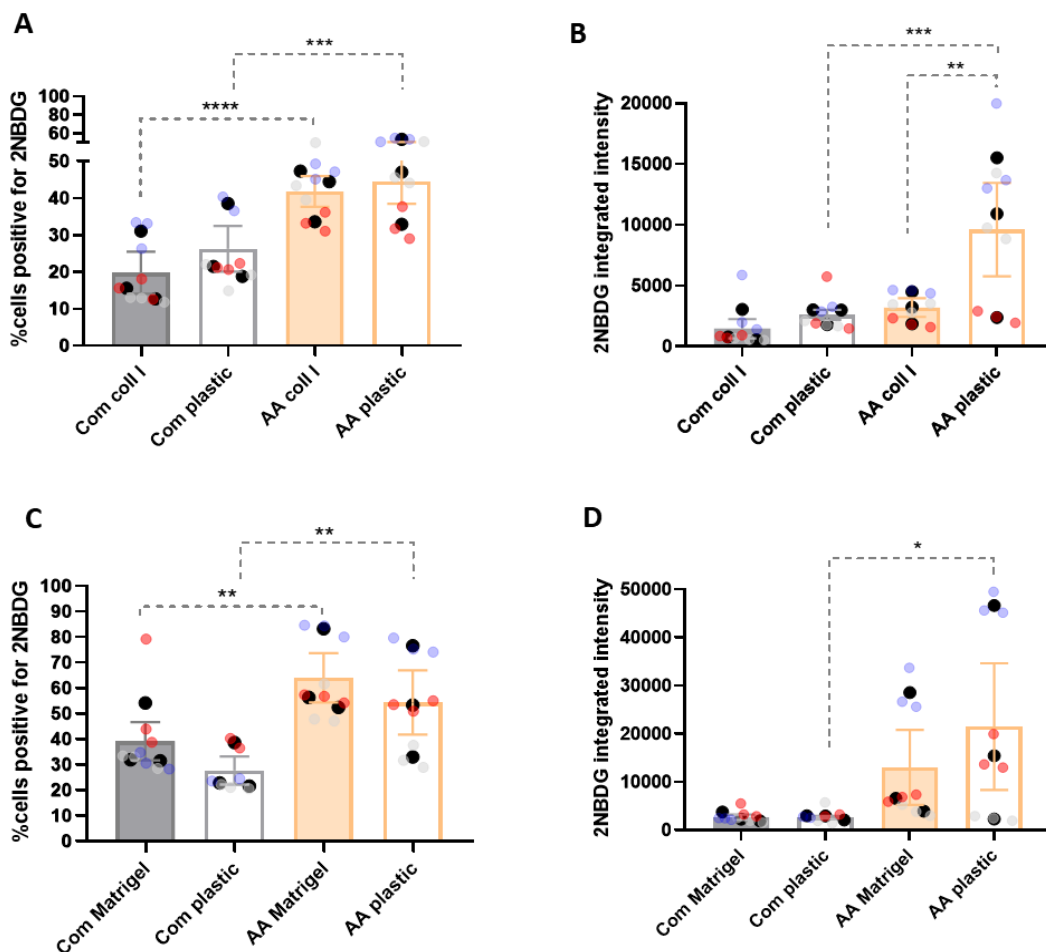


**Figure 4.7. The presence of ECM did not affect glucose uptake under amino acid starvation.** MDA-MB-231 cells were plated either on plastic or plastic coated with 2mg/ml collagen I (A and B) or 3mg/ml Matrigel (C and D) under complete media or AA starvation. Cells were incubated with 100 $\mu$ M 2-NBDG for 1 hr at day six. Cells were fixed and stained for nuclei. Images were collected by ImageXpress micro and analysed by CME software. Values are mean  $\pm$  SEM and are representative of three independent experiments. (The black dots represent the mean of individual experiments). \* $p < 0.05$ , \*\* $p < 0.01$ , \*\*\*  $p < 0.001$ , \*\*\*\*  $p < 0.0001$  ANOVA test.

#### 4.2.8 Cells on Matrigel had higher ATP content under amino acid starvation.

It has been recently shown that cells on higher ECM density have higher Glc uptake, ATP production and hydrolysis to meet the energy demand of migration. It was also shown that cells have higher intracellular ATP:ADP level in 3D environment compared to 2D environment (Zanotelli et al., 2018). Our previous data showed that higher Glc uptake might be an ECM-independent mechanism cells rely on to compensate for the lack of AAs (Figure 4.7). However, energy production in cells under different nutrient conditions was not determined. It is also important to define whether the glycolysis/OXPHOS ratio is changed on ECM under starvation

and whether these changes contribute to the ECM-dependent cell growth (Chp3 figure1). To assess whether the presence of ECM affected ATP content of cells, MDA-MB-231 were seeded either on collagen I, Matrigel or plastic under complete or AA depleted media. Cells received oligomycin A for 1hr. Oligomycin A inhibits OXPHOS and induces cells to produce ATP via glycolysis (Davis et al., 2020). To quantify cellular ATP content, MDA-MB-231 cells were incubated with bio-tracker ATP-red live cell dye for 15mins. ATP content of cells in the presence of oligomycin A was considered as the product of glycolysis. ATP generated by OXPHOS was measured by subtracting the ATP content in the presence of oligomycin A from the ATP content of the control group, as previously described (Mookerjee et al., 2017). The results showed that cells on Matrigel had a significantly higher amount of ATP compared to the cells on collagen I at day three regardless of their nutrient condition. In addition, the presence of Matrigel induced cells to rely more on glycolysis to produce ATP than OXPHOS at day three (Figure 4.8A). However, at day six post starvation, OXPHOS and glycolysis participated equally in ATP production in all groups. Cells under AA starvation on Matrigel produced a significantly higher amount of ATP compared to the cells on collagen I and plastic at day six. However, there was no difference between ATP content of cells under complete media regardless of their growth substrate (Figure 4.8B). Taken together, our data suggest that cells have more tendency to rely on glycolysis as a source of ATP on Matrigel compared to other substrates.

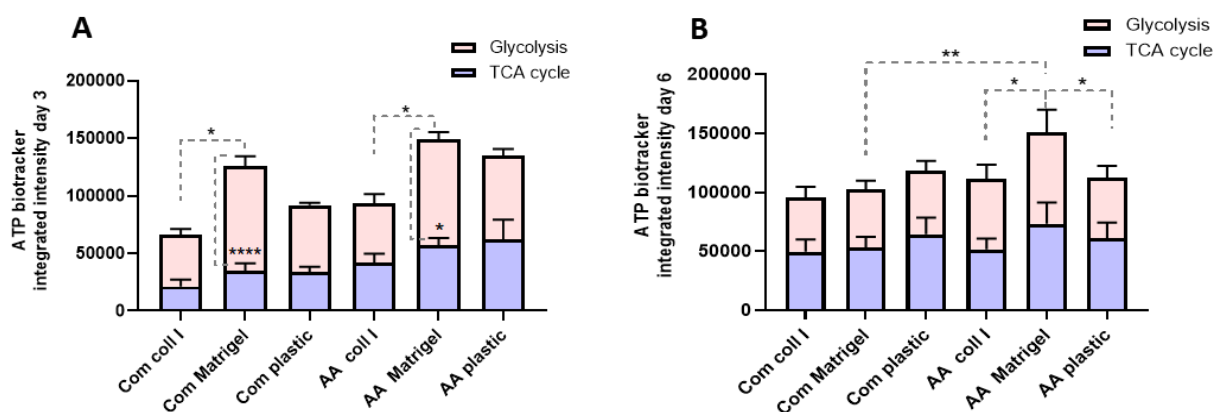


**Figure 4.8. Cells on Matrigel had higher ATP content under starvation.** MDA-MB-231 cells were plated either on plastic or plastic coated with collagen I (2mg/ml) or Matrigel (3mg/ml) under complete media and AA starvation. Cells were incubated with 126.4 $\mu$ M oligomycin A at 37°C and 5% CO<sub>2</sub> for 1 hr at day (A) three or (B) six post starvation. Cells' ATP content were measured by staining with 10 $\mu$ M BioTracker ATP-Red Live Cell Dye at 37°C and 5% CO<sub>2</sub> for 15 min. Live cell images were collected by ImageXpress micro and analysed by CME software. Values are mean  $\pm$  SEM and are representative of three independent experiments. \*p<0.05, \*\*p<0.01, \*\*\*\* p<0.0001 ANOVA test.

#### **4.2.9 The presence of ECM increased glycolysis and TCA cycle intermediates under starvation.**

We previously showed that the presence of ECM upregulated intracellular AA content in cells, that could be derived from collagen I and Matrigel through lysosomal degradation (Chp3 figure7 and supplementary figure 5). Many of these AAs can directly or indirectly feed the TCA cycle (Yang et al., 2017). Our previous data showed that there was no difference in ATP content between cells seeded on collagen I and plastic. However, after six days of AA starvation, cells on Matrigel had a significantly higher amount of ATP compared to the cells on plastic and collagen I (Figure 4.8). To further analyse whether being surrounded by ECM could also affect the activity of metabolic pathways responsible for energy production inside the cells, we assessed the amount of TCA cycle and glycolysis intermediates in cells on ECM or plastic under starvation. To do this, we performed direct infusion mass spectrometry (DI-MS) of MDA-MB-231 cells either on plastic, collagen I or Matrigel under six days of AA starvation. Our data showed that contrary to the data from 2-NBDG uptake (Figure 4.7), cells on both collagen I and Matrigel had higher Glc content compared to the cells on plastic. On collagen I, glycolysis intermediates downstream of Glc including fructose-1,6-bisphosphate and fructose-6-phosphate were upregulated compared to the plastic (Figure 4.9A). On Matrigel, fructose-1,6-bisphosphate was upregulated while amounts of 3-phosphoglycerate and 2-phosphoglycerate were downregulated (Figure 4.9C). Moreover, both collagen I and Matrigel induced upregulation of some TCA cycle intermediates including malate, succinate and fumarate compared to the cell growing on plastic (Figure 4.9B and D). Therefore, our results indicated that on collagen I, both TCA cycle and glycolysis could be more active compared to the cells on plastic under AA starvation, even though cellular ATP content was similar in both groups (Figure 4.8B). On Matrigel, cells' higher TCA cycle intermediates could imply that higher ATP content could be due the higher TCA cycle activity. However, while the early stage of glycolysis was upregulated on Matrigel, cells on plastic had higher content of glycolysis intermediates belonging to the later steps.



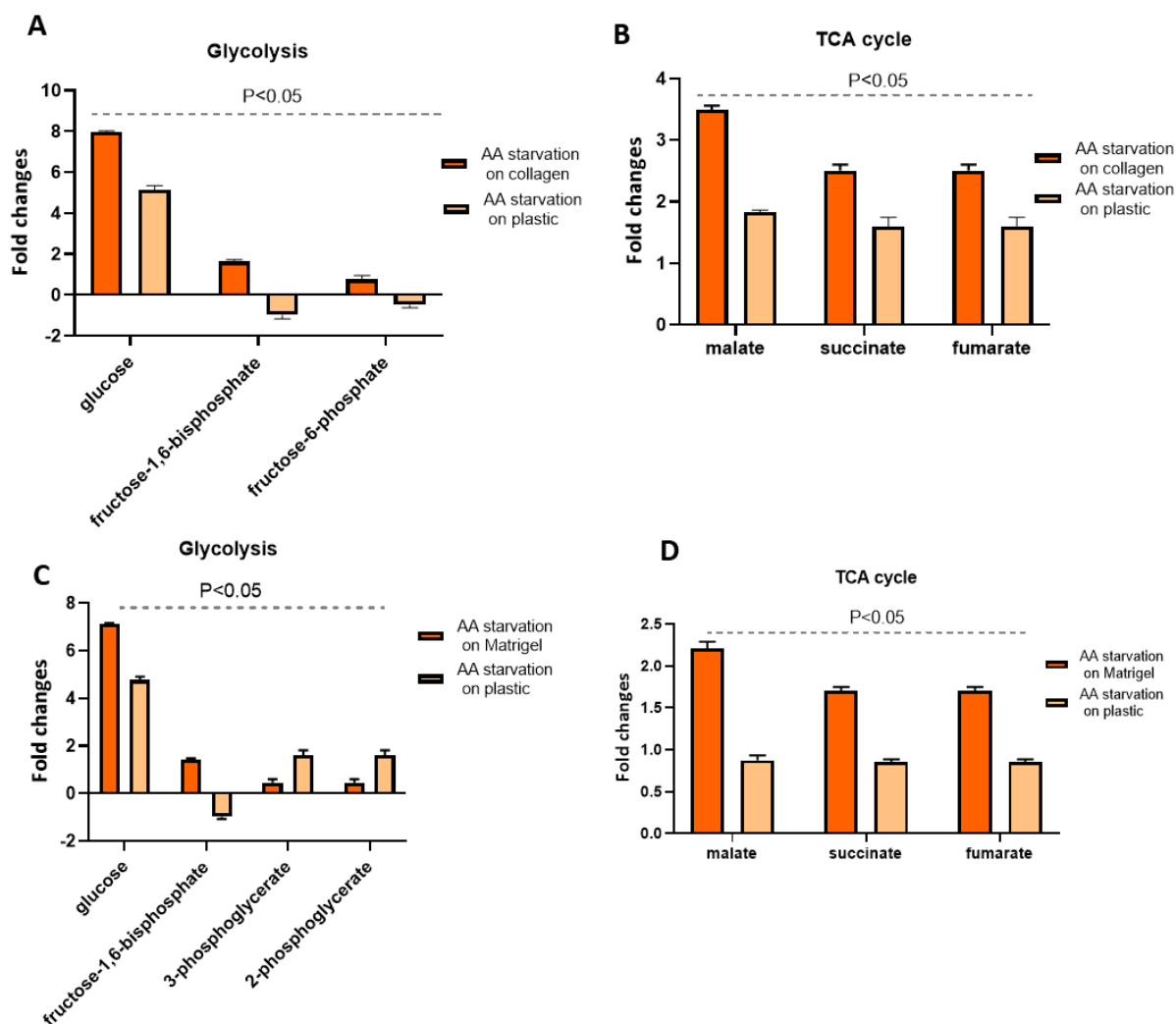


**Figure 4.9. TCA cycle and glycolysis intermediates on collagen I and Matrigel compared to the plastic under starvation.** Cells starved for six days either on (A-B) collagen I (2mg/ml), (B-C) Matrigel (3mg/ml) or plastic. Fold changes of metabolites in MDA-MB-231 normalized to the median of total metabolites in each condition. P values were measured by Student's t-test. Values are mean  $\pm$  SEM and are representative of three biological replicates.

### 4.3 Discussion

In this chapter we showed that laminin, like collagen I and Matrigel, induce the proliferation of invasive breast cancer cells. In addition, cells were able to internalize and degrade laminin under starvation conditions. However, the presence of laminin did not enhance mTORC1 activity. We also showed that decacidification of the lysosome prevented ECM-dependent cell growth without affecting mTORC1 activity under AA depleted media. Assessing Glc uptake and cell energy production revealed that AA starvation induced Glc uptake regardless of cells being on ECM or not. Cells on ECM upregulated Glc consumption via glycolysis under

starvation. Cells on ECMs also upregulated TCA cycle intermediates which could be the reason of higher ATP content on Matrigel compared to the plastic.

First, we tried to validate the technique we use to quantify the cell number and assess cell growth. DRAQ5 datasheet provided by the Licor company (<https://www.licor.com/documents/zfiq072j08h7bf4wgc4m>), suggests that it can be used as a cell number normalizing agents at least up to  $10^5$  cells/well in 96 well plates. However, we have been unable to seed more than  $2 \times 10^4$  cells/well without inducing the formation of clumps. We know that plating a very high number of cells for a short time is different from having cells growing in the well. Thus, it is likely that the linear range is bigger in the actual proliferation experiments. In addition, cell number under starvation conditions in our experiments were still within this range.

Along with the results showing that the compensatory effect of ECM under starvation is linked to the level of aggressiveness of the cells (Chp3 figure 2), here we tested the growth rate of non-invasive breast cancer cells on CDMs under starvation. Previously we showed that Matrigel, but not collagen I, was able to partially rescue MCF10A-DCIS growth under Gln, but not AA starvation (Chp3 figure 2G-H). Here, we examined the effect of TIF-CDM and CAF-CDM on MCF10A-DCIS cell growth. Our data demonstrated that TIF-CDM, but not CAF-CDM, rescued MCF10A-DCIS growth compared to plastic under Gln starvation. The composition of breast CAF-CDM and TIF-CDM has been characterised by mass spectrometry showing no significant differences in laminin and fibronectin content. However, CAF-CDM has been reported to contain a remarkably higher number of collagens including COL4A1, COL4A2 and COL8A1 (BM components) and COL1A1 and COL5A3 (IM components) (Hernandez-Fernaud et al., 2017). In addition, our data in chapter 3 showed that collagen I did not rescue the growth of MCF10A-DCIS cells under starvation (Chp3 figure 2E-F). Hence, higher density of collagen might have an adverse effect on non-invasive breast cancer cell growth under starvation. However, more studies are required to assess the effect of other types of collagens under the same conditions. Taken together, these data indicate that MCF10A-DCIS cells have the ability to use some types of ECM, but not others, to compensate for specific nutrient starvation. However, invasive breast cancer cells have potentially acquired more plasticity meaning that they are able to take advantage of the higher density matrix found in advanced tumours.

Here, we revealed that laminin induced MDA-MB-231 cell replication under Gln and AA starvation. In addition, cells were able to internalize laminin and degrade it inside the lysosome under starvation. In agreement with our data, a study showed that serum starvation induced soluble laminin uptake in mammary epithelial cells resulting in higher growth and lower cell death (Muranen et al., 2017). In addition, adding laminin to MCF10A cells under serum and AA starvation enhanced mTORC1 activity by providing AAs for the cells (Muranen et al., 2017). In our study, the presence of laminin did not affect mTORC1 activity in MDA-MB-231 cells under the Gln and AA starvation. In parallel, another study showed that adding collagen I or IV to PDAC cells suffering from either Gln or Glc deficiency did not impact downstream mTORC1 signalling pathway (Olivares et al., 2017). mTORC1 activation is a negative regulator of nutrient scavenging from alternative sources, such as ECPs under starvation (Muranen et al., 2017, Palm et al., 2015). Therefore, the absence of a rescue in mTORC1 activity in the presence of laminin under starvation might be a way for the cells to rescue the growth avoiding mTORC1 negative feedback on ECM uptake. It was previously shown that the presence of collagens under Glc and Gln starvation induced cell proliferation via ERK1/2 activation in PDAC cells (Olivares et al., 2017). Therefore, it is worth investigating whether laminin affects ERK1/2 activation in breast cancer cells under AA starvation, to find the mTORC1-independent signalling pathways induced by laminin to support cell growth.

It has been previously shown that inhibiting V-ATPase activity suppress the mTORC1 activity in the presence of laminin in starved cells (Muranen et al., 2017). V-ATPase maintains the activity of lysosomes via lowering the pH (Forgac, 2007). In addition, V-ATPase activity is required for AA sensing and mTORC1 activation and lysosomal recruitment (Zoncu et al., 2011a). It has been recently shown that the lack of V-ATPase activity, resulting in lower pH in lysosomes, negatively affected iron uptake. Lack of iron uptake in the cells can cause electron transport chain impairment and eventually inhibit proliferation (Weber et al., 2020). Hence, the reduction of growth under complete media in the presence of BA1 could be mediated by iron uptake inhibition. However, the effect of BA1 on cell growth under AA starvation might also be linked to inhibition of Matrigel lysosomal degradation limiting accessibility of cells to the source of AAs, as no effect on proliferation on plastic was observed. Assessment of mTORC1 activation in cells in complete media showed that V-ATPase inhibition reduced p-S6 intensity. It has been reported that there is an inside-out signalling pathway from lysosome

to promote mTORC1 lysosomal recruitment and activation. Accumulation of AAs inside the lysosome induces interaction between V-ATPase and Ragulator, a scaffolding complex that anchors the Rag GTPases to the lysosome, resulting in RagGTPase lysosomal recruitment followed by mTORC1 activation (Zoncu et al., 2011a). Therefore, inhibiting V-ATPase activity could impede mTORC1 activity regardless of the availability of nutrients. AA starvation has been shown to induce V-ATPase assembly, increasing H<sup>+</sup> content of lysosomes (Stransky and Forgac, 2015). This suggests that AA depletion might induce ECM lysosomal degradation and AA extraction by stimulating lysosomal acidification. In parallel, in chapter 3, we showed that cells had a lower amount of ECM accumulated inside the lysosome under AA starvation compared to the complete media. Therefore, under AA starvation, we expected to observe higher mTORC1 activity due to enhancement of V-ATPase assembly. In contrast, our data revealed that cells on Matrigel had similar p-S6 intensity regardless of them being treated by BA1 or not under AA depletion. These results suggest that there might be an alternative pathway cells benefit from to induce mTORC1 activity on ECM under AA starvation. In addition, lower cell growth in the presence of BA1 under AA starvation on ECM might be due to the lack of lysosome activity rather than an mTORC1 dependent effect.

Metastatic cancer cells have more plasticity in terms of using different metabolic pathways under different nutrient conditions. Cancer cells can compensate for lack of glutaminolysis via switching to glycolysis for energy production or vice versa (Méndez-Lucas et al., 2020). In this study, we asked whether cells on ECM under AA starvation could more efficiently rely on Glc uptake followed by glycolysis due to lack of AAs. To address this question, we tracked Glc uptake. Our data revealed that lack of AAs induced a greater number of cells to internalize Glc compared to the cells in complete media. Comparing the amount of Glc uptake in each cell did not show any significant changes between cells on ECMs regardless of their nutrient condition. However, cells on plastic had higher Glc uptake under AA deficiency compared to the cells in complete media. Thus, MDA-MB-231 cells might mainly rely on Glc during AA deficiency as a compensatory mechanism when plated on plastic. However, the presence of the ECM reduced the increase of Glc uptake induced by AA starvation, as the cells are mainly relying on AA, and potentially sugars, extracted from the ECM. We believe that extraction of AAs from the ECMs could be the reason why cells on collagen I and Matrigel had lower Glc uptake compared to the cells on plastic. However, there are studies showing that different

substrate stiffness changes cellular metabolic pathways. It was demonstrated that stiff environments such as glass induce glycolysis (Mah et al., 2018). Therefore, it is possible that changes in mechanosensing might be one of the reasons why cells on glass had higher Glc uptake under AA starvation. However, our data from cells in complete media are not consistent with this hypothesis, as cells on both ECM and glass showed similar Glc uptake.

It was recently shown that changes in matrix density affect the metabolic pathways that invasive breast cancer cells rely on to produce energy. However, normal mammary epithelial cells do not have this flexibility. Invasive breast cancer cells are more glycolytic on stiff collagen and glass. In contrast, they mainly produce energy via OXPHOS on soft collagen (Mah et al., 2018). In our study, we found that cells on Matrigel are more glycolytic and have higher ATP content compared to cells on collagen I and plastic. Concentration of Matrigel is higher in our study compared to the collagen I. However, further studies are needed to measure the stiffness differences between collagen I and Matrigel. Another study showed that cells on higher ECM density have higher ATP production and hydrolysis, as they need more energy for their migration (Zanotelli et al., 2018). In addition, higher ECM degradation resulted in higher Glc uptake and energy production during metastasis (Sullivan et al., 2018). Therefore, higher energy production in cells on Matrigel compared to collagen I could be due to differences in ECM density and energy needed for their degradation as we used higher concentration of Matrigel than collagen I. However, more studies are needed to characterise the contribution of matrix stiffness and the crosstalk between metabolism and mechanosensing. Furthermore, ATP content of cells under AA starvation was similar, or it was even higher on Matrigel, compared to the cells growing under the complete media. Recently it was demonstrated that the addition of a higher amount of Glc and serum increases ATP:ADP ratio of the cells (Zanotelli et al., 2018). We previously showed that cells have higher Glc uptake under AA starvation compared to the complete media. Taken together, it is possible that higher glucose consumption might result in higher ATP accumulation. However, to consolidate this, the ATP:ADP ratio will need to be tested, to find whether accumulation of ATP in cells is due to their higher ATP production or it is due to the lower energy consumption. Hence, there is the possibility that the higher ATP levels on plastic under starvation were due to lack of cell growth and therefore low ATP consumption.

In contrast to our previous data showing that Glc uptake of cells on collagen I and plastic was similar, data from non-targeted metabolomics revealed that cells on collagen I upregulated glycolysis and the TCA cycle compared to the cells on plastic in AA starved cells. In the previous chapter we showed that cells on Matrigel and collagen I have higher AA content compared to the cells on plastic. Many of these AAs can directly or indirectly feed the TCA cycle (Yang et al., 2017). Therefore, the presence of ECM as a source of AA could be the reason why cells had higher TCA cycle intermediates. Comparing Glc content of the cells via MS was inconsistent to the results assessing 2NBDG uptake. MS data revealed that cells on collagen I and Matrigel had higher Glc content compared to the plastic. 2NBDG cannot be utilized in the glycolysis pathway. Therefore, 2NBDG content of cells is not an indicator of Glc consumption rate and glycolysis. In addition, comparing glycolysis components of cells on Matrigel and plastic showed that while the intermediates of early stage of glycolysis was upregulated on Matrigel, cells on plastic had higher content of glycolysis intermediates belonging to the later steps. Therefore, there is this possibility that the uptake is the same, but the consumption rate is different on plastic and ECM resulting in higher Glc, detected by MS, inside the cells on ECM. In order to characterise how the ECM affects energy production, further work is required to follow incorporation of Glc in different metabolic pathways under AA starvation.

In conclusion, our data showed that invasive breast cancer cells can internalize laminin and degrade it inside the lysosome under Gln and AA starvation. Presence of laminin partially increase division rate of MDA-MB-231 cells under starvation conditions which is independent of mTORC1 activity. We also showed that AA starved cells on Matrigel have higher ATP content compared to the plastic. In addition, cells have higher TCA cycle and glycolysis intermediates on ECM compared to plastic in AA depleted media. Taken together, these data implying that cells on ECM produce more energy. To find whether Glc could be the source of energy in AA starved cells, we measured 2NBDG uptake and we did non-targeted MS to measure Glc content of the cells on ECM and plastic. Our data suggests that AA starvation increases Glc uptake compared to the complete media. We showed that in AA starved cells, Glc uptake is not affected by the substrate cells were growing on. However, Presence of ECM might reduce Glc consumption rate compared to the plastic. These data suggest that cells on ECM might rely more on ECM degradation to meet their need for energy while cells on plastic might rely on Glc consumption.

## Chapter 5: An RNAi screen identified AP3, RIN3 and MAPK8IP3 as novel regulators of ECM-dependent cell growth under starvation.

### 5.1 Introduction

In chapter 3 we showed that ECM internalization is essential to rescue cell growth under AA starvation. We also demonstrated that ECM uptake is followed by lysosomal degradation (Chp3 figure5). In addition, cells on ECM showed higher AA content compared to cells on plastic indicating that cells can extract AA from ECM (Chp3 figure7). Therefore, it is important to characterise how ECM trafficking is regulated.

ECM degradation facilitates invasion and metastasis in cancer cells. It happens either extracellularly via enzymes such as MMPs (more details in section 1.3.3), or intracellularly by ECM endocytosis followed by lysosomal degradation. Different pathways can control the internalisation of ECM components. Collagen had been shown to be internalized either through phagocytosis or clathrin-dependent endocytosis (Madsen et al., 2013). Collagen phagocytosis in fibroblast cells occurs via activation of stretch-activated  $Ca^{++}$  channel.  $Ca^{++}$  uptake induces interaction of an actin binding protein, gelsolin, to an actin motor protein, non-muscle myosin IIA (NMMIIA), to trigger actin assembly and collagen- $\alpha 2\beta 1$  integrin phagocytosis (Segal et al., 2001, Arora et al., 2013). Phagosomes containing collagen go through maturation by showing late endosome/lysosome marker and Cathepsin B resulting in collagen degradation (Arora et al., 2000). Another collagen binding receptor is Endo180 which is a member of the mannose receptor family (MRs). Endo180 can bind to both soluble and native collagen (Madsen et al., 2011). Collagen-bound Endo180 can be internalized and trafficked to early endosomes by clathrin-dependent endocytosis (Wienke et al., 2003). Collagen is then degraded in lysosomes in a cysteine proteases-dependent way while Endo180 is recycled back to the plasma membrane from the early endosomes (Melander et al., 2015). FN turnover also happens via its internalization and lysosomal degradation. In contrast to collagen, FN uptake is a caveolin-1 mediated endocytosis through its binding to  $\alpha 5\beta 1$  integrin (Sottile and Chandler, 2005, Shi and Sottile, 2008). Binding of FN to  $\alpha 5\beta 1$  in migratory fibroblasts causes  $\alpha 5$  ubiquitination.  $\alpha 5$  ubiquitination results in endosomal sorting complex required for transport (ESCRT) delivery of FN bound integrin to intraluminal vesicles (ILVs) and eventually lysosomes for degradation (Lobert et al., 2010). Laminin internalization

occurs via its binding to  $\alpha 3\beta 1$  integrin and phagocytosis.  $\alpha 3\beta 1$  in breast cancer cells is responsible for Matrigel, and gelatin trafficking and degradation inside the lysosomes. Binding of laminin to  $\alpha 3\beta 1$  activates the integrin and downstream signalling pathways that results in phagocytosis (Coopman et al., 1996). Laminin assembly and internalization has also been shown to be regulated by dystroglycan. Binding of laminin to dystroglycan results in its internalization to early endosome and finally degradation in lysosomes (Leonoudakis et al., 2014). Therefore, different ECM components might follow different trafficking routes inside the cells (Figure 5.1). However, all, finally, end up in the lysosome for degradation.

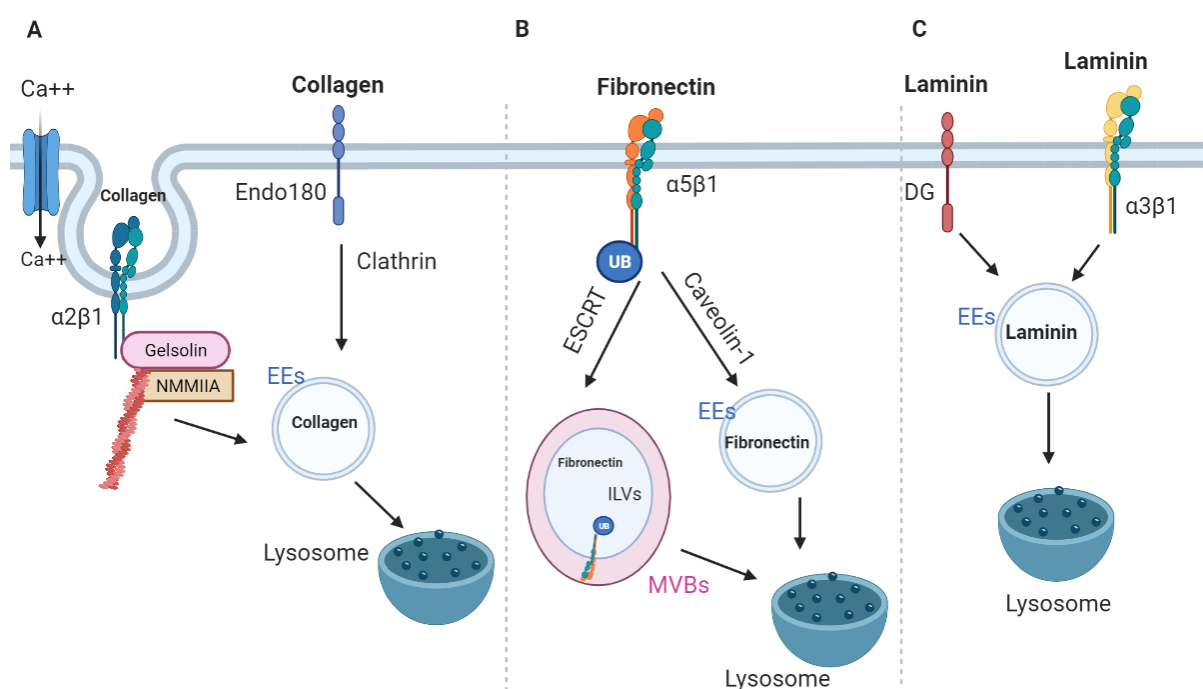


**Figure 5.1. Schematic representation of ECM internalization pathways.** (A) Collagen internalization happens through  $\alpha 2\beta 1$  integrin dependent phagocytosis activated by  $\text{Ca}^{++}$  or through Endo180 and clathrin dependent endocytosis. (B) Fibronectin uptake happens through  $\alpha 5\beta 1$  and ESCRT or caveolin-1 dependent pathways. (C) Laminin internalization happens via its binding to dystroglycan or  $\alpha 3\beta 1$  integrin. ECM internalization in the early endosome can be directed to lysosome for degradation (Figure is adapted from (Rainero, 2016)). Image is “Created with BioRender.com.”

In this chapter we characterised the genes participating in ECM trafficking under starvation via an siRNA gene silencing approach. The aim of this study is to find genes that are required for ECM-dependent cell growth under NEAA starvation. In cancer cells, high proliferation rates result in higher metabolic demand. Therefore, they rely on external sources to provide NEAAs, a process called NEAAs auxotrophy. NEAAs auxotrophy is linked to different mutations



in genes encoding for NEAAs synthesis enzymes (Szlosarek et al., 2006). NEAAs have roles in protein, lipid, and nucleotide biosynthesis in cancer cells and recently their metabolic pathway became a target for cancer therapy (Choi and Coloff, 2019). It has been shown in different studies that NEAA can induce metastasis, survival, and proliferation in cancer cells, while NEAA consumption can increase mortality rate and decrease relapse time in patients (further details in section 1.4.5) (Jain et al., 2012, Jeschke et al., 2013, Locasale et al., 2011, Pollari et al., 2011). Therefore, it is important to understand the compensatory mechanisms cancer cells can use to rescue their growth/survival under NEAA starvation.

## 5.2 Results

### 5.2.1 The presence of collagen I rescued breast cancer cell growth under non-essential amino acid starvation.

Chapter 3 showed that the presence of ECMs can partially rescue invasive breast cancer cell growth under AA starvation (Chp3 figure 1). To further characterise the role of the ECM in conditions where specific AAs were lacking, we assessed cell proliferation on collagen I in media containing different AA combinations. We added either essential (Table 2.10) or non-essential (Table 2.9) AAs to the AA depleted media and monitored cell growth between day two up to day eight post starvation in the presence or absence of Gln. Cells seeded under EAAs starvation, with or without addition of Gln, did not show any growth regardless of the substrate they were plated on (Figure 5.2A-B). In contrast, cells on collagen I under NEAAs and Gln starvation had significantly higher cell numbers between day four up to day eight (Figure 5.2C). Addition of Gln to the cells growing under NEAAs starvation promoted cell growth on plastic. However, there was still a significant increase on collagen I, suggesting that the effect of NEAA starvation is not entirely due to Gln starvation (Figure 5.2D). To examine MDA-MB-231 cell behaviour in a more physiologic environment, we assessed their growth on TIF-CDM and CAF-CDM under NEAA and Gln starvation. Similarly, to what we observed on collagen I, both types of CDMs significantly induced cell growth compared to the plastic (Figure 5.2E-F). Taken together, these data suggest that ECM can rescue cell growth under NEAA, but not EAA, starvation.

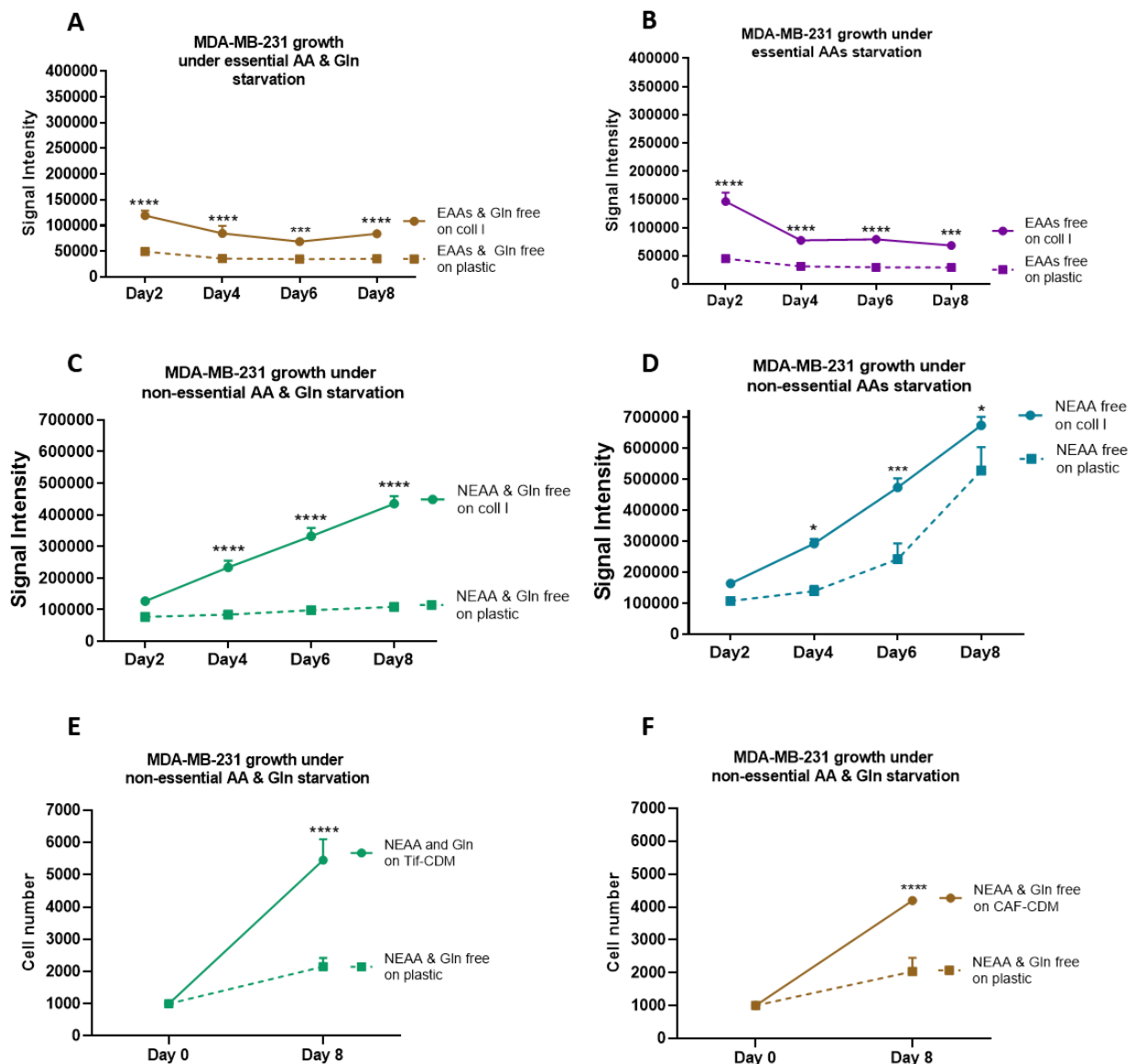


**Figure 5.2. Collagen I and CDMs partially rescued cell growth under NEAAs starvation.** MDA-MB-231 cells were seeded either on plastic or on plates coated with 2mg/ml collagen I under (A) essential AA (EAA) and Gln starvation (Gln), (B) EAA starvation in the presence of Gln, (C) non-essential AA (NEAA) and Gln starvation, and (D) NEAA starvation in the presence of Gln. Cell proliferation was measured by quantifying DRAQ5 nuclear staining with the Licor Odyssey system every two days up to day eight. MDA-MB-231 cells were seeded either on plastic or plates containing (E) TIFs-CDM or (F) CAF-CDM under Gln and NEAA starvation for eight days. Cell proliferation was measured via Hoechst nuclear staining. Images were collected by ImageXpress micro and analysed by MetaXpress software. Values are mean  $\pm$  SEM and are representative of at least three independent experiments. \* $p < 0.05$ , \*\*\* $p < 0.001$ , \*\*\*\* $p < 0.0001$  ANOVA test.

### 5.2.2 ECM cross-linking opposed cell growth under NEAAs starvation.

We showed in chapter 3 that lack of ECM internalization due to cross-linking opposed breast cancer cell growth under AA starvation (Chp3 figure 5F). To assess whether the inhibition of ECM uptake has a similar effect under NEAA starvation, we seeded cells on normal or cross-linked ECMs in NEAA depleted media. Henceforward, NEAA starvation refers to AA depleted media with the addition of EAAs (Table 2.10) in the absence of Gln. Our data revealed that cross-linking of Matrigel and CAF-CDM significantly reduced cell growth (Figure 5.3B-C); while on collagen I, cross-linking resulted in a small and not statistically significant reduction (Figure 5.3A). Altogether, our data indicate that ECM internalisation is required for ECM-dependent cell growth under NEAA starvation.

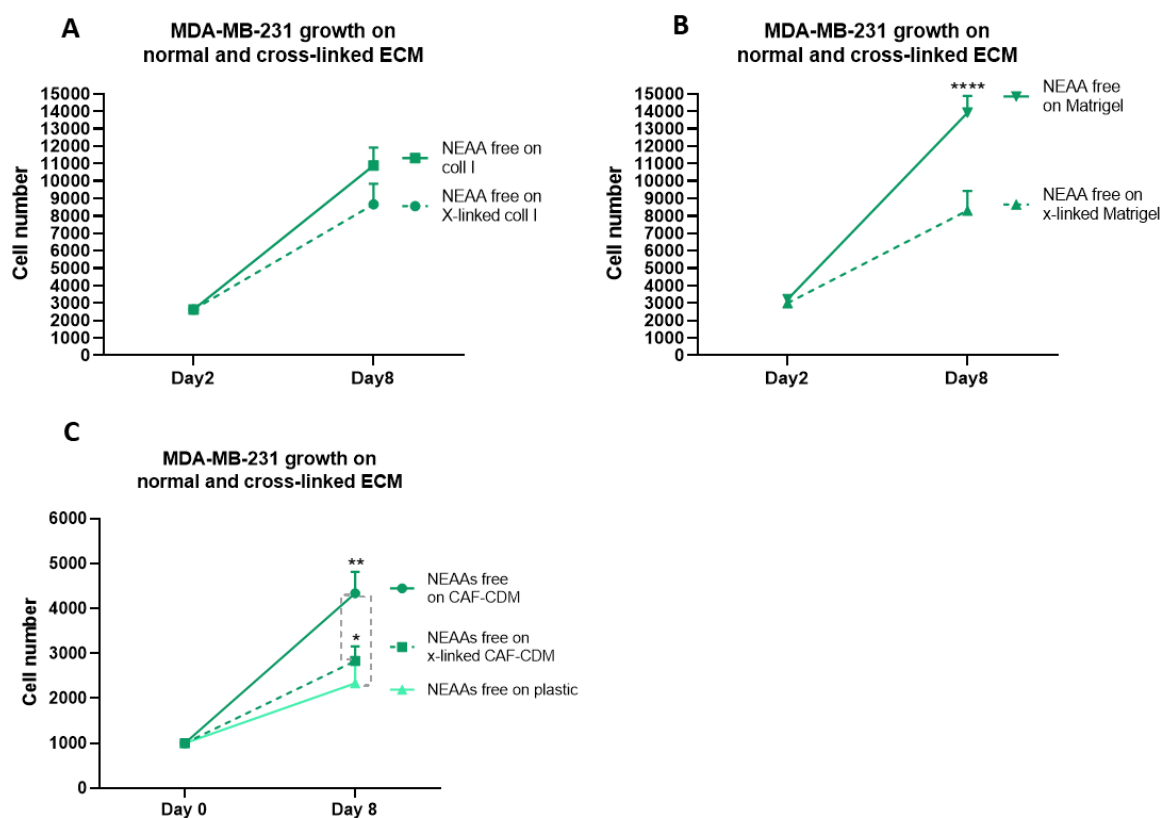


**Figure 5.3. ECM cross-linking opposed matrix-dependent cell growth under NEAA starvation.** MDA-MB-231 cells were seeded on untreated (control) or cross-linked (X-linked) (A) 2mg/ml collagen I, (B) 3mg/ml Matrigel or (C) CAF-CDM under NEAA starvation. Cell proliferation was measured through Hoechst nuclei staining. Images were collected by ImageXpress micro and analysed by MetaXpress software. Values are mean  $\pm$  SEM and are representative of three independent experiments. \* $p < 0.05$ , \*\* $p < 0.01$  and \*\*\*\*  $p < 0.0001$  ANOVA test.

### 5.2.3 RNAi screen setup and evaluation on Matrigel.

So far, we demonstrated that MDA-MB-231 cells had significantly higher growth on collagen I, Matrigel and CDM under NEAA starvation (Figure 5.2 and 5.3). In addition, lack of Matrigel and CDM uptake opposed cell growth (Figure 5.3). In addition, we showed in chapter 3 that endocytosis inhibition via Filipin addition reduced ECM internalisation and cell growth on Matrigel under AA starvation (Chp3 figure 5H). Thus, our data suggest that ECM trafficking might be required for ECM-dependent cell growth under AA starvation. To investigate this, we took an RNAi approach to downregulate the expression of genes controlling vesicular trafficking using the traffic-ome library, in collaboration with the SRSF. Since the RNAi screening was previously performed on plastic, further optimisation was needed to adapt the workflow in the presence of ECM. To measure the siRNA transfection efficiency in MDA-MB-231 cells plated on ECM, we used siGLO siRNA as a positive control. siGLO siRNA is a fluorescent control providing visual indication of siRNA transfection. We added siGLO and the transfection reagent into plates which were pre-coated with collagen I or Matrigel. Then, cells were seeded on top for the transfection to occur overnight in complete media. The media was exchanged the day after with the NEAA starvation condition. The data collected from siGLO transfection showed that on the Matrigel, the number of siGLO positive cells are substantially higher compared to the collagen I and plastic (Figure 5.4A). In addition, cells had better growth on Matrigel after transfection under NEAA starvation condition (Figure 5.4B). Therefore, we continued the rest of optimization on Matrigel.

Since our proliferation assays are performed up to six or eight days, we decided to examine whether siRNA-mediated transient gene knockdown (KD) was stable up to six days after transfection. To do this, we chose two genes whose lack of function induces cell death, ubiquitin B (UBB), and polo Like Kinase 1 (PLK1). PLK1 is essential for initiation of mitosis and its inhibition induces apoptosis and cell death (Colicino and Hehnly, 2018). In addition, PLK1 expression is usually upregulated in tumours with different origins (Holtrich et al., 1994). Ubiquitin's main role is targeting cellular proteins for degradation via the 26S proteasome. It has been reported that ubiquitin is upregulated in different tumours. In addition, downregulation of ubiquitin through UBB KD inhibits cancer cell proliferation and has a cytotoxic effect in MCF7 breast cancer cells (Oh et al., 2013). To examine whether gene KD could be effective up to day six on ECM, we coated the plates with Matrigel. Then, PLK1, UBB

and non-targeted (Nt) siRNA were added on top of Matrigel with transfection reagent. To do the reverse transfection, MDA-MB-231 cells were transferred to the ECM-coated plates containing the siRNAs and were incubated overnight. Cell media was exchanged with the fresh media the day after. Our data demonstrated that there is no significant cell growth between day three up to day six post UBB and PLK1 siRNA gene KD. In contrast, cells transfected with Nt siRNA displayed a significantly higher cell number at day six (Figure 5.4C). These data suggest that siRNA-mediated gene KD could be effective up to six days. However, we realized that for the siRNA library screening forward transfection was needed due to some technical difficulties (explained in detail in section 5.2.4). Therefore, to test effectiveness of forward siRNA transfection, we coated the plates with Matrigel. Cells were then seeded on Matrigel and incubated for 5 hrs to fully attach to the matrix. Then, media on the top of the cells were exchanged with PLK1 and Nt siRNA previously complexed with the transfection reagent. After an overnight transfection, the media was replaced by either complete or NEAA depleted media to assess cell growth under starvation. Our data revealed that cells transfected with PLK1 siRNA had substantially lower cell number six days after transfection under both complete and NEAA depleted media (Figure 5.4D). Taken together, our data suggests that cells can be transfected on Matrigel via both reverse and forward transfection protocols. In addition, siRNA transfection is effective at least up to six days.

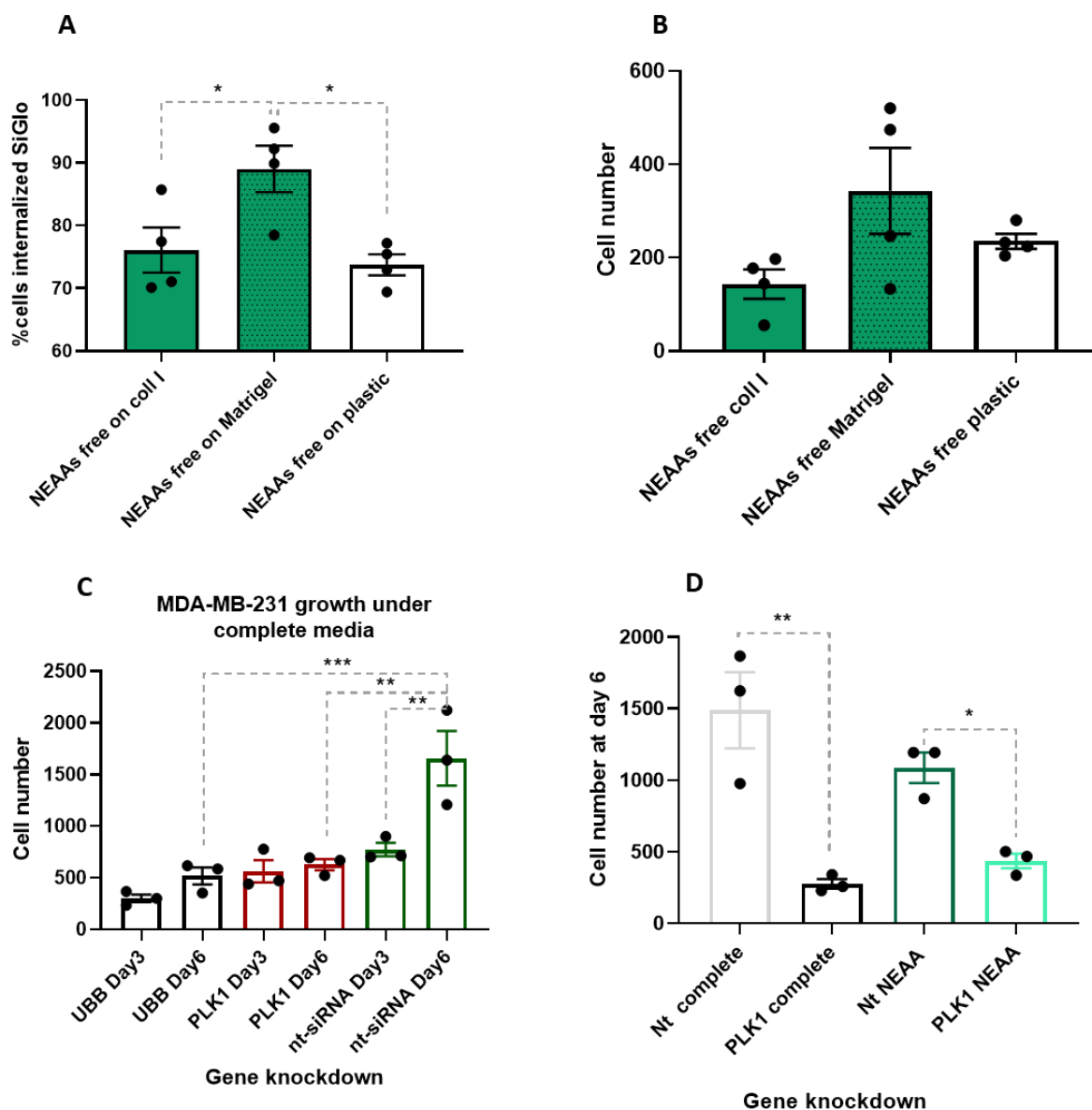


**Figure 5.4. Optimizing siRNA transfection on ECM.** (A-B) 150nM siGLO was added into the plates coated with collagen I (2mg/ml), Matrigel (3mg/ml) or plastic. The addition of the transfection reagent and the media containing the cells to the plates reduced the concentration of siRNA to 30nM per well. Cells were incubated under NEAA starvation for six days. Cells were fixed, stained with Hoechst, and imaged with ImageXpress micro and analysed by MetaXpress and CME software. (C) Reverse siRNA transfection. 150nM UBB, PLK1 or Nt siRNA were added into the plates coated with Matrigel (3mg/ml). Cells were seeded on top of the siRNAs as described in (A) and incubated overnight. Media was changed the day after. Cells were fixed and stained with Hoechst at day six post starvation. (D) Forward siRNA transfection. MDA-MB-231 cells were seeded on plates coated with Matrigel (3mg/ml). After 5 hrs of incubation, the media was removed, and cells were transfected with 30nM PLK1 and Nt siRNA overnight. Media was changed the day after. Cells were fixed, stained with Hoechst, and imaged with ImageXpress micro and analysed by MetaXpress software. \* $p < 0.05$ , \*\* $p < 0.01$  and \*\*\* $p < 0.001$  ANOVA test.

#### **5.2.4 The RNAi Traffic-ome screen.**

Having optimised the transfection condition, an RNAi screen was performed with siRNAs targeting mammalian genes involved in vesicular trafficking, called traffic-ome (Table 2.12). We received the traffic-ome library from Sheffield RNAi Screening Facility (SRSF), which was already printed into 384 well plates. The library comprised siRNA SMART pools (4 siRNA pooled per gene) for 75 genes. The single replicate of 75 individual siRNAs were distributed in one 384-well plate. After receiving the siRNA plate, positive control, PLK1 siRNA, and negative control, Nt siRNA, were added to the plate.

To perform the screen, we coated two 384-well plates with Matrigel. We seeded MDA-MB-231 cells on top and left it at 37°C for 5hrs for the cells to be fully attached to the Matrigel. Meanwhile, we added the transfection reagent to the plate containing pre-printed siRNAs. To do the transfection, the media on top of the cells was removed, while fresh media was added to the plate containing the siRNAs and transfection reagent. To transfer the siRNA-containing media onto the cells, we used the Hamilton robot in SRSF (programmed by the SRSF team). Cells were then incubated with siRNAs overnight (Figure 5.5). The day after, the media was replaced with either complete or NEAAs depleted media. Therefore, we had two sets of cells transfected with the traffic-ome library. One set of cells was growing in complete media and the other was growing under NEAA starvation. Six days post starvation, cells were fixed, stained with Hoechst and the cell number was measured.

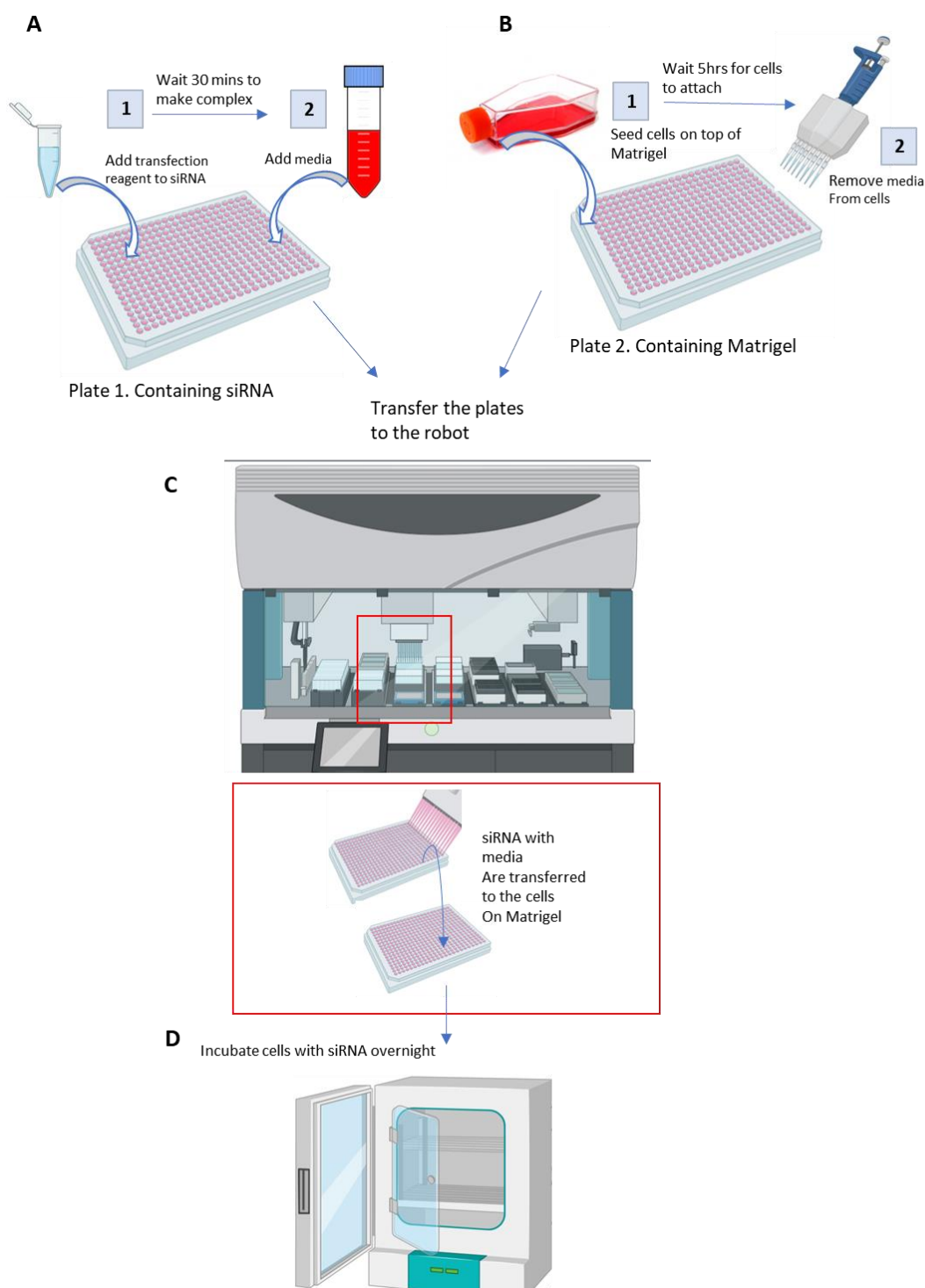


**Figure 5.5. High throughput RNAi screen set up.** (A) We Added Dharmafect 1(DF1) (Transfection reagent) to the plates containing traffic-ome siRNA (4 siRNA pools per gene) library. Cells were incubated for 30 minutes for the siRNA and DF1 to become complex. Then, we Added fresh media on top. (B) Cells were seeded in a separate plate which is coated with Matrigel (3mg/ml) and they were Incubated at 37°C for 5hrs. To do the transfection, we remove the media from cells, and (C) transfer four plates (two plates containing siRNA and two plates containing cells) to the Hamilton robot. The robot transfers the siRNA with the media to the plates containing cells. (D) Finally, Cells were incubated with siRNA overnight at 37°C.



Since we showed that ECM-dependent MDA-MB-231 cell growth required ECM internalization under NEAA starvation (Figure 5.3), we hypothesized that knocking down genes involved in ECM trafficking could reduce cell growth under starvation. We used the z-score (the number of standard deviations from the mean) to normalize the data to provide clearer information about the effect of each siRNA on cell number relative to the rest of the sample distribution. PLK1 KD, which has a direct effect on cell proliferation, had z scores between -1.5 to -2.5. Thus, we decided to nominate genes with z score < -1.5 as hits. In complete media, the following genes were listed as hits, SH3GLB2, COPA, PLK1, SEC22B, IHPK3, ACTR2, Myo5b, ARHGDI1, WASF2, ARF6, and RAB22A (Figure 5.6A-B). Under NEAA starvation the hits were PACSIN1, COPA, RAB3C, PLK1, GAPVD1, RIN3, SEC22B, AP3D1, MAPK8IP3, and Myo5b (Figure 5.6C-D). Among hits, there were some genes in common between complete media and NEAA starvation, indicating that their downregulation affected cell growth regardless of the nutrient condition. Therefore, we narrowed down the list of hits to the genes emerged as hits specifically under NEAA starvation for the further validation. To do this, we coated 96-well plates with collagen I and Matrigel. We seeded the cells on top of the ECMs and incubated for 5hrs. We prepared siRNAs against GAPVD1, AP3D1, MAPK8IP3, RIN3, PACSIN1 and RAB3C genes with transfection reagent in separate tubes. After 5hrs of incubation, we exchanged the media on top of the cells with siRNAs and fresh media. Due to some technical difficulties, we could not use the data from gene KD on Matrigel. The data from siRNA KD on collagen I confirmed that silencing of AP3D1, MAPK8IP3, and RIN3 significantly reduced cell number compared to the non-targeting siRNA control group under NEAA deficiency (Figure 5.6E). However, no interaction between these genes has been found so far (Figure 5.6F). AP-3 complex subunit delta-1 (AP3D1) is a subunit of AP3 adaptor-like complex, which plays role in transport of proteins from trans-Golgi network (TGN) and early endosomes to the lysosomes or other destined organelles (Petrenko et al., 2006). Mitogen-Activated Protein Kinase 8 Interacting Protein 3 (MAPK8IP3) has a role in axonal transport in the nervous system (Iwasawa et al., 2019). RIN3 is a Rab5-binding protein that participates in transport from the plasma membrane to the early endosomes (Kajiho et al., 2003). So far, our data suggests that AP3D, RIN3 and MAPK8IP3 are potential proteins playing a role in ECM trafficking under AA starvation. Further studies and validation are needed to characterise whether there is any link between them and to define how they control ECM trafficking and ECM-dependent cell growth.

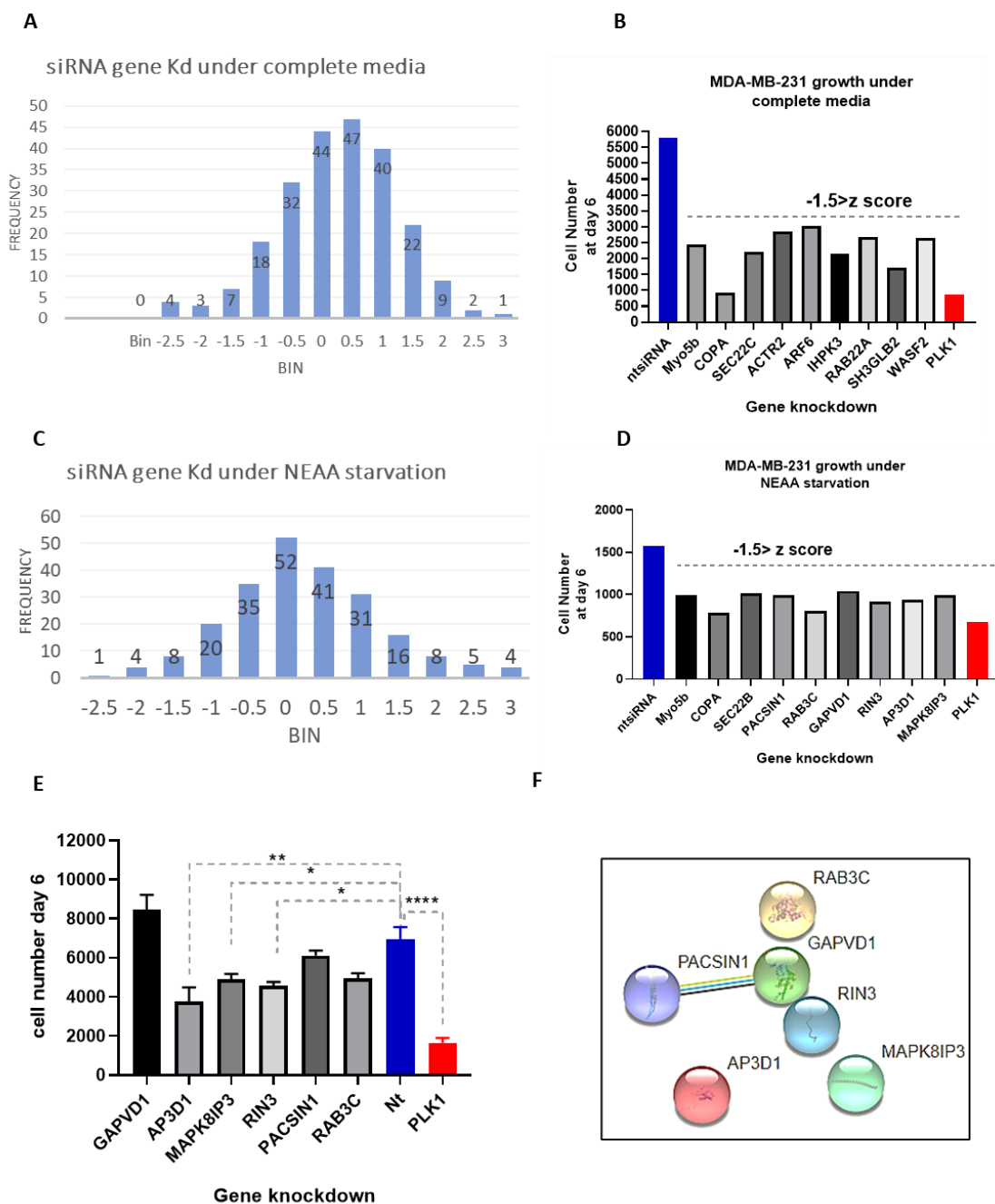


**Figure 5.6. Traffic-ome siRNA screening.** Histograms of z score value for number of cells after siRNA-mediated gene KD under (A) complete media or (C) NEAAs starvation. The graphs in B and D show the quantification of cell number for the proteins being identified as hits (z score <math><-1.5</math>) under (B) complete media or (D) NEAAS starvation. (E) MDA-MB-231 cells were plated on collagen I, transfected with GAPVD1, AP3D1, MAPK8IP3, RIN3, PACSN1 and RAB3C gene siRNA and starved for six days. Cells were fixed, stained with Hoechst, and imaged with ImageXpress micro and analysed by MetaXpress software. (F) Interaction network of Traffic-ome hits as visualized by STRING.

### 5.3 Discussion

In this chapter we showed that the presence of collagen I and Matrigel could rescue invasive breast cancer cell growth under NEAA starvation, but not EAA starvation. We also demonstrated that lack of ECM uptake opposed cell growth under NEAA deficiency, suggesting that cells need ECM internalization for their growth under nutrient depleted media. In addition, an RNAi screen identified AP3D1, MAPK8IP3 and RIN3 as potential genes participating in ECM trafficking under NEAA starvation.

Our data revealed that the presence of collagen I and Matrigel could induce cell growth under NEAA starvation. Interestingly, comparing the metabolite content of MDA-MB-231 cells on plastic and collagen I under AA starvation showed upregulation of some NEAAs on collagen I including cysteine, hydroxyproline, and tyrosine (Chp3 figure7). NEAAs play different roles in breast cancer cells survival, proliferation, and invasion. Higher catabolism of proline in breast cancer cells results in higher ATP production and metastasis (Elia et al., 2017). Serine synthesis is upregulated via higher expression of 3-phosphoglycerate dehydrogenase (PHGDH) in breast cancer cells, which is correlated to lower survival rate and shorter relapse time (Locasale et al., 2011, Pollari et al., 2011). Serine is also responsible for producing glycine and cysteine. Serine and glycine participate in one carbon metabolism, resulting in nucleotide production and proliferation. A previous study showed that blocking of serine, but not glycine, uptake inhibits proliferation in breast cancer cells (Labuschagne et al., 2014). Cancer cell glycine consumption and biosynthesis has also been shown to correlate with their proliferation and metastasis; and breast cancer patients with high reliance on glycine show higher mortality rate (Jain et al., 2012). In addition, in our study we showed that even in the presence of EAAs and Gln there is a significant difference in cell numbers between cells growing on collagen I and plastic. Taken together, it is suggested that NEAA could be important for breast cancer cell growth and cells rely on external sources of NEAAs.

However, invasive breast cancer cells could not grow under EAA starvation regardless of the substrate they were seeded on, in the presence or absence of Gln. Therefore, our data suggest that the mixture of exclusively NEAAs inhibits MDA-MB-231 cell growth, as we previously showed that the ECM was able to rescue cell growth under full AA starvation. In contrast, there is a study showing that the presence of dominantly EAAs (100% EAAs with no NEAAs or

mixture of 85% EAAs with 15% NEAAs) adversely affects cancer cells growth, including HeLa cells, while it does not have any effect on normal cells like MCF10A. It was shown that EAAs rich media inhibits proteasome activities results in accumulation of proteins associated with apoptosis and finally induces apoptosis (Bonfili et al., 2017). It should be considered that in the study by Bonfili et al (2017), measurement of cell growth was done on plastic, and we could speculate that in the presence of ECM cell behaviour might be different as we showed here. In parallel, another study revealed that branch chained AAs, including leucine, isoleucine, and valine, which all are EAAs, inhibit insulin induced hepatic tumour cell proliferation via inactivation of PI3K/Akt signalling pathways, causing upregulation of pro-apoptotic and downregulation of anti-apoptotic genes, leading to cell death (Hagiwara et al., 2012). Additionally, a study showed that addition of glycine solely into the media decreased the nucleotide pool of cells and inhibited cell proliferation while addition of serine as NEAA increases nucleotide production in cancer cells (Labuschagne et al., 2014). Taken together, further studies are needed to find the reason why 100% mixture of NEAAs has cytotoxic effect on MDA-MB-231 cells. In particular, it will be important to understand combination of NEAAs induces cell death. Is it either all together or is it a combination of some specific NEAAs without the presence of any EAAs that results in cell death?

In this study we showed ECM internalization is required for ECM-dependent MDA-MB-231 cell growth under starvation. Hence, we set out to investigate what genes could oversee ECM trafficking, by performing an siRNA screen for genes participating in vesicular trafficking. Our data so far revealed three genes whose silencing adversely impacted on cell proliferation under NEAA starvation but not under complete media, suggesting that they might be required for ECM internalisation and/or trafficking. One of these genes was AP3D1. AP3D1 is a subunit of the AP3 adaptor-like complex. The AP3 complex comprises two large subunits,  $\delta$ - and  $\beta$ 3A-adaptins, the medium subunit  $\mu$ 3A-adaptin, and the small subunit  $\sigma$ 3A-adaptin encoded by genes AP3D1, AP3B1, AP3M1, and AP3S1, respectively. The AP3 complex is a component of coating proteins recruited on the cytosolic side of membrane to sort the transport of the cargo to the intracellular vesicles (Lefrancois et al., 2004). It has been shown that there is a higher expression of AP-3 complex in cervical carcinoma which was not observed in normal tissue, and it has also been linked to metastasis (Petrenko et al., 2006). There are different studies aiming at characterizing AP3 function. One of the early studies showed that AP3 is

responsible for transport of lysosomal transmembrane protein I (LAMP I) and lysosomal integral membrane protein II (LAMP II), from the TGN to lysosomes (Le Borgne et al., 1998). Additional studies showed that AP3 can recruit clathrin to make clathrin-coated vesicles budding from the TGN or tubular endosomes (Drake et al., 2000). It was demonstrated that AP3 is associated with early endosome-associated tubules. These tubules are either AP1 or AP3 positive. The cargo vesicles emerging from AP1 positive tubules are destined to be recycled. However, it was revealed that the vesicle budding from tubular endosome coated with AP3, containing LAMP I and LAMP II, are transported to the lysosome (Peden et al., 2004). Therefore, loss of function of AP3 results in loss of function of lysosomes since the lysosomal transmembrane proteins cannot be delivered properly (Dell'Angelica et al., 1999). Further studies are necessary to define the role of AP3 in terms of ECM trafficking. So far, we can hypothesize that either lack of lysosome functionality upon AP3D1 KD might lead to lack of ECM degradation and AA extraction. Or, AP3 might have a direct role in ECM trafficking from early endosome to lysosome (Figure 5.7A). In support of the latter, recent data from our lab showed that AP3D1 KD significantly reduces Matrigel trafficking to lysosomes in MDA-MB-231 cells (Llanses Martinez, data not shown).

Another validated traffic-ome hit was MAPK8IP3, also known as JIN3. JIN3 is a scaffold protein for the MAPK signalling pathway. JIN3 has different trafficking roles inside the cells. Mostly the focus of the studies was on neurons, as JIN3 is essential for axonal transport (Iwasawa et al., 2019). However, there are some studies demonstrating other functions of JIN3 inside the cells. It was shown that JIN3 is a FAK/Src substrate. Src phosphorylates JIN3 and induces its recruitment to FA complexes. It was also demonstrated that the phosphorylation of JIN3 is more induced by the binding of cells to fibronectin compared to cells binding to poly L lysine or being held in suspension. At FAs, JIN3 helps the recruitment of other phosphorylated proteins with SH2 domains, including paxillin and results in the formation of actin stress fibres and cell spreading (Takino et al., 2002). It was also demonstrated that JIN3 induces invasive migration of MDA-MB-231 cells into the collagen I by controlling the exocytosis of MT-MMP1. JIN3 work as Arf6 effectors and direct the recruitment of dynamin-dynactin and kinesin-1 motor proteins to the late endosomes containing MT-MMP1, resulting in its exocytosis and ECM remodelling (Marchesin et al., 2015). In addition, in a fibrosarcoma cell line, Ras-driven macropinocytosis has been shown to be mediated by the recruitment of JIN3 to Arf6 on the

plasma membrane, followed by dynamin and kinesin motor protein engagement, resulting in macropinosome formation and transport inside the cell in a microtubule-dependent manner (Williamson and Donaldson, 2019). Taken together, here, JIN3 could affect ECM-dependent cell growth in multiple ways, by controlling FAK activation, ECM degradation or ECM macropinocytosis (Figure 5.7B). Our data presented in chapter 3 showed that ECM-dependent cell growth is independent of both FAK activation and MMP activity, suggesting that it is unlikely that JIN3 controls cell growth via the modulation of these pathways. Interestingly, it has previously been shown that the ECM can be internalised by macropinocytosis under nutrient starvation, resulting in AA extraction and cell growth (Commisso et al., 2013, Olivares et al., 2017). Therefore, further work is needed to investigate whether JIN3 controls breast cancer cell growth under starvation by controlling macropinocytosis-dependent ECM internalisation.

RIN3 is another gene that was selected as a hit of the Traffic-ome screen. It was demonstrated that RIN3 binds to Rab5 positive vesicles but not the vesicles containing early endosomes markers, EEA1, in Hela cells. Rab5 is involved not only in fusion of early endosome, but it also participates in the budding and transport of clathrin-coated vesicles from plasma membrane to the early endosome. RIN3 also interacts with amphiphysin II, which has a role in receptor mediated endocytosis and is internalised together with RIN3 and Rab5. Therefore, RIN3 positive vesicles are responsible for the transport between the plasma membrane and early endosomes (Kajiho et al., 2003). Taken together, this suggests that RIN3 downregulation might inhibit ECM endocytosis (Figure 5.7C). However, further studies are needed to characterise ECM trafficking upon RIN3 gene silencing.

In conclusion, our data indicate that ECM internalization is required for breast cancer cell growth under NEAA starvation. Moreover, we identified 3 candidate genes, RIN3, MAKP8IP3 and AP3D1 that might modulate ECM-dependent cell growth under starvation by controlling ECM endocytosis and/or trafficking to the lysosomes (Figure 5.7).

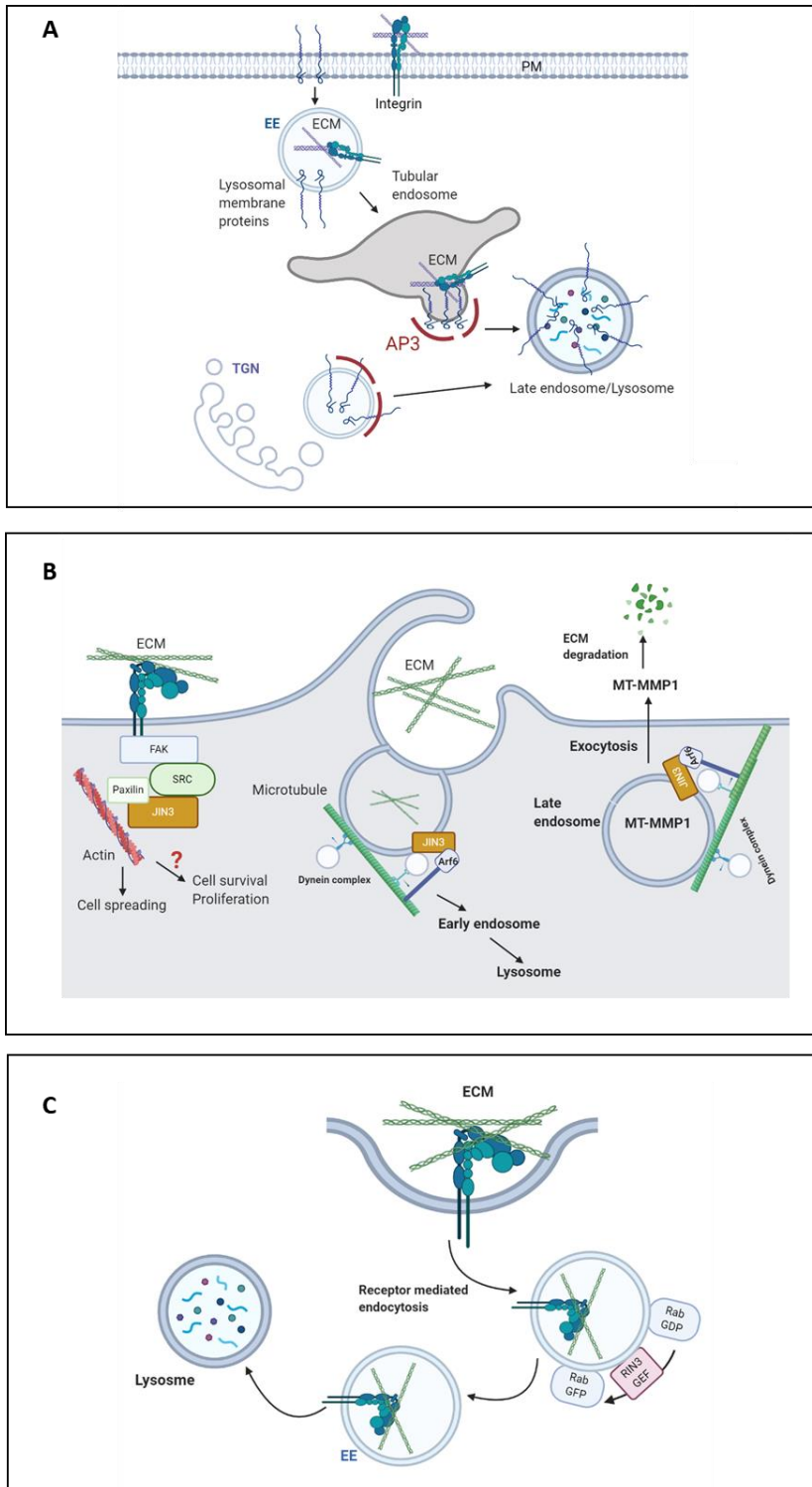


**Figure 5.7. Schematic representation of ECM trafficking pathways that AP3, JIN3 and RIN3 might be involved in under starvation conditions.** (A) AP3 might regulate ECM trafficking by transporting lysosomal membrane protein (LAMP I/II, LIMP II) or via transporting ECM from tubular endosome to lysosome. (B) JIN3 could promote ECM internalisation via Ras-driven macropinocytosis. JIN3 might also indirectly regulate ECM-dependent cell growth via recruiting FA proteins and triggering downstream signalling, or by exocytosis of MT-MMP1 resulting in ECM extracellular degradation. (C) RIN3 might play a role in ECM endocytosis controlling ECM transport between the plasma membrane and early endosomes. Image is “Created with BioRender.com.”

## Chapter 6: Signalling pathways downstream of cell-ECM interaction enhance the growth/survival of glucose starved breast cancer cells.

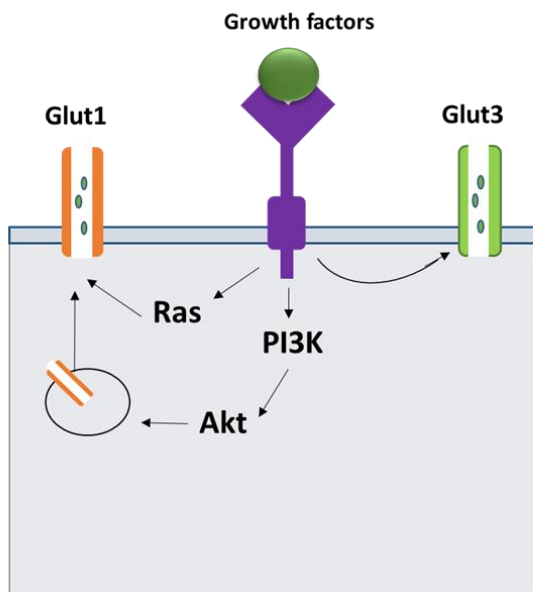
### 6.1 Introduction

In normal somatic cells, presence of nutrients in the environment does not solely trigger nutrient uptake. The interaction of cells with soluble GFs and extracellular matrix through membrane receptors is required to regulate nutrient consumption (Thompson, 2011, Grassian et al., 2011). The presence of GFs generally induces the expression of nutrient transporters. In the absence of GFs, however, nutrient transporter expression is downregulated, resulting in inadequate nutrient uptake and activation of pro-apoptotic molecules such as Bak and Bax and eventually causing cell death (Edinger, 2007). GFs trigger nutrient uptake via PI3K and Ras GTPase signalling. Activation of PI3K induces Akt and mTORC1 (for further details see section 4.1) activation (Palm and Thompson, 2017). PI3K/Akt signalling pathway promotes the translocation of Glc transporters to the plasma membrane (Cong et al., 1997, Barthel et al., 1999). Cells uptake and consume Glc to make energy via glycolysis. Glycolysis is composed of series of metabolic reactions that use one molecule of Glc to generate two molecules of pyruvate and two molecules of ATP (Pelicano et al., 2006). Akt activates hexokinase, which phosphorylates Glc to keep it intracellular. Akt also induces the activity of glycolytic enzymes (Broecker-Preuss et al., 2017). Ras GTPase signalling also induce the expression of a Glc transporter, GLUT1, hexokinase and glycolytic enzymes (Broecker-Preuss et al., 2017). Myc is a transcription factor being activated by growth-promoting signalling has been shown to induce the expression of Gln transporters, ASC2 and SNAT5 (Wise et al., 2008, Gao et al., 2009). Myc also induces expression and membrane translocation of L-type amino acid transporters (LAT1) (Hayashi et al., 2012). In around 70% of cancer types, mutations in these signalling molecules result in their constitutive activation leading to GF-independent nutrient uptake (Thompson and Bielska, 2019). For instance, RAS GTPase mutation could result in GF-independent constant activation, leading to macropinocytosis induction. It has been shown that under nutrient deficiency, macropinocytosis promotes the internalization of alternative nutrients, such as albumin or collagen (Figure 6.1) (Kim et al., 2018, Olivares et al., 2017, Commisso et al., 2013).

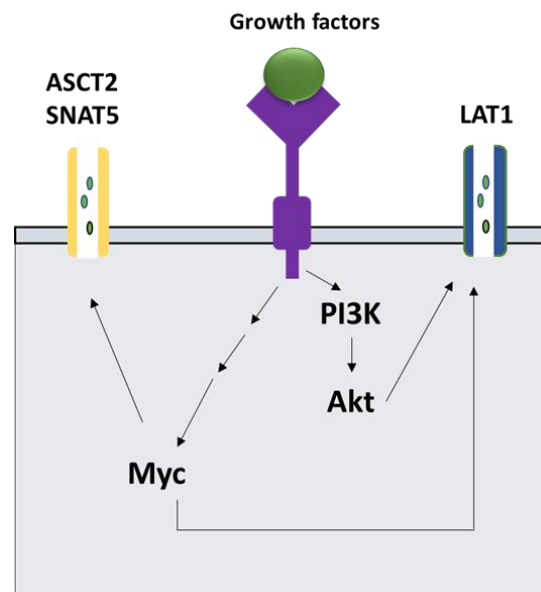


In this chapter, we evaluated the cancer cell growth, mTORC1 activation, ECM uptake, and energy production on different types of ECMs under serum and Glc starvation. Here, we showed that the presence of Matrigel and laminin cannot rescue cell growth under serum starvation. In addition, none of the ECMs could enhance cell division rate in serum starved cells. In contrast, under Glc starvation cells have higher cell number on ECM compared to the plastic. Interestingly, FAK inhibition, but not ECM internalisation, was required for cell growth on ECM under Glc starvation. Finally, the presence of ECM did not affect the cellular metabolite content in Glc-deprived conditions. Altogether, our data suggest that ECM-dependent signalling supports cell growth under Glc starvation.

## A. Glucose transporters



## B. Amino acids transporters



## C. Macropinocytosis

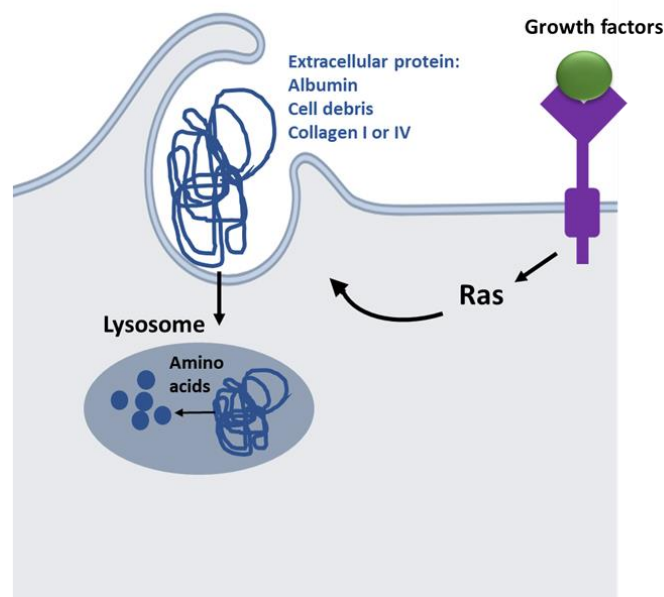


**Figure 6.1. Role of Growth factor signalling in nutrient consumption.** (A) Ras and Akt increased the expression of Glc transporter Glut1. PI3k/Akt signalling pathways also induce the membrane translocation of GLUT1 from cytoplasmic vesicles. GLUT3 concentration on the plasma membrane is increased by GFs. (B) Myc and Akt activation induce the expression of neutral amino acid transporter, LAT1. They also increase the expression of glutamine transporters, SLAT5 and ASCT2. (C) GFs induce macropinocytosis via Ras activation leading to ECP and ECM internalisation and lysosomal degradation to extract amino acids (Figure is adapted from (Palm and Thompson, 2017)).

## 6.2 Results

### 6.2.1 Optimising cell proliferation assays under glucose and serum starvation

To investigate the role of the ECM in supporting cell growth under serum and Glc starvation, we followed a similar approach to the one described in chapter three and four. To quantify the extent of ECM degradation during the proliferation assays, polymerized ECMs were incubated with a fluorescently conjugated N-Hydroxysuccinimide ester reactive dye (IRDye800) (as described in section 2.2.4). MDA-MB-231 cells were seeded the following day, and media was replaced with Glc and serum starvation conditions after 5hrs. Cells were fixed at day two and day eight post starvation. Intensity of N-Hydroxysuccinimide ester bound to collagen I or Matrigel under each condition was quantified via the Licor Odyssey imaging system. Our data revealed that the ECM was still detectable at the end of the experiments, suggesting that the cells did not completely digest the matrix (Figure 6.2). However, there was a substantial reduction in collagen I under all nutrient conditions at day eight compared to day two, without any starvation specific effect (Figure 6.2A). In contrast, the amount of Matrigel was not changed between day two and day eight, while serum and Glc starvation promoted Matrigel degradation compared to the complete media at day eight post starvation (Figure 6.2B).

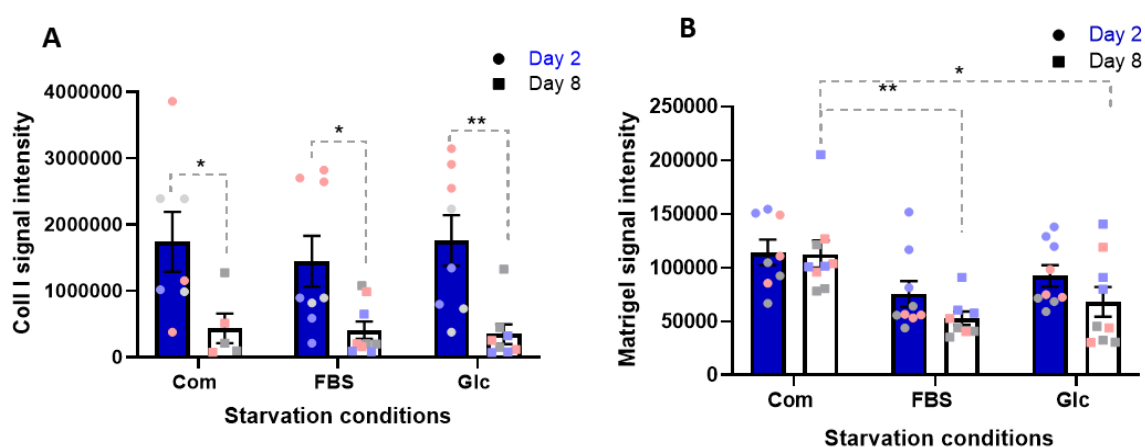


**Figure 6.2. Collagen degradation occurred during cell proliferation.** Plates were coated with 15 $\mu$ l of (A) 2mg/ml collagen I or (B) 3mg/ml Matrigel. Matrices were stained with 0.2 $\mu$ g/ml N-Hydroxysuccinimide ester. 10<sup>3</sup> MDA-MB-231 cells were seeded on ECMs. Cells were fixed at day two and eight. Signal intensity from N-Hydroxysuccinimide-labelled ECMs in each well was collected and quantified with the Licor Odyssey system. \*P < 0.05, \*\* p < 0.01 ANOVA test.

### **6.2.2 Fibrillar ECMs partially rescued breast cancer cell growth under serum starvation.**

To assess whether the presence of ECMs could enhance survival or growth of invasive breast cancer cells under GF deprivation, MDA-MB-231 cells were seeded either on plastic or on different ECM components under serum deficiency condition. On collagen I, cells had higher cell number and growth rate at day eight compared to the plastic (Figure 6.3A-B). In contrast, cells on Matrigel under serum starvation showed similar proliferation rate compared to the cells on plastic (Figure 6.3C-D). The results from cell growth on laminin was consistent with the results from cell growth on Matrigel. There was no difference between the patterns of cell growth under serum starvation on laminin or plastic (Figure 6.3E-F). To test the effect of serum deficiency on cell growth in a more physiologic condition, MDA-MB-231 were seeded on matrices derived from TIFs or CAFs extracted from breast tumours. Cells had higher proliferation rate on both TIF-CDM and CAF-CDM compared to the plastic on day eight post starvation. However, TIF-CDM resulted in a much bigger rescue on cell growth compared to CAF-CDM (Figure 6.3G-H). Altogether, these data demonstrated that fibrillar stromal-type matrices, like collagen I, TIF-CDM and CAF-CDM, rescued the growth of cells under serum depleted media, while basement-membrane-type matrices Matrigel and laminin, did not affect cell growth in the absence of serum.

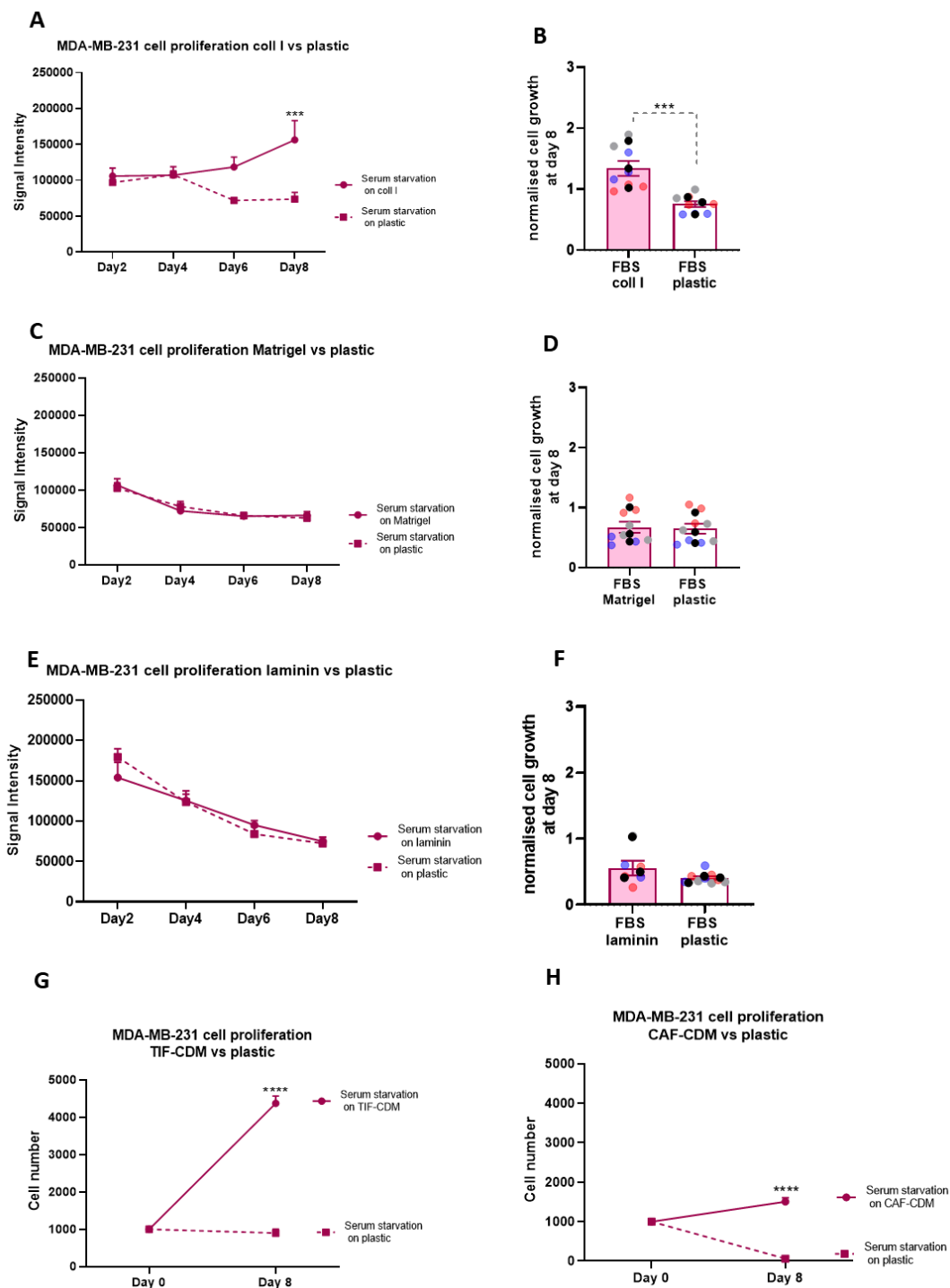


**Figure 6.3. Fibrillar matrices rescued cell growth under serum starvation.** MDA-MB-231 cells were seeded either on plastic or on plates coated with (A-B) 2mg/ml collagen I, (C-D) 3mg/ml Matrigel and (E-F) 3.5mg/ml laminin/entactin for eight days under serum (FBS) starvation. Cell proliferation was measured by DRAQ5 nuclear staining. Signal intensity was collected and quantified with the Licor Odyssey system every two days up to day eight. (G) MDA-MB-231 cells were seeded either on plastic or plates containing (G) TIFs-CDM or (H) CAF-CDM under serum starvation for eight days. Cell proliferation was measured via Hoechst nuclear staining. Images were collected by ImageXpress micro and analysed by MetaXpress software. Values are mean  $\pm$  SEM and are representative of at least three independent experiments (the black dots represent the mean of individual experiments). \*\*\* $P < 0.001$ , \*\*\*\*  $p < 0.0001$  ANOVA test.

### **6.2.3 The presence of ECM did not affect normal mammary epithelial cell and non-invasive breast cancer cell growth under serum starvation.**

To assess whether the fibrillar ECM-dependent rescue of cell growth was correlated to breast cancer cell invasiveness, the growth rate of normal mammary epithelial cells (MCF10A) and non-invasive breast cancer cells (MCF10A-DCIS) was tested. Interestingly, the presence of serum starvation only resulted in a little inhibition of cell growth on plastic compared to the complete media for both cell lines (Figure 6.4 and Chp3 supplementary figure 2 showing the growth rate in complete media). In terms of compensatory effect of ECMs, our data revealed that the presence of collagen I did not affect the growth pattern of both MCF10A and MCF10A-DCIS cells under starvation conditions (Figure 6.4A-B and E-F). However, on Matrigel both MCF10A and MCF10A-DCIS cells showed a small increase in cell number (Figure 6.C and G) and significantly higher growth rate at day eight compared to cells plated on plastic (Figure 6.4D and H). Taken together, these results demonstrate that normal mammary epithelial cells and non-invasive breast cancer cells are more tolerant to serum deficiency than invasive breast cancer cells. In addition, Matrigel, but not collagen I, slightly promotes cell growth under serum starvation while we saw the opposite effect in invasive breast cancer cells.

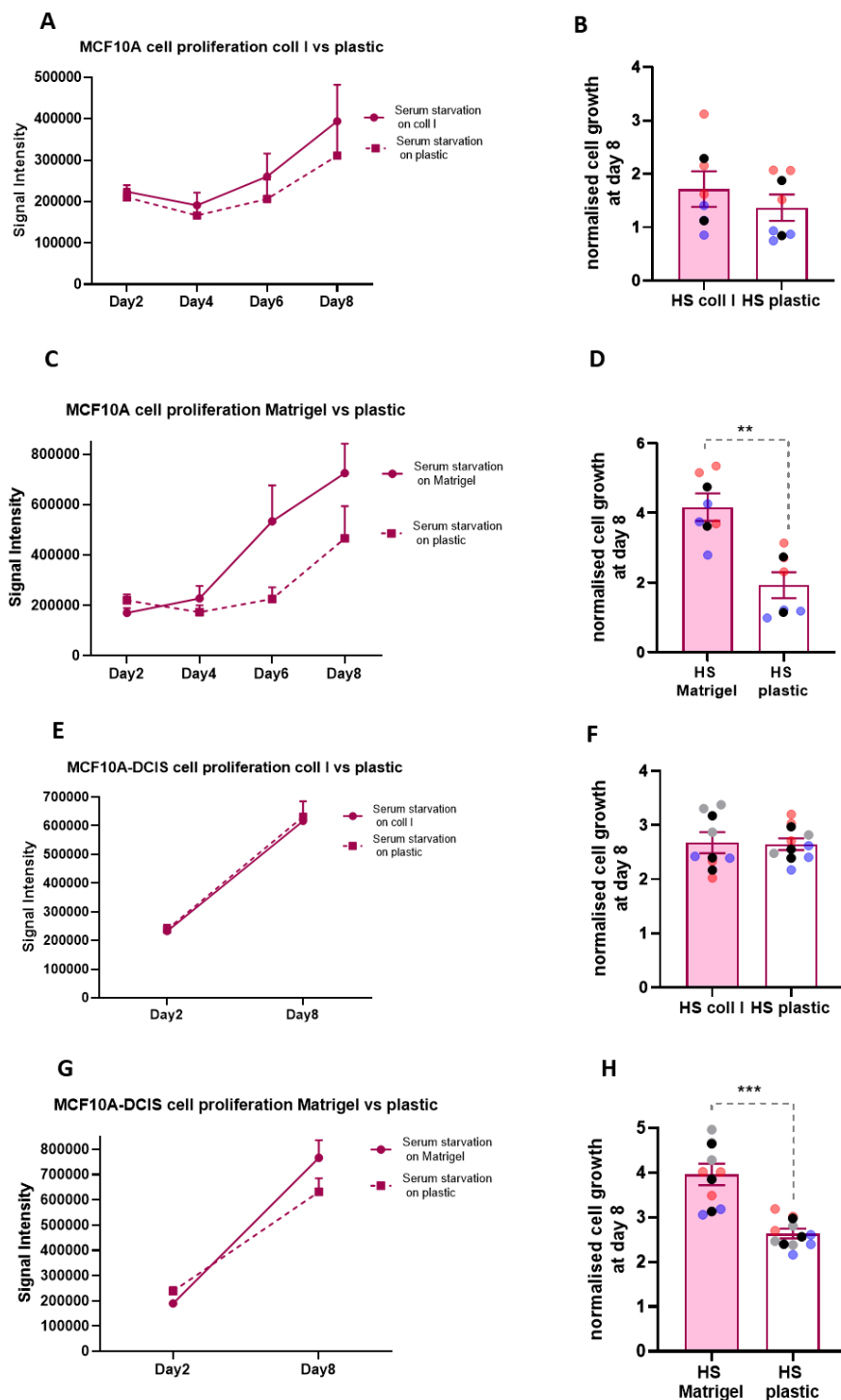


**Figure 6.4. MCF10A and MCF10A-DCIS growth under serum starvation.** MCF10A and MCF10A-DCIS cells were seeded either on plastic or on plates coated with (A-B and E-F) 2mg/ml collagen I, (C-D and G-H) 3mg/ml Matrigel for eight days under serum (HS) starvation. Cell proliferation was measured by DRAQ5 nuclear staining between day two up to day eight post starvation. Signal intensity was collected by Licor Odyssey and quantified by Image Studio Lit software. Values are mean  $\pm$  SEM and are representative of at least three replicated from two independent experiments (the black dots represent the mean of individual experiments). \*\* $p < 0.01$  and \*\*\* $p < 0.001$  ANOVA test.

### 6.2.4 The presence of ECMs did not promote cell division under serum starvation in invasive breast cancer cells.

Data presented above revealed that, under serum starvation, MDA-MB-231 was partially rescued in the presence of fibrillar matrices, like collagen I and CDMs, but not in the presence of Matrigel or laminin (Figure 6.3). Therefore, we hypothesized that cells might show an increased proliferation rates on collagen I compared to cells on Matrigel, laminin or plastic. Thus, we performed EdU incorporation experiments to identify cells which passed through DNA synthesis and mitosis (Figure 6.5). Cells were starved for six days when they received EdU. EdU incorporation was measured after two days at day eight post starvation. As shown in figure 6.5, serum starvation resulted in a significant inhibition of cell growth on plastic. MDA-MB-231 cells did not show any differences in terms of EdU incorporation on Matrigel or laminin under serum starvation condition compared to the cells seeded on plastic. However, there was a slight, but non-significant, increase in cell division rate in the presence of collagen I, which is consistent with the small increase in cell number we observed under serum depleted media. Cells growing in complete media were around 100% EdU positive on both ECM and plastic (Figure 6.5A-C). Taken together, our data suggest that collagen I, Matrigel and laminin does not substantially accelerate cell proliferation rate under serum starvation.

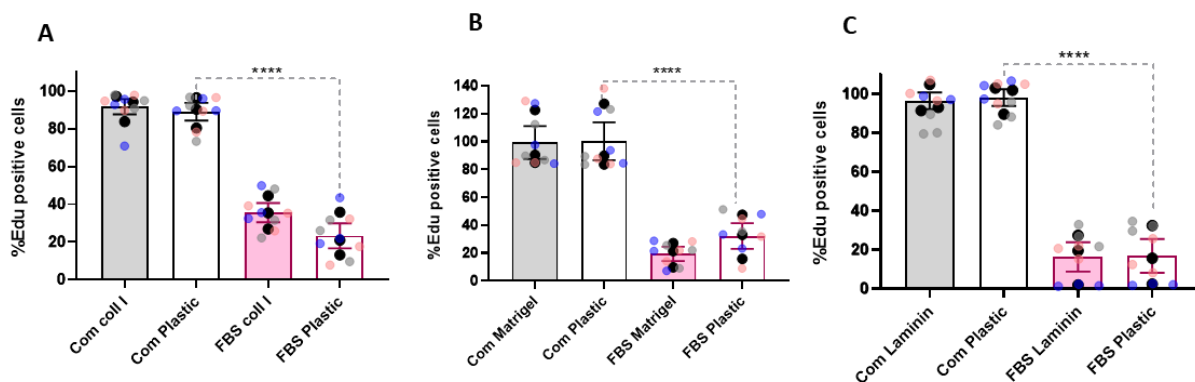


**Figure 6.5. ECMs did not affect cell division under serum starvation.** (A) MDA-MB-231 cells were seeded either on plastic or plastic coated with (B) 2mg/ml collagen I, (C) 3mg/ml Matrigel, or (D) 3.5mg/ml laminin/entactin in complete media (Com) or under serum starvation (FBS). Cells were incubated with EdU on day six post starvation, fixed and stained with Hoechst and Click iT EdU imaging kit on day 8. Images were collected by ImageXpress micro and analysed by MetaXpress and CME software. Values are mean  $\pm$  SEM and are representative of three independent experiments (the black dots represent the mean of individual experiments). \*\*\*\*  $p < 0.0001$  ANOVA test.



### **6.2.5 Collagen I, but not Matrigel or laminin, rescued the activity of mTORC1 under serum starvation.**

We previously showed that under serum starvation, only collagen I increased the growth rate of the MDA-MB-231 cells compared to the plastic (Figure 6.3). In chapter 3, we demonstrated that the presence of ECM rescued mTORC1 activity under AA starvation (Chp3 figure 4). Therefore, we wanted to test whether higher cell number on collagen I under serum starvation could correlate with higher mTORC1 anabolic activity (Mossmann et al., 2018). To do this, we examined the rate of phosphorylation of an mTORC1 downstream target, S6, as an indicator for mTORC1 activity. Cells were seeded on collagen I, Matrigel, laminin or plastic under complete media or serum depletion conditions for three days and p-S6 intensity was quantified. In agreement with our cell proliferation results, as expected serum starvation significantly reduced mTORC1 activity on plastic, while the presence of collagen I rescued the mTORC1 activity under serum starvation (Figure 6.6A). On Matrigel, even though the p-S6 intensity was higher compared to the plastic under nutrient deficient condition, the difference was not significant (Figure 6.6B). Laminin also did not induce mTORC1 activity under starvation as p-S6 intensity was very similar between cells growing on laminin or plastic (Figure 6.6C). Our data suggest that collagen I, but not Matrigel or laminin, was able to rescue mTORC1 activity under serum starvation in MDA-MB-231 cells.

One mechanism through which the ECM could promote mTOR activation is by ECM internalisation and lysosomal degradation. This can lead to an increase in AA content, promoting mTOR activation. Therefore, we wanted to test whether the ECM is internalised and degraded in the lysosomes under serum starvation. We tracked the journey of fluorescent-labelled collagen I, Matrigel and laminin under complete and serum depleted media in the presence or absence of a lysosomal protease inhibitor (E64d). Under complete media, cells significantly accumulate higher amounts of ECM in the presence of the lysosomal protease inhibitor, suggesting that cells internalize and degrade the ECMs inside the lysosomes. However, under serum starvation, lack of lysosomal degradation did not affect the amount of collagen I and laminin accumulation within the cells, suggesting that either ECM endocytosis or degradation was impaired under serum starvation (Figure 6.6D and F). Interestingly, the amount of internalised Matrigel, under serum depleted media, was significantly increased in the presence of E64d (Figure 6.6E). Taken together, these data did

not show any direct relation between ECM lysosomal degradation and mTORC1 activity under serum starvation.

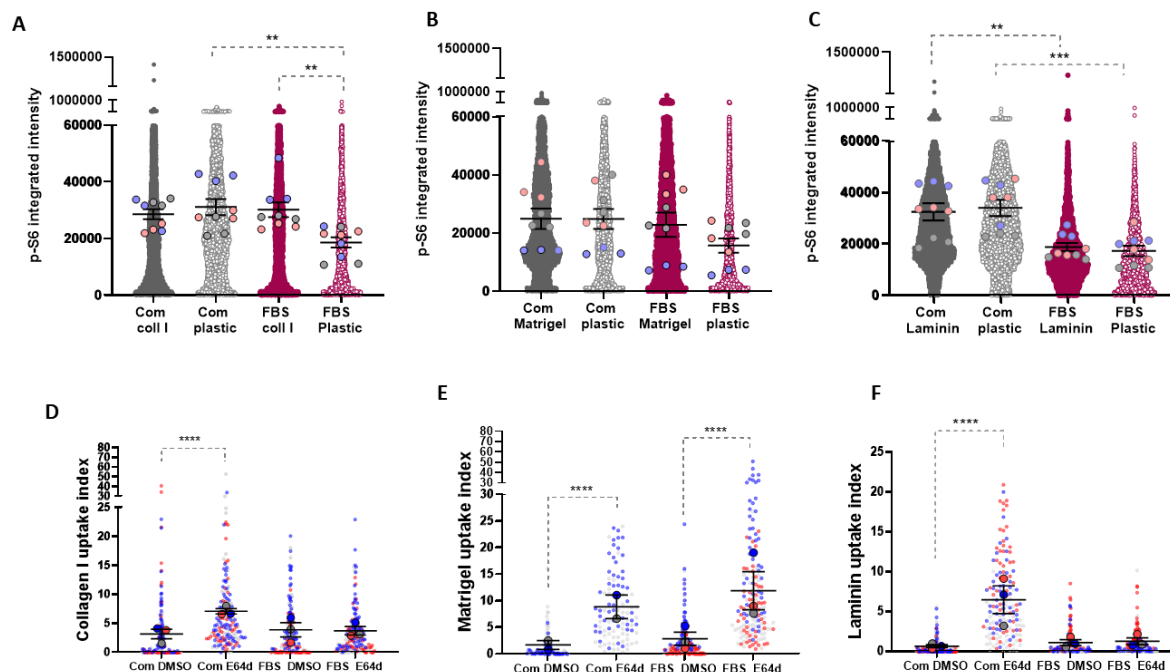


**Figure 6.6. Collagen I rescued mTORC1 activity in serum starved cells.** MDA-MB-231 cells were plated either on plastic or plastic coated with (A) 2mg/ml collagen I, (B) 3mg/ml Matrigel or (C) 3.5mg/ml laminin/entactin under complete media or FBS starvation conditions. Cells were fixed and stained for p-S6 and nuclei at day three. Images were collected by ImageXpress micro and analysed by CME software. MDA-MB-231 cells were plated under complete (Com), or FBS depleted media on dishes coated with NHS-fluorescein labelled (D) 1mg/ml collagen I, (E) 3mg/ml Matrigel or (F) 3.5mg/ml laminin/entactin for three days, in the presence of the lysosomal inhibitor E64d (20 $\mu$ M) or DMSO (control). Values are mean  $\pm$  SEM and are representative of three independent experiments except for Matrigel uptake under complete media which is the representative of two independent experiments. (The dots represent the mean of individual experiments). \*\* $p < 0.01$ , \*\*\*  $p < 0.001$ , and \*\*\*\*  $p < 0.0001$  ANOVA test.

### 6.2.6 The presence of ECM partially rescued breast cancer cell growth under glucose starvation.

To assess Glc dependency of invasive breast cancer cells, MDA-MB-231 cells were seeded on plastic under different Glc concentrations. A previous study showed that extraction of proline from collagen could recover the growth of pancreatic cancer cells under low Glc conditions, 1mM and 5mM Glc concentrations. In contrast, under full Glc starvation, proline did not have any impact on cell growth (Olivares et al., 2017). First, we compared the growth rate of MDA-MB-231 cells plated on plastic up to day seven post starvation to see under what Glc concentration the cells showed significant inhibition of growth compared to the complete

media. The data showed that the concentrations of Glc between 2.5mM to 0mM significantly reduced cell number on plastic compared to the 25mM, which is the concentration of Glc in complete media (Figure 6.7A). Thus, we decided to test the growth rate of cells between day two up to day eight on ECMs or on plastic under media containing 2.5mM, 1mM, or 0mM Glc. Under 2.5mM Glc, cell growth on collagen I and CAF-CDM was similar to plastic. However, on Matrigel, cell number was significantly higher at day eight post starvation (Figure 6.7B-D). Under 1mM Glc, on collagen I and Matrigel there were higher cell number compared to plastic from day six to eight. Cells on CAF-CDM on day eight also showed higher growth rate compared to the plastic (Figure 6.7E-G). In 0mM Glc, on collagen I, MDA-MB-231 cells had significantly higher growth rate and cell number at day six and eight post Glc starvation compared to the cells growing on plastic (Figure 6.8A-B). On Matrigel, cells had substantially higher cell number and growth rate from day four forward (Figure 6.8C-D). However, after day four, cell number on Matrigel reached a plateau (Figure 6.8C). The cell growth results on laminin were consistent with the ones on Matrigel. In 0mM Glc media, MDA-MB-231 cells had a higher cell number and growth rate on laminin compared to the cells seeded on plastic (Figure 6.8E-F). However, after day four post Glc starvation, cell number was decreasing on laminin (Figure 6.8E). To test the effect of a more physiologic environment on cell growth under Glc deficiency, MDA-MB-231 were seeded on TIF-CDM or CAF-CDM. Cells had higher proliferation rate on TIF-CDM and CAF-CDM compared to the plastic on day eight post starvation (Figure 6.8G-H). Therefore, since the most extreme difference in cell growth on ECM compared to plastic was observed in media fully depleted of Glc, 0mM Glc was selected to carry out further experiments.

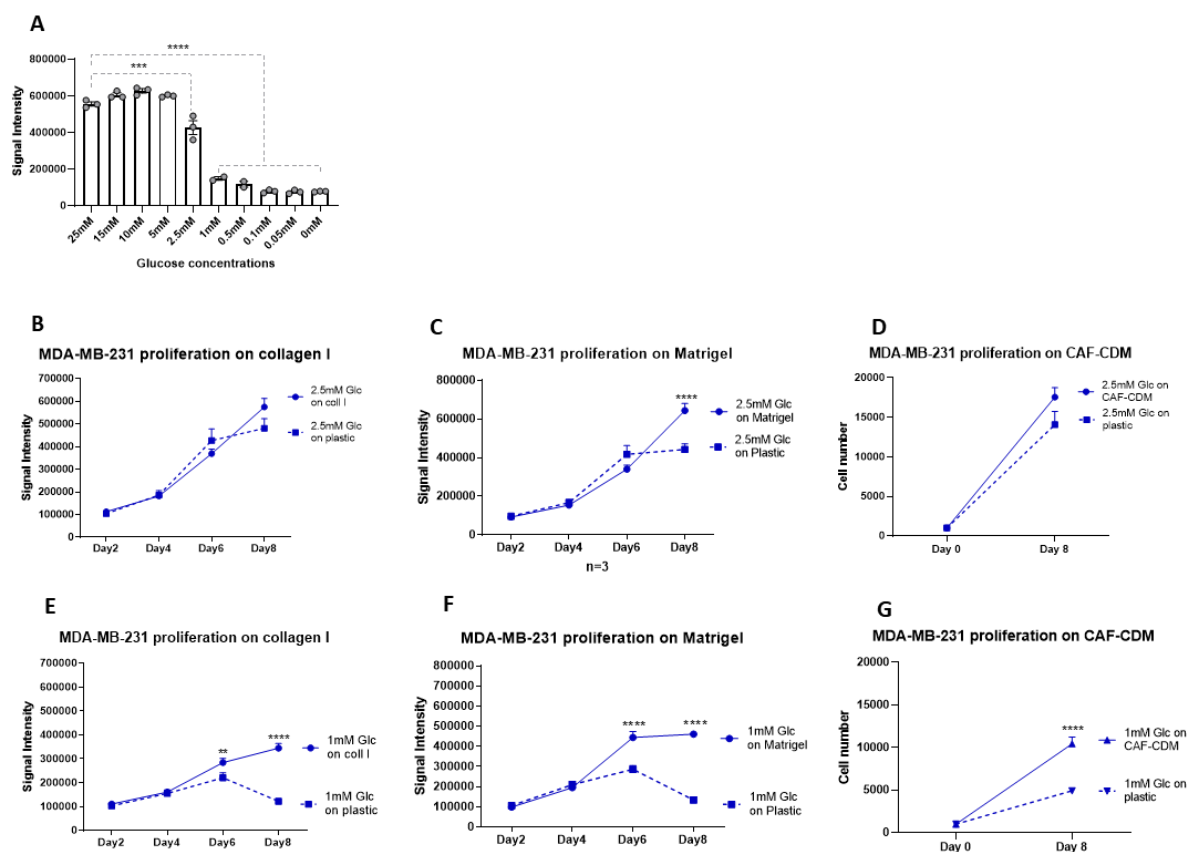


**Figure 6.7. Cell growth under different glucose concentration.** (A) MDA-MB-231 cells were seeded on plastic under different Glc concentrations. Cell proliferation was measured by DRAQ5 nuclear staining quantification with the Licor Odyssey system on day seven post starvation. MDA-MB-231 cells were seeded under 2.5mM Glc on plastic or plates coated with (B) 2mg/ml collagen I, (C) 3mg/ml Matrigel or (D) CAF-CDM. MDA-MB-231 cells were seeded under 1mM Glc on plates coated with (E) 2mg/ml collagen I, (F) 3mg/ml Matrigel or (G) CAF-CDM. (B, C, E, F) Cell proliferation was measured by DRAQ5 nuclear staining every two days up to day eight. Signal intensity was quantified by Image Studio Lit software. (D, G) cell proliferation was measured via Hoechst nuclear staining. Images were collected by ImageXpress micro and analysed by MetaXpress software. Values are mean  $\pm$  SEM and are representative of at least three independent experiments (the dots in A represent the mean of individual experiments). \*\* $p < 0.01$ , \*\*\* $P < 0.001$ , \*\*\*\* $p < 0.0001$  ANOVA test.

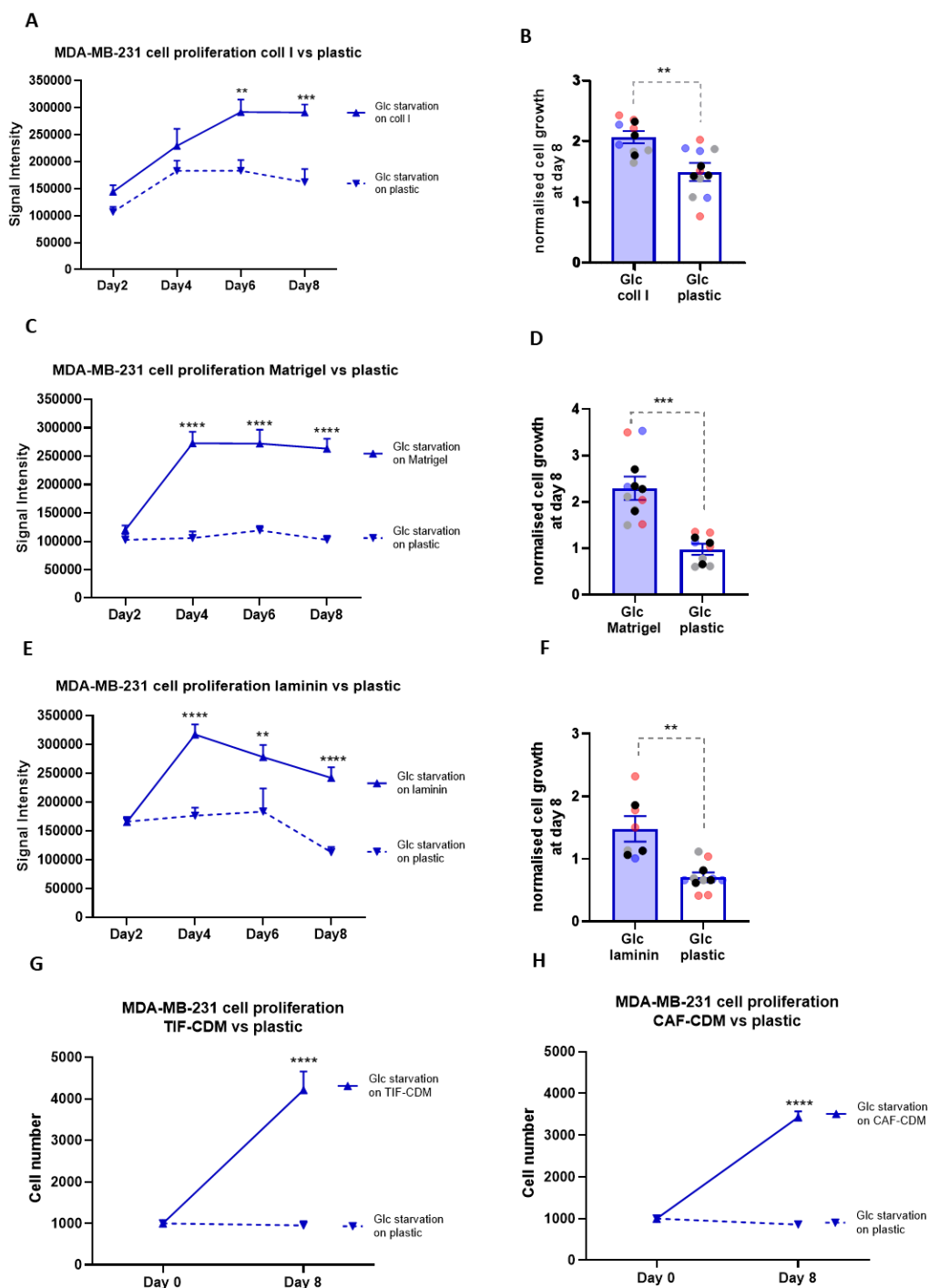


**Figure 6.8. The ECM rescued cell growth under glucose starvation.** MDA-MB-231 cells were seeded under Glc free media (Glc starvation) on plates coated with (A-B) 2mg/ml collagen I, (C-D) 3mg/ml Matrigel, (E-F) 3.5mg/ml laminin/entactin, (G) TIF-CDM or (H) CAF-CDM and starved for eight days. (A-F) Cell proliferation was measured by DRAQ5 nuclear staining quantification with the Licor Odyssey system every two days up to day eight on collagen, Matrigel and laminin. Signal intensity from cells under each condition were collected by Image Studio Lit software. (G, H) On TIF-CDM and CAF-CDM, cell proliferation was measured via Hoechst nuclear staining. Images were collected by ImageXpress micro and analysed by MetaXpress software. Values are mean  $\pm$  SEM and are representative of at least three independent experiments (the black dots represent the mean of individual experiments). \*\* $p < 0.01$ , \*\*\* $P < 0.001$ , \*\*\*\* $p < 0.0001$  ANOVA test.

### **6.2.7 The ECM did not affect cell growth of normal mammary epithelial cells and non-invasive breast cancer cells under glucose starvation.**

We showed that the presence of ECMs could partially rescue the growth of invasive breast cancer cells under Glc starvation (Figure 6.7 and 6.8). To assess whether the ability of the ECM to rescue cell growth under Glc starvation is correlated to the invasiveness of the cells, the growth rate of non-invasive breast cancer cells (MCF10A-DCIS) and normal mammary epithelial cells (MCF10A) was tested. Our data revealed that presence of collagen I or Matrigel did not affect the growth pattern of MCF10A-DCIS cell lines under 2.5mM, 1mM or 0mM Glc concentration (Figure 6.9). In Glc depleted media, MCF10A-DCIS cells were not proliferating regardless of the substrate they were growing on (Figure 6.9E-F). Under 1mM and 2.5mM Glc, cells were growing between day two up to day four. However, from day four up to day eight cell number started declining regardless of the presence of collagen I and Matrigel (Figure 6.9A and C). Despite a significant difference being observed in the growth rate of MCF10A-DCIS cells on Matrigel compared to the plastic at 2.5mM Glc, the growth pattern was very similar to the one observed on plastic (Figure 6.9A-B). Cells' growth rate on Matrigel and collagen I was like plastic under 1mM Glc concentration or Glc depleted media (Figure 6.9D and F).

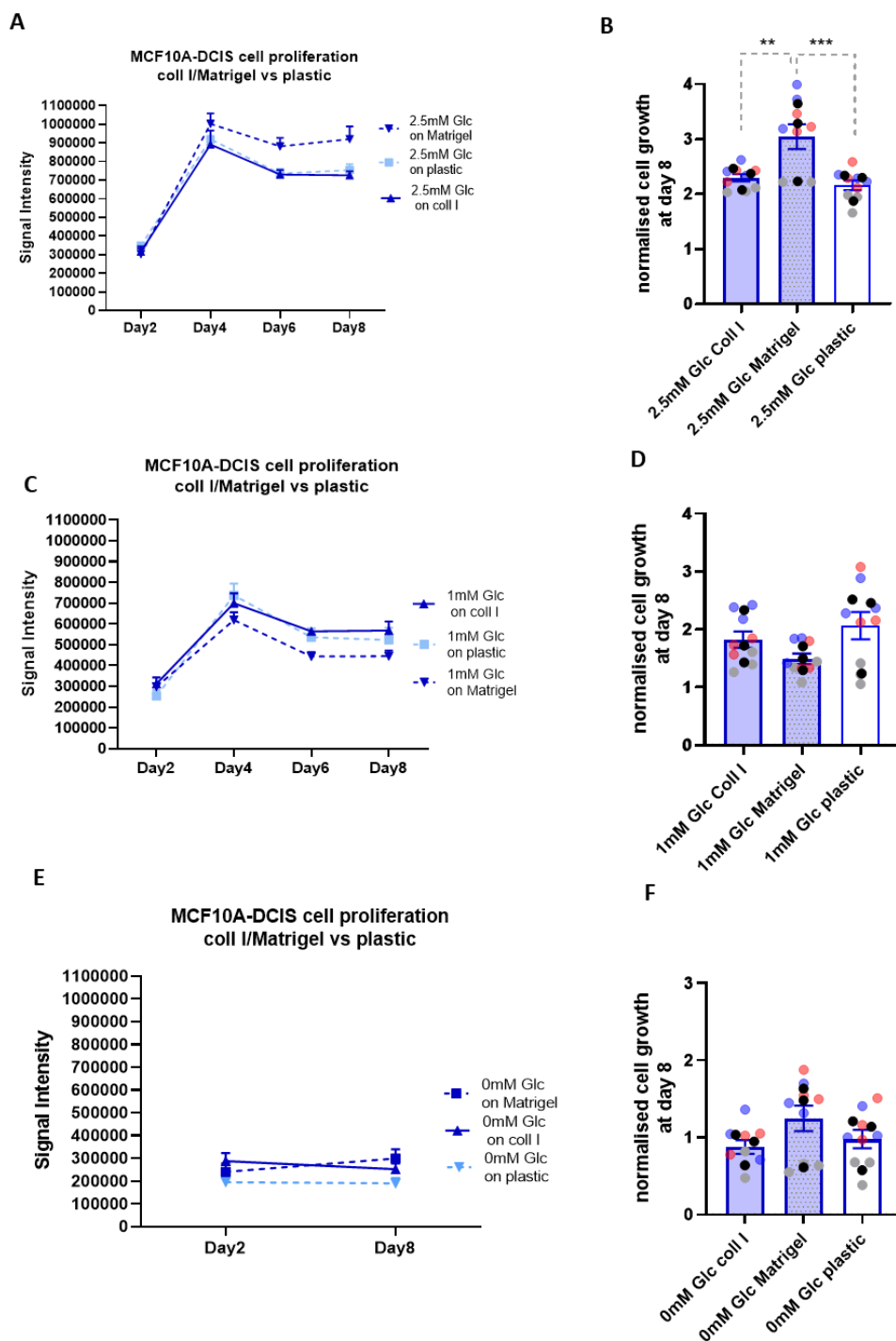


**Figure 6.9. The ECM did not affect MCF10A-DCIS growth under glucose starvation.** MCF10A-DCIS cells were seeded on 2mg/ml collagen I, 3mg/ml Matrigel and plastic in media containing (A-B) 2.5mM or (C-D) 1mM or (E-F) 0mM Glc. Cell proliferation was measured by DRAQ5 nuclear staining quantification with the Licor Odyssey system on day two up to day eight post starvation. Signal intensity from cells under each condition were collected by Image Studio Lit software. Values are mean  $\pm$  SEM and are representative of at least three independent experiments (the black dots represent the mean of individual experiments). \*\* $P < 0.01$  and \*\*\*  $p < 0.001$  ANOVA test.

Testing the effect of CAF-CDM on MCF10A-DCIS growth showed that cells on day eight had a significantly higher cell number on plastic under all Glc starvation conditions. In addition, cells with access to higher concentration of Glc showed higher growth rate regardless of the substrate they were growing on (Figure 6.10).

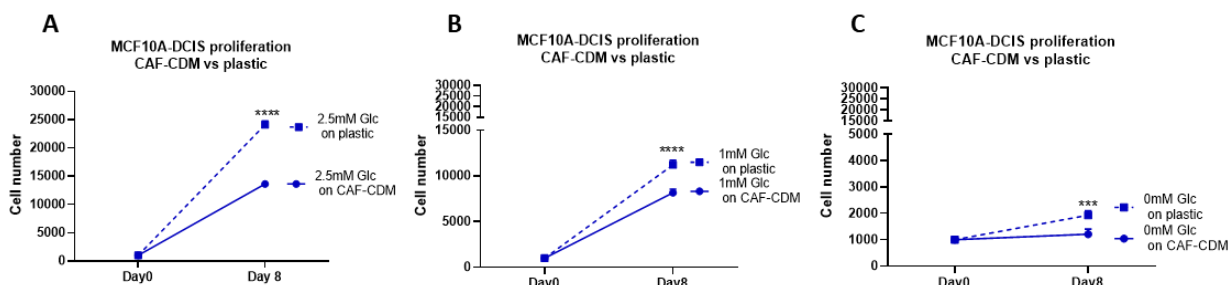


**Figure 6.10. MCF10A-DCIS growth on CAF-CDM.** MCF10A-DCIS cells were seeded either on plastic or on CAF-CDM in media with (A) 2.5mM, (B) 1mM Glc or (C) 0mM Glc. On day eight post starvation, cell proliferation was measured via Hoechst nuclear staining. Images were collected by ImageXpress micro and analysed by MetaXpress software. \*\* $p < 0.01$ , \*\*\* $P < 0.001$  ANOVA test.

Repeating the same experiments with MCF10A cells under Glc free media also revealed that the presence of collagen I and Matrigel could not recover cell growth. Cells' growth pattern on ECMs was the same as on plastic, showing a reduction in cell number between day two up to day eight of Glc starvation (Figure 6.11).

Altogether, these data suggest that the presence of ECM did not rescue the growth of non-invasive breast cancer cells and normal mammary epithelial cells. In addition, an increase in Glc concentration induced the cell growth regardless of the presence of ECM in non-invasive breast cancer cells.



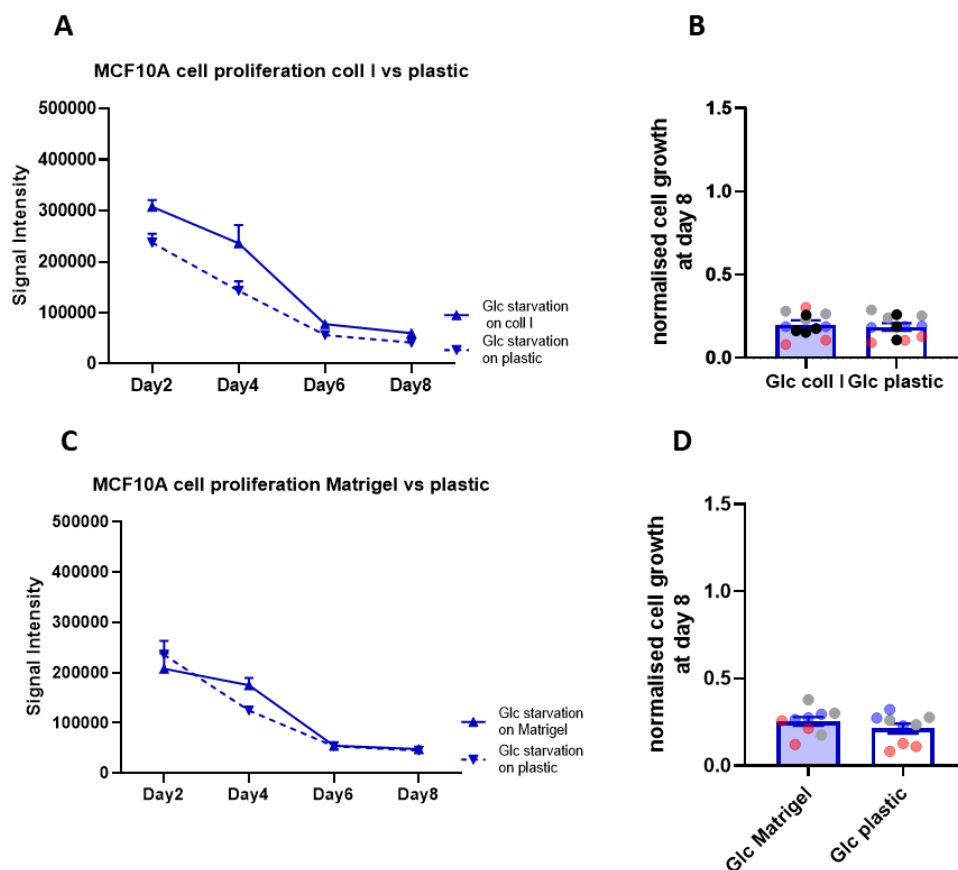


**Figure 6.11. ECMs did not rescue MCF10A growth under glucose starvation.** MCF10A cells were seeded either on plastic or on plates coated with (A-B) 2mg/ml collagen I, (C-D) 3mg/ml Matrigel for eight days under Glc starvation. Cell proliferation was measured by DRAQ5 nuclear staining quantification with the Licor Odyssey system on day two, four, six and day eight post starvation. Values are mean  $\pm$  SEM and are representative of three independent experiments (the black dots represent the mean of individual experiments).

### 6.2.8 The presence of ECMs did not promote cell division under glucose starvation in invasive breast cancer cells.

Data presented above revealed that MDA-MB-231 cell number was higher on collagen I, Matrigel and laminin compared to the plastic during eight days of complete Glc starvation (Figure 6.8). We therefore asked whether being surrounded by ECM either induced cell survival, proliferation, or both under Glc starvation. To answer this question, we performed EdU incorporation experiments (As described in 6.2.4). Cells were starved for six days when they received EdU. EdU incorporation was measured after two days on day eight of post starvation. Our data revealed that there was a gradual decrease in the percentage of EdU positive cells when the Glc concentration was reduced from 2.5mM to 0mM, regardless of

the substrate the cells were plated on (Figure 6.12A-B). MDA-MB-231 cells did not show any differences in terms of number of cells positive for EdU on ECMs under 1mM Glc or 0mM Glc compared to the cells seeded on plastic. Cells under 2.5mM Glc showed a significant but very small increase in EdU incorporation on Matrigel but not on collagen I in comparison to the plastic. (Figure 6.12A-B). In parallel, presence of laminin did not affect cell division rate under Glc depleted media (Figure 6.12C). Therefore, in general, the data demonstrate that the presence of ECM did not induce cell proliferation between six and eight days of Glc starvation.

It has previously been shown that binding of ECM to integrins activate downstream signalling pathways which can promote cell survival (Wozniak et al., 2004). In particular, cell-ECM interaction activates a FAK-dependent signalling pathway which has been shown to prevent apoptosis by sequestering pro apoptotic factors in the cytosol (Gilmore et al., 2000). Therefore, we investigated whether the higher cell number we observed on ECM under Glc deficiency was due to an anti-apoptotic role of collagen I and Matrigel. To assess this, we quantified the number of cells positive for an apoptosis marker, activated caspase 3/7, at day three or eight post starvation. Both caspase-3 and caspase-7 have a role in the intrinsic and extrinsic apoptosis pathway. Caspases are a group of cysteine protease enzymes whose cleavage results in their activation, which mediates DNA fragmentation, cytoskeletal and nuclear protein degradation, formation of apoptotic bodies and eventually cell death (Elmore, 2007). Our data revealed that the apoptosis rate increased between day three up to day eight under all nutrient conditions. In addition, Glc starvation significantly induced apoptosis in cells on plastic compared to the complete media. However, there were no significant differences between the apoptosis rate on collagen I or Matrigel compared to plastic either at day three or day eight in Glc depleted media (Figure 6.12D-E). Taken together, our data suggest that higher cell number on ECMs under Glc starvation compared to the plastic was linked neither to ECMs' impact on cell replication nor to their anti-apoptotic effect.

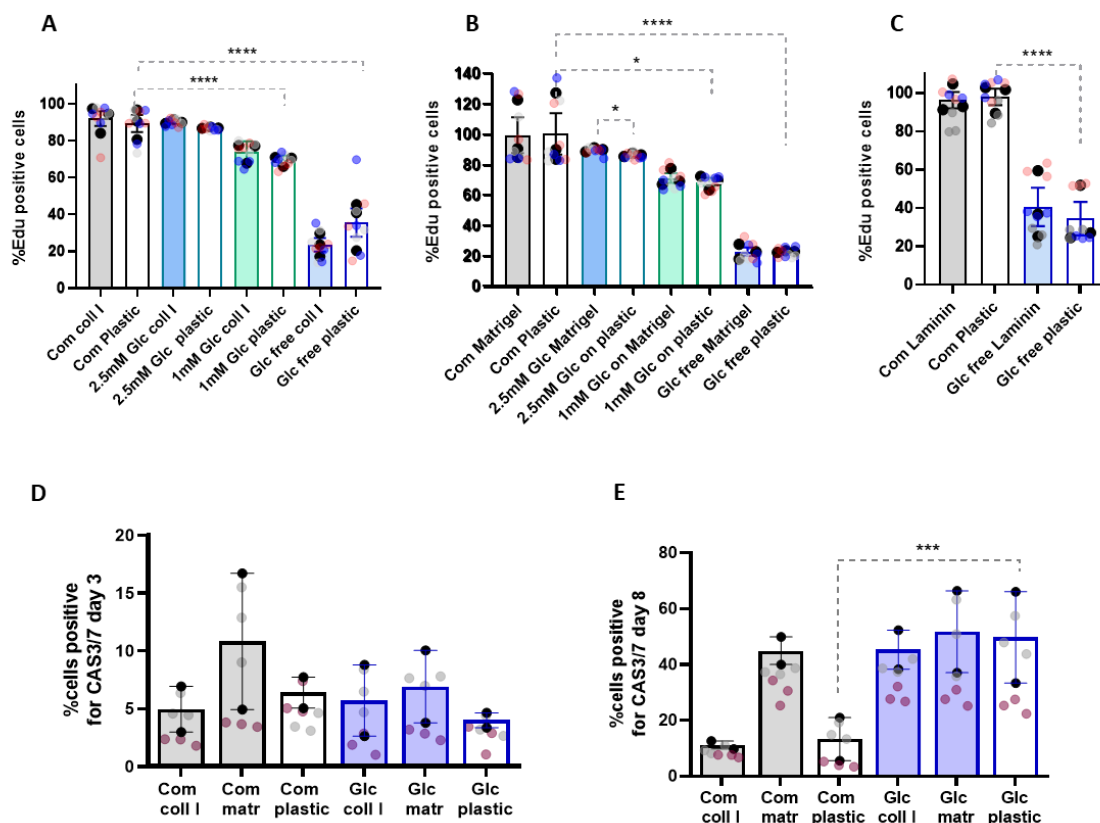


**Figure 6.12. ECMs did not affect cell division or apoptosis under glucose starvation.** MDA-MB-231 cells were seeded either on plastic or plastic coated with (A) 2mg/ml collagen I, (B) 3mg/ml Matrigel, under 2.5mM, 1mM and 0mM Glc (Glc free) or (C) 3.5mg/ml laminin/entactin under Glc free media. Cells were incubated with EdU on day six post starvation, fixed and stained with Hoechst and Click iT EdU imaging kit on day eight. Images were collected by ImageXpress micro and analysed by MetaXpress and CME software. Values are mean  $\pm$  SEM and are representative of three independent experiments (the black dots represent the mean of individual experiments). \* $p < 0.05$ , and \*\*\*\* $p < 0.0001$  ANOVA test. MDA-MB-231 cells were seeded on either plastic or plates coated with 2mg/ml collagen I or 3mg/ml Matrigel under Glc starvation or complete media. Cells were stained for activated cas-3/7 at day (D) three or (E) eight post starvation. Images were collected by ImageXpress micro and analysed by MetaXpress and CME software. Values are mean  $\pm$  SEM and are representative of two independent experiments (the black dots represent the mean of individual experiments). \*\*\* $p < 0.001$  ANOVA test.

### 6.2.9 ECM affected the activity of mTORC1 under glucose starvation.

In the previous chapter we showed that the ECM supports the activation of mTORC1 under nutrient starvation conditions (Chp3 figure 4). Therefore, we wanted to investigate whether the ECM-dependent increase in cell number was associated with higher mTORC1 anabolic activity. To do this, we examined the phosphorylation of an mTORC1 downstream target, S6. Cells were seeded on collagen I, Matrigel, laminin or plastic under Glc depleted media for

three days. mTORC1 activity was measured by quantifying p-S6 signal intensity using high-throughput microscopy. Effect of Glc on p-S6 was variable on plastic in our experiments (Figure 6.13A-C). Presence of collagen I rescued the mTORC1 activity under Glc starvation compared to the cells on plastic (Figure 6.13A). On Matrigel, even though the p-S6 intensity was higher, the difference was not significant (Figure 6.13B). Finally, p-S6 intensity was slightly lower in cells growing on laminin compared to the plastic (Figure 6.13C). Our data suggest that collagen I, and to a lesser extent Matrigel, supported mTORC1 activity under Glc starvation in MDA-MB-231 cells. To assess whether mTORC1 activation was required for ECM-dependent cell growth under Glc starvation, MDA-MB-231 cells were treated with Bafilomycin A1 (BA1) which is a V-ATPase inhibitor (For further details please refer to section 4.2.4). V-ATPase is a proton pump that acidifies lysosomes. In addition, accumulation of AAs inside the lysosomes induces a signal transferred to Rag GTPases via the V-ATPase–Ragulator interaction leading to mTORC1 lysosomal recruitment and activation (Zoncu et al., 2011a). Thus, we hypothesise that if ECM-dependent cell growth was mediated by mTORC1 activation, then, BA1 would inhibit mTORC1 reactivation and cell growth on collagen I and Matrigel. Previously, we showed that BA1 decreased both cell number and p-S6 intensity of MDA-MB-231 cells under complete media on both Matrigel and plastic (Figure 4.5A-B). Here, under Glc starvation BA1 decreased cell growth and p-S6 intensity on Matrigel compared to the DMSO control group, without affecting cell number or mTORC1 activation on plastic (Figure 6.13D-E). Moreover, comparing p-S6 intensity in the DMSO control groups confirms the observations that under Glc starvation, mTORC1 activity is enhanced on Matrigel compared to the plastic (Figure 6.13E). Therefore, our data suggest that ECM-driven cell growth on Matrigel under Glc starvation could be dependent on mTORC1 activation.

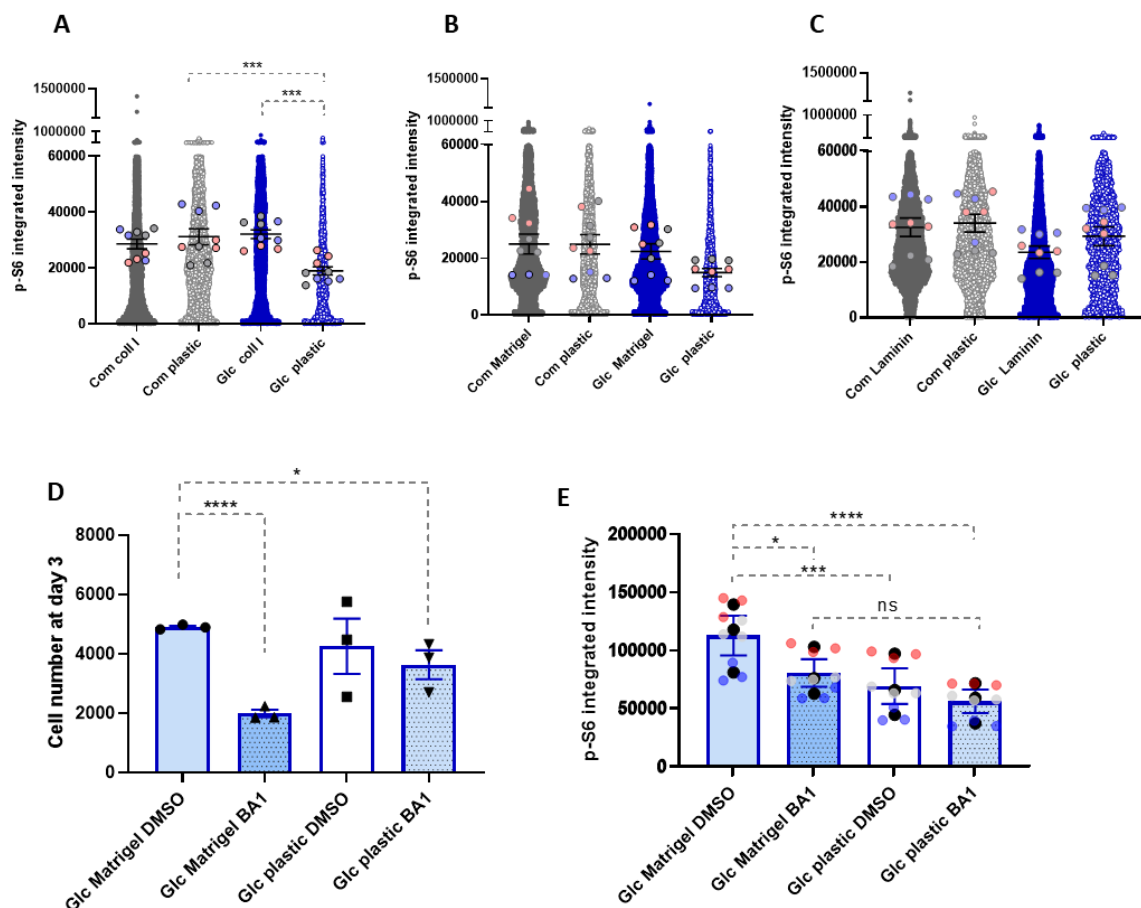


**Figure 6.13. The ECM supported mTORC1 activation in glucose starved cells, and this was required for ECM-dependent cell growth.** MDA-MB-231 cells were plated either on plastic or plastic coated with (A) 2mg/ml collagen I, (B) 3mg/ml Matrigel or (C) 3.5mg/ml laminin/entactin under complete media (Com) and 0mM glucose (Glc). (D-E) MDA-MB-231 cells were plated either on plastic or plastic coated 3mg/ml Matrigel in 0mM Glc. 200nM Bafilomycin A1 or DMSO (control) were added to each condition every day. Cells were fixed and stained for p-S6 and nuclei at day three. Images were collected by ImageXpress micro and analysed by CME software. Values are mean  $\pm$  SEM and are representative of three independent experiments (the dots represent the mean of individual experiments). \* $p < 0.05$ , \*\* $p < 0.01$ , \*\*\*  $p < 0.001$  and \*\*\*\* $p < 0.0001$  ANOVA test.

### 6.2.10 Blocking ECM internalization did not affect cell growth under glucose starvation.

We showed above that mTORC1 activity was required for cell growth under Glc starvation. One way in which the ECM could drive mTORC1 activation is by endocytosis and lysosomal degradation, leading to an increase in nutrient concentration in lysosomes. In parallel, our data in chapter 3 revealed that under AA starvation, ECM internalisation is required for invasive breast cancer cell growth (Chp3 figure5). Therefore, we examined whether cells were

still able to internalize the ECMs under Glc depleted conditions. We tracked the journey of fluorescently labelled collagen I, Matrigel and laminin under different Glc concentrations in the presence of the lysosomal protease inhibitor, E64d. Our data showed that, under full Glc starvation, there was a strong increase in Matrigel and collagen I internalisation and degradation, as the uptake index was significantly increased in both DMSO and E64d. In contrast, in the presence of 2.5mM Glc we did not observe any difference between DMSO and E64d, suggesting that this Glc concentration inhibited collagen I and Matrigel endocytosis and/or lysosomal degradation (Figure 6.14A-B). Presence of E64d also increased accumulation of laminin inside the cells under both complete and Glc depleted media (Figure 6.14C). We then wanted to investigate whether the growth of cancer cells relied on ECM internalization under Glc deficiency conditions. To assess this hypothesis, collagen I, Matrigel and CAF-CDM coated plates were treated with 10% glutaraldehyde to chemically cross-link amine groups of ECM proteins. We previously showed that MDA-MB-231 growth under complete media did not depend on ECM uptake as cell growth was similar on normal and cross-linked ECMs (Chp3 figure 5E). Surprisingly, under Glc starvation, matrix cross-linking did not oppose MDA-MB-231 growth (Figure 6.14D-E). Taken together, our data demonstrate that ECM internalization and lysosomal degradation were promoted under Glc deficiency, but they were dispensable for ECM-dependent cell growth. In addition, the presence of low Glc concentrations reduced ECM lysosomal degradation, suggesting that Glc deficiency might drive cells toward ECM lysosomal degradation.

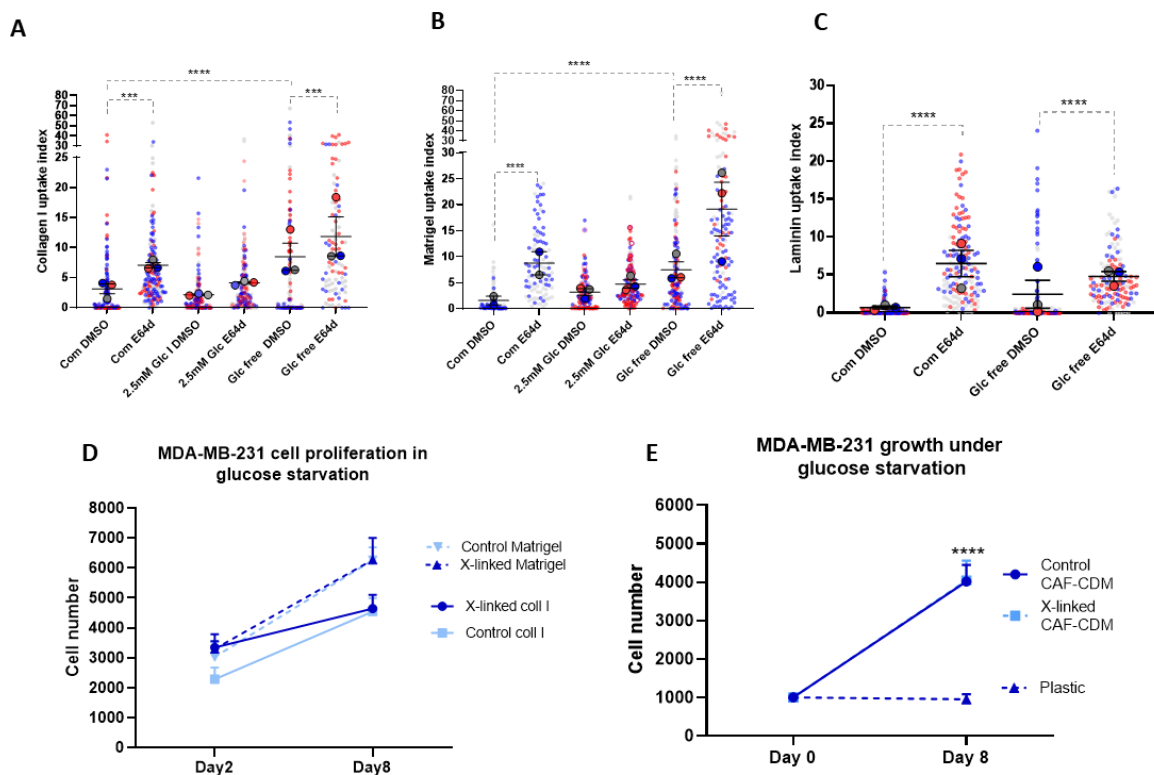


**Figure 6.14. MDA-MB-231 cells internalized and degraded ECMs under glucose starvation condition, but this was not required for cell growth.** MDA-MB-231 cells were plated under 0mM glucose (Glc free), 2.5mM Glc or complete (Com) media on dishes coated with NHS-fluorescein labelled (A) 1mg/ml collagen I, (B) 3mg/ml Matrigel or (C) 3.5mg/ml laminin/entactin for three days, in the presence of the lysosomal inhibitor E64d (20 $\mu$ M) or DMSO (control). Cells were fixed and stained for actin and nuclei. Images were collected by Nikon A1 confocal microscope. MDA-MB-231 cells were seeded on (D) untreated (control) or cross-linked 2mg/ml collagen I or 3mg/ml Matrigel or (E) normal and cross-linked (X-linked) CAF-CDM under Glc starvation. Cell proliferation were measured by Hoechst nuclei staining. Images were collected by ImageXpress micro and analysed by MetaXpress software. Values are mean  $\pm$  SEM and are representative of three independent experiments. Graphs in A, B and C are representative of around 150 cells per condition (the bigger dots represent the mean of individual experiments). \*\*\* $p$ <0.001 \*\*\*\*  $p$ <0.0001 ANOVA test.

We previously showed that mTORC1 activation is required for cell growth, and mTORC1 pathway has been shown to upregulate MMP expression (Chen et al., 2009). Therefore, we wanted to investigate whether extracellular ECM degradation was required for cell growth under Glc starvation. To do this, we treated cells with matrix metalloproteinase inhibitors (GM6001) under complete and Glc depleted media. Our data revealed that inhibition of extracellular degradation of collagen I and Matrigel did not affect cell growth as cell number was similar between control group and cells treated with the broad MMP inhibitor, GM6001, under Glc starvation (Figure 6.15A-C). Taken together, our data suggest that under Glc starvation cell growth was independent of ECM uptake and ECM extracellular degradation.

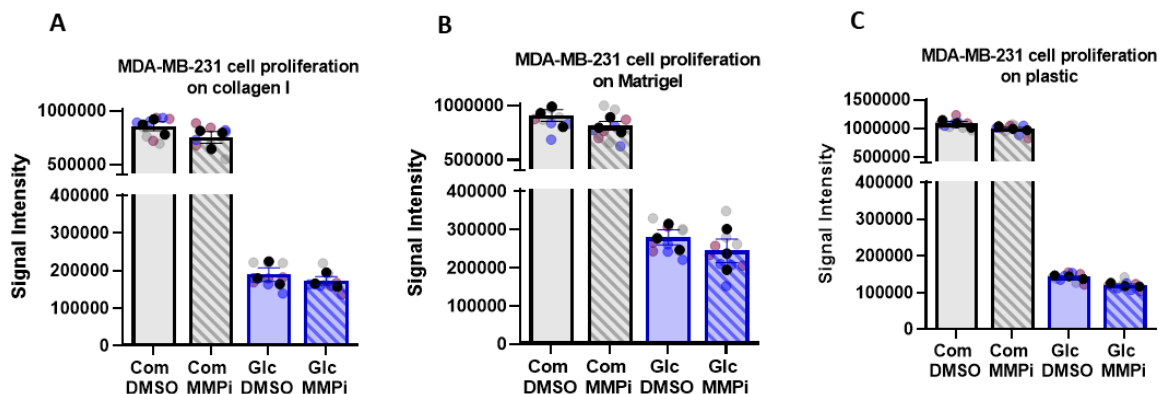


**Figure 6.15. MMP inhibition did not affect cell growth under glucose starvation.** MDA-MB-231 were seeded on (A) 2mg/ml collagen I, (B) 3mg/ml Matrigel, or (C) plastic under complete or Glc depleted media. GM6001 (10 $\mu$ M) or DMSO (control) were added to the cells every two days. Cell proliferation was measured by DRAQ5 nuclear staining quantification with the Licor Odyssey system on day six. Values are mean  $\pm$  SEM and are representative of three independent experiments (the black dots represent the mean of individual experiments).

### 6.2.11 FAK activity was required for cell growth on Matrigel and CDM under glucose starvation.

Our data previously revealed that even though cells can uptake ECM under Glc starvation, ECM internalization was not required for cell growth (Figure 6.14D-E). Therefore, we hypothesized that there might be another mechanism controlling ECM-dependent cell growth under Glc deficiency. FAK is a non-receptor kinase located in the FAs. Recent studies demonstrated that binding of ECM to integrin receptors trigger downstream signalling pathways mediated by FAK to regulate cell proliferation, migration, and survival (Aboubakar Nana et al., 2019). To test whether the inhibition of focal adhesion signalling affected cell growth under Glc starvation, MDA-MB-231 cells were treated with the FAK inhibitor, PF573228. We previously showed that treating cells with PF573228 in complete media did not change their proliferation rate on collagen I or Matrigel (Chp3 figure 6C). Here, our results revealed that treatment of cells with FAK inhibitor significantly reduced cell growth on Matrigel and CAF-CDM, but not on collagen I, under Glc starvation. (Figure 6.16). Taken together, these data suggest that the presence of Matrigel and CAF-CDM triggers FAK-dependent signalling pathways which could promote invasive breast cancer cell growth under Glc starvation.



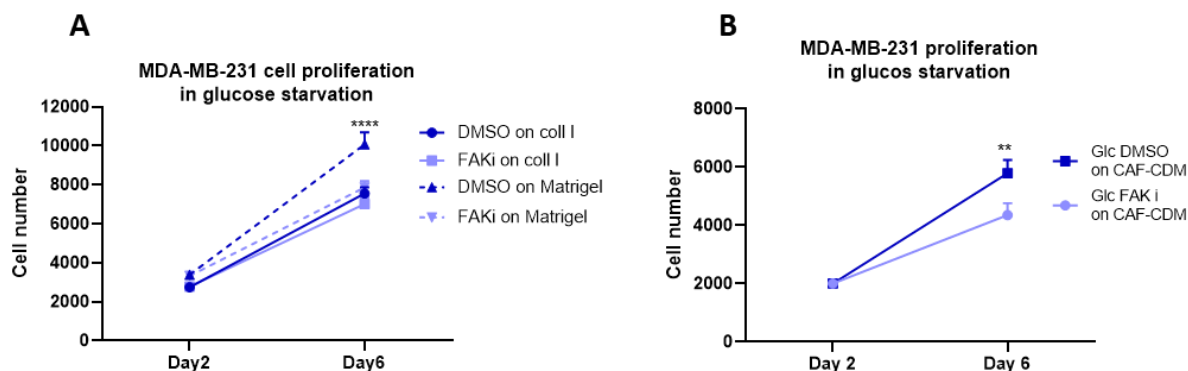


**Figure 6.16. FAK inhibition reduced cell growth on Matrigel and CAF-CDM under glucose starvation.** MDA-MB-231 cells were seeded on either (A) 2mg/ml collagen I, 3mg/ml Matrigel or (B) on CAF-CDM for six days under Glc starvation. Cells were treated with 0.5 $\mu$ M PF573228 (FAKi) or DMSO (control) every two days. Cell proliferation was measured by Hoechst nuclei staining. Images were collected by ImageXpress micro and analysed by MetaXpress software. Values are mean  $\pm$  SEM and are representative of three independent experiments. \*\* $p < 0.01$  and \*\*\*\* $p < 0.0001$  ANOVA test.

### 6.2.12 Cells on plastic internalized more glucose compared to the cells on ECM.

We have shown that the presence of ECMs partially rescued the growth of invasive breast cancer cells under Glc starvation (Figure 6.8). In addition, mTORC1 activity was enhanced by collagen I and Matrigel under starvation (Figure 6.13A-B). ECM proteins are heavily glycosylated, therefore we hypothesised that the ECM could provide an alternative source for sugars. Hence, cells on ECM might take up less Glc when being re-exposed to it after starvation. To investigate this, MDA-MB-231 cells were seeded either on collagen I, Matrigel or plastic, under Glc starvation for six days and treated with 2-NBDG, a fluorescent tracer for Glc, for 1hr. The percentage of cells positive for 2-NBDG was higher under glucose starvation compared to the complete media, regardless of the type of substrate they were growing on (Figure 6.17A and C). Under glucose depleted media, a higher percentage of cells on plastic internalized 2NBDG compared to the cell on collagen I, but not on Matrigel (Figure 6.17A and C). However, the amount of 2-NBDG being accumulated inside the cell was remarkably higher in cells on plastic under Glc deficiency compared to collagen I and Matrigel (Figure 6.17B and D). Altogether, these data suggest that presence of ECM could decrease the dependence of invasive breast cancer cells on Glc, thereby promoting cell growth during starvation.

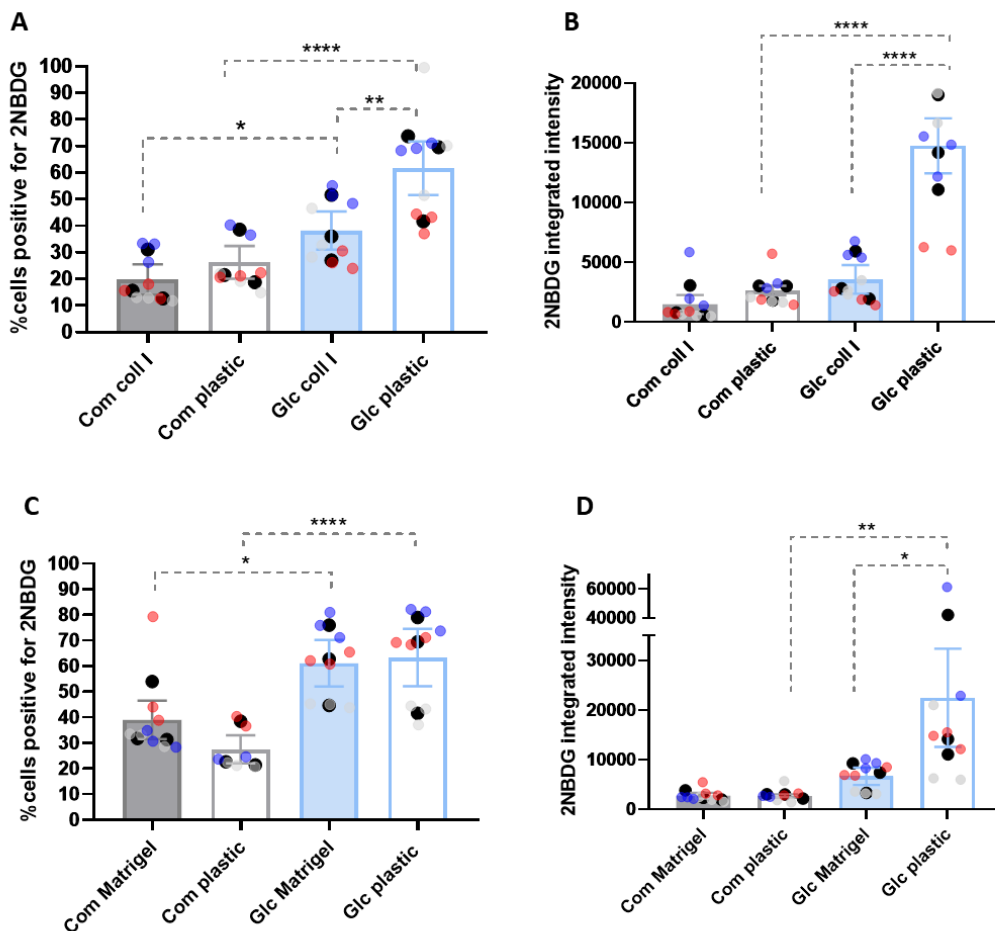


**Figure 6.17. The presence of ECM reduced 2-NBDG uptake under glucose starvation.** MDA-MB-231 cells were plated either on plastic or plastic coated with (A and B) 2mg/ml collagen I or (C and D) 3mg/ml Matrigel under complete media (Com) or glucose starvation (Glc) for six days. Cells were incubated with 100 $\mu$ M 2-NBDG for 1 hr, were fixed and stained for nuclei. Images were collected by ImageXpress micro and analysed by CME software. Values are mean  $\pm$  SEM and are representative of three independent experiments (the black dots represent the mean of individual experiments). \* $p$ <0.05, \*\* $p$ <0.01, \*\*\*\*  $p$ <0.0001 ANOVA test.

### 6.2.13 Cells on Matrigel had higher ATP content under glucose starvation.

Our previous results showed that cells on ECM internalized a lower amount of 2-NBDG under Glc starvation compared to the plastic suggesting that the ECM could compensate for the absence of Glc in the environment (Figure 6.17). We then wanted to investigate whether ECM could facilitate energy production in breast cancer cells and whether the glycolysis/OXPHOS ratio was changed on ECM under starvation. To assess whether the presence of ECM affected ATP content of cells, MDA-MB-231 were seeded either on collagen I, Matrigel or plastic under complete or Glc depleted media. To quantify cellular ATP content, MDA-MB-231 cells were

incubated with bio-tracker ATP-red live cell dye for 15mins, after 1 hr of incubation with the OXPPOS inhibitor Oligomycin A (for further details please check section 4.2.7). ATP content of cells treated with oligomycin A was considered as the product of glycolysis. ATP from OXPPOS was measured by subtracting the ATP content of cells treated with oligomycin A from the ATP content of the control group, as described in Davis et al (2020). Our data showed that three days post Glc starvation, cells on Matrigel had a remarkably higher content of ATP compared to the cells on collagen I and plastic. Cells on Matrigel under complete media and on collagen I under Glc depleted media relied more on glycolysis for their ATP production compared to OXPPOS (Figure 6.18A). However, after six days of starvation, ATP contents of cells were equally the result of glycolysis and TCA cycle. Cells on Matrigel still had higher ATP content under Glc starvation compared to the cells on plastic. In contrast, cells on collagen I under Glc starvation did show a small but not statistically significant increase in their ATP content. Moreover, on day six, cells under Glc starvation on ECMs showed higher ATP content compared to the cells on ECMs under the complete media (Figure 6.18B). Taken together, our data suggest that ECMs induced the accumulation of ATP inside the cells under Glc starvation.

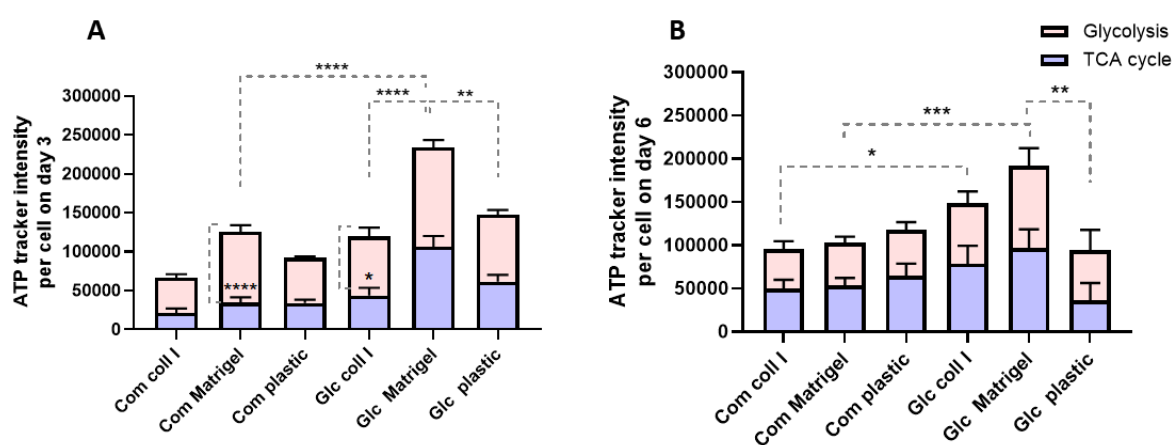


**Figure 6.18. Cells on Matrigel had higher ATP content under starvation.** MDA-MB-231 cells were plated either on plastic or plastic coated with collagen I (2mg/ml) or Matrigel (3mg/ml) under complete media (Com) and glucose starvation (Glc). Cells were incubated with 126.4 $\mu$ M oligomycin A at 37°C and 5% CO<sub>2</sub> for 1 hr at day (A) three or (B) six-day post starvation. Cells were stained with 10 $\mu$ M BioTracker ATP-Red Live Cell Dye at 37°C and 5% CO<sub>2</sub> for 15 min. Live cell images were collected by ImageXpress micro and analysed by CME software. Values are mean  $\pm$  SEM and are representative of three independent experiments. \* $p$ <0.05, \*\* $p$ <0.01, \*\*\*  $p$ <0.001 and \*\*\*\*  $p$ <0.0001 ANOVA test.

### 6.2.14 The presence of Matrigel did not change the metabolite content of cells under glucose starvation.

We previously showed Matrigel rescued cell growth and mTORC1 activation under Glc starvation. Moreover, cells growing on Matrigel had higher ATP content compared to the cells on plastic in the absence of Glc (Figure 6.18). Therefore, in order to highlight changes in metabolite content of cells, we use a non-targeted metabolomic approach in MDA-MB-231 under Glc starvation. Cells were seeded either on Matrigel or plastic for six days in Glc depleted media. Metabolites were collected from the cells and examined via direct infusion mass spectrometry (DI-MS). Our data show that there was no significant difference in metabolite content of cells between plastic and Matrigel under Glc starvation (Figure 6.19).

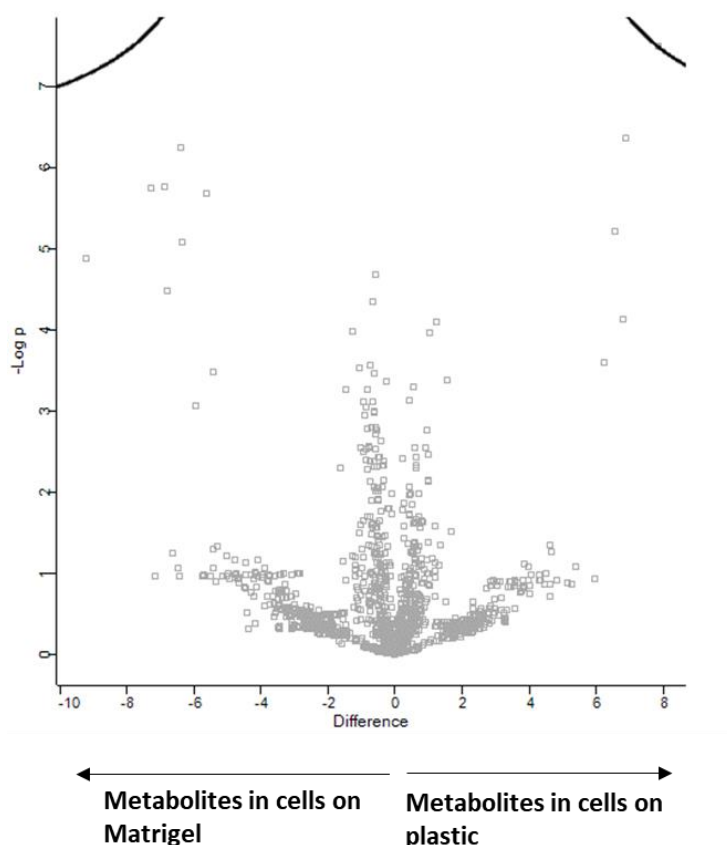


**Figure 6.19. The presence of Matrigel did not affect cellular metabolite content under glucose starvation.** Volcano plot of cells on Matrigel and plastic comparing the fold changes and P value of individual metabolites.

## 6.3 Discussion

### 6.3.1 Serum starvation

In this study we showed TIF-CDM, and to a lesser extent collagen I and CAF-CDM, partially rescued the growth of invasive breast cancer cells, but not normal mammary epithelial cells or non-invasive breast cancer cells, under serum starvation. Moreover, collagen I was the only type of ECM able to support mTORC1 activity in serum-starved cells.

In terms of invasive breast cancer cell growth under serum starvation, MDA-MB-231 cells had a higher growth rate on collagen I compared to the plastic under serum depletion condition, while Matrigel and laminin did not affect the growth at all. We also observed an increase in cell number on both TIF-CDM and CAF-CDM compared to the plastic. However, differences in cell number on CAF-CDM were mostly due to a more profound reduction of cell numbers on plastic, rather than a significant increase of cells growing on CAF-CDM. This suggests that CAF-CDM promoted cell survival, rather than stimulating cell growth. Consistent with our data on plastic, there are studies showing that serum starvation induces apoptosis in cancer cells, including adenocarcinoma and colon carcinoma (Braun et al., 2011, Levin et al., 2010). There was also some evidence that serum starvation could trigger senescence in cells, as a senescence marker, SA- $\beta$ -gal, was shown to be increased after serum depletion (Yurube et al., 2019). Another study demonstrated that addition of albumin to serum depleted cells induced PI3/Akt signalling pathway and inhibited apoptosis (Liu et al., 2012). Consistently, we showed that collagen I could partially rescue the growth of MDA-MB-231 cells under serum starvation. Further work is required to assess whether this is mediated by an inhibition of apoptosis.

Serum is the main source of GFs for the cells growing *in vitro*. Analysing the composition of the FBS we used revealed that it contains IGF-1, TGF- $\beta$ 1 and FGF-2 (<https://static.thermoscientific.com/images/D22225~.pdf>). There is also growing evidence that the ECM works as a GF reservoir. Different types of GFs including FGF, PDGF, TGF- $\beta$  can associate to the ECM via GF binding sites (Hynes, 2009, Zhu and Clark, 2014). Thus, we hypothesize that TIF-CDM could promote cell growth under serum starvation because of the presence of GFs in the matrix. The composition of TIF- and CAF-CDM has been analysed by mass spectrometry (Hernandez-Fernaund et al., 2017), showing that that fibroblast growth

factor 2, Insulin-like growth factor-binding protein 3 and 5 were slightly reduced in CAF-CDM compared to TIF-CDM; whereas some other GFs such as connective tissue growth factor, transforming growth factor beta-2, and insulin-like growth factor-binding protein 7 were upregulated. Therefore, more studies are required to elucidate the reason why TIF-CDM, but not CAF-CDM rescued cell growth and whether this was mediated by presence of specific GFs in TIF-CDM. It is important to note that other factors, such as ECM structure or stiffness, might contribute.

We also assessed the effect of serum starvation on normal mammary epithelial cells and non-invasive breast cancer cells. Our data revealed that serum starvation did not affect the cell number of normal epithelial cells and non-invasive breast cancer cells. While Matrigel partially rescued their growth rate. Consistently, another study showed that laminin internalization rescued normal mammary epithelial cell growth under serum and GF starvation (Muranen et al., 2017). Therefore, it is possible that we observed higher growth on Matrigel compared to collagen I because of the presence of laminin as a Matrigel component. Moreover, our data showed that non-invasive breast cancer cells and normal mammary epithelial cells were less dependent on serum for their growth compared to invasive breast cancer cells. A study showed that the response to the serum starvation is different between adenocarcinoma cells and glioma cells. Under serum starvation, glioma cells stop apoptosis via increasing antiapoptotic proteins such as Bcl2, Bcl-xl and Bax. Glioma cells also decrease p53 expression to hinder p53 dependant apoptosis. In contrast, adenocarcinoma cells under serum starvation increase the level of p53 and decrease the Bcl-xl (Levin et al., 2010). Therefore, differences in response to the serum starvation in our cell lines might be because normal mammary epithelial cells and non-invasive breast cancer cells switch on signalling pathways to promote their survival.

Assessing the rate of cell division showed that the presence of ECM did not increase cell proliferation under serum starvation, indicating that the increase in cell number observed on collagen I was not driven by an induction of cell proliferation. In addition, collagen I was the only ECM that could enhance mTORC1 activity under starvation, suggesting that higher mTORC1 activity might be the reason why collagen I could partially rescue cell growth. It was previously shown that laminin uptake and lysosomal degradation under serum and GF starvation increased the cellular AA content, inducing mTORC1 activity in mammary epithelial

cells (Muranen et al., 2017). However, in our study, we did not detect collagen I lysosomal degradation under serum starvation. In addition, even though cells were able to degrade Matrigel, the presence of Matrigel did not rescue invasive breast cancer cell growth. Therefore, positive effects of collagen I on cell growth might not be linked to collagen I-derived alternative nutrients. It was shown that albumin has an anti-oxidative effect under serum starvation. Presence of albumin inhibits nicotinamide adenine dinucleotide phosphate (NAPDH) oxidase (NOX) activation, ROS generation and eventually hinders mitochondrial apoptosis (Liu et al., 2012). Therefore, more studies are required to define whether collagen I has an anti-apoptotic role in invasive breast cancer cells.

### **6.3.2 Glucose starvation**

In this study we showed that the presence of ECM partially rescued invasive breast cancer cell growth and promoted mTORC1 activation under Glc starvation. Interestingly, non-invasive breast cancer and normal mammary epithelial cells did not grow under Glc starvation regardless of the presence of collagen I or Matrigel. Moreover, ECM internalization was not required for invasive breast cancer cell growth under Glc starvation, while treatment with a FAK inhibitor significantly reduced their growth, suggesting that presence of ECM promoted cell growth through the activation of adhesion signalling under Glc starvation.

A recent study revealed that Glc starvation causes selective turnover of lysosome membrane proteins in MCF10A cells (Lee et al., 2020), suggesting that full depletion of Glc from the media might disrupt lysosome function. This would in turn prevent ECM degradation. However, this was not the case in our study, as we observed a significant increase in the ECM intracellular content upon inhibition of lysosomal proteases under full Glc starvation. In addition, it was shown that extraction of proline from collagen partially rescued the survival of pancreatic cancer cells under low Glc but not in fully Glc depleted media (Olivares et al., 2017). On the contrary, our data clearly demonstrated that in invasive breast cancer cells the ECM had a more profound effect on cell growth under complete Glc starvation, rather than low Glc concentrations. Moreover, we showed that normal mammary epithelial cells were dying under Glc deficiency regardless of the substrate they were growing on, while non-invasive cancer cell growth was partially rescued on Matrigel but not collagen I. As we previously mentioned, non-invasive breast cancer cells reside inside the mammary duct and with direct

contact to the BM (Muschler and Streuli, 2010). Since Matrigel is a BM extract, it could more closely recapitulate the TME surrounding non-invasive breast tumours (Muschler and Streuli, 2010). This indicates that invasive cells can benefit more from the presence of ECM to support their survival under Glc starvation. However, our data demonstrated that there was no difference in invasive breast cancer cell proliferation, measured by EdU incorporation, when comparing ECM and plastic, suggesting that the higher cell number on ECM was not due to higher cell division. Similarly, there was no significant difference in the apoptosis rate of cells under Glc starvation on collagen I, Matrigel or plastic. Our data revealed that the apoptosis rate increased between day three up to day six post starvation, which is consistent with other study showing that Glc starvation induced apoptosis in MDA-MB-231 and MCF7 cells via increasing ROS generation and mitochondria dysfunction (Raut et al., 2019). It is important to note that cells under Glc deficiency can face other types of cell death such as autophagic cell death (Chiodi et al., 2019) or entosis (Hamann et al., 2017), which we did not assess in our study.

Lack of Glc has been shown to affect mTORC1 activity via the activation of AMPK (Kim et al., 2013a). There are conflicting pieces of evidence in the literature regarding the role of ECM internalisation in supporting mTORC1 activation under Glc starvation. It has been shown that the inhibition mTORC1 activation, via complete Glc depletion, induces fibronectin internalization in ovarian cancer cells (Rainero et al., 2015a); while collagen I and IV endocytosis did not affect mTORC1 downstream signalling under Glc free condition in pancreatic cancer cells (Olivares et al., 2017). In our study collagen I, and to a lesser extent Matrigel, induced mTORC1 activity under Glc starvation, suggesting that the role of the ECM in supporting mTORC1 activation could be cancer type specific. It was previously demonstrated that accumulation of AAs inside the lysosome induces a signal transferred to Rag GTPases via the v-ATPase–Ragulator interaction leading to mTORC1 lysosomal recruitment and activation (Zoncu et al., 2011a). In agreement with this, v-ATPase inhibition prevented ECM-dependent mTORC1 activation and cell growth, suggesting that the ECM could promote cell growth under Glc starvation by promoting mTORC1 activity. However, further work is needed to confirm that this is the case. Our data also showed that under Glc starvation cells were able to internalize and degrade the ECM. However, inhibiting ECM internalization did not have any impact on cell growth. These data indicate that cell-ECM



interaction, but not ECM uptake, might promote cell survival under Glc starvation. In parallel, our data showed that inhibition of FAK significantly reduced cell growth on Matrigel and CAF-CDM, but not collagen I. In addition, our data showed that there was no difference in cellular metabolite content between cells growing on Matrigel or plastic. Due to technical difficulties, we could not perform metabolomics on collagen I under Glc starvation. It would be informative to elucidate whether the presence of collagen I resulted in changes in metabolic pathways in the cells under Glc starvation, since we observed higher mTORC1 activity compared to Matrigel. Taken together these data suggest that the ECM mechanism of action to induce survival of cells under Glc starvation is mostly due adhesion-dependent signalling rather than a metabolic effect caused by ECM internalisation and lysosomal degradation, as we reported in the case of AA starvation (chapter 3). It was previously shown that the addition of collagen I and IV to PDAC cells under Glc starvation induced extracellular signal-regulated kinase-1/2 (ERK1/2) signalling pathway to increase the survival rate (Olivares et al., 2017). It has been reported that interaction of  $\beta$ 1 integrin with collagen IV triggers FAK and downstream ERK1/2 signalling via Ras activation. It was also shown that ERK1/2 activation induces invasion in pancreatic cancer cells with no significant effect on apoptosis (Sawai et al., 2005). Therefore, stimulation of ERK1/2 downstream of ECM-dependent FAK activation could be a candidate signalling pathway promoting cell growth/survival under Glc starvation. Thus, further experiments are needed to determine this.

Interestingly, we found that the presence of ECM changed Glc uptake and ATP content of cells under Glc starvation. Our data revealed that the cells growing on collagen I and Matrigel internalize a significantly lower amount of Glc compared to the plastic, when exposed to a Glc tracer after six days of Glc starvation. These data suggest that the presence of ECM might decrease the need of cells to Glc after starvation. It was recently reported that metastatic cancer cells have the ability to switch between different metabolic pathways and can compensate for lack of glycolysis by upregulating glutaminolysis to feed the TCA cycle (Méndez-Lucas et al., 2020). We also showed that cells had higher ATP content on collagen I (slightly) and on Matrigel (significantly) compared to the plastic under Glc starvation, suggesting that they could rely on different metabolic pathways for energy production. It has been shown that macropinocytosis of yeast proteins increased the survival rate of Glc-independent lung cancer cells under serum and Glc deficiency. Degradation of internalized

proteins produced AAs, like alanine, which fed into the TCA cycle and gluconeogenesis via the conversion of alanine to pyruvate. Interestingly, they showed that Glc-dependent lung cancer cells did not have this ability and the addition of soluble proteins did not rescue their growth (Hodakoski et al., 2019). Even though in our study we showed that breast cancer cells did not need ECM internalization to rescue their growth, the presence of ECM might make them glucose-independent and enable them to use AAs in the media to support gluconeogenesis. The fact that our non-targeted metabolomics data did not show any difference suggests that more subtle changes could be behind this, and more detailed analysis are needed. For instance, using <sup>13</sup>C-labeled AA could help us to track the journey of AAs inside the Glc starved cells on plastic and ECM. In addition, it was shown that invasive breast cancer cells are more glycolytic on stiff matrices and glass; while they mainly produce energy via OXPHOS on soft ECMs (Mah et al., 2018). Therefore, one reason why MDA-MB-231 cells produce higher ATP on Matrigel compared to plastic might be mediated by their metabolic shift toward OXPHOS due to changes in the stiffness. However, in our study, we did not see any difference between the level of ATP produced by OXPHOS or glycolysis. More studies are needed to assess the ATP to ADP conversion, as it is possible that higher ATP content is due to lower energy consumption. In addition, on plastic, cells were treated with the OXPHOS inhibitor (Oligomycin A) could still produce ATP under Glc starvation. This result brings this question that how cells with no access to Glc and under Oligomycin A can still produce ATP. To complement these data and assess whether the ECM affects metabolic plasticity, <sup>13</sup>C isotope-assisted methods for Gln tracing could be performed by mass spectrometry. Moreover, using the Seahorse XF technique to measure oxygen consumption rate (OCR) and extracellular acidification rate (ECAR) of live cells on Matrigel and collagen I under Glc starvation could allow us to establish whether different ECM components affect cell metabolism. Taken together, our data suggest that the presence of ECM can direct cells toward a glucose-independent metabolic pathway for energy production, to compensate for lack of Glc.

In conclusion, our data suggest that the presence of ECM can trigger signalling pathways downstream of FAK activation inducing cell survival. Concomitantly, the ECM might promote cancer cell ability to switch to different metabolic pathways independent of glucose. Therefore, further studies are needed to characterise which signalling pathways downstream of FAK induce cell survival on ECM under Glc starvation. This could be followed by assessing

whether these signalling pathways affect cell metabolism either via enhancing mTORC1 activity, activating specific metabolic pathways such as OXPHOS or increasing the transport of other nutrients, like Gln.

## Chapter 7. General discussion

### 7.1 Summary

Using extracellular proteins as a substitute source of food during starvation is a mechanism cancer cells benefit from to survive (Commisso et al., 2013, Muranen et al., 2017, Olivares et al., 2017, Palm et al., 2015). ECMs are a major component of the TME and they are in direct contact with tumour cells. Increased secretion of ECM is linked to higher tumour initiation, adhesion, sprouting, invasiveness, and survival of breast cancer cells (Kim et al., 2014, Yao et al., 2007, Chang et al., 2015). In this study, we investigated the role of ECM components in controlling breast cancer cells growth under different starvation conditions. We demonstrated that the presence of ECM under AA starvation induced cell proliferation, enhanced mTORC1 activity and upregulated AA content of cells, suggesting that cells could extract AA from ECMs to compensate for the AA deficiency. Under serum starvation, only collagen I, TIF-CDM and CAF-CDM could partially rescue cell growth. Presence of collagen I did not increase the division rate but it significantly enhanced mTORC1 activity under serum starvation. TIF-CDM has the strongest effect on cell growth under serum starvation implying that it might provide GFs for serum starved cells. Under Glc starvation, ECMs enhanced mTORC1 activity. However, after an initial increase in cell proliferation after Glc starvation, cell growth was not sustained and at a later point there was no difference in cell division. In addition, there was no substantial difference in the metabolite content of cells on ECM compared to plastic. Interestingly, inhibiting focal adhesion signalling adversely affected the growth on ECM in Glc starved cells. Hence, we hypothesized that under Glc starvation, presence of ECM trigger signalling pathways downstream of FAK to induce cell growth/survival (Figure 7.1).

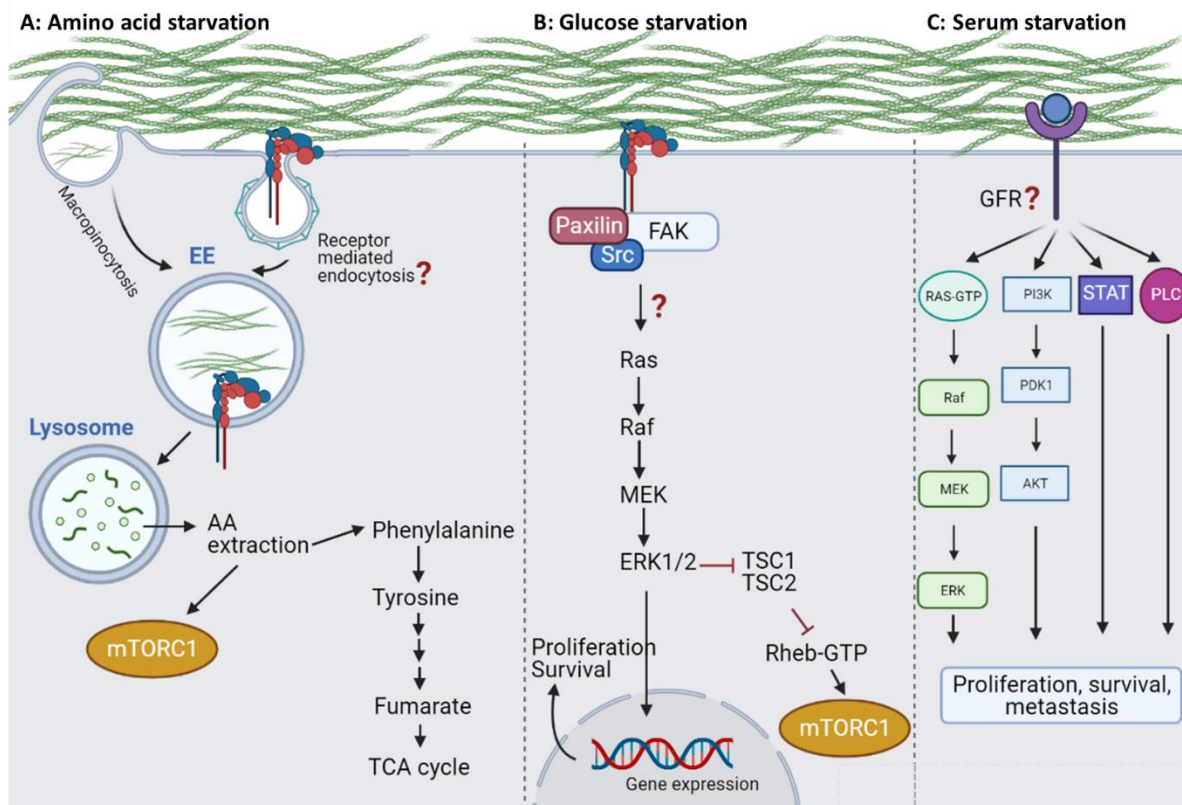


**Figure 7.1. Mechanism of cell ECM interaction under different starvation conditions.** (A) Under AA starvation, invasive breast cancer cells internalize ECM and extract AA via lysosomal degradation. Upregulation AA content enhances phenylalanine and tyrosine metabolism pathway and mTORC1 activity. ECM internalization might happen via macropinocytosis or receptor mediated endocytosis. (B) Under Glc starvation, interaction of ECM with integrin receptors triggers signalling pathways downstream of FAK that result in higher cell growth. (C) Under serum starvation, we propose that cells might use the ECM as a GFs reservoir to induce their growth/survival.

## 7.2 ECMs partially rescued cell growth under different starvation conditions.

Under Gln and AA starvation, the presence of collagen I, Matrigel, laminin and CAF-CDM rescued breast cancer cell growth. Cells on TIF-CDM promoted cell growth under Gln but not AA depleted media. Analysing the rate of cell division via EdU labelling also revealed that the number of MDA-MB-231 cells positive for EdU is significantly higher on ECM compared to the plastic in AA starved cells. Consistently, under NEAA starvation, cells had higher cell growth on Matrigel, collagen I and CAF-CDM compared to the plastic. Under Glc starvation, all types of ECM partially rescued cell growth up to day eight. However, from around day four onwards the graph representative of cell growth on ECM showed plateau on collagen I, Matrigel and laminin (Table 7.1). Cell growth on CDM data was collected on day eight. Therefore, it was not possible to assess whether cell growth ceased after the first four days or not. We could

detect a similar amount of extracellular ECM under all starvation conditions, it is unlikely that cell growth was prevented under Glc deficiency because of lack of ECM. Taken together, our data suggest that under Glc starvation the presence of ECM might be sufficient to enhance invasive breast cancer cell survival, but not their proliferation in the long term. Under serum starvation, only collagen I, TIF-CDM and CAF-CDM enhanced invasive breast cancer cell growth. Among them, TIF-CDM had the greatest effect. However, none of the matrices tested could increase cell division rate. The CDM is composed of many different components. *In vivo* characterization of normal and tumour ECMs revealed that the core matrisome includes around 300 genes. 35 genes for proteoglycans, 43 genes for collagens and the rest are for glycoproteins including fibronectin, laminin, tenascins, thrombospondin. Matrisome-associated proteins include around 778 genes subcategorized to ECM regulators such as MMPs and LOX, and secreted factors including cytokines and GFs (Naba et al., 2012). Therefore, it is important to consider that more than one factor could potentially enhance cell growth under serum starvation on CDM. There is growing evidence that the ECM works as a GF reservoir. Different types of GFs including FGF, PDGF, TGF- $\beta$  can associate to the ECMs via their specific GF binding sites (Hynes, 2009, Zhu and Clark, 2014). In addition, CDMs can show different mechanical properties due to different levels of remodelling and cross-linking, mediated by MMPs and LOX enzymes. Higher ECM stiffness has been linked to the integrin clustering, resulting in activation of FAK and PI3K and eventually breast malignancy (Levental et al., 2009). So far, we can hypothesize that upregulation of signalling pathways linked to cell proliferation, such as PI3K, could promote on CDM either via GFs or CDM-dependent signalling pathways due to their mechanical properties.

**Table 7.1. Effect of different matrices on MDA-MB-231 growth under various starvation conditions.**

Starvations	Collagen I	Matrigel	Laminin	TIF-CDM	CAF-CDM
Amino acid	+	+	+	-	+
Nonessential amino acids	+	+	NA	NA	+
Glutamine	+	+	+	+	+
Glucose	+	+	+	+	+

serum	+	-	-	+	+
-------	---	---	---	---	---

(+) matrix can partially rescue cell growth. (-) no difference in cell growth between matrix and plastic. (NA) it was not tested.

### 7.3 Normal mammary epithelial cells and non-invasive breast cancer cells behaved differently on ECM under different starvation conditions.

To investigate whether the ability to take advantage of the ECM to promote cell growth under starvation is a common feature of mammary epithelial cells or is acquired during carcinoma progression, we examined the growth rate of normal mammary epithelial cells (MCF10A) and non-invasive breast cancer cells (MCF10A-DCIS). Under Glc and AA starvation, the growth rate of MCF10A and MCF10A-DCIS was not changed on collagen I and Matrigel compared to the plastic. Alongside, it has been shown that deprivation of arginine induced cell cycle arrest in both MCF10A cells and MCF7 (invasive breast cancer cells). However, addition of arginine to the media after 5 days of starvation rescued cell growth for invasive breast cancer cells while normal mammary epithelial cells were not responsive to it, as arginine starvation induced irreversible senescence in normal mammary epithelial cells (Chiaviello et al., 2012). In our study, we showed that arginine biosynthesis pathway is upregulated in AA starved invasive breast cancer cells on collagen I compared to the plastic. Since ECM proteins contain arginine, it is possible that invasive breast cancer cells, but not normal mammary epithelial cells, could support their growth under AA deficiency by extracting arginine from internalised ECM components. In contrast, the presence of Matrigel, but not collagen I, was able to rescue MCF10A-DCIS and MCF10A growth under Gln and serum starvation, respectively. Non-invasive breast cancer cells reside inside the mammary duct and in contact with the BM (Muschler and Streuli, 2010). Hence, the reason why cells have better growth on Matrigel under Gln starvation could be because Matrigel more closely recapitulates the BM environment. It has been shown that under 24hrs serum starvation followed by 2hrs AA starvation, laminin supported the growth of MCF10A cells (Muranen et al., 2017). Since Matrigel contains laminin, this could be the reason why MCF10A cells have better growth on Matrigel under serum starvation. Taken together, our data reveal that the ECM did not rescue the growth of non-invasive breast cancer cells and normal mammary epithelial cells under AA and Glc starvation, suggesting that invasive breast cancer cells have acquired the ability to use ECM to overcome nutrient scarcity. Further studies are needed to characterise how this

is developed during carcinoma progression. Our data showing a significantly higher growth rate of non-invasive breast cancer cells on Matrigel under Gln starvation suggest that they achieve this ability on their way to becoming invasive.

#### **7.4 The ECM promoted cell growth via different mechanisms under various starvation conditions.**

Our data demonstrate that the presence of ECM supports cell growth via different mechanisms under different starvation conditions. In general, cells respond to Glc and AA deficiency by activating distinct signalling pathways. Therefore, it is possible that these in turn could determine how cells take advantage of the ECM. Under Glc starvation, liver kinase B1 (LKB1)-adenosine monophosphate-activated kinase (AMPK) signalling plays an important role in sensing nutrient stress and controlling energy homeostasis via different mechanisms. Excessive level of ROS inside the cells triggers LKB1/AMPK to promote cell survival during Glc deficiency via (1) decreasing consumption of NADPH to prevent ROS accumulation (Jeon et al., 2012); (2) activation of p53, which is a cell cycle checkpoint and induces senescence (Jones et al., 2005), or (3) activation of an mTORC1 inhibitor, TSC1/2, leading to reduction of protein translation and induction of autophagy (Corradetti et al., 2004). It was also shown that the activation of LKB1/AMPK induces the expression of Nrf1, a transcription factor resulting in higher expression of MMP-9 and cell invasion (Endo et al., 2018). Future work will determine how the presence of ECM impinges on Glc sensing and whether this in turn affect cell-ECM interaction.

AA deficiency is sensed by the integrated stress response and has been shown to trigger activation of eIF2 $\alpha$ -kinases, such as General Control Non-depressible 2 (GCN2), promoting eukaryotic Initiation Factor 2 $\alpha$  (eIF2 $\alpha$ ). eIF2 $\alpha$  induces the translation of transcription factors, C/EBP-homologous protein (CHOP) and transcription factor 4 (ATF4), responsible for the transcription of different sets of genes controlling autophagy (B'Chir et al., 2013). AA starved cells could also induce autophagy and inhibit anabolic processes via mTORC1 inactivation. AA deficiency causes Rag inactivation, to induce mTORC1 release from lysosome via two independent mechanisms. First, Rag reduces its binding to mTORC1. Second, it recruits TSC2 on the lysosomes, which inhibits Rheb and consequently induces mTORC1 release to the cytoplasm (Demetriades et al., 2014). However, it was shown that cells adopt different



mechanisms for their survival in long-term AA depletion compared to the short-term starvation. Cells able to tolerate long-term AA deficiency did not show any difference in mTORC1 and GCN2/elf2 $\alpha$  activity, compared to cells in which AA starvation induces apoptosis. In contrast, cells with higher tolerance to AA starvation had lower ATF4 activity, which prevents apoptosis (Mesclon et al., 2017). Future work will address whether ATF4 activity is linked to ECM-dependent cell growth under AA starvation and whether the integrated stress response promotes ECM internalisation and/or degradation.

#### **7.4.1 Assessing rate of cell division and apoptosis on different ECMs and starvation conditions.**

Under AA starvation, ECMs enhanced cell division while under Glc and serum starvation the percentage of cells positive for EdU was similar on ECM and plastic. There are few studies showing that ECPs can enhance cell growth under full AA deficiency (Kamphorst et al., 2015), 5% EAA (Palm et al., 2015) or Gln depleted conditions (Olivares et al., 2017). In contrast, in full Glc deficiency cells did not show higher growth in the presence of albumin (Palm et al., 2015) or collagen (Olivares et al., 2017). Those studies were mostly performed adding soluble proteins, while our work uses polymerised ECMs. It is possible that only assembled ECM (and not soluble components) are able to support cell growth under Glc starvation. Therefore, we can hypothesize that the reason why under Glc starvation cells on ECM have higher cell numbers could be due the ECM signalling downstream of the interaction with their plasma membrane receptors.

We examined whether the presence of collagen I and Matrigel can have anti-apoptotic effects. Our data revealed that Glc starvation enhanced apoptosis regardless of the substrate the cells were growing on and cells on ECM did not reduce apoptosis rate. In parallel, another study revealed that Glc starvation induces apoptosis in MDA-MB-231 and MCF7 cells via increasing ROS generation and mitochondria dysfunction (Raut et al., 2019). Taken together, the ECM function to increase cell number under Glc starvation is not an anti-apoptotic mechanism.

Our data demonstrated that CAF-CDM, but not TIF-CDM, supported MDA-MB-231 cell growth under AA starvation, while TIF-CDM had a stronger growth promoting effect under serum starvation. It was previously shown that CAF-CDM is denser with more uniform collagen and

FN fibres compared to TIF-CDM. Mechanically, CAF-CDM is stiffer than TIF-CDM, which could influence cancer cell proliferation. It was demonstrated that TIF-CDM has an anti-proliferation effect on breast cancer cells. Low stiffness of TIF-CDM enhances histone demethylase, JMJD1a, translocation from the nucleus to the cytoplasm. Lack of JMJD1a activity downregulates Yap/Taz transcription resulting in lower proliferation. CAF-CDM, in contrast, does not change Yap/Taz activity and proliferation rate. On CAF-CDM, JMJD1a is localized in the nucleus resulting in Yap/Taz upregulation and proliferation (Kaukonen et al., 2016). In our study, MDA-MB-231 cells under complete media did not show any lower growth rate on TIF-CDM compared to the plastic. However, it has been shown that under nutrient stress such as Glc deficiency, Yap/Taz activity could be inhibited (DeRan et al., 2014). Or, in nutrient limited conditions when AA starved cells just have access to Gln and leucine, Yap/Taz enhanced transcription of leucine transporter results in higher mTORC1 activity and proliferation (Hansen et al., 2015). Therefore, different cell behaviour on TIF-CDM and CAF-CDM in our study could be the result of interplay between mechanosensing and metabolism which needs to be investigated further. A study demonstrated that in higher density collagen, cells rely more on the contribution of Gln to the TCA cycle; whereas, on low density collagen, they mostly use Glc to feed the TCA cycle (Morris et al., 2016). It was also shown that collagen stiffness enhances the shift of breast cancer cells metabolism from OXPHOs to glycolysis (Mah et al., 2018). Taken together, we can hypothesize that the higher growth rate of invasive breast cancer cells on CAF-CDM, but not -TIF-CDM, under AA starvation might be because (1) cells rely on Glc and glycolysis to produce energy and feed the TCA cycle because of the higher stiffness of CAF-CDM, (2) mechanosensing signalling pathways, like Yap/Taz, are upregulated because of the mechanical properties of CAF-CDM, resulting in higher proliferation and/or mTORC1 activity, or (3) cells can internalise and extract AAs more efficiently from CAF-CDM. In contrast, under serum starvation cells had better growth on TIF-CDM compared to CAF-CDM. Since CAF-CDM provides more favourable environment in terms of mechanosensing related signalling pathways resulting in higher proliferation (Kaukonen et al., 2016), we can hypothesize that specific structure/composition of TIF-CDM might make the GFs more available compared to the CAF-CDM. However, further studies are required to find whether that is the reason why serum starved invasive breast cancer cells have better growth rate on TIF-CDM.

#### **7.4.2 Potential mechanisms controlling mTORC1 activity on ECMs under different nutrient conditions.**

Our data showed that under AA starvation collagen I and Matrigel, but not laminin, enhanced mTORC1 activity compared to the plastic. Even though mTORC1 is enhanced on specific ECMs under Glc and AA starvation, all the ECMs promoted cell growth. Thus, mTORC1 activation might not be the only reason for the greater growth rate. A study revealed that under EEA starvation, albumin scavenging can rescue mTORC1 activity via providing AA (Palm et al., 2015). Similarly, we also showed that under AA starvation cells can internalize and degrade collagen I and Matrigel inside the lysosomes, which might provide AAs leading to the activation of mTORC1. Under Glc and serum starvation, however, only the presence of collagen I, but not Matrigel or laminin, could rescue mTORC1 activity. All the tested ECMs were shown to be internalised and degraded in lysosomes in the absence of Glc, suggesting that the mechanism through which collagen I support mTORC1 activation is independent from the generation of nutrients in the lysosomes. Similarly, no collagen I intracellular degradation was observed under serum starvation, suggesting that collagen I-dependent signalling might promote mTORC1 activation.

In addition to lysosomal degradation, there were other variables that could have affected mTORC1 activity. We used different concentrations of the different ECMs (in order to polymerise them correctly), and the matrices might have different stiffnesses and morphologies. Moreover, different ECM components can interact with different receptors. It was previously shown that interaction of stiff ECM with  $\beta 1$  and  $\beta 3$  integrin stabilizes insulin receptors (IR) and results in activation of IR/Akt/mTORC1 pathway. It was also shown that engagement of integrin with stiff ECM reinforces this pathway, via inhibiting IR lysosomal degradation (Bui et al., 2019). It was also demonstrated that inhibition of FAK in mammary tumours results in downregulation of Akt/mTORC1 pathway, inducing apoptosis (Paul et al., 2020). FAK can also activate Ras/Raf/MEK/ERK1/2 pathway, which could enhance mTORC1 activity via TSC1/2 inhibition. Taken together, our data and previous studies suggest that cells might benefit from different mechanisms downstream of cell-ECM interaction to compensate for nutrient starvation and induce mTORC1 activation. In addition, these mechanisms might vary under different starvation conditions. We can hypothesize that under AA starvation cells

might rely on AA extraction while under Glc starvation signalling pathways downstream of integrin-FAK activation might result in enhanced mTORC1 activity (Figure 7.1).

#### **7.4.3 Does the presence of ECM have signalling or metabolic impact?**

It was previously shown that cancer cells rely on scavenging extracellular proteins and extracting AAs from them under starvation to maintain their survival and growth (Olivares et al., 2017, Commisso et al., 2013). We showed that under both AA and Glc depleted media, MDA-MB-231 cells internalize ECM followed by lysosomal degradation. However, inhibition of ECM internalisation opposed cell growth under AA starvation, but not Glc starvation. In addition, FAK inhibition did not affect cell growth under AA starvation on ECMs while it reduced cell growth on Matrigel and CAF-CDM for Glc starved cells. Taken together, since cell growth on ECM was dependent on FAK activation but not ECM uptake under Glc depleted media, we conclude that ECMs partially rescue cell growth via triggering signalling pathways downstream of FAK. It was previously shown that addition of collagen I and IV under Glc starvation enhances ERK1/2 signalling pathway to increase survival rate of cancer cells (Olivares et al., 2017). Interaction of  $\beta 1$  integrin with collagen IV triggers FAK ERK1/2 activation, resulting in higher invasion in pancreatic cancer cells (Sawai et al., 2005). Alongside, in fibroblasts, binding of collagen I, but no FN, to  $\alpha 11$  integrin increases focal adhesion formation, followed by FAK/ERK activation and cell proliferation (Erusappan et al., 2019). Therefore, it is possible that matrix-specific or integrin isoform-specific adhesion signalling promotes cell growth. Thus, further studies are needed to identify which signalling pathways downstream of FAK are being activated in this situation. However, we can hypothesize that binding of the ECM to an integrin receptor might activate ERK1/2 signalling, resulting in higher resistance to Glc starvation in invasive breast cancer cells. It is also important to test whether this solely relies on a signalling pathway downstream integrins located in plasma membrane or there is also a contribution from signalling from endosomes, since we could detect ECM internalization under Glc starvation. It was previously shown that Integrin-ECM located in EEs cause the assembly of FAK-containing signalling complexes on the endosomal surface, resulting in anoikis resistance and cell growth (Alanko et al., 2015, Nader et al., 2016).

The observation that inhibition of ECM internalization adversely affected cells growth under AA depleted media while FAK inhibition did not suggest that that ECM has different mechanisms of action under AA starvation compared to the Glc depletion. In parallel, our non-targeted metabolomic data revealed that the presence of both collagen I and Matrigel significantly changed the cellular metabolite content compared to the plastic in AA starved cells. Cells on both collagen I and Matrigel had higher AA content, suggesting that the ECM supports breast cancer cell growth by providing an alternative source of AA. Several studies showed that scavenging ECPs can upregulate AA content in AA starved cells. It was shown that addition of yeast protein to the cells increases AA content which feeds into TCA cycle and cause lactate, and pyruvate production (Commisso et al., 2013). It was also revealed that addition of albumin to AA starved cancer cells can increase EAAs cellular concentration more than the complete media (Kamphorst et al., 2015). *In vivo* study also observed significantly higher AA extracted from heavy carbon labelled albumin in pancreatic cancer cells compared to adjacent healthy tissue (Davidson et al., 2017).

In this study, we used an RNAi screening approach to identify vesicular trafficking regulators potentially involved in controlling ECM-dependent cell growth under NEAA starvation. We found silencing of three genes, AP3, JIN3 and RIN3, can substantially reduce cell growth under starvation on Matrigel and collagen I. These data suggests that these genes are involved in ECM trafficking and their silencing might result in lack of ECM internalization and/or lysosomal degradation and impede the access of cells to AA from ECMs (Peden et al., 2004, Williamson and Donaldson, 2019, Kajiho et al., 2003). In addition, JIN3 could also be important in Glc starvation due to its role in adhesion signalling (Takino et al., 2002).

### **7.5 Metabolic pathways were enhanced on ECMs in AA starved cells.**

Our non-targeted metabolomic approach showed the upregulation of different metabolic pathways under AA starvation in the presence of ECM, including phenylalanine and tyrosine metabolism. This leads to the production of fumarate, working as TCA cycle intermediate. Our data showed that the downregulation of HPDL, but not HPD, completely opposed ECM-dependent cell growth under AA starvation, suggesting that HPDL might specifically be activated in metabolic pathways downstream of ECM degradation. Further studies are required to find whether HPDL activation is related to the presence of ECM. In addition, it will

be important to confirm that the lack of growth upon HPDL KD is related to phenylalanine and tyrosine metabolism dysfunction, as it was shown that HPDL could also have a role in mitochondria metabolic functions (Ghosh et al., 2020). Interestingly, we found other metabolic pathways potentially being upregulated on ECM compared to the plastic in AA starved cells, including arginine biosynthesis, purine metabolism and valine, leucine, and isoleucine biosynthesis. It was previously shown that lack of arginine in the media causes cell cycle arrest in invasive breast cancer cells which can be reverted by the re-addition of arginine (Chiaviello et al., 2012). Valine, leucine, and isoleucine are all branched chained AAs (BCAAs). BCAAs are upregulated in both plasma and tissue of breast cancer patients. Catabolism of BCAAs in breast cancer cells is mediated by branched-chain AA transaminase 1 (BCAT1). BCAT1 expression is elevated in breast cancer cells and has a role in enhancing mitochondria biogenesis, ATP production and mTORC1 activation, resulting in cell growth and colony formation (Zhang and Han, 2017). In terms of purine metabolism, in hepatocellular carcinoma (HCC) enhanced purine metabolism was shown *in vitro*, in mouse models and patient tissues. Purine metabolism is linked to tumour grade and prognosis while KD of the enzymes participating in this process reduce cell proliferation and tumour burden (Chong et al., 2020). Taken together, upregulation of all these metabolic pathways on ECM could potentially assist cell growth. Further studies are needed to define how the presence of ECM enhances these metabolic pathways and whether it is related to AA starvation or not.

These data raise the possibility that ECM proteins could provide AA for AA starved invasive breast cancer cells to promote cell proliferation and energy production by upregulating metabolic pathways that could also feed TCA cycle. It has been previously shown that the level of nutrients that tumour's cells have access to is different from normal tissues. Cells receive the nutrients via the vasculature that releases the nutrients from the circulating system into the interstitial area of tissues. Nutrient and waste exchange happens between the interstitial fluid (IF) and capillaries and lymph system (Sullivan et al., 2019). However, tumour blood vessels are highly branched, leaky, enlarged with inconsistent blood flow (Nagy et al., 2010, Baluk et al., 2005). Therefore, the nutrient content of the IF is different from the plasma. *In vivo* study of PDAC and lung tumours in mice showed that nutrient composition of IF varies by the tumour location, tissue of origin and diet. The nutrients that tumour cells rely on are mostly depleted in IF compared to the plasma. For instance, in PDAC the amount of

Glc, arginine, tryptophan and cysteine were lower in IF compared to the plasma (Sullivan et al., 2019). Thus, it is essential to know what metabolites cancer cells rely on and whether it is possible to reduce their access to them via changing the diet. However, focusing on the diet alone might not be enough. In our study we showed that even under complete AA depletion, invasive breast cancer cells had higher phenylalanine and tyrosine metabolism on ECM compared to the plastic. It was previously demonstrated that phenylalanine and tyrosine metabolism is higher in invasive breast cancer tissue compared to the non-invasive and normal mammary epithelial cells suggesting that they rely on this metabolic pathway for AA or energy production (More et al., 2018). Taken together, this suggests that even in low AA levels in IF, cancer cells can rely on alternative sources of AA like ECM. Therefore, diet restriction might not be a viable approach to induce tumour starvation. Since it is unlikely that *in vivo* cells are under full Glc or AA starvation, we used diluted Plasmax media to reduce up to 75% the accessibility of all the nutrients compared to the plasma. The presence of ECM partially rescued invasive breast cancer cell growth under diluted Plasmax, suggesting that ECM can promote cell growth under starvation in a more physiological environment as well. However, further studies are needed to determine whether cell growth is ECM internalisation- or signalling dependent. In addition, HPD and HPDL KD on collagen I Under Plasmax (data not shown) showed similar effect as in AA starved cells implying that they might rely on common pathways to compensate their growth. Therefore, in addition to the level of nutrients in IF, plasma, or diet, it is very important to consider accessibility of cells to ECM while metabolic conditions of tumours are assessed.

## 7.6 Conclusion and future directions

Overall, the data presented in this thesis highlights that under different starvation conditions, invasive breast cancer cells can benefit from the presence of ECM. However, the ECM mechanism of action is different depending on the starvation condition. In this thesis we showed that under Glc starvation, cells have higher survival rate on ECM compared to plastic, which might be the result of signalling pathways being triggered downstream of ECM-integrin binding and FAK activation. In contrast, under AA starvation, cells need ECM uptake to enhance their proliferation. We showed that ECM internalization is followed by lysosomal degradation and AA extraction, eventually feeding into the TCA cycle. Several studies revealed

that normal tissue stroma is transformed into a very dense and fibrotic stroma in breast (Kim et al., 2014), lung, pancreatic (Neesse et al., 2015) and colon (Brauchle et al., 2018) tumours, and this correlates with cancer formation and progression. Therefore, the findings of this study could potentially be generalized to other highly fibrotic cancers, although further studies are needed.

This study has raised many questions about the mechanism of cell-ECM interaction under starvation which are interesting for future investigation. Here is a summary of the main questions which could be addressed in the future:

- Elucidate the mechanism through which TIF-CDM partially induces cell growth under serum starvation. Is it because the CDM works as a GF reservoir or does ECM-integrin interaction trigger signalling pathways that induce growth/survival?
- Characterise the signalling pathway(s) downstream of FAK activation under Glc starvation on ECM and define whether this signalling pathway occurs via activation of integrins at plasma membrane or on endosomes.
- Perform phenylalanine and tyrosine metabolic tracing to assess whether they are fed into TCA cycle under AA starvation on ECM.
- Compare activity of phenylalanine and tyrosine metabolism pathway between invasive breast cancer cells and normal mammary epithelial cells.
- Define the molecular mechanisms controlling ECM internalization in AA starved cells.
- Use the Seahorse XF technique to define the metabolic status of cells on different ECM and starvation conditions.
- Expand this study to include different cancer cell lines, to establish whether the ability to use ECM to support cell growth under starvation is a common feature of different cancer types.

This study reinforces the need for a better understanding of the impact of the ECM on breast cancer cell growth/survival under different starvation conditions. It strengthens the idea that during the study of cancer cell metabolism, the effect of the TME and especially the ECM should be considered. I hope the findings in this thesis will be beneficial for developing efficient therapy for cancer patients in the future.



## Chapter 8: References

- ABOUBAKAR NANA, F., LECOCQ, M., LADJEMI, M. Z., DETRY, B., DUPASQUIER, S., FERON, O., MASSION, P. P., SIBILLE, Y., PILETTE, C. & OCAK, S. 2019. Therapeutic Potential of Focal Adhesion Kinase Inhibition in Small Cell Lung Cancer. *Mol Cancer Ther*, 18, 17-27.
- ABU-REMAILEH, M., WYANT, G. A., KIM, C., LAQTOM, N. N., ABBASI, M., CHAN, S. H., FREINKMAN, E. & SABATINI, D. M. 2017. Lysosomal metabolomics reveals V-ATPase- and mTOR-dependent regulation of amino acid efflux from lysosomes. *Science*, 358, 807-813.
- ADAMS, J. M. & CORY, S. 2007. The Bcl-2 apoptotic switch in cancer development and therapy. *Oncogene*, 26, 1324-37.
- AHMADZADEH, M. & ROSENBERG, S. A. 2005. TGF-beta 1 attenuates the acquisition and expression of effector function by tumor antigen-specific human memory CD8 T cells. *J Immunol*, 174, 5215-23.
- AKINS, N. S., NIELSON, T. C. & LE, H. V. 2018. Inhibition of Glycolysis and Glutaminolysis: An Emerging Drug Discovery Approach to Combat Cancer. *Curr Top Med Chem*, 18, 494-504.
- AKRAM, M. 2014. Citric acid cycle and role of its intermediates in metabolism. *Cell Biochem Biophys*, 68, 475-8.
- AL-AWADI, F., YANG, M., TAN, Y., HAN, Q., LI, S. & HOFFMAN, R. M. 2008. Human tumor growth in nude mice is associated with decreased plasma cysteine and homocysteine. *Anticancer Res*, 28, 2541-4.
- ALANKO, J., MAI, A., JACQUEMET, G., SCHAUER, K., KAUKONEN, R., SAARI, M., GOUD, B. & IVASKA, J. 2015. Integrin endosomal signalling suppresses anoikis. *Nat Cell Biol*, 17, 1412-21.
- ANDERS, C. & CAREY, L. A. 2008. Understanding and treating triple-negative breast cancer. *Oncology (Williston Park)*, 22, 1233-9; discussion 1239-40, 1243.
- ANDERSON, N. M., MUCKA, P., KERN, J. G. & FENG, H. 2018. The emerging role and targetability of the TCA cycle in cancer metabolism. *Protein Cell*, 9, 216-237.
- ARMSTRONG, T., PACKHAM, G., MURPHY, L. B., BATEMAN, A. C., CONTI, J. A., FINE, D. R., JOHNSON, C. D., BENYON, R. C. & IREDALE, J. P. 2004. Type I collagen promotes the malignant phenotype of pancreatic ductal adenocarcinoma. *Clin Cancer Res*, 10, 7427-37.
- ARORA, P. D., MANOLSON, M. F., DOWNEY, G. P., SODEK, J. & MCCULLOCH, C. A. 2000. A novel model system for characterization of phagosomal maturation, acidification, and intracellular collagen degradation in fibroblasts. *J Biol Chem*, 275, 35432-41.
- ARORA, P. D., WANG, Y., BRESNICK, A., DAWSON, J., JANMEY, P. A. & MCCULLOCH, C. A. 2013. Collagen remodeling by phagocytosis is determined by collagen substrate topology and calcium-dependent interactions of gelsolin with nonmuscle myosin IIA in cell adhesions. *Mol Biol Cell*, 24, 734-47.
- ARRIBAS, J., BASELGA, J., PEDERSEN, K. & PARRA-PALAU, J. L. 2011. p95HER2 and breast cancer. *Cancer Res*, 71, 1515-9.
- AUMAILLEY, M. 2013. The laminin family. *Cell Adh Migr*, 7, 48-55.
- B'CHIR, W., MAURIN, A. C., CARRARO, V., AVEROUS, J., JOUSSE, C., MURANISHI, Y., PARRY, L., STEPIEN, G., FAFOURNOUX, P. & BRUHAT, A. 2013. The eIF2alpha/ATF4 pathway is essential for stress-induced autophagy gene expression. *Nucleic Acids Res*, 41, 7683-99.
- BADAQUI, M., MIMSY-JULIENNE, C., SABY, C., VAN GULICK, L., PERETTI, M., JEANNESSON, P., MORJANI, H. & OUADID-AHIDOUCH, H. 2018. Collagen type 1 promotes survival of human breast cancer cells by overexpressing Kv10.1 potassium and Orai1 calcium channels through DDR1-dependent pathway. *Oncotarget*, 9, 24653-24671.
- BAE, Y. K., KIM, A., KIM, M. K., CHOI, J. E., KANG, S. H. & LEE, S. J. 2013. Fibronectin expression in carcinoma cells correlates with tumor aggressiveness and poor clinical outcome in patients with invasive breast cancer. *Hum Pathol*, 44, 2028-37.
- BAENKE, F. 2012. *Metabolic dependencies of breast cancer cells*. Ph.D., University College London.

- BALANIS, N., WENDT, M. K., SCHIEMANN, B. J., WANG, Z., SCHIEMANN, W. P. & CARLIN, C. R. 2013. Epithelial to mesenchymal transition promotes breast cancer progression via a fibronectin-dependent STAT3 signaling pathway. *J Biol Chem*, 288, 17954-67.
- BALKWILL, F., CHARLES, K. A. & MANTOVANI, A. 2005. Smoldering and polarized inflammation in the initiation and promotion of malignant disease. *Cancer Cell*, 7, 211-7.
- BALUK, P., HASHIZUME, H. & MCDONALD, D. M. 2005. Cellular abnormalities of blood vessels as targets in cancer. *Curr Opin Genet Dev*, 15, 102-11.
- BARTH, P. J., EBRAHIMSADDE, S., RAMASWAMY, A. & MOLL, R. 2002. CD34+ fibrocytes in invasive ductal carcinoma, ductal carcinoma in situ, and benign breast lesions. *Virchows Arch*, 440, 298-303.
- BARTHEL, A., OKINO, S. T., LIAO, J., NAKATANI, K., LI, J., WHITLOCK, J. P., JR. & ROTH, R. A. 1999. Regulation of GLUT1 gene transcription by the serine/threonine kinase Akt1. *J Biol Chem*, 274, 20281-6.
- BASSET, P., BELLOCQ, J. P., WOLF, C., STOLL, I., HUTIN, P., LIMACHER, J. M., PODHAJECER, O. L., CHENARD, M. P., RIO, M. C. & CHAMBON, P. 1990. A novel metalloproteinase gene specifically expressed in stromal cells of breast carcinomas. *Nature*, 348, 699-704.
- BEGUM, A., EWACHIW, T., JUNG, C., HUANG, A., NORBERG, K. J., MARCHIONNI, L., MCMILLAN, R., PENCHEV, V., RAJESHKUMAR, N. V., MAITRA, A., WOOD, L., WANG, C., WOLFGANG, C., DEJESUS-ACOSTA, A., LAHERU, D., SHAPIRO, I. M., PADVAL, M., PACTER, J. A., WEAVER, D. T., RASHEED, Z. A. & MATSUI, W. 2017. The extracellular matrix and focal adhesion kinase signaling regulate cancer stem cell function in pancreatic ductal adenocarcinoma. *PLoS One*, 12, e0180181.
- BELLA, J., EATON, M., BRODSKY, B. & BERMAN, H. M. 1994. Crystal and molecular structure of a collagen-like peptide at 1.9 Å resolution. *Science*, 266, 75-81.
- BENTON, G., CROOKE, E. & GEORGE, J. 2009. Laminin-1 induces E-cadherin expression in 3-dimensional cultured breast cancer cells by inhibiting DNA methyltransferase 1 and reversing promoter methylation status. *FASEB J*, 23, 3884-95.
- BERGAMASCHI, A., TAGLIABUE, E., SORLIE, T., NAUME, B., TRIULZI, T., ORLANDI, R., RUSSNES, H. G., NESLAND, J. M., TAMMI, R., AUVINEN, P., KOSMA, V. M., MENARD, S. & BORRESEN-DALE, A. L. 2008. Extracellular matrix signature identifies breast cancer subgroups with different clinical outcome. *J Pathol*, 214, 357-67.
- BERGSTROM, J., FURST, P., NOREE, L. O. & VINNARS, E. 1974. Intracellular free amino acid concentration in human muscle tissue. *J Appl Physiol*, 36, 693-7.
- BERTERO, T., OLDHAM, W. M., GRASSET, E. M., BOURGET, I., BOULTER, E., PISANO, S., HOFMAN, P., BELLVERT, F., MENEGUZZI, G., BULAVIN, D. V., ESTRACH, S., FERL, C. C., CHAN, S. Y., BOZEC, A. & GAGGIOLI, C. 2018. Tumor-Stroma Mechanics Coordinate Amino Acid Availability to Sustain Tumor Growth and Malignancy. *Cell Metab*.
- BERTERO, T., OLDHAM, W. M., GRASSET, E. M., BOURGET, I., BOULTER, E., PISANO, S., HOFMAN, P., BELLVERT, F., MENEGUZZI, G., BULAVIN, D. V., ESTRACH, S., FERL, C. C., CHAN, S. Y., BOZEC, A. & GAGGIOLI, C. 2019. Tumor-Stroma Mechanics Coordinate Amino Acid Availability to Sustain Tumor Growth and Malignancy. *Cell Metab*, 29, 124-140 e10.
- BERX, G. & VAN ROY, F. 2009. Involvement of members of the cadherin superfamily in cancer. *Cold Spring Harb Perspect Biol*, 1, a003129.
- BHOWMICK, N. A., NEILSON, E. G. & MOSES, H. L. 2004. Stromal fibroblasts in cancer initiation and progression. *Nature*, 432, 332-7.
- BHUTIA, Y. D. & GANAPATHY, V. 2016. Glutamine transporters in mammalian cells and their functions in physiology and cancer. *Biochim Biophys Acta*, 1863, 2531-9.
- BLASCO, M. A. 2005. Telomeres and human disease: ageing, cancer and beyond. *Nat Rev Genet*, 6, 611-22.
- BLOOM, H. J. & RICHARDSON, W. W. 1957. Histological grading and prognosis in breast cancer; a study of 1409 cases of which 359 have been followed for 15 years. *Br J Cancer*, 11, 359-77.

- BONFILI, L., CECARINI, V., CUCCIOLONI, M., ANGELETTI, M., FLATI, V., CORSETTI, G., PASINI, E., DIOGUARDI, F. S. & ELEUTERI, A. M. 2017. Essential amino acid mixtures drive cancer cells to apoptosis through proteasome inhibition and autophagy activation. *FEBS J*, 284, 1726-1737.
- BOULTER, E., ESTRACH, S., TISSOT, F. S., HENNRICH, M. L., TOSELLO, L., CAILLETEAU, L., DE LA BALLINA, L. R., PISANO, S., GAVIN, A. C. & FERAL, C. C. 2018. Cell metabolism regulates integrin mechanosensing via an SLC3A2-dependent sphingolipid biosynthesis pathway. *Nat Commun*, 9, 4862.
- BOWDITCH, R. D., HARIHARAN, M., TOMINNA, E. F., SMITH, J. W., YAMADA, K. M., GETZOFF, E. D. & GINSBERG, M. H. 1994. Identification of a novel integrin binding site in fibronectin. Differential utilization by beta 3 integrins. *J Biol Chem*, 269, 10856-63.
- BOWMAN, E. J., SIEBERS, A. & ALTENDORF, K. 1988. Bafilomycins: a class of inhibitors of membrane ATPases from microorganisms, animal cells, and plant cells. *Proc Natl Acad Sci U S A*, 85, 7972-6.
- BRAND, K., LEIBOLD, W., LUPPA, P., SCHOERNER, C. & SCHULZ, A. 1986. Metabolic alterations associated with proliferation of mitogen-activated lymphocytes and of lymphoblastoid cell lines: evaluation of glucose and glutamine metabolism. *Immunobiology*, 173, 23-34.
- BRAND, T. M., IIDA, M., DUNN, E. F., LUTHAR, N., KOSTOPOULOS, K. T., CORRIGAN, K. L., WLEKLINSKI, M. J., YANG, D., WISINSKI, K. B., SALGIA, R. & WHEELER, D. L. 2014. Nuclear epidermal growth factor receptor is a functional molecular target in triple-negative breast cancer. *Mol Cancer Ther*, 13, 1356-68.
- BRAUCHLE, E., KASPER, J., DAUM, R., SCHIERBAUM, N., FALCH, C., KIRSCHNIAK, A., SCHAFFER, T. E. & SCHENKE-LAYLAND, K. 2018. Biomechanical and biomolecular characterization of extracellular matrix structures in human colon carcinomas. *Matrix Biol*, 68-69, 180-193.
- BRAUN, F., BERTIN-CIFTCI, J., GALLOUET, A. S., MILLOUR, J. & JUIN, P. 2011. Serum-nutrient starvation induces cell death mediated by Bax and Puma that is counteracted by p21 and unmasked by Bcl-x(L) inhibition. *PLoS One*, 6, e23577.
- BROECKER-PREUSS, M., BECHER-BOVELETH, N., BOCKISCH, A., DUHRSEN, U. & MULLER, S. 2017. Regulation of glucose uptake in lymphoma cell lines by c-MYC- and PI3K-dependent signaling pathways and impact of glycolytic pathways on cell viability. *J Transl Med*, 15, 158.
- BROWN, J. M. 2014. Vasculogenesis: a crucial player in the resistance of solid tumours to radiotherapy. *Br J Radiol*, 87, 20130686.
- BUI, T., RENNHACK, J., MOK, S., LING, C., PEREZ, M., ROCCAMO, J., ANDRECHEK, E. R., MORAES, C. & MULLER, W. J. 2019. Functional Redundancy between beta1 and beta3 Integrin in Activating the IR/Akt/mTORC1 Signaling Axis to Promote ErbB2-Driven Breast Cancer. *Cell Rep*, 29, 589-602 e6.
- BURNS, K. A. & KORACH, K. S. 2012. Estrogen receptors and human disease: an update. *Arch Toxicol*, 86, 1491-504.
- BURRIDGE, K., TURNER, C. E. & ROMER, L. H. 1992. Tyrosine phosphorylation of paxillin and pp125FAK accompanies cell adhesion to extracellular matrix: a role in cytoskeletal assembly. *J Cell Biol*, 119, 893-903.
- CAILLEAU, R., YOUNG, R., OLIVE, M. & REEVES, W. J., JR. 1974. Breast tumor cell lines from pleural effusions. *J Natl Cancer Inst*, 53, 661-74.
- Cancer research UK 2020, Breast Cancer Statistics, viewed on 15 April 2020, <<https://www.cancerresearchuk.org/health-professional/cancer-statistics/statistics-by-cancer-type/breast-cancer/incidence>>
- CARMELIET, P. 2005. VEGF as a key mediator of angiogenesis in cancer. *Oncology*, 69 Suppl 3, 4-10.
- CARPENTER, P. M., DAO, A. V., ARAIN, Z. S., CHANG, M. K., NGUYEN, H. P., ARAIN, S., WANG-RODRIGUEZ, J., KWON, S. Y. & WILCZYNSKI, S. P. 2009. Motility induction in breast carcinoma by mammary epithelial laminin 332 (laminin 5). *Mol Cancer Res*, 7, 462-75.
- CARVAJAL-CARMONA, L. G., ALAM, N. A., POLLARD, P. J., JONES, A. M., BARCLAY, E., WORTHAM, N., PIGNATELLI, M., FREEMAN, A., POMPLUN, S., ELLIS, I., POULSOM, R., EL-BAHRAWY, M. A.,

- BERNEY, D. M. & TOMLINSON, I. P. 2006. Adult leydig cell tumors of the testis caused by germline fumarate hydratase mutations. *J Clin Endocrinol Metab*, 91, 3071-5.
- CAVALLI, L. R., VARELLA-GARCIA, M. & LIANG, B. C. 1997. Diminished tumorigenic phenotype after depletion of mitochondrial DNA. *Cell Growth Differ*, 8, 1189-98.
- CHAFFER, C. L. & WEINBERG, R. A. 2011. A perspective on cancer cell metastasis. *Science*, 331, 1559-64.
- CHANG, C., GOEL, H. L., GAO, H., PURSELL, B., SHULTZ, L. D., GREINER, D. L., INGERPUU, S., PATARROYO, M., CAO, S., LIM, E., MAO, J., MCKEE, K. K., YURCHENCO, P. D. & MERCURIO, A. M. 2015. A laminin 511 matrix is regulated by TAZ and functions as the ligand for the alpha6Bbeta1 integrin to sustain breast cancer stem cells. *Genes Dev*, 29, 1-6.
- CHENG, N., CHYTIL, A., SHYR, Y., JOLY, A. & MOSES, H. L. 2008. Transforming growth factor-beta signaling-deficient fibroblasts enhance hepatocyte growth factor signaling in mammary carcinoma cells to promote scattering and invasion. *Mol Cancer Res*, 6, 1521-33.
- CHEN, J. S., WANG, Q., FU, X. H., HUANG, X. H., CHEN, X. L., CAO, L. Q., CHEN, L. Z., TAN, H. X., LI, W., BI, J. & ZHANG, L. J. 2009. Involvement of PI3K/PTEN/AKT/mTOR pathway in invasion and metastasis in hepatocellular carcinoma: Association with MMP-9. *Hepatol Res*, 39, 177-86.
- CHIAVIELLO, A., PACIELLO, I., VENEZIANI, B. M., PALUMBO, G. & ALOJ, S. M. 2012. Cells derived from normal or cancer breast tissue exhibit different growth properties when deprived of arginine. *Med Oncol*, 29, 2543-51.
- CHIODI, I., PICCO, G., MARTINO, C. & MONDELLO, C. 2019. Cellular response to glutamine and/or glucose deprivation in in vitro transformed human fibroblasts. *Oncol Rep*, 41, 3555-3564.
- CHOI, B. H. & COLOFF, J. L. 2019. The Diverse Functions of Non-Essential Amino Acids in Cancer. *Cancers (Basel)*, 11.
- CHOI, J., CHA, Y. J. & KOO, J. S. 2018. Adipocyte biology in breast cancer: From silent bystander to active facilitator. *Prog Lipid Res*, 69, 11-20.
- CHONG, Y. C., TOH, T. B., CHAN, Z., LIN, Q. X. X., THNG, D. K. H., HOOI, L., DING, Z., SHUEN, T., TOH, H. C., DAN, Y. Y., BONNEY, G. K., ZHOU, L., CHOW, P., WANG, Y., BENOUKRAF, T., CHOW, E. K. & HAN, W. 2020. Targeted Inhibition of Purine Metabolism Is Effective in Suppressing Hepatocellular Carcinoma Progression. *Hepatol Commun*, 4, 1362-1381.
- COLICINO, E. G. & HEHNLY, H. 2018. Regulating a key mitotic regulator, polo-like kinase 1 (PLK1). *Cytoskeleton (Hoboken)*, 75, 481-494.
- COMMISSO, C., DAVIDSON, S. M., SOYDANER-AZELOGLU, R. G., PARKER, S. J., KAMPHORST, J. J., HACKETT, S., GRABOCKA, E., NOFAL, M., DREBIN, J. A., THOMPSON, C. B., RABINOWITZ, J. D., METALLO, C. M., VANDER HEIDEN, M. G. & BAR-SAGI, D. 2013. Macropinocytosis of protein is an amino acid supply route in Ras-transformed cells. *Nature*, 497, 633-7.
- COMMISSO, C., FLINN, R. J. & BAR-SAGI, D. 2014. Determining the macropinocytic index of cells through a quantitative image-based assay. *Nat Protoc*, 9, 182-92.
- CONG, L. N., CHEN, H., LI, Y., ZHOU, L., MCGIBBON, M. A., TAYLOR, S. I. & QUON, M. J. 1997. Physiological role of Akt in insulin-stimulated translocation of GLUT4 in transfected rat adipose cells. *Mol Endocrinol*, 11, 1881-90.
- COOPMAN, P. J., THOMAS, D. M., GEHLSSEN, K. R. & MUELLER, S. C. 1996. Integrin alpha 3 beta 1 participates in the phagocytosis of extracellular matrix molecules by human breast cancer cells. *Mol Biol Cell*, 7, 1789-804.
- CORRADETTI, M. N., INOKI, K., BARDEESY, N., DEPINHO, R. A. & GUAN, K. L. 2004. Regulation of the TSC pathway by LKB1: evidence of a molecular link between tuberous sclerosis complex and Peutz-Jeghers syndrome. *Genes Dev*, 18, 1533-8.
- COUGHLIN, S. S. 2019. Epidemiology of Breast Cancer in Women. *Adv Exp Med Biol*, 1152, 9-29.
- COX, T. R., BIRD, D., BAKER, A. M., BARKER, H. E., HO, M. W., LANG, G. & ERLER, J. T. 2013. LOX-mediated collagen crosslinking is responsible for fibrosis-enhanced metastasis. *Cancer Res*, 73, 1721-32.

- CRAWFORD, Y., KASMAN, I., YU, L., ZHONG, C., WU, X., MODRUSAN, Z., KAMINKER, J. & FERRARA, N. 2009. PDGF-C mediates the angiogenic and tumorigenic properties of fibroblasts associated with tumors refractory to anti-VEGF treatment. *Cancer Cell*, 15, 21-34.
- CURTIS, M., KENNY, H. A., ASHCROFT, B., MUKHERJEE, A., JOHNSON, A., ZHANG, Y., HELOU, Y., BATLLE, R., LIU, X., GUTIERREZ, N., GAO, X., YAMADA, S. D., LASTRA, R., MONTAG, A., AHSAN, N., LOCASALE, J. W., SALOMON, A. R., NEBREDA, A. R. & LENGYEL, E. 2019. Fibroblasts Mobilize Tumor Cell Glycogen to Promote Proliferation and Metastasis. *Cell Metab*, 29, 141-155 e9.
- CURTO, M., COLE, B. K., LALLEMAND, D., LIU, C. H. & MCCLATCHEY, A. I. 2007. Contact-dependent inhibition of EGFR signaling by Nf2/Merlin. *J Cell Biol*, 177, 893-903.
- DAVIDSON, S. M., JONAS, O., KEIBLER, M. A., HOU, H. W., LUENGO, A., MAYERS, J. R., WYCKOFF, J., DEL ROSARIO, A. M., WHITMAN, M., CHIN, C. R., CONDON, K. J., LAMMERS, A., KELLERSBERGER, K. A., STALL, B. K., STEPHANOPOULOS, G., BAR-SAGI, D., HAN, J., RABINOWITZ, J. D., CIMA, M. J., LANGER, R. & VANDER HEIDEN, M. G. 2017. Direct evidence for cancer-cell-autonomous extracellular protein catabolism in pancreatic tumors. *Nat Med*, 23, 235-241.
- DAVIS, R. T., BLAKE, K., MA, D., GABRA, M. B. I., HERNANDEZ, G. A., PHUNG, A. T., YANG, Y., MAURER, D., LEFEBVRE, A., ALSHETAIWI, H., XIAO, Z., LIU, J., LOCASALE, J. W., DIGMAN, M. A., MJOLSNESS, E., KONG, M., WERB, Z. & LAWSON, D. A. 2020. Transcriptional diversity and bioenergetic shift in human breast cancer metastasis revealed by single-cell RNA sequencing. *Nat Cell Biol*, 22, 310-320.
- DAWSON, P. J., WOLMAN, S. R., TAIT, L., HEPNER, G. H. & MILLER, F. R. 1996. MCF10AT: a model for the evolution of cancer from proliferative breast disease. *Am J Pathol*, 148, 313-9.
- DE FRANCESCHI, N., HAMIDI, H., ALANKO, J., SAHGAL, P. & IVASKA, J. 2015. Integrin traffic - the update. *J Cell Sci*, 128, 839-52.
- DEBERARDINIS, R. J., MANCUSO, A., DAIKHIN, E., NISSIM, I., YUDKOFF, M., WEHRLI, S. & THOMPSON, C. B. 2007. Beyond aerobic glycolysis: transformed cells can engage in glutamine metabolism that exceeds the requirement for protein and nucleotide synthesis. *Proc Natl Acad Sci U S A*, 104, 19345-50.
- DELL'ANGELICA, E. C., SHOTELERSUK, V., AGUILAR, R. C., GAHL, W. A. & BONIFACINO, J. S. 1999. Altered trafficking of lysosomal proteins in Hermansky-Pudlak syndrome due to mutations in the beta 3A subunit of the AP-3 adaptor. *Mol Cell*, 3, 11-21.
- DEMAS, D. M., DEMO, S., FALLAH, Y., CLARKE, R., NEPHEW, K. P., ALTHOUSE, S., SANDUSKY, G., HE, W. & SHAJAHAN-HAQ, A. N. 2019. Glutamine Metabolism Drives Growth in Advanced Hormone Receptor Positive Breast Cancer. *Front Oncol*, 9, 686.
- DEMETRIADES, C., DOUMPAS, N. & TELEMANN, A. A. 2014. Regulation of TORC1 in response to amino acid starvation via lysosomal recruitment of TSC2. *Cell*, 156, 786-99.
- DENARDO, D. G., ANDREU, P. & COUSSENS, L. M. 2010. Interactions between lymphocytes and myeloid cells regulate pro- versus anti-tumor immunity. *Cancer Metastasis Rev*, 29, 309-16.
- DENT, R., TRUDEAU, M., PRITCHARD, K. I., HANNA, W. M., KAHN, H. K., SAWKA, C. A., LICKLEY, L. A., RAWLINSON, E., SUN, P. & NAROD, S. A. 2007. Triple-negative breast cancer: clinical features and patterns of recurrence. *Clin Cancer Res*, 13, 4429-34.
- DERAN, M., YANG, J., SHEN, C. H., PETERS, E. C., FITAMANT, J., CHAN, P., HSIEH, M., ZHU, S., ASARA, J. M., ZHENG, B., BARDEESY, N., LIU, J. & WU, X. 2014. Energy stress regulates hippo-YAP signaling involving AMPK-mediated regulation of angiomin-like 1 protein. *Cell Rep*, 9, 495-503.
- DESGROSELLIER, J. S., BARNES, L. A., SHIELDS, D. J., HUANG, M., LAU, S. K., PREVOST, N., TARIN, D., SHATTIL, S. J. & CHERESH, D. A. 2009. An integrin alpha(v)beta(3)-c-Src oncogenic unit promotes anchorage-independence and tumor progression. *Nat Med*, 15, 1163-9.

- DI SALVO, M. L., CONTESTABILE, R., PAIARDINI, A. & MARAS, B. 2013. Glycine consumption and mitochondrial serine hydroxymethyltransferase in cancer cells: the heme connection. *Med Hypotheses*, 80, 633-6.
- DORNIER, E., RABAS, N., MITCHELL, L., NOVO, D., DHAYADE, S., MARCO, S., MACKAY, G., SUMPTON, D., PALLARES, M., NIXON, C., BLYTH, K., MACPHERSON, I. R., RAINERO, E. & NORMAN, J. C. 2017. Glutaminolysis drives membrane trafficking to promote invasiveness of breast cancer cells. *Nat Commun*, 8, 2255.
- DOZYNKIEWICZ, M. A., JAMIESON, N. B., MACPHERSON, I., GRINDLAY, J., VAN DEN BERGHE, P. V., VON THUN, A., MORTON, J. P., GOURLEY, C., TIMPSON, P., NIXON, C., MCKAY, C. J., CARTER, R., STRACHAN, D., ANDERSON, K., SANSOM, O. J., CASWELL, P. T. & NORMAN, J. C. 2012. Rab25 and CLIC3 collaborate to promote integrin recycling from late endosomes/lysosomes and drive cancer progression. *Dev Cell*, 22, 131-45.
- DRAKE, M. T., ZHU, Y. & KORNFELD, S. 2000. The assembly of AP-3 adaptor complex-containing clathrin-coated vesicles on synthetic liposomes. *Mol Biol Cell*, 11, 3723-36.
- DURBEEJ, M. 2010. Laminins. *Cell Tissue Res*, 339, 259-68.
- DUTTA, D. & DONALDSON, J. G. 2012. Search for inhibitors of endocytosis: Intended specificity and unintended consequences. *Cell Logist*, 2, 203-208.
- EAGLE, H. 1955. The minimum vitamin requirements of the L and HeLa cells in tissue culture, the production of specific vitamin deficiencies, and their cure. *J Exp Med*, 102, 595-600.
- EDINGER, A. L. 2007. Controlling cell growth and survival through regulated nutrient transporter expression. *Biochem J*, 406, 1-12.
- ELIA, I., BROEKAERT, D., CHRISTEN, S., BOON, R., RADAELLI, E., ORTH, M. F., VERFAILLIE, C., GRUNEWALD, T. G. P. & FENDT, S. M. 2017. Proline metabolism supports metastasis formation and could be inhibited to selectively target metastasizing cancer cells. *Nat Commun*, 8, 15267.
- ELIYATKIN, N., YALCIN, E., ZENGEL, B., AKTAS, S. & VARDAR, E. 2015. Molecular Classification of Breast Carcinoma: From Traditional, Old-Fashioned Way to A New Age, and A New Way. *J Breast Health*, 11, 59-66.
- ELMORE, S. 2007. Apoptosis: a review of programmed cell death. *Toxicol Pathol*, 35, 495-516.
- ENDO, H., OWADA, S., INAGAKI, Y., SHIDA, Y. & TATEMACHI, M. 2018. Glucose starvation induces LKB1-AMPK-mediated MMP-9 expression in cancer cells. *Sci Rep*, 8, 10122.
- ERDOGAN, B., AO, M., WHITE, L. M., MEANS, A. L., BREWER, B. M., YANG, L., WASHINGTON, M. K., SHI, C., FRANCO, O. E., WEAVER, A. M., HAYWARD, S. W., LI, D. & WEBB, D. J. 2017. Cancer-associated fibroblasts promote directional cancer cell migration by aligning fibronectin. *J Cell Biol*, 216, 3799-3816.
- ERUSAPPAN, P., ALAM, J., LU, N., ZELTZ, C. & GULLBERG, D. 2019. Integrin alpha11 cytoplasmic tail is required for FAK activation to initiate 3D cell invasion and ERK-mediated cell proliferation. *Sci Rep*, 9, 15283.
- EVERTS, V., HEMBRY, R. M., REYNOLDS, J. J. & BEERTSEN, W. 1989. Metalloproteinases are not involved in the phagocytosis of collagen fibrils by fibroblasts. *Matrix*, 9, 266-76.
- FANG, M., YUAN, J., PENG, C. & LI, Y. 2014. Collagen as a double-edged sword in tumor progression. *Tumour Biol*, 35, 2871-82.
- FARMER, P., BONNEFOI, H., BECETTE, V., TUBIANA-HULIN, M., FUMOLEAU, P., LARSIMONT, D., MACGROGAN, G., BERGH, J., CAMERON, D., GOLDSTEIN, D., DUSS, S., NICOU LAZ, A. L., BRISKEN, C., FICHE, M., DELORENZI, M. & IGGO, R. 2005. Identification of molecular apocrine breast tumours by microarray analysis. *Oncogene*, 24, 4660-71.
- FEARON, K. C., FALCONER, J. S., SLATER, C., MCMILLAN, D. C., ROSS, J. A. & PRESTON, T. 1998. Albumin synthesis rates are not decreased in hypoalbuminemic cachectic cancer patients with an ongoing acute-phase protein response. *Ann Surg*, 227, 249-54.
- FEIG, C., JONES, J. O., KRAMAN, M., WELLS, R. J., DEONARINE, A., CHAN, D. S., CONNELL, C. M., ROBERTS, E. W., ZHAO, Q., CABALLERO, O. L., TEICHMANN, S. A., JANOWITZ, T., JODRELL, D.

- I., TUVESON, D. A. & FEARON, D. T. 2013. Targeting CXCL12 from FAP-expressing carcinoma-associated fibroblasts synergizes with anti-PD-L1 immunotherapy in pancreatic cancer. *Proc Natl Acad Sci U S A*, 110, 20212-7.
- FERNANDEZ-GARCIA, B., EIRO, N., MARIN, L., GONZALEZ-REYES, S., GONZALEZ, L. O., LAMELAS, M. L. & VIZOSO, F. J. 2014. Expression and prognostic significance of fibronectin and matrix metalloproteases in breast cancer metastasis. *Histopathology*, 64, 512-22.
- FORGAC, M. 2007. Vacuolar ATPases: rotary proton pumps in physiology and pathophysiology. *Nat Rev Mol Cell Biol*, 8, 917-29.
- FORSTER, J. C., HARRISS-PHILLIPS, W. M., DOUGLASS, M. J. & BEZAK, E. 2017. A review of the development of tumor vasculature and its effects on the tumor microenvironment. *Hypoxia (Auckl)*, 5, 21-32.
- GALLUZZI, L. & KROEMER, G. 2008. Necroptosis: a specialized pathway of programmed necrosis. *Cell*, 135, 1161-3.
- GALLUZZI, L., VITALE, I., AARONSON, S. A., ABRAMS, J. M., ADAM, D., AGOSTINIS, P., ALNEMRI, E. S., ALTUCCI, L., AMELIO, I., ANDREWS, D. W., ANNICCHIARICO-PETRUZZELLI, M., ANTONOV, A. V., ARAMA, E., BAEHRECKE, E. H., BARLEV, N. A., BAZAN, N. G., BERNASSOLA, F., BERTRAND, M. J. M., BIANCHI, K., BLAGOSKLONNY, M. V., BLOMGREN, K., BORNER, C., BOYA, P., BRENNER, C., CAMPANELLA, M., CANDI, E., CARMONA-GUTIERREZ, D., CECCONI, F., CHAN, F. K., CHANDEL, N. S., CHENG, E. H., CHIPUK, J. E., CIDLOWSKI, J. A., CIECHANOVER, A., COHEN, G. M., CONRAD, M., CUBILLOS-RUIZ, J. R., CZABOTAR, P. E., D'ANGIOLELLA, V., DAWSON, T. M., DAWSON, V. L., DE LAURENZI, V., DE MARIA, R., DEBATIN, K. M., DEBERARDINIS, R. J., DESHMUKH, M., DI DANIELE, N., DI VIRGILIO, F., DIXIT, V. M., DIXON, S. J., DUCKETT, C. S., DYNLACHT, B. D., EL-DEIRY, W. S., ELROD, J. W., FIMIA, G. M., FULDA, S., GARCIA-SAEZ, A. J., GARG, A. D., GARRIDO, C., GAVATHIOTIS, E., GOLSTEIN, P., GOTTLIEB, E., GREEN, D. R., GREENE, L. A., GRONEMEYER, H., GROSS, A., HAJNOCZKY, G., HARDWICK, J. M., HARRIS, I. S., HENGARTNER, M. O., HETZ, C., ICHIJO, H., JAATTELA, M., JOSEPH, B., JOST, P. J., JUIN, P. P., KAISER, W. J., KARIN, M., KAUFMANN, T., KEPP, O., KIMCHI, A., KITSIS, R. N., KLIONSKY, D. J., KNIGHT, R. A., KUMAR, S., LEE, S. W., LEMASTERS, J. J., LEVINE, B., LINKERMANN, A., LIPTON, S. A., LOCKSHIN, R. A., LOPEZ-OTIN, C., LOWE, S. W., LUEDDE, T., LUGLI, E., MACFARLANE, M., MADEO, F., MALEWICZ, M., MALORNI, W., MANIC, G., et al. 2018. Molecular mechanisms of cell death: recommendations of the Nomenclature Committee on Cell Death 2018. *Cell Death Differ*, 25, 486-541.
- GAO, P., TCHERNYSHYOV, I., CHANG, T. C., LEE, Y. S., KITA, K., OCHI, T., ZELLER, K. I., DE MARZO, A. M., VAN EYK, J. E., MENDELL, J. T. & DANG, C. V. 2009. c-Myc suppression of miR-23a/b enhances mitochondrial glutaminase expression and glutamine metabolism. *Nature*, 458, 762-5.
- GECK, R. C. & TOKER, A. 2016. Nonessential amino acid metabolism in breast cancer. *Adv Biol Regul*, 62, 11-17.
- GELSE, K., POSCHL, E. & AIGNER, T. 2003. Collagens--structure, function, and biosynthesis. *Adv Drug Deliv Rev*, 55, 1531-46.
- GEORGIADOU, M., LILJA, J., JACQUEMET, G., GUZMAN, C., RAFAEVA, M., ALIBERT, C., YAN, Y., SAHGAL, P., LERCHE, M., MANNEVILLE, J. B., MAKELA, T. P. & IVASKA, J. 2017. AMPK negatively regulates tensin-dependent integrin activity. *J Cell Biol*, 216, 1107-1121.
- GHOSH, S. G., LEE, S., FABUNAN, R., CHAI, G., ZAKI, M. S., ABDEL-SALAM, G., SULTAN, T., BEN-OMRAN, T., ALVI, J. R., MCEVOY-VENNERI, J., STANLEY, V., PATEL, A., ROSS, D., DING, J., JAIN, M., PAN, D., LUBBERT, P., KAMMERER, B., WIEDEMANN, N., VERHOEVEN-DUIF, N. M., JANS, J. J., MURPHY, D., TOOSI, M. B., ASHRAFZADEH, F., IMANNEZHAD, S., KARIMIYANI, E. G., IBRAHIM, K., WATERS, E. R., MAROOFIAN, R. & GLEESON, J. G. 2020. Biallelic variants in HPDL, encoding 4-hydroxyphenylpyruvate dioxygenase-like protein, lead to an infantile neurodegenerative condition. *Genet Med*.

- GILMORE, A. P., METCALFE, A. D., ROMER, L. H. & STREULI, C. H. 2000. Integrin-mediated survival signals regulate the apoptotic function of Bax through its conformation and subcellular localization. *J Cell Biol*, 149, 431-46.
- GIOVANNELLI, P., DI DONATO, M., GALASSO, G., DI ZAZZO, E., BILANCIO, A. & MIGLIACCIO, A. 2018. The Androgen Receptor in Breast Cancer. *Front Endocrinol (Lausanne)*, 9, 492.
- GOTTLIEB, E. & TOMLINSON, I. P. 2005. Mitochondrial tumour suppressors: a genetic and biochemical update. *Nat Rev Cancer*, 5, 857-66.
- GRASHOFF, C., HOFFMAN, B. D., BRENNER, M. D., ZHOU, R., PARSONS, M., YANG, M. T., MCLEAN, M. A., SLIGAR, S. G., CHEN, C. S., HA, T. & SCHWARTZ, M. A. 2010. Measuring mechanical tension across vinculin reveals regulation of focal adhesion dynamics. *Nature*, 466, 263-6.
- GRASSIAN, A. R., COLOFF, J. L. & BRUGGE, J. S. 2011. Extracellular matrix regulation of metabolism and implications for tumorigenesis. *Cold Spring Harb Symp Quant Biol*, 76, 313-24.
- GRIVENNIKOV, S. I., GRETEN, F. R. & KARIN, M. 2010. Immunity, inflammation, and cancer. *Cell*, 140, 883-99.
- GU, Z., NOSS, E. H., HSU, V. W. & BRENNER, M. B. 2011. Integrins traffic rapidly via circular dorsal ruffles and macropinocytosis during stimulated cell migration. *J Cell Biol*, 193, 61-70.
- GUO, L., CUI, C., ZHANG, K., WANG, J., WANG, Y., LU, Y., CHEN, K., YUAN, J., XIAO, G., TANG, B., SUN, Y. & WU, C. 2019. Kindlin-2 links mechano-environment to proline synthesis and tumor growth. *Nat Commun*, 10, 845.
- HAGIWARA, A., NISHIYAMA, M. & ISHIZAKI, S. 2012. Branched-chain amino acids prevent insulin-induced hepatic tumor cell proliferation by inducing apoptosis through mTORC1 and mTORC2-dependent mechanisms. *J Cell Physiol*, 227, 2097-105.
- HAMANN, J. C., SURCEL, A., CHEN, R., TERAGAWA, C., ALBECK, J. G., ROBINSON, D. N. & OVERHOLTZER, M. 2017. Entosis Is Induced by Glucose Starvation. *Cell Rep*, 20, 201-210.
- HAN, S., LI, Y. Y. & CHAN, B. P. 2015. Protease inhibitors enhance extracellular collagen fibril deposition in human mesenchymal stem cells. *Stem Cell Res Ther*, 6, 197.
- HANAHAHAN, D. & COUSSENS, L. M. 2012. Accessories to the crime: functions of cells recruited to the tumor microenvironment. *Cancer Cell*, 21, 309-22.
- HANAHAHAN, D. & WEINBERG, R. A. 2011. Hallmarks of cancer: the next generation. *Cell*, 144, 646-74.
- HANLEY, C. J., NOBLE, F., WARD, M., BULLOCK, M., DRIFKA, C., MELLONE, M., MANOUSOPOULOU, A., JOHNSTON, H. E., HAYDEN, A., THIRDBOROUGH, S., LIU, Y., SMITH, D. M., MELLOWS, T., KAO, W. J., GARBIS, S. D., MIRNEZAMI, A., UNDERWOOD, T. J., ELICEIRI, K. W. & THOMAS, G. J. 2016. A subset of myofibroblastic cancer-associated fibroblasts regulate collagen fiber elongation, which is prognostic in multiple cancers. *Oncotarget*, 7, 6159-74.
- HANSEN, C. G., NG, Y. L., LAM, W. L., PLOUFFE, S. W. & GUAN, K. L. 2015. The Hippo pathway effectors YAP and TAZ promote cell growth by modulating amino acid signaling to mTORC1. *Cell Res*, 25, 1299-313.
- HARDIE, D. G., ROSS, F. A. & HAWLEY, S. A. 2012. AMPK: a nutrient and energy sensor that maintains energy homeostasis. *Nat Rev Mol Cell Biol*, 13, 251-62.
- HAYASHI, K., JUTABHA, P., ENDOU, H. & ANZAI, N. 2012. c-Myc is crucial for the expression of LAT1 in MIA Paca-2 human pancreatic cancer cells. *Oncol Rep*, 28, 862-6.
- HERNANDEZ-FERNAUD, J. R., RUENGELER, E., CASAZZA, A., NEILSON, L. J., PULLEINE, E., SANTI, A., ISMAIL, S., LILLA, S., DHAYADE, S., MACPHERSON, I. R., MCNEISH, I., ENNIS, D., ALI, H., KUGERATSKI, F. G., AL KHAMICI, H., VAN DEN BIGGELAAR, M., VAN DEN BERGHE, P. V., CLOIX, C., MCDONALD, L., MILLAN, D., HOYLE, A., KUCHNIO, A., CARMELIET, P., VALENZUELA, S. M., BLYTH, K., YIN, H., MAZZONE, M., NORMAN, J. C. & ZANIVAN, S. 2017. Secreted CLIC3 drives cancer progression through its glutathione-dependent oxidoreductase activity. *Nat Commun*, 8, 14206.
- HIDA, K., AKIYAMA, K., OHGA, N., MAISHI, N. & HIDA, Y. 2013. Tumour endothelial cells acquire drug resistance in a tumour microenvironment. *J Biochem*, 153, 243-9.



- HODAKOSKI, C., HOPKINS, B. D., ZHANG, G., SU, T., CHENG, Z., MORRIS, R., RHEE, K. Y., GONCALVES, M. D. & CANTLEY, L. C. 2019. Rac-Mediated Macropinocytosis of Extracellular Protein Promotes Glucose Independence in Non-Small Cell Lung Cancer. *Cancers (Basel)*, 11.
- HOLTRICH, U., WOLF, G., BRAUNINGER, A., KARN, T., BOHME, B., RUBSAMEN-WAIGMANN, H. & STREBHARDT, K. 1994. Induction and down-regulation of PLK, a human serine/threonine kinase expressed in proliferating cells and tumors. *Proc Natl Acad Sci U S A*, 91, 1736-40.
- HONG, H., ZHOU, T., FANG, S., JIA, M., XU, Z., DAI, Z., LI, C., LI, S., LI, L., ZHANG, T., QI, W., BARDEESI, A. S., YANG, Z., CAI, W., YANG, X. & GAO, G. 2014. Pigment epithelium-derived factor (PEDF) inhibits breast cancer metastasis by down-regulating fibronectin. *Breast Cancer Res Treat*, 148, 61-72.
- HUDIS, C. A. 2007. Trastuzumab--mechanism of action and use in clinical practice. *N Engl J Med*, 357, 39-51.
- HUMPHRIES, J. D., BYRON, A. & HUMPHRIES, M. J. 2006. Integrin ligands at a glance. *J Cell Sci*, 119, 3901-3.
- HYNES, R. O. 2009. The extracellular matrix: not just pretty fibrils. *Science*, 326, 1216-9.
- INOKI, K., KIM, J. & GUAN, K. L. 2012. AMPK and mTOR in cellular energy homeostasis and drug targets. *Annu Rev Pharmacol Toxicol*, 52, 381-400.
- INSUA-RODRIGUEZ, J. & OSKARSSON, T. 2016. The extracellular matrix in breast cancer. *Adv Drug Deliv Rev*, 97, 41-55.
- IPPOLITO, L., MORANDI, A., TADDEI, M. L., PARRI, M., COMITO, G., ISCARO, A., RASPOLINI, M. R., MAGHERINI, F., RAPIZZI, E., MASQUELIER, J., MUCCIOLI, G. G., SONVEAUX, P., CHIARUGI, P. & GIANNONI, E. 2019. Cancer-associated fibroblasts promote prostate cancer malignancy via metabolic rewiring and mitochondrial transfer. *Oncogene*, 38, 5339-5355.
- ITKONEN, H. M., MINNER, S., GULDVIK, I. J., SANDMANN, M. J., TSOURLAKIS, M. C., BERGE, V., SVINDLAND, A., SCHLOMM, T. & MILLS, I. G. 2013. O-GlcNAc transferase integrates metabolic pathways to regulate the stability of c-MYC in human prostate cancer cells. *Cancer Res*, 73, 5277-87.
- IWANO, M., PLIETH, D., DANOFF, T. M., XUE, C., OKADA, H. & NEILSON, E. G. 2002. Evidence that fibroblasts derive from epithelium during tissue fibrosis. *J Clin Invest*, 110, 341-50.
- IWASAWA, S., YANAGI, K., KIKUCHI, A., KOBAYASHI, Y., HAGINOYA, K., MATSUMOTO, H., KUROSAWA, K., OCHIAI, M., SAKAI, Y., FUJITA, A., MIYAKE, N., NIIHORI, T., SHIROTA, M., FUNAYAMA, R., NONOYAMA, S., OHGA, S., KAWAME, H., NAKAYAMA, K., AOKI, Y., MATSUMOTO, N., KANAME, T., MATSUBARA, Y., SHOJI, W. & KURE, S. 2019. Recurrent de novo MAPK8IP3 variants cause neurological phenotypes. *Ann Neurol*, 85, 927-933.
- JACKSON, S. P. & BARTEK, J. 2009. The DNA-damage response in human biology and disease. *Nature*, 461, 1071-8.
- JAIN, M., NILSSON, R., SHARMA, S., MADHUSUDHAN, N., KITAMI, T., SOUZA, A. L., KAFRI, R., KIRSCHNER, M. W., CLISH, C. B. & MOOTHA, V. K. 2012. Metabolite profiling identifies a key role for glycine in rapid cancer cell proliferation. *Science*, 336, 1040-4.
- JEON, S. M., CHANDEL, N. S. & HAY, N. 2012. AMPK regulates NADPH homeostasis to promote tumour cell survival during energy stress. *Nature*, 485, 661-5.
- JESCHKE, J., O'HAGAN, H. M., ZHANG, W., VATAPALLI, R., CALMON, M. F., DANILOVA, L., NELKENBRECHER, C., VAN NESTE, L., BIJSMANS, I. T., VAN ENGELAND, M., GABRIELSON, E., SCHUEBEL, K. E., WINTERPACHT, A., BAYLIN, S. B., HERMAN, J. G. & AHUJA, N. 2013. Frequent inactivation of cysteine dioxygenase type 1 contributes to survival of breast cancer cells and resistance to anthracyclines. *Clin Cancer Res*, 19, 3201-11.
- JEWELL, J. L., KIM, Y. C., RUSSELL, R. C., YU, F. X., PARK, H. W., PLOUFFE, S. W., TAGLIABRACCI, V. S. & GUAN, K. L. 2015. Metabolism. Differential regulation of mTORC1 by leucine and glutamine. *Science*, 347, 194-8.

- JIANG, P., DU, W., WANG, X., MANCUSO, A., GAO, X., WU, M. & YANG, X. 2011. p53 regulates biosynthesis through direct inactivation of glucose-6-phosphate dehydrogenase. *Nat Cell Biol*, 13, 310-6.
- JING, Z., HENG, W., AIPING, D., YAFEI, Q. & SHULAN, Z. 2013. Expression and clinical significance of phosphoglycerate dehydrogenase and squamous cell carcinoma antigen in cervical cancer. *Int J Gynecol Cancer*, 23, 1465-9.
- JONES, C. L., STEVENS, B. M., D'ALESSANDRO, A., REISZ, J. A., CULP-HILL, R., NEMKOV, T., PEI, S., KHAN, N., ADANE, B., YE, H., KRUG, A., REINHOLD, D., SMITH, C., DEGREGORI, J., POLLYEA, D. A. & JORDAN, C. T. 2018. Inhibition of Amino Acid Metabolism Selectively Targets Human Leukemia Stem Cells. *Cancer Cell*, 34, 724-740 e4.
- JONES, R. G., PLAS, D. R., KUBEK, S., BUZZAI, M., MU, J., XU, Y., BIRNBAUM, M. J. & THOMPSON, C. B. 2005. AMP-activated protein kinase induces a p53-dependent metabolic checkpoint. *Mol Cell*, 18, 283-93.
- JOTZU, C., ALT, E., WELTE, G., LI, J., HENNESSY, B. T., DEVARAJAN, E., KRISHNAPPA, S., PINILLA, S., DROLL, L. & SONG, Y. H. 2010. Adipose tissue-derived stem cells differentiate into carcinoma-associated fibroblast-like cells under the influence of tumor-derived factors. *Anal Cell Pathol (Amst)*, 33, 61-79.
- JUNG, Y., KIM, J. K., SHIOZAWA, Y., WANG, J., MISHRA, A., JOSEPH, J., BERRY, J. E., MCGEE, S., LEE, E., SUN, H., WANG, J., JIN, T., ZHANG, H., DAI, J., KREBSBACH, P. H., KELLER, E. T., PIENTA, K. J. & TAICHMAN, R. S. 2013. Recruitment of mesenchymal stem cells into prostate tumours promotes metastasis. *Nat Commun*, 4, 1795.
- JUNTTILA, M. R. & EVAN, G. I. 2009. p53--a Jack of all trades but master of none. *Nat Rev Cancer*, 9, 821-9.
- KAJIHO, H., SAITO, K., TSUJITA, K., KONTANI, K., ARAKI, Y., KUROSU, H. & KATADA, T. 2003. RIN3: a novel Rab5 GEF interacting with amphiphysin II involved in the early endocytic pathway. *J Cell Sci*, 116, 4159-68.
- KALLURI, R. 2016. The biology and function of fibroblasts in cancer. *Nat Rev Cancer*, 16, 582-98.
- KALLURI, R. & ZEISBERG, M. 2006. Fibroblasts in cancer. *Nat Rev Cancer*, 6, 392-401.
- KAMPHORST, J. J., NOFAL, M., COMMISSO, C., HACKETT, S. R., LU, W., GRABOCKA, E., VANDER HEIDEN, M. G., MILLER, G., DREBIN, J. A., BAR-SAGI, D., THOMPSON, C. B. & RABINOWITZ, J. D. 2015. Human pancreatic cancer tumors are nutrient poor and tumor cells actively scavenge extracellular protein. *Cancer Res*, 75, 544-53.
- KAPLAN, R. N., RIBA, R. D., ZACHAROULIS, S., BRAMLEY, A. H., VINCENT, L., COSTA, C., MACDONALD, D. D., JIN, D. K., SHIDO, K., KERNS, S. A., ZHU, Z., HICKLIN, D., WU, Y., PORT, J. L., ALTORKI, N., PORT, E. R., RUGGERO, D., SHMELKOV, S. V., JENSEN, K. K., RAFII, S. & LYDEN, D. 2005. VEGFR1-positive haematopoietic bone marrow progenitors initiate the pre-metastatic niche. *Nature*, 438, 820-7.
- KAUKONEN, R., JACQUEMET, G., HAMIDI, H. & IVASKA, J. 2017. Cell-derived matrices for studying cell proliferation and directional migration in a complex 3D microenvironment. *Nat Protoc*, 12, 2376-2390.
- KAUKONEN, R., MAI, A., GEORGIADOU, M., SAARI, M., DE FRANCESCHI, N., BETZ, T., SIHTO, H., VENTELA, S., ELO, L., JOKITALO, E., WESTERMARCK, J., KELLOKUMPU-LEHTINEN, P. L., JOENSUU, H., GRENMAN, R. & IVASKA, J. 2016. Normal stroma suppresses cancer cell proliferation via mechanosensitive regulation of JMJD1a-mediated transcription. *Nat Commun*, 7, 12237.
- KAUPPILA, S., STENBACK, F., RISTELI, J., JUKKOLA, A. & RISTELI, L. 1998. Aberrant type I and type III collagen gene expression in human breast cancer in vivo. *J Pathol*, 186, 262-8.
- KAUSHIK, S., PICKUP, M. W. & WEAVER, V. M. 2016. From transformation to metastasis: deconstructing the extracellular matrix in breast cancer. *Cancer Metastasis Rev*, 35, 655-667.

- KELLERMANN, M. G., SOBRAL, L. M., DA SILVA, S. D., ZECCHIN, K. G., GRANER, E., LOPES, M. A., NISHIMOTO, I., KOWALSKI, L. P. & COLETTA, R. D. 2007. Myofibroblasts in the stroma of oral squamous cell carcinoma are associated with poor prognosis. *Histopathology*, 51, 849-53.
- KESSENBROCK, K., PLAKS, V. & WERB, Z. 2010. Matrix metalloproteinases: regulators of the tumor microenvironment. *Cell*, 141, 52-67.
- KIM, R., EMI, M. & TANABE, K. 2007. Cancer immunoediting from immune surveillance to immune escape. *Immunology*, 121, 1-14.
- KIM, S. G., BUEL, G. R. & BLENIS, J. 2013a. Nutrient regulation of the mTOR complex 1 signaling pathway. *Mol Cells*, 35, 463-73.
- KIM, S. G., HOFFMAN, G. R., POULOGIANNIS, G., BUEL, G. R., JANG, Y. J., LEE, K. W., KIM, B. Y., ERIKSON, R. L., CANTLEY, L. C., CHOO, A. Y. & BLENIS, J. 2013b. Metabolic stress controls mTORC1 lysosomal localization and dimerization by regulating the TTT-RUVBL1/2 complex. *Mol Cell*, 49, 172-85.
- KIM, S. H., LEE, H. Y., JUNG, S. P., KIM, S., LEE, J. E., NAM, S. J. & BAE, J. W. 2014. Role of secreted type I collagen derived from stromal cells in two breast cancer cell lines. *Oncol Lett*, 8, 507-512.
- KIM, S. M., NGUYEN, T. T., RAVI, A., KUBINIOK, P., FINICLE, B. T., JAYASHANKAR, V., MALACRIDA, L., HOU, J., ROBERTSON, J., GAO, D., CHERNOFF, J., DIGMAN, M. A., POTMA, E. O., TROMBERG, B. J., THIBAUT, P. & EDINGER, A. L. 2018. PTEN Deficiency and AMPK Activation Promote Nutrient Scavenging and Anabolism in Prostate Cancer Cells. *Cancer Discov*, 8, 866-883.
- KLOTZSCH, E., SMITH, M. L., KUBOW, K. E., MUNTWYLER, S., LITTLE, W. C., BEYELER, F., GOURDON, D., NELSON, B. J. & VOGEL, V. 2009. Fibronectin forms the most extensible biological fibers displaying switchable force-exposed cryptic binding sites. *Proc Natl Acad Sci U S A*, 106, 18267-72.
- KO, Y. H., PEDERSEN, P. L. & GESCHWIND, J. F. 2001. Glucose catabolism in the rabbit VX2 tumor model for liver cancer: characterization and targeting hexokinase. *Cancer Lett*, 173, 83-91.
- KOROLCHUK, V. I., SAIKI, S., LICHTENBERG, M., SIDDIQI, F. H., ROBERTS, E. A., IMARISIO, S., JAHREISS, L., SARKAR, S., FUTTER, M., MENZIES, F. M., O'KANE, C. J., DERETIC, V. & RUBINSZTEIN, D. C. 2011. Lysosomal positioning coordinates cellular nutrient responses. *Nat Cell Biol*, 13, 453-60.
- KOZIN, S. V., KAMOUN, W. S., HUANG, Y., DAWSON, M. R., JAIN, R. K. & DUDA, D. G. 2010. Recruitment of myeloid but not endothelial precursor cells facilitates tumor regrowth after local irradiation. *Cancer Res*, 70, 5679-85.
- KWIATKOWSKA, E., WOJTALA, M., GAJEWSKA, A., SOSZYNSKI, M., BARTOSZ, G. & SADOWSKA-BARTOSZ, I. 2016. Effect of 3-bromopyruvate acid on the redox equilibrium in non-invasive MCF-7 and invasive MDA-MB-231 breast cancer cells. *J Bioenerg Biomembr*, 48, 23-32.
- KWON, S. Y., CHAE, S. W., WILCZYNSKI, S. P., ARAIN, A., CARPENTER & PHILIP, M. 2012. Laminin 332 expression in breast carcinoma. *Appl Immunohistochem Mol Morphol*, 20, 159-64.
- LABUSCHAGNE, C. F., VAN DEN BROEK, N. J., MACKAY, G. M., VOUSDEN, K. H. & MADDOCKS, O. D. 2014. Serine, but not glycine, supports one-carbon metabolism and proliferation of cancer cells. *Cell Rep*, 7, 1248-58.
- LACEY, J. M. & WILMORE, D. W. 1990. Is glutamine a conditionally essential amino acid? *Nutr Rev*, 48, 297-309.
- LAI, J. Y. & MA, D. H. 2013. Glutaraldehyde cross-linking of amniotic membranes affects their nanofibrous structures and limbal epithelial cell culture characteristics. *Int J Nanomedicine*, 8, 4157-68.
- LE BORGNE, R., ALCONADA, A., BAUER, U. & HOFACK, B. 1998. The mammalian AP-3 adaptor-like complex mediates the intracellular transport of lysosomal membrane glycoproteins. *J Biol Chem*, 273, 29451-61.
- LEE, B. Y., TIMPSON, P., HORVATH, L. G. & DALY, R. J. 2015. FAK signaling in human cancer as a target for therapeutics. *Pharmacol Ther*, 146, 132-49.

- LEE, C., LAMECH, L., JOHNS, E. & OVERHOLTZER, M. 2020. Selective Lysosome Membrane Turnover Is Induced by Nutrient Starvation. *Dev Cell*, 55, 289-297 e4.
- LEE, S. W., ZHANG, Y., JUNG, M., CRUZ, N., ALAS, B. & COMMISSO, C. 2019. EGFR-Pak Signaling Selectively Regulates Glutamine Deprivation-Induced Macropinocytosis. *Dev Cell*, 50, 381-392 e5.
- LEFRANCOIS, S., JANVIER, K., BOEHM, M., OOI, C. E. & BONIFACINO, J. S. 2004. An ear-core interaction regulates the recruitment of the AP-3 complex to membranes. *Dev Cell*, 7, 619-25.
- LEONOUDAKIS, D., HUANG, G., AKHAVAN, A., FATA, J. E., SINGH, M., GRAY, J. W. & MUSCHLER, J. L. 2014. Endocytic trafficking of laminin is controlled by dystroglycan and is disrupted in cancers. *J Cell Sci*, 127, 4894-903.
- LEVENTAL, K. R., YU, H., KASS, L., LAKINS, J. N., EGEHLAD, M., ERLER, J. T., FONG, S. F., CSISZAR, K., GIACCIA, A., WENINGER, W., YAMAUCHI, M., GASSER, D. L. & WEAVER, V. M. 2009. Matrix crosslinking forces tumor progression by enhancing integrin signaling. *Cell*, 139, 891-906.
- LEVIN, V. A., PANCHABHAI, S. C., SHEN, L., KORNBLOU, S. M., QIU, Y. & BAGGERLY, K. A. 2010. Different changes in protein and phosphoprotein levels result from serum starvation of high-grade glioma and adenocarcinoma cell lines. *J Proteome Res*, 9, 179-91.
- LIU, G. Y. & SABATINI, D. M. 2020. mTOR at the nexus of nutrition, growth, ageing and disease. *Nat Rev Mol Cell Biol*, 21, 183-203.
- LIU, J., GUO, S., LI, Q., YANG, L., XIA, Z., ZHANG, L., HUANG, Z. & ZHANG, N. 2013. Phosphoglycerate dehydrogenase induces glioma cells proliferation and invasion by stabilizing forkhead box M1. *J Neurooncol*, 111, 245-55.
- LIU, S. Y., CHEN, C. L., YANG, T. T., HUANG, W. C., HSIEH, C. Y., SHEN, W. J., TSAI, T. T., SHIEH, C. C. & LIN, C. F. 2012. Albumin prevents reactive oxygen species-induced mitochondrial damage, autophagy, and apoptosis during serum starvation. *Apoptosis*, 17, 1156-69.
- LIU, T., HAN, C., WANG, S., FANG, P., MA, Z., XU, L. & YIN, R. 2019. Cancer-associated fibroblasts: an emerging target of anti-cancer immunotherapy. *J Hematol Oncol*, 12, 86.
- LIVERANI, C., MERCATALI, L., CRISTOFOLINI, L., GIORDANO, E., MINARDI, S., PORTA, G. D., DE VITA, A., MISEROCCHI, G., SPADAZZI, C., TASCIOTTI, E., AMADORI, D. & IBRAHIM, T. 2017. Investigating the Mechanobiology of Cancer Cell-ECM Interaction Through Collagen-Based 3D Scaffolds. *Cell Mol Bioeng*, 10, 223-234.
- LOBERT, V. H., BRECH, A., PEDERSEN, N. M., WESCHE, J., OPPELT, A., MALEROD, L. & STENMARK, H. 2010. Ubiquitination of alpha 5 beta 1 integrin controls fibroblast migration through lysosomal degradation of fibronectin-integrin complexes. *Dev Cell*, 19, 148-59.
- LOCASALE, J. W., GRASSIAN, A. R., MELMAN, T., LYSSIOTIS, C. A., MATTAINI, K. R., BASS, A. J., HEFFRON, G., METALLO, C. M., MURANEN, T., SHARFI, H., SASAKI, A. T., ANASTASIOU, D., MULLARKY, E., VOKES, N. I., SASAKI, M., BEROUKHIM, R., STEPHANOPOULOS, G., LIGON, A. H., MEYERSON, M., RICHARDSON, A. L., CHIN, L., WAGNER, G., ASARA, J. M., BRUGGE, J. S., CANTLEY, L. C. & VANDER HEIDEN, M. G. 2011. Phosphoglycerate dehydrogenase diverts glycolytic flux and contributes to oncogenesis. *Nat Genet*, 43, 869-74.
- LOWE, S. W., CEPERO, E. & EVAN, G. 2004. Intrinsic tumour suppression. *Nature*, 432, 307-15.
- LU, P., TAKAI, K., WEAVER, V. M. & WERB, Z. 2011. Extracellular matrix degradation and remodeling in development and disease. *Cold Spring Harb Perspect Biol*, 3.
- LU, P., WEAVER, V. M. & WERB, Z. 2012. The extracellular matrix: a dynamic niche in cancer progression. *J Cell Biol*, 196, 395-406.
- MADSEN, D. H., INGVARSEN, S., JURGENSEN, H. J., MELANDER, M. C., KJOLLER, L., MOYER, A., HONORE, C., MADSEN, C. A., GARRED, P., BURGDORF, S., BUGGE, T. H., BEHRENDT, N. & ENGELHOLM, L. H. 2011. The non-phagocytic route of collagen uptake: a distinct degradation pathway. *J Biol Chem*, 286, 26996-7010.
- MADSEN, D. H., LEONARD, D., MASEDUNSKAS, A., MOYER, A., JURGENSEN, H. J., PETERS, D. E., AMORNPHIMOLTHAM, P., SELVARAJ, A., YAMADA, S. S., BRENNER, D. A., BURGDORF, S.,

- ENGELHOLM, L. H., BEHRENDT, N., HOLMBECK, K., WEIGERT, R. & BUGGE, T. H. 2013. M2-like macrophages are responsible for collagen degradation through a mannose receptor-mediated pathway. *J Cell Biol*, 202, 951-66.
- MAH, E. J., LEFEBVRE, A., MCGAHEY, G. E., YEE, A. F. & DIGMAN, M. A. 2018. Collagen density modulates triple-negative breast cancer cell metabolism through adhesion-mediated contractility. *Sci Rep*, 8, 17094.
- MALINDA, K. M., WYSOCKI, A. B., KOBLINSKI, J. E., KLEINMAN, H. K. & PONCE, M. L. 2008. Angiogenic laminin-derived peptides stimulate wound healing. *Int J Biochem Cell Biol*, 40, 2771-80.
- MAMAN, S. & WITZ, I. P. 2018. A history of exploring cancer in context. *Nat Rev Cancer*, 18, 359-376.
- MARCHESIN, V., CASTRO-CASTRO, A., LODILLINSKY, C., CASTAGNINO, A., CYRTA, J., BONSANG-KITZIS, H., FUHRMANN, L., IRONDELLE, M., INFANTE, E., MONTAGNAC, G., REYAL, F., VINCENT-SALOMON, A. & CHAVRIER, P. 2015. ARF6-JIP3/4 regulate endosomal tubules for MT1-MMP exocytosis in cancer invasion. *J Cell Biol*, 211, 339-58.
- MARTINEZ-CARRERES, L., NASRALLAH, A. & FAJAS, L. 2017. Cancer: Linking Powerhouses to Suicidal Bags. *Front Oncol*, 7, 204.
- MATHEW, R., KARANTZA-WADSWORTH, V. & WHITE, E. 2007. Role of autophagy in cancer. *Nat Rev Cancer*, 7, 961-7.
- MAZIVEYI, M. & ALAHARI, S. K. 2017. Cell matrix adhesions in cancer: The proteins that form the glue. *Oncotarget*, 8, 48471-48487.
- MCDANIEL, S. M., RUMER, K. K., BIROC, S. L., METZ, R. P., SINGH, M., PORTER, W. & SCHEDIN, P. 2006. Remodeling of the mammary microenvironment after lactation promotes breast tumor cell metastasis. *Am J Pathol*, 168, 608-20.
- MELANDER, M. C., JURGENSEN, H. J., MADSEN, D. H., ENGELHOLM, L. H. & BEHRENDT, N. 2015. The collagen receptor uPARAP/Endo180 in tissue degradation and cancer (Review). *Int J Oncol*, 47, 1177-88.
- MÉNDEZ-LUCAS, A., LIN, W., DRISCOLL, P. C., LEGRIVE, N., NOVELLASDEMUNT, L., XIE, C., CHARLES, M., WILSON, Z., JONES, N. P., RAYPORT, S., RODRÍGUEZ-JUSTO, M., LI, V., MACRAE, J. I., HAY, N., CHEN, X. & YUNEVA, M. 2020. Identifying strategies to target the metabolic flexibility of tumours. *Nature Metabolism*, 2, 335-350.
- MENDOZA, M. C., ER, E. E. & BLENIS, J. 2011. The Ras-ERK and PI3K-mTOR pathways: cross-talk and compensation. *Trends Biochem Sci*, 36, 320-8.
- MESCLON, F., LAMBERT-LANGLAIS, S., CARRARO, V., PARRY, L., HAINAULT, I., JOUSSE, C., MAURIN, A. C., BRUHAT, A., FAFOURNOUX, P. & AVEROUS, J. 2017. Decreased ATF4 expression as a mechanism of acquired resistance to long-term amino acid limitation in cancer cells. *Oncotarget*, 8, 27440-27453.
- MINN, A. J., KANG, Y., SERGANOVA, I., GUPTA, G. P., GIRI, D. D., DOUBROVIN, M., PONOMAREV, V., GERALD, W. L., BLASBERG, R. & MASSAGUE, J. 2005. Distinct organ-specific metastatic potential of individual breast cancer cells and primary tumors. *J Clin Invest*, 115, 44-55.
- MOHAN, V., DAS, A. & SAGI, I. 2020. Emerging roles of ECM remodeling processes in cancer. *Semin Cancer Biol*, 62, 192-200.
- MOOKERJEE, S. A., GERENCSE, A. A., NICHOLLS, D. G. & BRAND, M. D. 2017. Quantifying intracellular rates of glycolytic and oxidative ATP production and consumption using extracellular flux measurements. *J Biol Chem*, 292, 7189-7207.
- MORE, T. H., ROYCHOUDHURY, S., CHRISTIE, J., TAUNK, K., MANE, A., SANTRA, M. K., CHAUDHURY, K. & RAPOLE, S. 2018. Metabolomic alterations in invasive ductal carcinoma of breast: A comprehensive metabolomic study using tissue and serum samples. *Oncotarget*, 9, 2678-2696.
- MORRIS, B. A., BURKEL, B., PONIK, S. M., FAN, J., CONDEELIS, J. S., AGUIRRE-GHISO, J. A., CASTRACANE, J., DENU, J. M. & KEELY, P. J. 2016. Collagen Matrix Density Drives the Metabolic Shift in Breast Cancer Cells. *EBioMedicine*, 13, 146-156.

- MOSSMANN, D., PARK, S. & HALL, M. N. 2018. mTOR signalling and cellular metabolism are mutual determinants in cancer. *Nat Rev Cancer*, 18, 744-757.
- MOUW, J. K., OU, G. & WEAVER, V. M. 2014. Extracellular matrix assembly: a multiscale deconstruction. *Nat Rev Mol Cell Biol*, 15, 771-85.
- MURAKAMI, T., NISHIYAMA, T., SHIROTANI, T., SHINOHARA, Y., KAN, M., ISHII, K., KANAI, F., NAKAZURU, S. & EBINA, Y. 1992. Identification of two enhancer elements in the gene encoding the type 1 glucose transporter from the mouse which are responsive to serum, growth factor, and oncogenes. *J Biol Chem*, 267, 9300-6.
- MURANEN, T., IWANICKI, M. P., CURRY, N. L., HWANG, J., DUBOIS, C. D., COLOFF, J. L., HITCHCOCK, D. S., CLISH, C. B., BRUGGE, J. S. & KALAANY, N. Y. 2017. Starved epithelial cells uptake extracellular matrix for survival. *Nat Commun*, 8, 13989.
- MUSCHLER, J. & STREULI, C. H. 2010. Cell-matrix interactions in mammary gland development and breast cancer. *Cold Spring Harb Perspect Biol*, 2, a003202.
- MYLLYHARJU, J. & KIVIRIKKO, K. I. 2004. Collagens, modifying enzymes and their mutations in humans, flies and worms. *Trends Genet*, 20, 33-43.
- NABA, A., CLAUSER, K. R., HOERSCH, S., LIU, H., CARR, S. A. & HYNES, R. O. 2012. The matrisome: in silico definition and in vivo characterization by proteomics of normal and tumor extracellular matrices. *Mol Cell Proteomics*, 11, M111 014647.
- NADER, G. P., EZRATTY, E. J. & GUNDERSEN, G. G. 2016. FAK, talin and PIPK1gamma regulate endocytosed integrin activation to polarize focal adhesion assembly. *Nat Cell Biol*, 18, 491-503.
- NAGY, J. A., CHANG, S. H., SHIH, S. C., DVORAK, A. M. & DVORAK, H. F. 2010. Heterogeneity of the tumor vasculature. *Semin Thromb Hemost*, 36, 321-31.
- NAKANO, A., TSUJI, D., MIKI, H., CUI, Q., EL SAYED, S. M., IKEGAME, A., ODA, A., AMOU, H., NAKAMURA, S., HARADA, T., FUJII, S., KAGAWA, K., TAKEUCHI, K., SAKAI, A., OZAKI, S., OKANO, K., NAKAMURA, T., ITOH, K., MATSUMOTO, T. & ABE, M. 2011. Glycolysis inhibition inactivates ABC transporters to restore drug sensitivity in malignant cells. *PLoS One*, 6, e27222.
- NASS, N. & KALINSKI, T. 2015. Tamoxifen resistance: from cell culture experiments towards novel biomarkers. *Pathol Res Pract*, 211, 189-97.
- NAZEMI, M. & RAINERO, E. 2020. Cross-Talk Between the Tumor Microenvironment, Extracellular Matrix, and Cell Metabolism in Cancer. *Front Oncol*, 10, 239.
- National Disease Registration Service 2020, Cancer Incidence, viewed 15 April 2020  
<<https://www.ndrs.nhs.uk/#>>
- NEESSE, A., ALGUL, H., TUVESON, D. A. & GRESS, T. M. 2015. Stromal biology and therapy in pancreatic cancer: a changing paradigm. *Gut*, 64, 1476-84.
- NEGRINI, S., GORGOLIS, V. G. & HALAZONETIS, T. D. 2010. Genomic instability--an evolving hallmark of cancer. *Nat Rev Mol Cell Biol*, 11, 220-8.
- NELSON, B. H. 2008. The impact of T-cell immunity on ovarian cancer outcomes. *Immunol Rev*, 222, 101-16.
- NICKLIN, P., BERGMAN, P., ZHANG, B., TRIANTAFELLOW, E., WANG, H., NYFELER, B., YANG, H., HILD, M., KUNG, C., WILSON, C., MYER, V. E., MACKEIGAN, J. P., PORTER, J. A., WANG, Y. K., CANTLEY, L. C., FINAN, P. M. & MURPHY, L. O. 2009. Bidirectional transport of amino acids regulates mTOR and autophagy. *Cell*, 136, 521-34.
- NISHIDA, N., YANO, H., NISHIDA, T., KAMURA, T. & KOJIRO, M. 2006. Angiogenesis in cancer. *Vasc Health Risk Manag*, 2, 213-9.
- NISSEN, N. I., KARSDAL, M. & WILLUMSEN, N. 2019. Collagens and Cancer associated fibroblasts in the reactive stroma and its relation to Cancer biology. *J Exp Clin Cancer Res*, 38, 115.
- NOFAL, M., ZHANG, K., HAN, S. & RABINOWITZ, J. D. 2017. mTOR Inhibition Restores Amino Acid Balance in Cells Dependent on Catabolism of Extracellular Protein. *Mol Cell*, 67, 936-946 e5.

- O'SHAUGHNESSY, J. 2005. Extending survival with chemotherapy in metastatic breast cancer. *Oncologist*, 10 Suppl 3, 20-9.
- OH, C., PARK, S., LEE, E. K. & YOO, Y. J. 2013. Downregulation of ubiquitin level via knockdown of polyubiquitin gene Ubb as potential cancer therapeutic intervention. *Sci Rep*, 3, 2623.
- OHGAKI, H. & KLEIHUES, P. 2013. The definition of primary and secondary glioblastoma. *Clin Cancer Res*, 19, 764-72.
- OHLUND, D., LUNDIN, C., ARDNOR, B., OMAN, M., NAREDI, P. & SUND, M. 2009. Type IV collagen is a tumour stroma-derived biomarker for pancreas cancer. *Br J Cancer*, 101, 91-7.
- OKADA, T., LOPEZ-LAGO, M. & GIANCOTTI, F. G. 2005. Merlin/NF-2 mediates contact inhibition of growth by suppressing recruitment of Rac to the plasma membrane. *J Cell Biol*, 171, 361-71.
- OKUYAMA, K., OKUYAMA, K., ARNOTT, S., TAKAYANAGI, M. & KAKUDO, M. 1981. Crystal and molecular structure of a collagen-like polypeptide (Pro-Pro-Gly)<sub>10</sub>. *J Mol Biol*, 152, 427-43.
- OLIVARES, O., MAYERS, J. R., GOUIRAND, V., TORRENCE, M. E., GICQUEL, T., BORGE, L., LAC, S., ROQUES, J., LAVAUT, M. N., BERTHEZENE, P., RUBIS, M., SECQ, V., GARCIA, S., MOUTARDIER, V., LOMBARDO, D., IOVANNA, J. L., TOMASINI, R., GUILLAUMOND, F., VANDER HEIDEN, M. G. & VASSEUR, S. 2017. Collagen-derived proline promotes pancreatic ductal adenocarcinoma cell survival under nutrient limited conditions. *Nat Commun*, 8, 16031.
- ONRUST, S. V., HARTL, P. M., ROSEN, S. D. & HANAHAN, D. 1996. Modulation of L-selectin ligand expression during an immune response accompanying tumorigenesis in transgenic mice. *J Clin Invest*, 97, 54-64.
- ORYAN, A., KAMALI, A., MOSHIRI, A., BAHARVAND, H. & DAEMI, H. 2018. Chemical crosslinking of biopolymeric scaffolds: Current knowledge and future directions of crosslinked engineered bone scaffolds. *Int J Biol Macromol*, 107, 678-688.
- PAGE-MCCAW, A., EWALD, A. J. & WERB, Z. 2007. Matrix metalloproteinases and the regulation of tissue remodelling. *Nat Rev Mol Cell Biol*, 8, 221-33.
- PAGES, F., GALON, J., DIEU-NOSJEAN, M. C., TARTOUR, E., SAUTES-FRIDMAN, C. & FRIDMAN, W. H. 2010. Immune infiltration in human tumors: a prognostic factor that should not be ignored. *Oncogene*, 29, 1093-102.
- PALM, W., ARAKI, J., KING, B., DEMATTEO, R. G. & THOMPSON, C. B. 2017. Critical role for PI3-kinase in regulating the use of proteins as an amino acid source. *Proc Natl Acad Sci U S A*, 114, E8628-E8636.
- PALM, W., PARK, Y., WRIGHT, K., PAVLOVA, N. N., TUVESON, D. A. & THOMPSON, C. B. 2015. The Utilization of Extracellular Proteins as Nutrients Is Suppressed by mTORC1. *Cell*, 162, 259-270.
- PALM, W. & THOMPSON, C. B. 2017. Nutrient acquisition strategies of mammalian cells. *Nature*, 546, 234-242.
- PANKOVA, D., CHEN, Y., TERAJIMA, M., SCHLIEKELMAN, M. J., BAIRD, B. N., FAHRENHOLTZ, M., SUN, L., GILL, B. J., VADAKKAN, T. J., KIM, M. P., AHN, Y. H., ROYBAL, J. D., LIU, X., PARRA CUENTAS, E. R., RODRIGUEZ, J., WISTUBA, II, CREIGHTON, C. J., GIBBONS, D. L., HICKS, J. M., DICKINSON, M. E., WEST, J. L., GRANDE-ALLEN, K. J., HANASH, S. M., YAMAUCHI, M. & KURIE, J. M. 2016. Cancer-Associated Fibroblasts Induce a Collagen Cross-link Switch in Tumor Stroma. *Mol Cancer Res*, 14, 287-95.
- PAUL, R., LUO, M., MO, X., LU, J., YEO, S. K. & GUAN, J. L. 2020. FAK activates AKT-mTOR signaling to promote the growth and progression of MMTV-Wnt1-driven basal-like mammary tumors. *Breast Cancer Res*, 22, 59.
- PAVLOVA, N. N. & THOMPSON, C. B. 2016. The Emerging Hallmarks of Cancer Metabolism. *Cell Metab*, 23, 27-47.
- PEDEN, A. A., OORSCHOT, V., HESSER, B. A., AUSTIN, C. D., SCHELLER, R. H. & KLUMPERMAN, J. 2004. Localization of the AP-3 adaptor complex defines a novel endosomal exit site for lysosomal membrane proteins. *J Cell Biol*, 164, 1065-76.

- PEGRAM, M. D., KONECNY, G. E., O'CALLAGHAN, C., BERYT, M., PIETRAS, R. & SLAMON, D. J. 2004. Rational combinations of trastuzumab with chemotherapeutic drugs used in the treatment of breast cancer. *J Natl Cancer Inst*, 96, 739-49.
- PEINADO, H., LAVOTSHKIN, S. & LYDEN, D. 2011. The secreted factors responsible for pre-metastatic niche formation: old sayings and new thoughts. *Semin Cancer Biol*, 21, 139-46.
- PELICANO, H., MARTIN, D. S., XU, R. H. & HUANG, P. 2006. Glycolysis inhibition for anticancer treatment. *Oncogene*, 25, 4633-46.
- PEREZ, E. A. 2009. Impact, mechanisms, and novel chemotherapy strategies for overcoming resistance to anthracyclines and taxanes in metastatic breast cancer. *Breast Cancer Res Treat*, 114, 195-201.
- PETERSEN, T. E., THOGERSEN, H. C., SKORSTENGAARD, K., VIBE-PEDERSEN, K., SAHL, P., SOTTRUP-JENSEN, L. & MAGNUSSON, S. 1983. Partial primary structure of bovine plasma fibronectin: three types of internal homology. *Proc Natl Acad Sci U S A*, 80, 137-41.
- PETRENKO, A. A., PAVLOVA, L. S., KARSELADZE, A. I., KISSELJOV, F. L. & KISSELJOVA, N. P. 2006. Downregulation of genes encoding for subunits of adaptor complex-3 in cervical carcinomas. *Biochemistry (Mosc)*, 71, 1153-60.
- PFEIFFER, T., SCHUSTER, S. & BONHOEFFER, S. 2001. Cooperation and competition in the evolution of ATP-producing pathways. *Science*, 292, 504-7.
- PICKUP, M. W., LAKLAI, H., ACERBI, I., OWENS, P., GORSKA, A. E., CHYTIL, A., AAKRE, M., WEAVER, V. M. & MOSES, H. L. 2013. Stromally derived lysyl oxidase promotes metastasis of transforming growth factor-beta-deficient mouse mammary carcinomas. *Cancer Res*, 73, 5336-46.
- PIRONE, D. M., LIU, W. F., RUIZ, S. A., GAO, L., RAGHAVAN, S., LEMMON, C. A., ROMER, L. H. & CHEN, C. S. 2006. An inhibitory role for FAK in regulating proliferation: a link between limited adhesion and RhoA-ROCK signaling. *J Cell Biol*, 174, 277-88.
- POLLARI, S., KAKONEN, S. M., EDGREN, H., WOLF, M., KOHONEN, P., SARA, H., GUISE, T., NEES, M. & KALLIONIEMI, O. 2011. Enhanced serine production by bone metastatic breast cancer cells stimulates osteoclastogenesis. *Breast Cancer Res Treat*, 125, 421-30.
- POLTAVETS, V., KOCHETKOVA, M., PITSON, S. M. & SAMUEL, M. S. 2018. The Role of the Extracellular Matrix and Its Molecular and Cellular Regulators in Cancer Cell Plasticity. *Front Oncol*, 8, 431.
- PRASAD, R., PAL, D. & MOHAMMAD, W. 2020. Therapeutic Targets in Telomerase and Telomere Biology of Cancers. *Indian J Clin Biochem*, 35, 135-146.
- POURFARHANGI, K. E., BERGMAN, A. & GLIGORIJEVIC, B. 2018. ECM Cross-Linking Regulates Invadopodia Dynamics. *Biophys J*, 114, 1455-1466.
- PRAT, A., PARKER, J. S., KARGINOVA, O., FAN, C., LIVASY, C., HERSCHKOWITZ, J. I., HE, X. & PEROU, C. M. 2010. Phenotypic and molecular characterization of the claudin-low intrinsic subtype of breast cancer. *Breast Cancer Res*, 12, R68.
- PROVENZANO, P. P., INMAN, D. R., ELICEIRI, K. W., KNITTEL, J. G., YAN, L., RUEDEN, C. T., WHITE, J. G. & KEELY, P. J. 2008. Collagen density promotes mammary tumor initiation and progression. *BMC Med*, 6, 11.
- QIAN, P., ZUO, Z., WU, Z., MENG, X., LI, G., WU, Z., ZHANG, W., TAN, S., PANDEY, V., YAO, Y., WANG, P., ZHAO, L., WANG, J., WU, Q., SONG, E., LOBIE, P. E., YIN, Z. & ZHU, T. 2011. Pivotal role of reduced let-7g expression in breast cancer invasion and metastasis. *Cancer Res*, 71, 6463-74.
- QIAN, B. Z. & POLLARD, J. W. 2010. Macrophage diversity enhances tumor progression and metastasis. *Cell*, 141, 39-51.
- QIE, S., CHU, C., LI, W., WANG, C. & SANG, N. 2014. ErbB2 activation upregulates glutaminase 1 expression which promotes breast cancer cell proliferation. *J Cell Biochem*, 115, 498-509.
- RAINERO, E. 2016. Extracellular matrix endocytosis in controlling matrix turnover and beyond: emerging roles in cancer. *Biochem Soc Trans*, 44, 1347-1354.



- RAINERO, E., HOWE, J. D., CASWELL, P. T., JAMIESON, N. B., ANDERSON, K., CRITCHLEY, D. R., MACHESKY, L. & NORMAN, J. C. 2015a. Ligand-Occupied Integrin Internalization Links Nutrient Signaling to Invasive Migration. *Cell Rep*, 10, 398-413.
- RAINERO, E., HOWE, J. D., CASWELL, P. T., JAMIESON, N. B., ANDERSON, K., CRITCHLEY, D. R., MACHESKY, L. & NORMAN, J. C. 2015b. Ligand-Occupied Integrin Internalization Links Nutrient Signaling to Invasive Migration. *Cell Rep*.
- RASANEN, K. & VAHERI, A. 2010. Activation of fibroblasts in cancer stroma. *Exp Cell Res*, 316, 2713-22.
- RAUT, G. K., CHAKRABARTI, M., PAMARTHY, D. & BHADRA, M. P. 2019. Glucose starvation-induced oxidative stress causes mitochondrial dysfunction and apoptosis via Prohibitin 1 upregulation in human breast cancer cells. *Free Radic Biol Med*, 145, 428-441.
- REYNOLDS, M. R., LANE, A. N., ROBERTSON, B., KEMP, S., LIU, Y., HILL, B. G., DEAN, D. C. & CLEM, B. F. 2014. Control of glutamine metabolism by the tumor suppressor Rb. *Oncogene*, 33, 556-66.
- RHEE, D. K., PARK, S. H. & JANG, Y. K. 2008. Molecular signatures associated with transformation and progression to breast cancer in the isogenic MCF10 model. *Genomics*, 92, 419-28.
- RICHARDS, N. G. & KILBERG, M. S. 2006. Asparagine synthetase chemotherapy. *Annu Rev Biochem*, 75, 629-54.
- RING, A. & DOWSETT, M. 2004. Mechanisms of tamoxifen resistance. *Endocr Relat Cancer*, 11, 643-58.
- RUFFELL, B., AU, A., RUGO, H. S., ESSERMAN, L. J., HWANG, E. S. & COUSSENS, L. M. 2012. Leukocyte composition of human breast cancer. *Proc Natl Acad Sci U S A*, 109, 2796-801.
- RUFFELL, B. & COUSSENS, L. M. 2015. Macrophages and therapeutic resistance in cancer. *Cancer Cell*, 27, 462-72.
- SAAD, S., GOTTLIEB, D. J., BRADSTOCK, K. F., OVERALL, C. M. & BENDALL, L. J. 2002. Cancer cell-associated fibronectin induces release of matrix metalloproteinase-2 from normal fibroblasts. *Cancer Res*, 62, 283-9.
- SAADI, A., SHANNON, N. B., LAO-SIRIEIX, P., O'DONOVAN, M., WALKER, E., CLEMONS, N. J., HARDWICK, J. S., ZHANG, C., DAS, M., SAVE, V., NOVELLI, M., BALKWILL, F. & FITZGERALD, R. C. 2010. Stromal genes discriminate preinvasive from invasive disease, predict outcome, and highlight inflammatory pathways in digestive cancers. *Proc Natl Acad Sci U S A*, 107, 2177-82.
- SABEH, F., SHIMIZU-HIROTA, R. & WEISS, S. J. 2009. Protease-dependent versus -independent cancer cell invasion programs: three-dimensional amoeboid movement revisited. *J Cell Biol*, 185, 11-9.
- SAINIO, A. & JARVELAINEN, H. 2020. Extracellular matrix-cell interactions: Focus on therapeutic applications. *Cell Signal*, 66, 109487.
- SAKAMOTO, A., KUNOU, S., SHIMADA, K., TSUNODA, M., AOKI, T., IRIYAMA, C., TOMITA, A., NAKAMURA, S., HAYAKAWA, F. & KIYOI, H. 2019. Pyruvate secreted from patient-derived cancer-associated fibroblasts supports survival of primary lymphoma cells. *Cancer Sci*, 110, 269-278.
- SATO, T., UMETSU, A. & TAMANOI, F. 2008. Characterization of the Rheb-mTOR signaling pathway in mammalian cells: constitutive active mutants of Rheb and mTOR. *Methods Enzymol*, 438, 307-20.
- SAWAI, H., OKADA, Y., FUNAHASHI, H., MATSUO, Y., TAKAHASHI, H., TAKEYAMA, H. & MANABE, T. 2005. Activation of focal adhesion kinase enhances the adhesion and invasion of pancreatic cancer cells via extracellular signal-regulated kinase-1/2 signaling pathway activation. *Mol Cancer*, 4, 37.
- SCALTRITI, M., ROJO, F., OCANA, A., ANIDO, J., GUZMAN, M., CORTES, J., DI COSIMO, S., MATIAS-GUIU, X., RAMON Y CAJAL, S., ARRIBAS, J. & BASELGA, J. 2007. Expression of p95HER2, a

- truncated form of the HER2 receptor, and response to anti-HER2 therapies in breast cancer. *J Natl Cancer Inst*, 99, 628-38.
- SCHENK, S., HINTERMANN, E., BILBAN, M., KOSHIKAWA, N., HOJILLA, C., KHOKHA, R. & QUARANTA, V. 2003. Binding to EGF receptor of a laminin-5 EGF-like fragment liberated during MMP-dependent mammary gland involution. *J Cell Biol*, 161, 197-209.
- SCHWARZBAUER, J. E. & DESIMONE, D. W. 2011. Fibronectins, their fibrillogenesis, and in vivo functions. *Cold Spring Harb Perspect Biol*, 3.
- SCHWARZBAUER, J. E., TAMKUN, J. W., LEMISCHKA, I. R. & HYNES, R. O. 1983. Three different fibronectin mRNAs arise by alternative splicing within the coding region. *Cell*, 35, 421-31.
- SEGAL, G., LEE, W., ARORA, P. D., MCKEE, M., DOWNEY, G. & MCCULLOCH, C. A. 2001. Involvement of actin filaments and integrins in the binding step in collagen phagocytosis by human fibroblasts. *J Cell Sci*, 114, 119-129.
- SERRELS, A., MCLEOD, K., CANEL, M., KINNAIRD, A., GRAHAM, K., FRAME, M. C. & BRUNTON, V. G. 2012. The role of focal adhesion kinase catalytic activity on the proliferation and migration of squamous cell carcinoma cells. *Int J Cancer*, 131, 287-97.
- SHAY, J. W. & WRIGHT, W. E. 2000. Hayflick, his limit, and cellular ageing. *Nat Rev Mol Cell Biol*, 1, 72-6.
- SHI, F. & SOTTILE, J. 2008. Caveolin-1-dependent beta1 integrin endocytosis is a critical regulator of fibronectin turnover. *J Cell Sci*, 121, 2360-71.
- SHI, F. & SOTTILE, J. 2011. MT1-MMP regulates the turnover and endocytosis of extracellular matrix fibronectin. *J Cell Sci*, 124, 4039-50.
- SHI, H. S., LI, D., ZHANG, J., WANG, Y. S., YANG, L., ZHANG, H. L., WANG, X. H., MU, B., WANG, W., MA, Y., GUO, F. C. & WEI, Y. Q. 2010. Silencing of pkm2 increases the efficacy of docetaxel in human lung cancer xenografts in mice. *Cancer Sci*, 101, 1447-53.
- SHIBUE, T. & WEINBERG, R. A. 2009. Integrin beta1-focal adhesion kinase signaling directs the proliferation of metastatic cancer cells disseminated in the lungs. *Proc Natl Acad Sci U S A*, 106, 10290-5.
- SHIELDS, J. D., KOURTIS, I. C., TOMEI, A. A., ROBERTS, J. M. & SWARTZ, M. A. 2010. Induction of lymphoidlike stroma and immune escape by tumors that express the chemokine CCL21. *Science*, 328, 749-52.
- SIMOES, R. V., SERGANOVA, I. S., KRUCHEVSKY, N., LEFTIN, A., SHESTOV, A. A., THALER, H. T., SUKENICK, G., LOCASALE, J. W., BLASBERG, R. G., KOUTCHER, J. A. & ACKERSTAFF, E. 2015. Metabolic plasticity of metastatic breast cancer cells: adaptation to changes in the microenvironment. *Neoplasia*, 17, 671-84.
- SLACK-DAVIS, J. K., MARTIN, K. H., TILGHMAN, R. W., IWANICKI, M., UNG, E. J., AUTRY, C., LUZZIO, M. J., COOPER, B., KATH, J. C., ROBERTS, W. G. & PARSONS, J. T. 2007. Cellular characterization of a novel focal adhesion kinase inhibitor. *J Biol Chem*, 282, 14845-52.
- SMYTH, M. J., DUNN, G. P. & SCHREIBER, R. D. 2006. Cancer immunosurveillance and immunoediting: the roles of immunity in suppressing tumor development and shaping tumor immunogenicity. *Adv Immunol*, 90, 1-50.
- SO, J. Y., LEE, H. J., KRAMATA, P., MINDEN, A. & SUH, N. 2012. Differential Expression of Key Signaling Proteins in MCF10 Cell Lines, a Human Breast Cancer Progression Model. *Mol Cell Pharmacol*, 4, 31-40.
- SOM, P., ATKINS, H. L., BANDOYPADHYAY, D., FOWLER, J. S., MACGREGOR, R. R., MATSUI, K., OSTER, Z. H., SACKER, D. F., SHIUE, C. Y., TURNER, H., WAN, C. N., WOLF, A. P. & ZABINSKI, S. V. 1980. A fluorinated glucose analog, 2-fluoro-2-deoxy-D-glucose (F-18): nontoxic tracer for rapid tumor detection. *J Nucl Med*, 21, 670-5.
- SON, J., LYSSIOTIS, C. A., YING, H., WANG, X., HUA, S., LIGORIO, M., PERERA, R. M., FERRONE, C. R., MULLARKY, E., SHYH-CHANG, N., KANG, Y., FLEMING, J. B., BARDEESY, N., ASARA, J. M., HAIGIS, M. C., DEPINHO, R. A., CANTLEY, L. C. & KIMMELMAN, A. C. 2013. Glutamine

- supports pancreatic cancer growth through a KRAS-regulated metabolic pathway. *Nature*, 496, 101-5.
- SORLIE, T., PEROU, C. M., TIBSHIRANI, R., AAS, T., GEISLER, S., JOHNSEN, H., HASTIE, T., EISEN, M. B., VAN DE RIJN, M., JEFFREY, S. S., THORSEN, T., QUIST, H., MATESE, J. C., BROWN, P. O., BOTSTEIN, D., LONNING, P. E. & BORRESEN-DALE, A. L. 2001. Gene expression patterns of breast carcinomas distinguish tumor subclasses with clinical implications. *Proc Natl Acad Sci U S A*, 98, 10869-74.
- SORLIE, T., TIBSHIRANI, R., PARKER, J., HASTIE, T., MARRON, J. S., NOBEL, A., DENG, S., JOHNSEN, H., PESICH, R., GEISLER, S., DEMETER, J., PEROU, C. M., LONNING, P. E., BROWN, P. O., BORRESEN-DALE, A. L. & BOTSTEIN, D. 2003. Repeated observation of breast tumor subtypes in independent gene expression data sets. *Proc Natl Acad Sci U S A*, 100, 8418-23.
- SOTTILE, J. & CHANDLER, J. 2005. Fibronectin matrix turnover occurs through a caveolin-1-dependent process. *Mol Biol Cell*, 16, 757-68.
- SOULE, H. D., MALONEY, T. M., WOLMAN, S. R., PETERSON, W. D., JR., BRENZ, R., MCGRATH, C. M., RUSSO, J., PAULEY, R. J., JONES, R. F. & BROOKS, S. C. 1990. Isolation and characterization of a spontaneously immortalized human breast epithelial cell line, MCF-10. *Cancer Res*, 50, 6075-86.
- SOUSA, C. M., BIANCUR, D. E., WANG, X., HALBROOK, C. J., SHERMAN, M. H., ZHANG, L., KREMER, D., HWANG, R. F., WITKIEWICZ, A. K., YING, H., ASARA, J. M., EVANS, R. M., CANTLEY, L. C., LYSSIOTIS, C. A. & KIMMELMAN, A. C. 2016. Pancreatic stellate cells support tumour metabolism through autophagic alanine secretion. *Nature*, 536, 479-83.
- SPIRO, R. G. 2002. Protein glycosylation: nature, distribution, enzymatic formation, and disease implications of glycopeptide bonds. *Glycobiology*, 12, 43R-56R.
- STEHLE, G., SINN, H., WUNDER, A., SCHRENK, H. H., STEWART, J. C., HARTUNG, G., MAIER-BORST, W. & HEENE, D. L. 1997. Plasma protein (albumin) catabolism by the tumor itself--implications for tumor metabolism and the genesis of cachexia. *Crit Rev Oncol Hematol*, 26, 77-100.
- STOVER, D. G., BIERIE, B. & MOSES, H. L. 2007. A delicate balance: TGF-beta and the tumor microenvironment. *J Cell Biochem*, 101, 851-61.
- STRAMER, B. & MAYOR, R. 2017. Mechanisms and in vivo functions of contact inhibition of locomotion. *Nat Rev Mol Cell Biol*, 18, 43-55.
- STRANSKY, L. A. & FORGAC, M. 2015. Amino Acid Availability Modulates Vacuolar H<sup>+</sup>-ATPase Assembly. *J Biol Chem*, 290, 27360-9.
- STUELTEN, C. H., DACOSTA BYFIELD, S., ARANY, P. R., KARPOVA, T. S., STETLER-STEVENSON, W. G. & ROBERTS, A. B. 2005. Breast cancer cells induce stromal fibroblasts to express MMP-9 via secretion of TNF-alpha and TGF-beta. *J Cell Sci*, 118, 2143-53.
- SUBIK, K., LEE, J. F., BAXTER, L., STRZEPEK, T., COSTELLO, D., CROWLEY, P., XING, L., HUNG, M. C., BONFIGLIO, T., HICKS, D. G. & TANG, P. 2010. The Expression Patterns of ER, PR, HER2, CK5/6, EGFR, Ki-67 and AR by Immunohistochemical Analysis in Breast Cancer Cell Lines. *Breast Cancer (Auckl)*, 4, 35-41.
- SULLIVAN, M. R., DANAI, L. V., LEWIS, C. A., CHAN, S. H., GUI, D. Y., KUNCHOK, T., DENNSTEDT, E. A., VANDER HEIDEN, M. G. & MUIR, A. 2019. Quantification of microenvironmental metabolites in murine cancers reveals determinants of tumor nutrient availability. *Elife*, 8.
- SULLIVAN, W. J., MULLEN, P. J., SCHMID, E. W., FLORES, A., MOMCILOVIC, M., SHARPLEY, M. S., JELINEK, D., WHITELEY, A. E., MAXWELL, M. B., WILDE, B. R., BANERJEE, U., COLLIER, H. A., SHACKELFORD, D. B., BRAAS, D., AYER, D. E., DE AGUIAR VALLIM, T. Q., LOWRY, W. E. & CHRISTOFK, H. R. 2018. Extracellular Matrix Remodeling Regulates Glucose Metabolism through TXNIP Destabilization. *Cell*, 175, 117-132 e21.
- SUROWIAK, P., MURAWA, D., MATERNA, V., MACIEJCZYK, A., PUDELKO, M., CIESLA, S., BREBOROWICZ, J., MURAWA, P., ZABEL, M., DIETEL, M. & LAGE, H. 2007. Occurrence of stromal myofibroblasts in the invasive ductal breast cancer tissue is an unfavourable prognostic factor. *Anticancer Res*, 27, 2917-24.

- SZLOSAREK, P. W., KLABATSA, A., PALLASKA, A., SHEAFF, M., SMITH, P., CROOK, T., GRIMSHAW, M. J., STEELE, J. P., RUDD, R. M., BALKWILL, F. R. & FENNELL, D. A. 2006. In vivo loss of expression of argininosuccinate synthetase in malignant pleural mesothelioma is a biomarker for susceptibility to arginine depletion. *Clin Cancer Res*, 12, 7126-31.
- TAKADA, Y., YE, X. & SIMON, S. 2007. The integrins. *Genome Biol*, 8, 215.
- TAKINO, T., YOSHIOKA, K., MIYAMORI, H., YAMADA, K. M. & SATO, H. 2002. A scaffold protein in the c-Jun N-terminal kinase signaling pathway is associated with focal adhesion kinase and tyrosine-phosphorylated. *Oncogene*, 21, 6488-97.
- TALMADGE, J. E. & FIDLER, I. J. 2010. AACR centennial series: the biology of cancer metastasis: historical perspective. *Cancer Res*, 70, 5649-69.
- TALVENSAARI-MATTILA, A., PAAKKO, P., HOYHTYA, M., BLANCO-SEQUEIROS, G. & TURPEENNIEMI-HUJANEN, T. 1998. Matrix metalloproteinase-2 immunoreactive protein: a marker of aggressiveness in breast carcinoma. *Cancer*, 83, 1153-62.
- TANG, X., HOU, Y., YANG, G., WANG, X., TANG, S., DU, Y. E., YANG, L., YU, T., ZHANG, H., ZHOU, M., WEN, S., XU, L. & LIU, M. 2016a. Stromal miR-200s contribute to breast cancer cell invasion through CAF activation and ECM remodeling. *Cell Death Differ*, 23, 132-45.
- TANG, Y., WANG, Y., KIANI, M. F. & WANG, B. 2016b. Classification, Treatment Strategy, and Associated Drug Resistance in Breast Cancer. *Clin Breast Cancer*, 16, 335-343.
- TARDITO, S., OUDIN, A., AHMED, S. U., FACK, F., KEUNEN, O., ZHENG, L., MILETIC, H., SAKARIASSEN, P. O., WEINSTOCK, A., WAGNER, A., LINDSAY, S. L., HOCK, A. K., BARNETT, S. C., RUPPIN, E., MORKVE, S. H., LUND-JOHANSEN, M., CHALMERS, A. J., BJERKVIG, R., NICLOU, S. P. & GOTTLIEB, E. 2015. Glutamine synthetase activity fuels nucleotide biosynthesis and supports growth of glutamine-restricted glioblastoma. *Nat Cell Biol*, 17, 1556-68.
- TENG, M. W., SWANN, J. B., KOEBEL, C. M., SCHREIBER, R. D. & SMYTH, M. J. 2008. Immune-mediated dormancy: an equilibrium with cancer. *J Leukoc Biol*, 84, 988-93.
- TETU, B., BRISSON, J., WANG, C. S., LAPOINTE, H., BEAUDRY, G., BLANCHETTE, C. & TRUDEL, D. 2006. The influence of MMP-14, TIMP-2 and MMP-2 expression on breast cancer prognosis. *Breast Cancer Res*, 8, R28.
- THEOCHARIS, A. D., SKANDALIS, S. S., GIALELI, C. & KARAMANOS, N. K. 2016. Extracellular matrix structure. *Adv Drug Deliv Rev*, 97, 4-27.
- THOMPSON, C. B. 2011. Rethinking the regulation of cellular metabolism. *Cold Spring Harb Symp Quant Biol*, 76, 23-9.
- THOMPSON, C. B. & BIELSKA, A. A. 2019. Growth factors stimulate anabolic metabolism by directing nutrient uptake. *J Biol Chem*, 294, 17883-17888.
- TIAN, T., LI, X. & ZHANG, J. 2019. mTOR Signaling in Cancer and mTOR Inhibitors in Solid Tumor Targeting Therapy. *Int J Mol Sci*, 20.
- TIMPL, R. & BROWN, J. C. 1994. The laminins. *Matrix Biol*, 14, 275-81.
- TIWARI, S., ASKARI, J. A., HUMPHRIES, M. J. & BULLEID, N. J. 2011. Divalent cations regulate the folding and activation status of integrins during their intracellular trafficking. *J Cell Sci*, 124, 1672-80.
- TURASHVILI, G. & BROGI, E. 2017. Tumor Heterogeneity in Breast Cancer. *Front Med (Lausanne)*, 4, 227.
- TURLEY, S. J., CREMASCO, V. & ASTARITA, J. L. 2015. Immunological hallmarks of stromal cells in the tumour microenvironment. *Nat Rev Immunol*, 15, 669-82.
- VALKENBURG, K. C., DE GROOT, A. E. & PIENTA, K. J. 2018. Targeting the tumour stroma to improve cancer therapy. *Nat Rev Clin Oncol*, 15, 366-381.
- VAN BEIJNUM, J. R., NOWAK-SLIWINSKA, P., HUIJBERS, E. J., THIJSEN, V. L. & GRIFFIOEN, A. W. 2015. The great escape; the hallmarks of resistance to antiangiogenic therapy. *Pharmacol Rev*, 67, 441-61.

- VANDE VOORDE, J., ACKERMANN, T., PFETZER, N., SUMPTON, D., MACKAY, G., KALNA, G., NIXON, C., BLYTH, K., GOTTLIEB, E. & TARDITO, S. 2019. Improving the metabolic fidelity of cancer models with a physiological cell culture medium. *Sci Adv*, 5, eaau7314.
- VANDER HEIDEN, M. G., CANTLEY, L. C. & THOMPSON, C. B. 2009. Understanding the Warburg effect: the metabolic requirements of cell proliferation. *Science*, 324, 1029-33.
- VETTORE, L., WESTBROOK, R. L. & TENNANT, D. A. 2020. New aspects of amino acid metabolism in cancer. *Br J Cancer*, 122, 150-156.
- VU, T. & CLARET, F. X. 2012. Trastuzumab: updated mechanisms of action and resistance in breast cancer. *Front Oncol*, 2, 62.
- VUONG, D., SIMPSON, P. T., GREEN, B., CUMMINGS, M. C. & LAKHANI, S. R. 2014. Molecular classification of breast cancer. *Virchows Arch*, 465, 1-14.
- WAGNER, D. D. & HYNES, R. O. 1979. Domain structure of fibronectin and its relation to function. Disulfides and sulfhydryl groups. *J Biol Chem*, 254, 6746-54.
- WANG, R., DILLON, C. P., SHI, L. Z., MILASTA, S., CARTER, R., FINKELSTEIN, D., MCCORMICK, L. L., FITZGERALD, P., CHI, H., MUNGER, J. & GREEN, D. R. 2011. The transcription factor Myc controls metabolic reprogramming upon T lymphocyte activation. *Immunity*, 35, 871-82.
- WANG, X., SHANG, Y., YANG, L., TAN, X., ZHANG, H., SHAN, C. & LIU, S. 2019. HPD overexpression predicts poor prognosis in breast cancer. *Pathol Res Pract*, 215, 152524.
- WARBURG, O. 1956. On respiratory impairment in cancer cells. *Science*, 124, 269-70.
- WARBURG, O., WIND, F. & NEGELEIN, E. 1927. The Metabolism of Tumors in the Body. *J Gen Physiol*, 8, 519-30.
- WEBER, R. A., YEN, F. S., NICHOLSON, S. P. V., ALWASEEM, H., BAYRAKTAR, E. C., ALAM, M., TIMSON, R. C., LA, K., ABU-REMAILEH, M., MOLINA, H. & BIRSOY, K. 2020. Maintaining Iron Homeostasis Is the Key Role of Lysosomal Acidity for Cell Proliferation. *Mol Cell*, 77, 645-655 e7.
- WEIS, S. M. & CHERESH, D. A. 2011. Tumor angiogenesis: molecular pathways and therapeutic targets. *Nat Med*, 17, 1359-70.
- WELLEN, K. E., LU, C., MANCUSO, A., LEMONS, J. M., RYCZKO, M., DENNIS, J. W., RABINOWITZ, J. D., COLLER, H. A. & THOMPSON, C. B. 2010. The hexosamine biosynthetic pathway couples growth factor-induced glutamine uptake to glucose metabolism. *Genes Dev*, 24, 2784-99.
- WHITE, E., KARP, C., STROHECKER, A. M., GUO, Y. & MATHEW, R. 2010. Role of autophagy in suppression of inflammation and cancer. *Curr Opin Cell Biol*, 22, 212-7.
- WIEMAN, H. L., WOFFORD, J. A. & RATHMELL, J. C. 2007. Cytokine stimulation promotes glucose uptake via phosphatidylinositol-3 kinase/Akt regulation of Glut1 activity and trafficking. *Mol Biol Cell*, 18, 1437-46.
- WIENKE, D., MACFADYEN, J. R. & ISACKE, C. M. 2003. Identification and characterization of the endocytic transmembrane glycoprotein Endo180 as a novel collagen receptor. *Mol Biol Cell*, 14, 3592-604.
- WILLEM, M., MIOSGE, N., HALFTER, W., SMYTH, N., JANNETTI, I., BURGHART, E., TIMPL, R. & MAYER, U. 2002. Specific ablation of the nidogen-binding site in the laminin gamma1 chain interferes with kidney and lung development. *Development*, 129, 2711-22.
- WILLIAMSON, C. D. & DONALDSON, J. G. 2019. Arf6, JIP3, and dynein shape and mediate macropinocytosis. *Mol Biol Cell*, 30, 1477-1489.
- WILLUMSEN, N., JORGENSEN, L. N. & KARSDAL, M. A. 2019. Vastatin (the NC1 domain of human type VIII collagen a1 chain) is linked to stromal reactivity and elevated in serum from patients with colorectal cancer. *Cancer Biol Ther*, 20, 692-699.
- WISE, D. R., DEBERARDINIS, R. J., MANCUSO, A., SAYED, N., ZHANG, X. Y., PFEIFFER, H. K., NISSIM, I., DAIKHIN, E., YUDKOFF, M., MCMAHON, S. B. & THOMPSON, C. B. 2008. Myc regulates a transcriptional program that stimulates mitochondrial glutaminolysis and leads to glutamine addiction. *Proc Natl Acad Sci U S A*, 105, 18782-7.

- WOLFSON, R. L. & SABATINI, D. M. 2017. The Dawn of the Age of Amino Acid Sensors for the mTORC1 Pathway. *Cell Metab*, 26, 301-309.
- WOZNIAK, M. A., MODZELEWSKA, K., KWONG, L. & KEELY, P. J. 2004. Focal adhesion regulation of cell behavior. *Biochim Biophys Acta*, 1692, 103-19.
- XIONG, J. P., STEHLE, T., DIEFENBACH, B., ZHANG, R., DUNKER, R., SCOTT, D. L., JOACHIMIAK, A., GOODMAN, S. L. & ARNAOUT, M. A. 2001. Crystal structure of the extracellular segment of integrin alpha Vbeta3. *Science*, 294, 339-45.
- YANAGIDA, O., KANAI, Y., CHAIROUNGDUA, A., KIM, D. K., SEGAWA, H., NII, T., CHA, S. H., MATSUO, H., FUKUSHIMA, J., FUKASAWA, Y., TANI, Y., TAKETANI, Y., UCHINO, H., KIM, J. Y., INATOMI, J., OKAYASU, I., MIYAMOTO, K., TAKEDA, E., GOYA, T. & ENDOU, H. 2001. Human L-type amino acid transporter 1 (LAT1): characterization of function and expression in tumor cell lines. *Biochim Biophys Acta*, 1514, 291-302.
- YANG, J. & WEINBERG, R. A. 2008. Epithelial-mesenchymal transition: at the crossroads of development and tumor metastasis. *Dev Cell*, 14, 818-29.
- YANG, L., ACHREJA, A., YEUNG, T. L., MANGALA, L. S., JIANG, D., HAN, C., BADDOUR, J., MARINI, J. C., NI, J., NAKAHARA, R., WAHLIG, S., CHIBA, L., KIM, S. H., MORSE, J., PRADEEP, S., NAGARAJA, A. S., HAEMMERLE, M., KYUNGHEE, N., DERICHSWEILER, M., PLACKEMEIER, T., MERCADO-URIBE, I., LOPEZ-BERESTEIN, G., MOSS, T., RAM, P. T., LIU, J., LU, X., MOK, S. C., SOOD, A. K. & NAGRATH, D. 2016. Targeting Stromal Glutamine Synthetase in Tumors Disrupts Tumor Microenvironment-Regulated Cancer Cell Growth. *Cell Metab*, 24, 685-700.
- YANG, L., MOSS, T., MANGALA, L. S., MARINI, J., ZHAO, H., WAHLIG, S., ARMAIZ-PENA, G., JIANG, D., ACHREJA, A., WIN, J., ROOPAIMOOLE, R., RODRIGUEZ-AGUAYO, C., MERCADO-URIBE, I., LOPEZ-BERESTEIN, G., LIU, J., TSUKAMOTO, T., SOOD, A. K., RAM, P. T. & NAGRATH, D. 2014. Metabolic shifts toward glutamine regulate tumor growth, invasion and bioenergetics in ovarian cancer. *Mol Syst Biol*, 10, 728.
- YANG, L., VENNETI, S. & NAGRATH, D. 2017. Glutaminolysis: A Hallmark of Cancer Metabolism. *Annu Rev Biomed Eng*, 19, 163-194.
- YANG, S., WANG, X., CONTINO, G., LIESA, M., SAHIN, E., YING, H., BAUSE, A., LI, Y., STOMMEL, J. M., DELL'ANTONIO, G., MAUTNER, J., TONON, G., HAIGIS, M., SHIRIHAI, O. S., DOGLIONI, C., BARDEESY, N. & KIMMELMAN, A. C. 2011. Pancreatic cancers require autophagy for tumor growth. *Genes Dev*, 25, 717-29.
- YAO, E. S., ZHANG, H., CHEN, Y. Y., LEE, B., CHEW, K., MOORE, D. & PARK, C. 2007. Increased beta1 integrin is associated with decreased survival in invasive breast cancer. *Cancer Res*, 67, 659-64.
- YEN, K., TRAVINS, J., WANG, F., DAVID, M. D., ARTIN, E., STRALEY, K., PADYANA, A., GROSS, S., DELABARRE, B., TOBIN, E., CHEN, Y., NAGARAJA, R., CHOE, S., JIN, L., KONTEATIS, Z., CIANCHETTA, G., SAUNDERS, J. O., SALITURO, F. G., QUIVORON, C., OPOLON, P., BAWA, O., SAADA, V., PACI, A., BROUTIN, S., BERNARD, O. A., DE BOTTON, S., MARTEYN, B. S., PILICHOWSKA, M., XU, Y., FANG, C., JIANG, F., WEI, W., JIN, S., SILVERMAN, L., LIU, W., YANG, H., DANG, L., DORSCH, M., PENARD-LACRONIQUE, V., BILLER, S. A. & SU, S. M. 2017. AG-221, a First-in-Class Therapy Targeting Acute Myeloid Leukemia Harboring Oncogenic IDH2 Mutations. *Cancer Discov*, 7, 478-493.
- YLISAUKKO-OJA, S. K., CYBULSKI, C., LEHTONEN, R., KIURU, M., MATYJASIK, J., SZYMANSKA, A., SZYMANSKA-PASTERNAK, J., DYRSKJOT, L., BUTZOW, R., ORNTOFT, T. F., LAUNONEN, V., LUBINSKI, J. & AALTONEN, L. A. 2006. Germline fumarate hydratase mutations in patients with ovarian mucinous cystadenoma. *Eur J Hum Genet*, 14, 880-3.
- YOSHIMORI, T., YAMAMOTO, A., MORIYAMA, Y., FUTAI, M. & TASHIRO, Y. 1991. Bafilomycin A1, a specific inhibitor of vacuolar-type H(+)-ATPase, inhibits acidification and protein degradation in lysosomes of cultured cells. *J Biol Chem*, 266, 17707-12.
- YOUSEF, E. M., TAHIR, M. R., ST-PIERRE, Y. & GABOURY, L. A. 2014. MMP-9 expression varies according to molecular subtypes of breast cancer. *BMC Cancer*, 14, 609.

- YURUBE, T., BUCHSER, W. J., MOON, H. J., HARTMAN, R. A., TAKAYAMA, K., KAWAKAMI, Y., NISHIDA, K., KUROSAKA, M., VO, N. V., KANG, J. D., LOTZE, M. T. & SOWA, G. A. 2019. Serum and nutrient deprivation increase autophagic flux in intervertebral disc annulus fibrosus cells: an in vitro experimental study. *Eur Spine J*, 28, 993-1004.
- ZANOTELLI, M. R., GOLDBLATT, Z. E., MILLER, J. P., BORDELEAU, F., LI, J., VANDERBURGH, J. A., LAMPI, M. C., KING, M. R. & REINHART-KING, C. A. 2018. Regulation of ATP utilization during metastatic cell migration by collagen architecture. *Mol Biol Cell*, 29, 1-9.
- ZEISBERG, E. M., POTENTA, S., XIE, L., ZEISBERG, M. & KALLURI, R. 2007. Discovery of endothelial to mesenchymal transition as a source for carcinoma-associated fibroblasts. *Cancer Res*, 67, 10123-8.
- ZHANG, J., FAN, J., VENNETI, S., CROSS, J. R., TAKAGI, T., BHINDER, B., DJABALLAH, H., KANAI, M., CHENG, E. H., JUDKINS, A. R., PAWEL, B., BAGGS, J., CHERRY, S., RABINOWITZ, J. D. & THOMPSON, C. B. 2014. Asparagine plays a critical role in regulating cellular adaptation to glutamine depletion. *Mol Cell*, 56, 205-218.
- ZHANG, L. & HAN, J. 2017. Branched-chain amino acid transaminase 1 (BCAT1) promotes the growth of breast cancer cells through improving mTOR-mediated mitochondrial biogenesis and function. *Biochem Biophys Res Commun*, 486, 224-231.
- ZHAO, H., YANG, L., BADDOUR, J., ACHREJA, A., BERNARD, V., MOSS, T., MARINI, J. C., TUDAWE, T., SEVIOUR, E. G., SAN LUCAS, F. A., ALVAREZ, H., GUPTA, S., MAITI, S. N., COOPER, L., PEEHL, D., RAM, P. T., MAITRA, A. & NAGRATH, D. 2016. Tumor microenvironment derived exosomes pleiotropically modulate cancer cell metabolism. *Elife*, 5, e10250.
- ZHU, J. & CLARK, R. A. F. 2014. Fibronectin at select sites binds multiple growth factors and enhances their activity: expansion of the collaborative ECM-GF paradigm. *J Invest Dermatol*, 134, 895-901.
- ZHU, Q., ZHANG, X., ZHANG, L., LI, W., WU, H., YUAN, X., MAO, F., WANG, M., ZHU, W., QIAN, H. & XU, W. 2014. The IL-6-STAT3 axis mediates a reciprocal crosstalk between cancer-derived mesenchymal stem cells and neutrophils to synergistically prompt gastric cancer progression. *Cell Death Dis*, 5, e1295.
- ZHUANG, X., ZHANG, H. & HU, G. 2019. Cancer and Microenvironment Plasticity: Double-Edged Swords in Metastasis. *Trends Pharmacol Sci*, 40, 419-429.
- ZONCU, R., BAR-PELED, L., EFEYAN, A., WANG, S., SANCAK, Y. & SABATINI, D. M. 2011a. mTORC1 senses lysosomal amino acids through an inside-out mechanism that requires the vacuolar H(+)-ATPase. *Science*, 334, 678-83.
- ZONCU, R., EFEYAN, A. & SABATINI, D. M. 2011b. mTOR: from growth signal integration to cancer, diabetes and ageing. *Nat Rev Mol Cell Biol*, 12, 21-35.